Pieces of a Puzzle

Fitting Electromagnetic Induction into Geophysical Strategies to Produce Enhanced Archaeological Characterisation

Jane Chrys HARRIS

Submitted for the Degree of
Doctor of Philosophy

Faculty of Archaeological Sciences
University of Bradford
2016

J. Chrys Harris

Pieces of a Puzzle: Fitting Electromagnetic Induction into Geophysical Strategies to Produce Enhanced Archaeological Characterisation

Keywords: geophysics, archaeology, earth resistance, electromagnetic induction, magnetometry, archaeological geophysics, data combination, characterisation

Abstract

Electromagnetic induction (EM) methods have been utilised in a recent surge of archaeological applications across continental Europe, Ireland and Scandinavia. Development of multi-exploration depth instruments and improvements to instrument stability have improved its reputation as an effective method for mapping archaeological remains. Despite these advances, EM methods are comparatively lacking in rigour when for British sites. Through a structured scheme of experimental analysis and fieldwork, this thesis develops an understanding of the responses of EM instruments over a range of British archaeology, including earthworks, field systems, burials, modern remains, and a Cistercian abbey; the results of which demonstrate its effective over a diversity of environments. The impact of instrument-based issues on the collected measurements was quantified through a scheme of experiments targeting instrument drift, calibration and elevation. Dedicated instrument operation and processing workflows were developed based on the collective field and experimental results, which recommend best practice guidelines for improving the quality and accuracy of collected data. The link between instrument measurements and buried archaeology was further developed through a structured analysis of the EM datasets with complementary earth resistance and magnetic results. The integration of the EM, earth resistance and magnetic datasets was utilised to develop an enhanced archaeological characterisation of subsurface features. While the earth resistance and magnetic methods generally responded to different aspects of the buried archaeology, the EM surveys were able to detect a range of responses evident in the results of the former methods. Therefore, the role of EM methods within this characterisation are shown to “bridge the gap” between the earth resistance and magnetic methods, while providing a comprehensive characterisation of the remains in their own right.

Dedication

To Finn—my husband, colleague and inspiration. Our ArchaeoPY days were the most fun of the PhD and challenged me to develop the thesis into what it is today.

And to my Mom—hopefully now you will finally understand what it is that I do!

Acknowledgements

I am grateful to my supervisors, Drs. Chris Gaffney and Cathy Batt, for allowing me to explore my own research, learn from my mistakes, and reel me in when I had gone off too far. The amount of data collected and made available for this project could not have been accomplished without the dedication of the years of Archaeological Prospection MSc students, with the support of Stuart Fox and Tom Sparrow. My fellow Bradford compatriots have also contributed to this endeavour both in fieldwork and discussions, which have enriched the development of this project. Thank you, Finnegan Pope-Carter, Hannah Brown, Peter Turner, Alex Corkhum, Mary Saunders, Mariah Ottersen, Emily Fioccoprile, James Bonsall and Rob Fry. The support of this research by Geoscan Research and Geomatrix Earth Science Ltd is immensely appreciated. Thank you to my family for the support, as well my Magnitude family, particularly Graeme Attwood, for picking up the slack during my academic sabbaticals. And finally, to my German Shepherd Laika, who contributed valuable insights into this project.

Table of Contents

List of Equations

List of Tables

Chapter 1 Research Introduction

Geophysical methods can provide a rapid evaluation of the presence or absence of buried archaeological remains. The well-established reliability of magnetometers in detecting a range of different types of archaeological features has led to the preference for magnetic methods as the primary geophysical technique for archaeological investigations (David et al. 2008; Jordan 2009; Kvamme 2006a). Magnetometers also provide faster sampling rates than other geophysical sensors and can easily be configured in multi-sensor and cart-based systems to further increase survey speed. These advantages make magnetic methods particularly efficient for field survey, which allows the technique to be suitable for surveys ranging from site-specific (Lowe and Fogel 2010; Payne 1996; Rogers et al 2010) to landscape-wide (Becker 2009; Gaffney et al. 2012; Powlesland 2009) in size. Following magnetic methods, earth resistance methods have also experienced widespread usage for archaeological applications (Schmidt 2013). The application of earth resistance for archaeological applications is reasonably understood owing to a long history of use and development (Clark 1996). Earth resistance methods have been proven particularly effective for detecting stone or other insulating materials, but can respond to ditch-like and earthen features as well.

Despite their history of use and development, magnetic and earth resistance methods are not infallible. For example, while magnetic methods can provide a rapid assessment of the presence or absence of buried remains, they lack the straightforward ability to characterise the vertical extent and nature of the anomaly's source feature. Direct magnetometer measurements cannot quantify the specific depth extent of buried archaeological remains (Benech et al. 2002; Dalan et al. 2011). Shallow or deep feature depth can be roughly approximated by examining anomaly width in the XY traces, but this analysis is unsophisticated for accurately determining feature depth due to the dependency of the anomaly response on other variables (Aspinall et al. 2008; Kvamme 2006a; Neubauer and Eder-Hinterleitner 1997). For example, a magnetic anomaly may not directly represent the dimensions or extent of the anomaly source due to the dependencies of its magnitude and form on the site conditions, instrument used and operator-induced effects (Neubauer and Eder-Hinterleitner 1997; Fassbinder

2015). In addition to these factors, disentangling individual magnetic anomalies can be difficult at complex or multi-phase sites (Aspinall et al. 2008; Fassbinder 2015). Quantifying the exact depths of magnetic anomalies is possible through analytical data analysis and modelling, but these algorithms require a detailed understanding of the archaeological feature and site-specific soil properties, parameters which may not be easily available to the practitioner (Cheyney 2012; Neubauer and Eder-Hinterleitner 1997). As a result, the accuracy of magnetic modelling may be unreliable. Three-dimensional analysis of buried features is more practical with earth resistance methods because the separation of electrodes can easily be changed to target different exploration depths. Still, the effectiveness of earth resistance on any given site is not as reliable as magnetic methods due to the complex dependency of soil resistivity on climatic and soil moisture conditions: the so-called “seasonality” effect (David et al. 2008; Bonsall et al. 2013a). Magnetic methods are independent of seasonal changes because the method relies on magnetic enhancement to detect archaeological remains; whereas earth resistance requires adequate physical contrast between the feature and the soil matrix to be detected.

A less widespread archaeological prospection technique in Britain is electromagnetic induction (EM), which measure magnetic susceptibility and electrical conductivity properties simultaneously. EM methods have experienced a recent surge in publication for a range of different archaeological applications extending from Europe (Cella et al. 2015; Dabas et al. 2016; De Smedt et al. 2014a; Di Maio et al. 2016; Gheyle et al. 2016; Saey et al. 2016; Verhegge et al. 2016), to the Arctic (Landry et al. 2015; Wunderlich et al. 2015) and to Africa (Welham et al. 2014; Klehm and Ernenwein 2016). While EM methods have been explored since the mid-20th century, the improved stability of the latest instruments has helped the method become a more reliable option for archaeological applications. Furthermore, multi-coil EM instruments now offer multiple exploration depths, which allows for the vertical discrimination of archaeological features (Bonsall et al. 2013b; De Smedt et al. 2013). The ability to simultaneously measure magnetic susceptibility and electrical conductivity soil properties can also provide information on soil texture, organic matter and moisture content. Thus, EM methods have found particular success in marginal environments where geological conditions and poor physical contrast of

archaeological remains has resulted in poor performance by magnetic and earth resistance methods (Bonsall et al. 2013a; Wunderlich et al. 2015).

For these reasons, the application of EM methods for British archaeology is attractive. However, EM methods have not experienced widespread usage in Britain, which means their application lacks the confidence and reliability that the well-established magnetic and earth resistance methods have. Furthermore, there are no comprehensive guidelines for EM survey in Britain. While Historic England's archaeological geophysics guidelines contain an EM section, the methodology for the collection, processing and visualisation of EM data is not fully developed (David et al. 2008). The poorly defined methodology for EM surveys is problematic since "the potential of even the 'best'… data set may not be realized without a properly designed display that maximizes conveyance of information it contains" (Kvamme 2006b). Some texts suggest that EM processing steps should be similar to those of earth resistance and magnetic data for the respective quadrature-phase and in-phase datasets (Clay 2006; Gaffney and Gater 2003). At face value, the basis for this assertion is that conductivity and magnetic susceptibility datasets represent comparable physical properties as to earth resistance and magnetometer datasets. The problem with this view, is that many of the steps for earth resistance and magnetic data processing are to correct for the operation of the instruments themselves—not as a reflection of some actual physical property. Given the lack of guidance for the application and handling of EM methods at British sites, an important part of this research is the structured development of an effective, dedicated methodology for EM data collection, processing, visualisation and interpretation.

By developing an effective EM methodology, this thesis will improve the confidence in the responses of EM methods by exploring their application and results over a range of typical British archaeological sites. Magnetic and earth resistance results will be used as the standard control methods in order to understand how the output measurements represent buried archaeological features in a variety of British environments. The separate magnetic, earth resistance and electromagnetic induction results will be interpreted individually first to establish the nature of the respective measurements, which will guide how the individual results can be most effectively integrated. Next, the individual

results will be integrated to derive the most information from the techniques together, in order to develop a more comprehensive characterisation of the nature of the buried archaeology and the context in which it lies. This combined approach will go beyond the interpretation of the discrete archaeological anomaly and will further develop the information that can be learned about the background and contextual information from this combined approach. By characterising a range of sites, this thesis will also serve as a resource to consult for which techniques are suited to what particular types of archaeology, how their measured responses represent the type of archaeology and how the techniques collectively can be used to comprehensively characterise the type of archaeology.

1.1 Research Aim

The aim of this research to evaluate the role of electromagnetic induction methods for British archaeology within a combined magnetic and earth resistance approach, to develop a comprehensive characterisation of archaeological remains.

1.2 Research Questions and Objectives

1. What is the most effective methodology for the collection, processing and visualisation of electromagnetic induction data?

    1a. Employ and assess different survey strategies to determine a dedicated methodology for the collection of high-quality, positionally accurate EM data.

    1b. Assess recommended processing and visualisation guides for EM data in order to develop new processing and visualisation software.

2. How do the resulting electromagnetic induction measurements relate to buried archaeology at a range of typical British sites?

    a. Compare EM results with magnetic and earth resistance results to understand how the EM instrument responds to these individual properties.

b. Apply novel graphical and data combination techniques to quantify the comparison between EM results and magnetic and earth resistance methods.

3. How can the individual magnetic, earth resistance and EM techniques be effectively used in combination to better assess and characterise buried archaeology?

    a. Derive conclusions from the integrated results of the geophysical methods.

1.3 Thesis Outline

Chapter 2 will present the background and theory of the magnetic, earth resistance and electromagnetic induction methods utilised for this research. The methods will initially be discussed individually then cross-analysed in relation to one another through a selection of case studies. Chapter 2 will finish by exploring the different data integration techniques and how these techniques can improve the interpretation of the geophysical results.

From there, presentation of this thesis' research methods in Chapter 3 will structure how the fieldwork and experimental investigations were accomplished to answer the research questions. Chapter 3 will cover the methods used for the lab experiments, fieldwork, data processing and visualisation. The location and background information for the test sides used for the experimental work and field surveys will be presented as well.

The fieldwork results will be presented in Chapter 4. Following the presentation of results, the sites will be analysed in further detail using the graphical and data combination approaches to develop a more accurate archaeological characterisation of the geophysical measurements. This chapter will address research questions two and three.

Chapter 5 will present the results of the EM experiments. The experimental results and the fieldwork results will be analysed together to quantify the relationship between the instrument's measurements with archaeological

features, environmental variables and operator effects. This chapter will address research question two.

The comprehensive analysis of the EM results in Chapter 5 will develop the basis for the EM methodology that will be presented in Chapter 6. This chapter will address research question one.

Chapter 7 will conclude the thesis. This chapter will answer the research questions using the cumulative thesis work as support. A final overall statement on the aim of the research project, including the value and impact of this research on the field of archaeological prospection will bring the research to a close. Suggestion for further work will end the chapter and bring the thesis to a close.

Chapter 2 Defining the Roles of Geophysical Methods Within Archaeological Investigations

Chapter 2 is important for constructing the foundation for the research methodology that will be presented in Chapter 3. The development and theory of the earth resistance, magnetic, and electromagnetic induction methods will be presented to establish their roles within archaeological prospection today. Greater detail will be given to the EM section, because the application and usage of earth resistance and magnetic methods for British archaeology is already well-established.

2.1 Development of Earth Resistance Methods for Archaeological Applications

As one of the oldest prospection techniques utilised for archaeological applications, earth resistance has experienced a long history of research and development. Much of the early development for archaeological earth resistance applications occurred in England, as recalled by Anthony Clark (1996). Unfortunately, there are limited accessible records of these early surveys outside of Clark (1996), as many of the results apparently disappeared into grey literature reports to funding agencies (Weymouth 1986).

Richard Atkinson conducted the first archaeological earth resistance survey in 1946, applying the method over English monumental henges. The earliest resistance meters were relatively simple in electronics, but cumbersome and time-consuming to use. Manual balancing of the instrument's potentiometer to an appropriate circuit voltage was required to obtain accurate resistance measurements. Because the operation of these instruments required focus, patience and time, earth resistance fell out of favour with practitioners in preference of magnetometer survey. In the early 1950s, developments in electronic engineering facilitated the design of more reliable, complex and compact resistance meters. One such instrument was the Martin-Clark resistivity meter, which offered easier in-field operation to its predecessors owing to its smaller size and streamlined electrode leapfrogging system. Despite these advances, the new resistance meters still required manual null balancing of the circuits through audio feedback. By 1960, a commercial version of the Martin-Clark resistivity meter was available for purchase (Clark 1996).

Carr (1982) highlights the varied success of early survey work, comparing the success of earth resistance surveys against the site location and type of archaeology detected. Of the successful earth resistance surveys, 95% were conducted over masonry or tomb features in the “Old World” (i.e. collectively Europe, Asia and northern Africa); of the unsuccessful surveys, 42% were conducted over earthen pit features in the “New World” (i.e. the Americas collectively). The difference in success between New World and Old World surveys can likely be attributed in part to the type of feature being surveyed. In the New World, the prehistoric and early historic test sites were comprised of low-contrast, earthen features. As the signal-to-noise ratio between earthen features and the soil is typically lower for earthen features, earth resistance is more effective for detecting masonry features, which typically present as high-contrast from the surrounding soil (David et al. 2008). The magnitude of feature contrast is dependent on the soil moisture content, which has led to the notion that earth resistance measurements are dependent on seasonal moisture conditions. While direct correlation between seasonal soil moisture variation and measured resistance has never been consistently proven, there is an accepted general relationship between rain, temperature and climatic conditions with measured resistance (Figure 1). The unpredictability of soil moisture conditions lead to the preference of magnetometers over early earth resistance systems (Clark 1996; Weymouth 1986). Weymouth (1986) also cites greater interpretative uncertainties and weather dependences as further disadvantages of earth resistance compared to magnetic methods. Still, surveys through the 1970s and 1980s proved the method can be successful for detecting earthen archaeological features, such as houses, pits and middens; on the condition there is preferential moisture saturation between the feature and the surrounding soil and an adequate sampling strategy is used (Weymouth 1986).

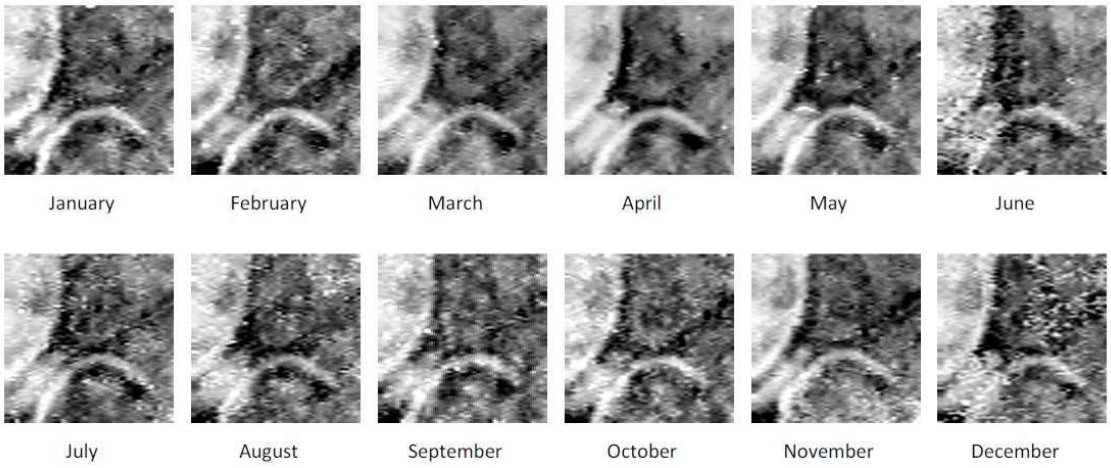

Figure 1: Earth resistance measurements collected over the same 40m x 40m grid every month over for one year to demonstrate a “seasonality effect”. From Bonsall et al. (2013b).

Through the 20th century, the development of earth resistance methods focused heavily on the configuration of the electrodes. The earliest archaeological applications utilised standard linear electrode configurations, such as the Wenner and double-dipole arrays. The most important development for the advancement of archaeological earth resistance survey was the refinement of the twin-probe system in the mid-to-late 1960s (Clark 1996:22). The twin-probe array separates the current and potential electrode pairs, which produces several advantages over the traditional linear configurations. For example, the twin-probe array is less sensitive to geological noise than the Wenner array; the resulting twin-probe anomalies more accurately represent the true extent of the source features. Design wise, the twin-probe array was faster and less cumbersome to use in the field than early generations of Wenner and double-dipole systems (Gaffney and Gater 2003: 32).

Another important development for earth resistance applications was Anthony Clark’s research into non-linear arrays. Clark was the sole member of the Ancient Monuments Laboratory’s Geophysics Section, which motivated him to develop compact earth resistance systems that could be operated by a lone surveyor. Clark dedicated particular focus to the development of square arrays (Clark 1996:20). Despite Clark’s research, the square array did not create as significant of an impact on earth resistance methodologies as the twin-probe array. However, the application of non-linear arrays has experienced a resurgence in the past decades as practitioners have utilised non-linear configurations in the creation of cart-based systems (Dabas 2009; Lueck and Ruehlmann 2013;

Gaffney et al. 2015). Compared to linear arrays, the compact form of non-linear arrays, such as square, rectangular and trapezoid configurations, is suited for configuration into cart-based systems. The ability to collect measurements continuously in a cart-based system facilitates faster and more efficient survey strategies (Dabas 2009; Lueck and Ruehlmann 2013; Terron et al. 2015). The most prolific modern practitioners for cart-based earth resistance survey is the French company Geocarta, an offshoot of the National Centre for Scientific Research (CNRS). Geocarta has been on the forefront of the development of cart-based earth resistance systems over the past few decades. Their current Automatic Resistivity Profiling (ARP) system consists of one current bipole and three potential bipoles, which are of different lengths and distances from the current bipole (Figure 4). The arrangement of ARP's current and potential bipoles eliminates the need for electrode multiplexing, allowing data to be continually collected at a rate of 80Hz, which corresponds to a sampling interval of roughly 0.05m (Dechezlepretre et al. 2009).The manufacturers claim the combination of square and trapezoid electrode arrangements also produces orientation independent responses of three different volumes, maintaining resolution and reducing superficial geology noise on the two lower depths (Panissod et al. 1998).

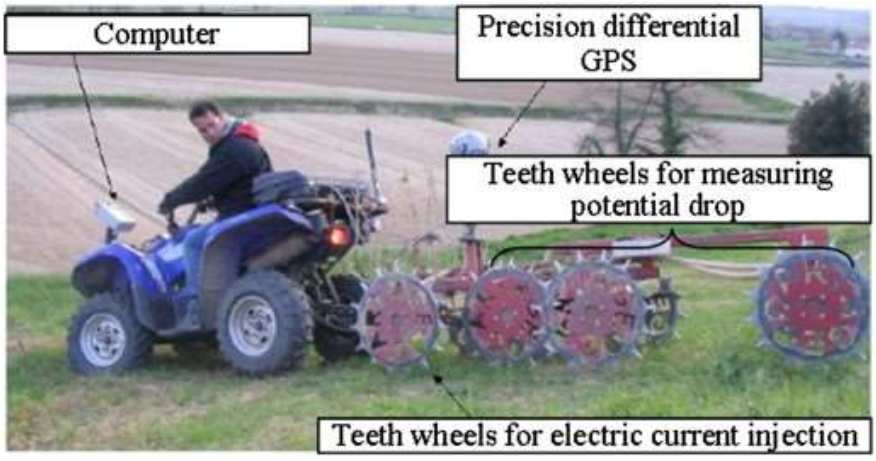

Figure 2: Geocarta's Automatic Resistivity Profiling cart-based earth resistance system. Image source: Andrenelli et al 2013.

In 2004, Geocarta released an ARP system designed specifically for archaeological applications. ARP results for archaeological investigations are encouraging, demonstrating earth resistance methods are capable of providing rapid, landscape-wide coverage with a high sampling density (Boschi 2011; Campana and Dabas 2011; Dabas 2009).

Another contemporary cart-based earth resistance system is the Geoscan Research MSP25. An a=0.75m square configuration of four electrodes forms the base of the MSP25 system. Current is injected through two of the wheels; while the other two measure the resulting potential difference. Using multiplexing technology, the electrodes can be individually triggered as the current and potential electrodes, which allows the near simultaneous collection of the unique alpha, beta and gamma configurations (Aspinall and Saunders 2005; Tsokas et al. 1997). Typical square electrode configurations measure the alpha configuration with the electrodes in-line with the direction of traverse; the beta configuration with the current electrodes normal to the direction of traverse; and the gamma configuration with the current electrodes at 45° to the direction of traverse (Figure 3).

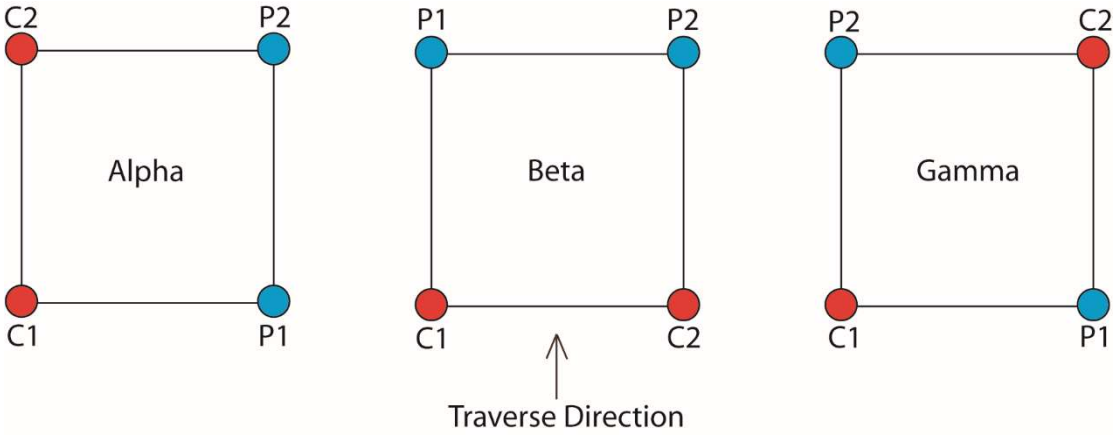

Figure 3: Conventional square array alpha, beta and gamma configurations in relation to the direction of traverse. Source: author.

Mathematically, the alpha, beta and gamma configurations relate such that:

$$R_\gamma = R_\alpha - R_\beta$$

Equation 1: The theoretical relationship between the earth resistance alpha, beta and gamma configurations.

In a homogeneous earth, current flow between two electrodes forms regular hemispheric bowls. Because there are no inhomogeneities to disrupt the regular flow of current, measured resistance is uniform between alpha, beta and gamma orientations. Therefore, from Equation 1, $R_\alpha = R_\beta$ and $R_\gamma = 0$, in a homogeneous

earth. In the presence of inhomogeneities, such as archaeological remains, the regular flow of current will distort around the feature in order to find the easiest path of travel. Because current flow is not uniform, R_α may not equal R_β depending where the measurement is observed relative to the feature. As a result, R_γ may not equal zero and the gamma measurement will represent the variation between the alpha and beta measurements, which can help describe subsurface inhomogeneity. Since traditional linear configurations only measure resistance in one direction, the square array offers a more holistic understanding of subsurface properties (Habberjam 1979: 18-23; Tsokas et al 1997).

For an analogous trapezoid electrode arrangement, Harris' (2011) work shows that Equation 1 does not describe the relationship between the trapezoid's alpha, beta and gamma configurations. As the difference of trapezoid alpha and beta does not equal trapezoid gamma, because trapezoid alpha and beta are not orthogonal, the trapezoid configurations are described as the longitudinal, broadside and theta configurations (Harris 2011; Figure 4).

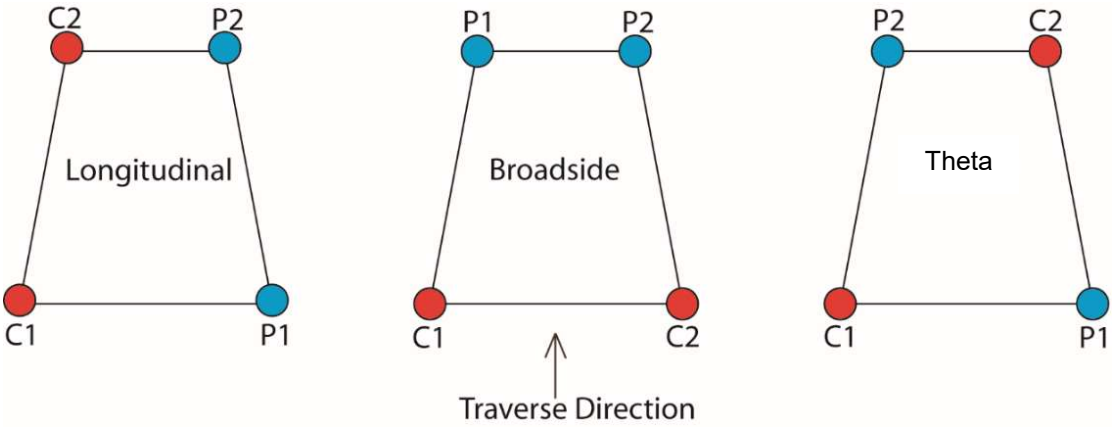

Figure 4: Trapezoid array longitudinal, broadside and theta configurations in relation to the direction of traverse. Source: author.

Whether employing a cart-based survey strategy or a traditional handheld apparatus, earth resistance survey still relies on the fundamental ability of the soil's interstitial moisture content to conduct an electric current. The types of archaeology for which earth resistance is effective for detecting are:

1. **Cut Features:** These include earthen features, such as pits and ditches, where disturbances to the surrounding soil matrix cause the features to retain moisture differently to the surrounding soil. Depending on the properties of the feature's soil moisture context, texture, and drainage, relative to the surrounding soil matrix, the feature's anomalous response can exhibit positive or negative changes from background soil resistance (Kvamme 2003).

2. **Intrusive Features:** Earth resistance is particularly suited for detecting stone or stone-like intrusive features, as such materials are typically poor conductors of an electric current. Unlike cut features, intrusive features are more predicable in their resolution. For British archaeology, intrusive features often exhibit a positive change from background soil resistance and high resistance. Even in dry soil conditions, intrusive features will typically maintain higher resistance to the surrounding soil (Schmidt 2013). Although intrusive features can sometimes exhibit a negative change from background soil resistance if there is water pooling on the top surface of the feature.

The depth to which an array can measure these features depends both on the separation of the current electrodes, whose distance governs the density of current flow with depth, and on the separation of the potential electrodes to the current electrodes. Traditionally, an array's depth of investigation (DOI) is calculated by multiplying the distance between C1 and P1 with a constant relating to the array's geometry. DOI is indicative for determining the approximate depth of buried features, but cannot quantify exact feature depth as measured resistance represents a bulk soil volume (Loke et al. 2013; Schmidt 2013: 80). The bulk measurement creates a problem of non-uniqueness, because the same feature can produce a range of resistance measurements depending on the soil properties or ground conditions. True resistivity distribution is better understood through electrical resistivity tomography (ERT), which utilises many different electrode configurations over a targeted area. The survey results are run through an inversion scheme, which produces the "optimum electrical model" (Papadopoulos et al. 2006) of the subsurface. This model represents a more accurate resistivity distribution, showing the depth and three-dimensional extent

of buried features. A drawback of ERT survey, is that even with modern technological advancements, true three-dimensional ERT surveys are still time consuming and data intensive; semi-three dimensional surveys are often conducted instead (Papadopoulos et al. 2006). Semi-three dimensional surveys collect resistivity measurements along a two-dimensional profile with increasing inner electrode spacing. As the electrode spacing increases, depth of investigation increases, building up a pseudo-two-dimensional image of resistivity change with depth (Figure 2). To simulate a three-dimensional survey, a series of equally spaced profiles are individually collected (Tsokas et al 2009). Recent improvements with multiplexing technology facilitate the collection and production of quasi-three-dimensional imaging using mobile platforms (Brinon et al 2012; Lueck and Ruehlmann 2013; Papadopoulos et al 2009). While the actual forward modelling process itself is still time and computational consuming, which limits the inversion process to small, targeted areas (Brinon et al 2012).

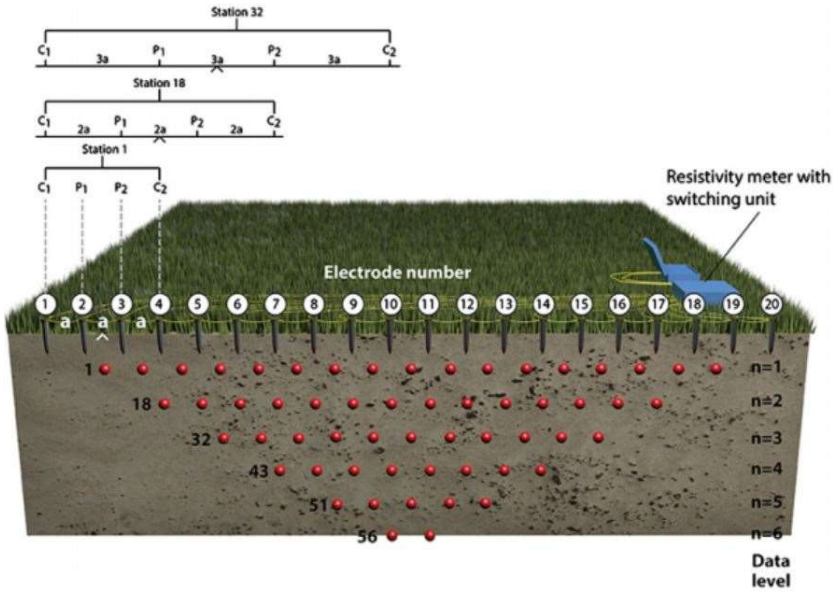

Figure 5: Two-dimensional resistivity profile. From Loke et al (2013).

The development of earth resistance methods has been driven by the need to collect data more rapidly and more efficiently. The more rapid collection of data, the more feasible large-scale surveys become—allowing a wider contextual understanding of the buried archaeology to be understood. Furthermore, improved sampling densities facilitated by cart-based systems produce higher-resolution survey results that allows the detection of features of limited vertical and lateral extent. The ability to collect alpha, beta and gamma configurations

provides further information on the nature of the subsurface, allowing a more accurate delineation of the lateral extent of archaeological features. Overall, these developments in the improvement earth resistance methods have had an overall similar result: the ability to improve the archaeological characterisation of the geophysical results.

2.2 Development of Magnetic Methods for Archaeological Applications

Magnetic methods also have a long history of development for archaeological applications. Martin Aitken conducted one of the earliest successful magnetic surveys for archaeological applications in 1958. Using a proton precession magnetometer, the instrument proved effective for detecting kilns, as well as pottery filled pits and ditches. The instrument gained favour over earth resistance methods of the time owing to the magnetometer's simplicity and ease of use compared to contemporary earth resistance meters (Clark 1996: 12-7). Furthermore, the magnetometer's lack of dependence on seasonal moisture content was also considered advantageous (Linington 1963).

While the proton magnetometer demonstrated its ability to detect British archaeology, its efficacy over other regions was unknown. Driven by the success of Aitken and Hall's work, Black and Johnston (1962) evaluated the efficacy of magnetometry for mapping historic sites in the United States. Black and Johnston's magnetic results demonstrate successful detection of the archaeological features at their test sites, but the authors would not deliver absolute conclusions regarding the efficacy of the method for American sites without further testing. Still, they recognised the potential for geophysical prospection for archaeology. Von Frese and Noble (1984a) summarises a comprehensive evaluation on the efficacy of magnetometer survey for American historical sites, conducted through the mid to late 1970s. After correcting their data for diurnal and drift variations, Von Frese and Noble (1984b) applied a comprehensive characterisation strategy for data interpretation. The archaeological nature of the magnetic anomalies was characterised through careful examination of the form and amplitude of the geophysical response. The nature of magnetisation was described by analysing the results of a reduction to pole, which revealed those anomalies with remenant moments. Von Frese and Noble's detailed characterisation of the anomalies' properties is presented as an

interpretative figure where pit types are described by their geophysical response (Figure 6).

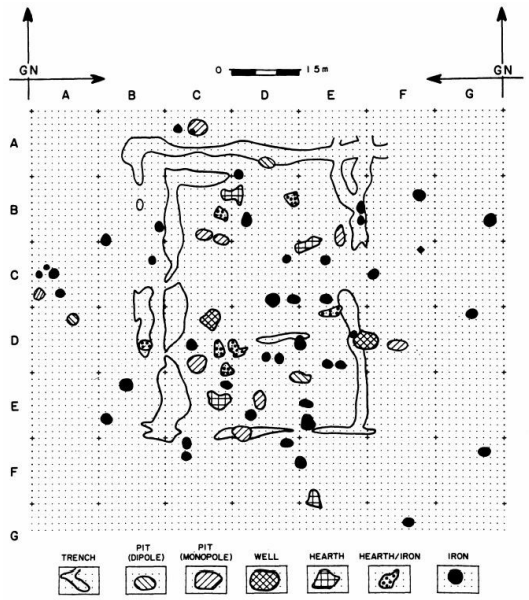

Figure 6: Characterisation of archaeological features through the analytical analysis of magnetic anomalies. From Von Frese and Noble (1984b).

Excavation results confirmed Von Frese and Noble's interpretation of cultural remains, including iron slag refuse, daub, hearths, and stockade trench lines, as well as the interpretation of areas that did not contain any features. Overall, Von Frese and Noble (1984b) demonstrated the wealth of information that can be derived on the nature archaeological targets through analysis of the anomalous signal. Von Frese and Noble (1984b) concluded that further similar interpretation strategies should be conducted at a variety of sites to increase the accuracy and confidence characterising geophysical responses.

One of the most important developments for the magnetic method, and archaeological geophysics as whole, was the development of the fluxgate gradiometer. The Plessey company's "Philpot" fluxgate gradiometer featured continuous output, which when linked with an XY plotter, could produce real-time traces of collected data. Anthony Clark marks this invention as the beginning of "the fluxgate revolution" (Clark 1996: 24). The fluxgate gradiometer is still predominant for magnetic applications to this day, with the basic design of the sensors relatively unchanged (Bartington and Chapman 2004).

Magnetometers in gradiometer configuration are the preferred systems for archaeological applications; the reduction of external interference helps to provide a more straightforward understanding of site-specific magnetic measurements (Clark 1996). The difference of the sensors' vertical components represents the contrast between the target material and the surrounding soil matrix; this contrast can be positive or negative depending on the magnetic properties of the materials. Due to the widespread application of magnetic methods for archaeological surveys, the expected magnetic response of particular archaeological features is well understood and reasonably predictable (David et al. 2008). The types of archaeology for which magnetic methods are particularly effective at detecting are:

1. **Burnt Features:** An asset of magnetic methods for archaeological applications is their ability to detect fired or burnt remains. Due to the prevalence of burnt features across space and time in the archaeological record, the magnetic methods are a versatile technique that can be applied to a range of different sites (Aspinall et al. 2008; Fassbinder 2015). Features, such as hearths and kilns, retain a strong remenant magnetism, which typically produces a characteristic double-peaking response over the anomaly's centre (Bevan 1996).

2. **Cut Features:** Cut features are detected when they exhibit magnetic contrast from the surrounding soil. The contrast of cut features is due to the fill material exhibiting different magnetic properties to the surrounding soil. Soil obtains magnetic enhancement through organic and chemical processes, which can have natural or anthropogenic origins (Evans and Heller 2003). Cut features generally exhibit a weaker induced magnetisation due to the enhanced magnetic susceptibility of the fill material. However, cut features can exhibit a strong remenant magnetisation if the fill material contains a high quantity of magnetically enhanced materials, such as pottery or ferrous debris (Clark 1996).

3. **Intrusive Features:** Intrusive features are detected if they exhibit magnetic contrast from the surrounding soil. For example, building materials using sandstone may show as negative contrast from the surrounding soil due to their low magnetic properties. Conversely, fired

building materials, such as brick and clay, may show as positive contrast from the surrounding soil due to their high magnetic properties (Bevan 1996). However, fired materials can produce a noisy dipolar effect depending on their orientation and state of preservation (Mohamed-Ali et al. 2012).

4. **Ferrous features:** Ferrous materials exhibit strong, remenant magnetisation, which manifests as a high contrast, bipolar response. Ferrous materials produce strong responses that will overwhelm any nearby weaker archaeological signals.

Overall, these examples demonstrate how the type of magnetisation producing the anomaly is helpful for characterising the source target. However, because magnetometers measure the magnitude of the ambient magnetic field, remenant and induced magnetisation cannot be directly discriminated through the output measurements. As a result, the shape and centre of magnetometer anomalies may not accurately reflect the extent of the feature being measured. To better characterise magnetometer anomalies, data processing methods can be applied to correct magnetic anomalies to more accurately represent their source feature.

Signal processing algorithms are commonly used to enhance the archaeological features within magnetic results. Signal processing techniques rely on the basis that magnetometer measurements comprise signals from different sources: archaeological signals exhibit a medium wavenumber; surface noise has a high wavenumber; and geology has a low wavenumber Scollar (1969). Black and Scollar's (1969) signal processing approach utilises Fourier transforms to separate out the noise and represent the measured signal in the frequency domain. By representing the resulting signal as a sum of sinusoidal functions, particular signals can be amplified or supressed to enhance the archaeological signal. Specific processes that use a Fourier transform, such as the reduction to pole and analytic signal, rectify the measured anomaly to more accurately represent the source target.

Von Frese (1984) describes reduction to pole (RTP) methodologies for archaeological magnetic anomalies. The RTP adjusts the anomaly's local ambient field to the polarisation if the anomaly were in a vertical magnetic field.

For dipolar anomalies exhibiting induced magnetism, the RTP shifts the peak anomaly response directly over the target source, while removing the secondary smaller peak; for dipolar anomalies exhibiting remenant magnetism, the peaking is unaffected by the RTP. RTP can therefore be useful for classifying anomaly feature types, as different types of archaeological features will exhibit different types of magnetism (Von Frese and Noble 1984). MacLeod et al. (1993) question the suitability of a RTP on features possessing strong, remenant magnetism and instead recommend applying an analytic signal to correct the complex responses of remenant anomalies. The analytic signal corrects complex peaking by removing the negative signal components. For a 2D representation of the archaeological target, the analytic signal produces a simplified response that is independent of the direction of magnetisation. However, this should still be interpreted with caution because in comparison to an RTP, synthetic and model data show the analytic signal produces broader anomalous responses (Figure 7; Tsokas and Hansen 2000).

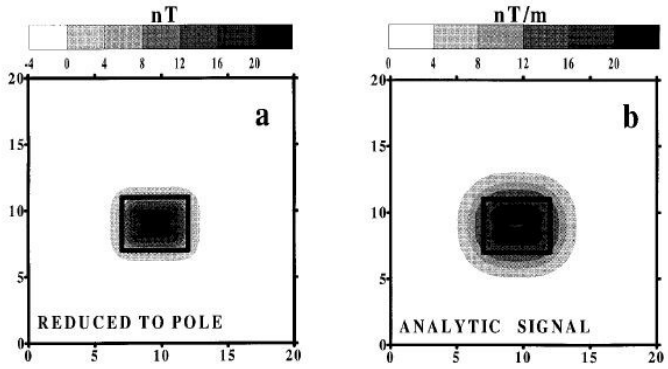

Figure 7: Comparison of the form of the anomalous response of a synthetic target derived from the reduction to pole (left) and analytic signal (right) processing techniques. From Tsokas and Hansen (2000).

Tabbagh et al. (1997) conclude that the usefulness of the analytic signal may vary depending on the source target and the survey environment. Research published within the past five years focuses on RTP and analytic signal methods for edge detection schemes (Arisoy 2014; Cheyney et al. 2011; Stampolidis and Tsokas 2012) and for simplifying data interpretation (Cocchi et al. 2012; Mojica et al. 2014; Ard et al. 2015). Gaffney et al. (2015) demonstrate the usefulness of analytic signal derivations for more accurately pinpointing the source location of burial plot markers from their complex, dipolar responses.

The previous examples focus on a two-dimensional approach to anomaly rectification. A 3D approach requires the inversion of magnetic data to derive depth information from the magnetic anomaly. The difficulty of inversions is the requirement for a thorough understanding of the source target and the site conditions, which may not be known to the practitioner. As a result, magnetic inversions for archaeological targets are not commonly employed (Cheyney 2012; Neubauer and Eder-Hinterleitner 1997).

Overall, while these processing methods help correct the magnetic anomaly to better represent the source target, the effectiveness of these algorithms depends on the quality and reliability of the collected data. While signal processing algorithms can rectify the locational dependences of the magnetic anomalies, they cannot accurately correct for the operational dependences of the anomalies as well. Factors such as operator gait, sway and magnetic cleanliness also affect the magnitude and form of the anomalous response. Due to the uncontrolled or random nature of these errors, these factors are difficult to correct for (Fassbinder 2015; Neubauer and Eder-Hinterleitner 1997). However, the modern development of GNSS positioned cart-based systems reduce or even eliminate many of these operator-induced effects (Pope-Carter et al 2014a).

Modern development of magnetic survey strategies has focused on innovations to improve the quality and accuracy of magnetic results through the improved collection, handling, and management of digital data. Improved technology has also facilitated the rapid collection of high resolution surveys. Previous magnetic work was often limited to lower spatial resolution by instrument storage capacities and the slower sampling rates of previous instrument. Lower spatial resolutions can results in detected archaeological targets being undefined or poorly resolved, making them difficult to interpret (Weymouth 1986; Viberg et al. 2011). Viberg et al. 2011 states this problem limited the development and efficacy of archaeological prospection in Sweden, as archaeological targets were small and isolated, requiring very high resolution (e.g. less than 0.25m traverse separation) for detection.

Overall, the push behind the development of improved magnetic data collection, processing and interpretation methodologies focuses on producing a more

accurate characterisation of the buried archaeology; the methodology may vary, but the objective is the same.

2.3 Development of Electromagnetic Induction Methods for Archaeological Applications

The previous sections have explored the development of archaeological earth resistance and magnetic methods through the mid-20th century to the present day. Electromagnetic induction methods, in contrast, have experienced a different trajectory of development and application. Early proto-EM work began with the application of low-frequency mine detectors following World War II. While these early surveys are mostly undocumented, the technique was reported to have been effective for detecting not only metal, but for detecting pottery as well. The development of EM methods for archaeological applications was stimulated in the early 1960s as a reaction to the slow and cumbersome nature of earth resistance systems at the time (Scollar et al. 1990: 545; Thiesson et al 2009); the Wenner and double-dipole systems were also prone to geological noise (McNeill 1980), a problem which was exacerbated by the requirement to maintain adequate contact between the soil and the electrodes. The contactless nature of EM techniques was thought to be a solution to these problems; particularly with slingram instruments, where the transmitting and receiving coils are housed within a self-contained sensor (Scollar et al. 1990: 525).

From the 1960s, research into coil orientation, coil separation, and operating frequency of EM slingram instruments was tested to develop a more sensitive and sophisticated instrument that could measure both soil electrical conductivity and magnetic properties simultaneously (Weymouth 1986; Scollar et al. 1990: 524-5). Early research into the development of a system that could measure electrical conductivity was met with challenges when tests concluded the instruments were responding more to the magnetic properties of the soil rather than electrical properties (Tite and Mullins 1973); these failed conductivity meters were considered by practitioners as having no advantage over contemporary proton magnetometers (Weymouth 1986). Tite and Mullins' (1973) work concluded that to measure electrical conductivity, the instruments required a higher operating frequency and should measure the quadrature component of the

signal as well. However, these solutions were difficult to implement using the available technology of the time (Weymouth 1986).

In the 1980s, improved circuity design facilitated the creation of instruments that could measure both the quadrature-phase and in-phase signal components (Weymouth 1986). Work by the CNRS in France demonstrated that quadrature-phase and in-phase measurements correlated with earth resistance and magnetic data, respectively (Parchas and Tabbagh 1978; Tabbagh 1984). The Canadian company Geonics was an early manufacturer of commercial EM instruments. Weymouth (1986) lists the marketed price of the Geonics EM31 and EM38 as $7200 and $3800 (USD) respectively, which was considerably more expensive than contemporary earth resistance systems at the time. Weymouth (1986) reasons the continued preference of earth resistance methods over these early EM systems was in part due to the higher equipment cost of the EM instruments. Despite the initial higher retail price of EM instruments, EM survey were overall more cost-effective than contemporary earth resistance survey. Weymouth (1986) cites an EM survey required only one operator and could be conducted at speeds comparable to a contemporary magnetometer survey; whereas earth resistance survey was more time consuming and required multiple personnel for data collection.

Despite these advantages, EM methods have not experienced the same widespread adoption in Britain as earth resistance and magnetic methods have. The potential limiting factors that EM methods are still notorious to suffer from, although to a lesser degree than previous generations, include instrument drift, inadequate understanding of instrument measurements and their relation to soil properties, and uncertainties regarding the three-dimensional spatial sensitivity of the instrument (Bonsall et al. 2013b; Thiesson et al. 2009). Much of the recent EM research focuses on technique development to improve the effectiveness and accuracy of EM survey for archaeological applications. A fundamental basis of the technique development lies in a solid understanding of EM theory.

EM slingram instruments consist of a transmitting coil (T_x) and at least one receiving coil (R_x). Instrument operation uses a low-frequency, time-varying electric current to stimulate the transmitting coil to produce a mutually

perpendicular primary magnetic field (H_P). H_P will propagate in a direction normal to the orientation of the coil (Figure 9) and will induce eddy currents within conductive material as it propagates through the subsurface. These eddy currents in turn will produce a secondary time-varying magnetic field (H_S). The primary and secondary fields will induce a voltage across the receiving coil(s) that is proportional to the magnitude of combined fields (Callegary et al. 2012). Because the amplitude of the primary field is known, the amplitude and phase of the secondary field can be derived from the received signal. The in-phase amplitude change from the primary and secondary signal is indicative of subsurface magnetic susceptibility. This measurement is dimensionless and output in SI parts per thousand (ppt) or parts per million (ppm) units.

Electrical conductivity is approximated through the quadrature-phase component of the secondary signal. The quadrature-phase component is π/2 radians out of phase with the primary field, due to the lag in inducing eddy currents within a conductive body. The ratio of the quadrature-phase to the primary field is proportional to apparent electrical conductivity under "low induction number" (LIN) conditions (Equation 2).

$$\sigma = \frac{4}{2\pi f \mu_0 s^2}\left(\frac{H_s}{H_p}\right)$$

Where σ = apparent soil conductivity (mS m^{-1}); f = instrument frequency (Hz); μ_0 = the permeability of free space ($4\pi\times10^{7}$ H m^{-1}); s = Tx and Rx spacing (m).

Equation 2: Calculation of apparent conductivity from slingram instrument.

The induction number (B) is the ratio of the coil separation to the skin depth. The skin depth refers to the depth in which a plane wave's amplitude is attenuated to 1/*e,* ≈37%, taking e as ≈2.71828, of its surface value. From McNeill (1980), the absolute conditions required for low induction number conditions require:

1. B << 1. In practice, the soil should not be extremely conductive, as the skin depth will decrease and the induction number will increase. As soil conductivity increases, the skin depth approaches zero, which increases the induction number. As the induction number increases, apparent conductivity is less accurately approximated by the quadrature-phase.

Saey et al. (2015) state that as a result, true conductivity is underestimated with larger coil separations as the relationship between the induction number and apparent conductivity varies between the coil configurations.

2. The centre of the instrument's transmitting and receiving coils must be at zero elevation. This condition is impossible to strictly hold with slingram instruments as the instrument's casing elevates the coils above the ground surface. Furthermore, to meet this requirement in HCP configuration, the coils would have to be located partially above and below the ground surface! These minute coil elevations must be considered negligible by instrument manufacturers, but more substantial elevation heights produce a noticeable effect (Figure 8). Therefore, this elevation effect must be considered, especially for handheld or cart-based configurations where the instrument is suspended above the ground. Figure 8 depicts how the quadrature-phase measurements decrease as the instrument height increases, depending on the orientation of the instrument's coils.

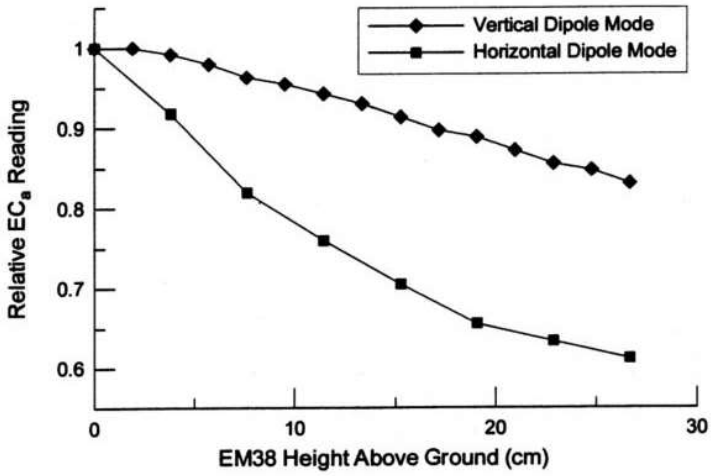

Figure 8: As the instrument height above the ground surface increases, the quadrature-phase measures an associated decrease in measured electrical conductivity. From Sudduth et al. (2001).

The orientation and separation of the transmitting and receiving coils governs the transmitting wave's maximum depth of exploration. Three primary orientations of these coils are standard for archaeological applications: horizontal coplanar (HCP), vertical coplanar (VCP), and perpendicular (PERP). These orientations are also interchangeably described as vertical dipoles, horizontal dipoles and perpendicular dipoles (Figure 9).

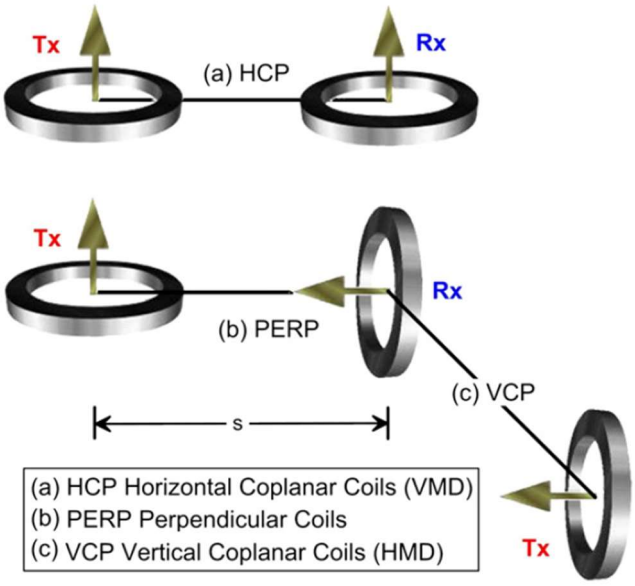

Figure 9: The horizontal coplanar (a), perpendicular (b) and vertical coplanar (c) coil orientations available for slingram EM instruments. The arrows indicate the direction of the induced field. From Beamish (2011).

Multiple exploration depths can be measured by using additional receiving coils at different distances from the transmitting coil (Benech and Marmet 1999). However, these depths are only approximate, as the received signal represents a combined measurement of the bulk soil volume. By McNeill 1980, the signal contribution of material at different depths can be calculated and used to derive an approximate exploration depths for the different coil separations.

$$R_{HCP}(z) = (4z^2 + 1)^{-0.5}$$
$$R_{VCP}(z) = (4z^2 + 1)^{-0.5} - 2z$$

Where R(z) is the cumulative response (% of measured signal) from the soil volume below a depth z.

Equation 3: The depth-weighted EM quadrature-phase response.

The preceding EM theory demonstrates the complexity of how conductivity and magnetic susceptibility properties are derived from EM measurements. The challenge in improving the interpretation of EM results requires the collection of high-quality, accurate data. Previous generations of EM instruments were prone to temporal drift and drift with temperature variation (Dos Santos and Porsani 2011; Thiesson et al. 2009). Drift effects have been reduced in the latest instrument models, but not eliminated. The difficulty of rectifying instrument drift, is that drift is not a singular phenomenon, but is a collective term for describing systematic instrument error that originates from a range of sources. As Delefortrie

et al. (2014) succinctly state, “[drift is the] systematic variation that exceeds the random signal noise over time, despite no apparent changes above or underneath the surface.” The vagueness of this definition eludes to how drift manifests in unpredictable ways between different instruments and different coil configurations, and cannot be correlated with climatic or weather conditions (Robinson et al. 2004; Sudduth et al. 2001). Operators take their own initiative to reduce instrument drift by applying attentive instrument set-up and calibration steps; however, these steps vary between practitioners. Before survey work commences, the instrument should first warm or cool to ambient survey temperature, to allow the measurements to adjust to the present survey conditions. Robinson et al. (2004) recommend powering on the instrument in a shaded area a full two hours before commencing survey; whereas Delefortrie et al. (2014) recommend only 20 minutes for an instrument warm-up time.

Another important step in EM instrument set-up is the calibration of the coils to the survey environment. Ideally the calibration should be performed in a uniform free-space by raising the instrument >1.0 m off the ground surface (Dabas et al. 2016); although for ease of use, calibration is regularly performed on the ground surface. Some practitioners recommend returning to a reference calibration location throughout the survey to recalibrate the instrument back to the established background level (Abraham et al. 2006; Sudduth et al. 2001), while other practitioners argue discrete measurements may be too infrequent to get an accurate trend of drift over time (Delefortrie et al. 2014). For GPS-positioned surveys, calibration lines are used as an alternative to a set reference point. Calibration lines are collected in ‘W’ patterns across the survey area to collect reference values for positions along every traverse (Figure 10). These reference values correct the coincident collected survey data for drift variations (Delefortrie et al. 2014). The issue with using calibration lines for drift correction is that the calibration data must accurate and of good quality—free from drift itself. To improve reliability in the accuracy of the calibration line, De Smedt et al. (2015) recommend collecting multiple calibration lines and even revisit sites to assess the stability of the calibration line.

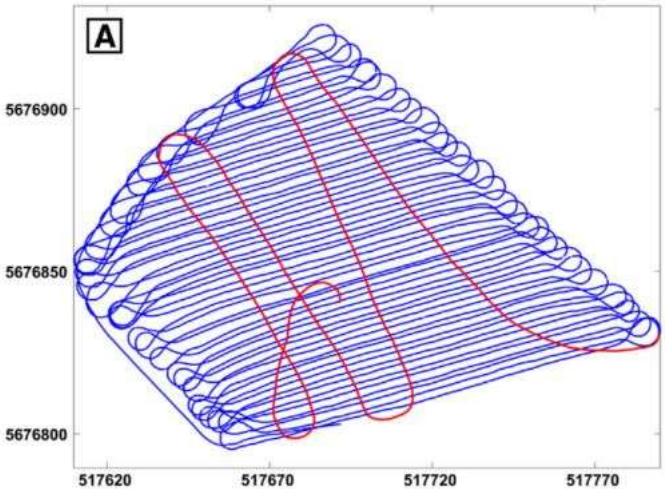

Figure 10: The M-shaped calibration line (in red) was collected as part of a quad-towed, GPS-positioned EM survey (GPS traces in blue), to correct instrument drift. From Delefortrie et al. (2014).

The variability in approaches to instrument set-up and calibration signifies that practitioners have developed workflows particular to their specific instrument, survey strategy and field conditions. While magnetic and earth resistance methods have standard field operation and processing strategies that have been developed over years of experience of working with different instruments in different environments, EM methods do not. For example, Historic England's 2008 guidelines recommend a sampling density of 1m x 1m be employed for EM surveys, but do not provide justification or support for these recommendations, as the authors admit that the method is not widely employed in the UK (David et al. 2008). Furthermore, the range of variables that may affect the quality and accuracy of EM data collection are not addressed. These variables include operating speed, sampling rate and instrument calibration. As a result, compared to the magnetic and earth resistance methods, there is need to verify effective EM procedures, particularly in the UK where the application is not as common or widespread as it is in other countries, such as the United States and Belgium.

In Belgium, for example, EM methods have been applied with regularity. Ghent University researchers are responsible for a recent surge in publications. Their EM survey strategies have been refined to suit the topography of their survey landscapes and the nature of their targeted features. Given the relatively flat topography of their survey landscapes, large-scale quad-towed surveys are an effective survey strategy (De Smedt et al. 2013). The Ghent quad-towed surveys can be more rapidly completed owing to a fast collection speed and wide traverse

interval employed (e.g. 5-8 km/h speed using 1.4 m line spacing in Gheyle et al. 2016). This sampling strategy is suitable for resolving the scale of the features these surveys are targeting, which includes geomorphological features (De Smedt et al. 2011; Verhegge et al. 2016), trenches (e.g. conflict landscapes in Gheyle et al. 2016) and ditch features (Saey et al. 2012; Saey et al. 2014). Furthermore, the nature of EM methods provides further information on the nature of the soil material, which helps to contextualise the geophysical results (Saey et al. 2013; Saey et al. 2016).

EM's advantage over magnetic and earth resistance methods is in its ability to simultaneously measure electrical and magnetic subsurface properties with a single instrument. As a result, the nature of the EM response will vary between the phases depending on the type of feature being resolved. The types of archaeology for which EM has shown to be effective for detecting are:

1. **Cut and Earthen Features:** Both the in-phase and quadrature-phase signal components respond well to features created through the cutting and deposition of soil. Henry et al. (2014) present a good example of EM results over a burial mound feature in the United States (Figure 11).

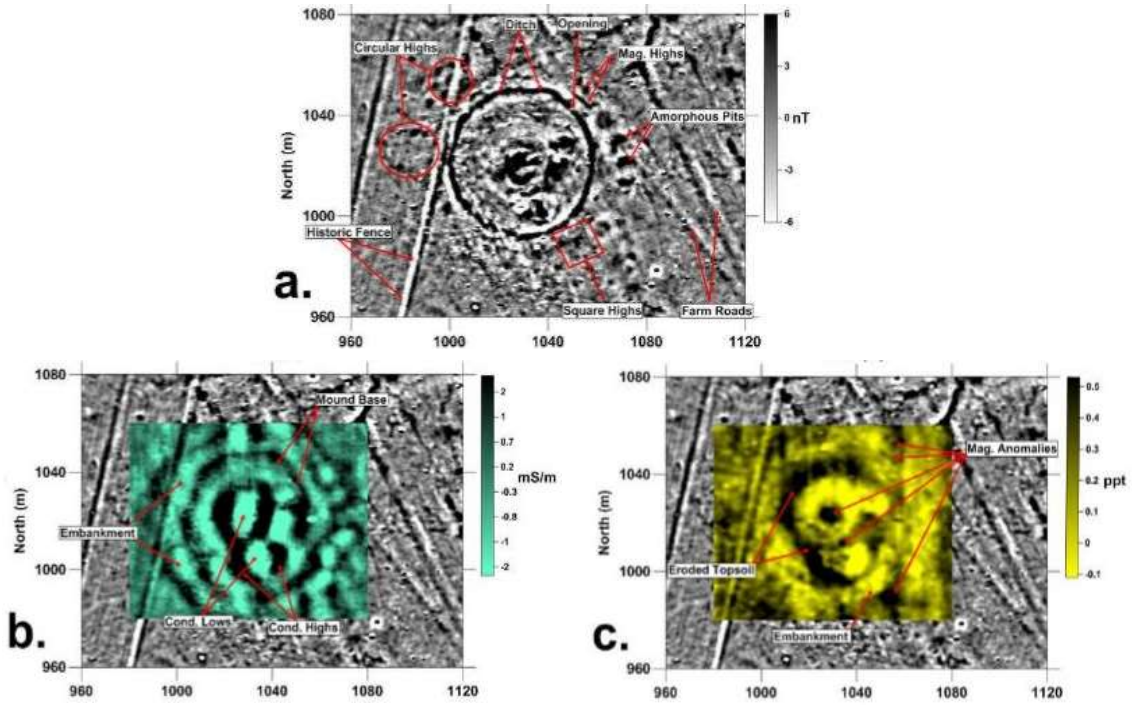

Figure 11: Example EM results, in reference to magnetic results, over earthen features as part of a burial mound complex in North America (a) magnetic results (b) EM quadrature-phase results (c) and EM in-phase results. From Henry et al. (2014).

The magnetic results are included in Figure 11 to provide context for the EM responses. The magnetic results reveal the burial mound situated within a circular ditch and embankment feature; to the east of the ditch lie a series of pit-like anomalies. The quadrature-phase and in-phase both detect the embankment feature, but the quadrature-phase detects the ditch feature as well. Both phases also show anomalies relating to the burial mound feature, but the differences in responses between the in-phase and quadrature-phase demonstrates the phases are responding to different aspects of the feature. The quadrature-phase also resolves the pit-like anomalies in the magnetic results, which are surprisingly absent in the in-phase results, given their strong magnetic response.

Bonsall et al. (2013a) present an example of EM results over a hengiform monument in the greater landscape surrounding Stonehenge. The in-phase results at Stonehenge mirror the magnetic results over the example hengiform feature. The in-phase resolves the hengiform's pit features and the internal features as discrete anomalies. In contrast, the quadrature-phase pit anomalies are more ambiguous in form.

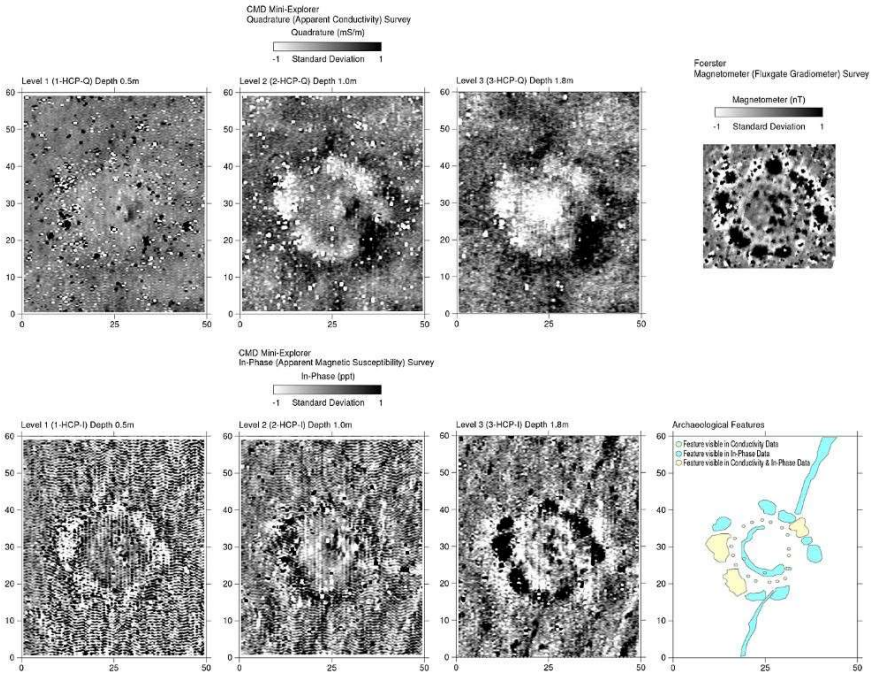

Figure 12: An example of EM results over a pit-like hengiform feature at Stonehenge. The HCP quadrature-phase results (top) and the HCP in-phase results (bottom) are presented in comparison with magnetic results (top, righthand corner). From Bonsall et al. (2013a)

2. **Resistive Features:** Resistive features are notorious for being difficult to reliably detect with EM methods (Thiesson et al. 2009; Dabas et al. 2016). Simpson et al. (2009) present a case study that compares the results of EM and magnetic surveys over the remains of a castle in western Belgium. Soil augering over the survey area revealed areas containing brick rubble, ceramics and wall fragments. EM data were collected in a quad-towed sledge system while the magnetic data were collected handheld using a gridded survey strategy. The structural footprint of the castle is coherent in the magnetic and in-phase results, but less clear in the quadrature-phase results (Figure 13).

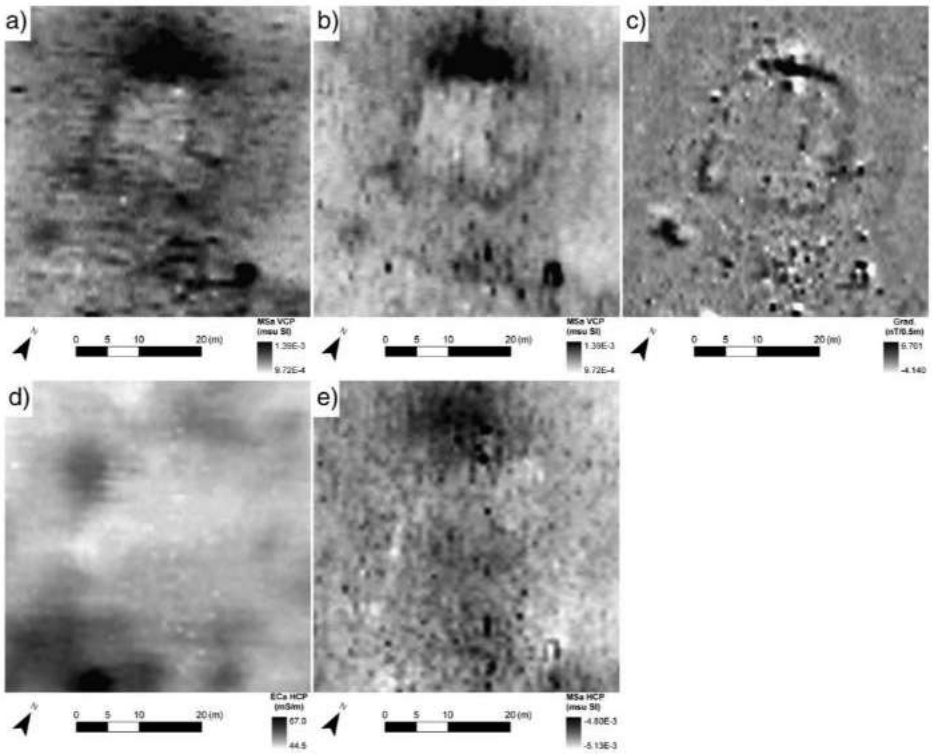

Figure 13: An example comparing the results of different EM surveys over the remains of a castle in Belgium: a) In-phase results, collected in an E-W direction in VCP orientation b) In-phase results, collected in a N-S direction in VCP orientation c) magnetic results d) quadrature-phase results collected in an E-W direction in HCP orientation e) quadrature-phase results, collected in a N-S direction in HCP orientation. From Simpson et al. (2009).

Direct comparison of the EM and magnetic results is limited by the fact that the EM results suffer from operation induced effects. The instrument's spatial sensitivity, combined with positional inaccuracies, cause the elongation of responses along the direction of traverse, which is exacerbated by a staggering effect between the lines. Despite these differences in data quality, the EM in-phase and magnetic results are well

correlated and both techniques appear to respond well to the presence of the fired material. Simpson et al. (2009) attribute the success of the in-phase for delineating the castle's structure to the enhanced magnetism of the material remains. The EM quadrature-phase is less successful for detecting the structural remains, which Simpson et al. (2009) attribute to either low electrical contrast of the materials or sub-optimal spatial sensitivity of the HCP orientation to the archaeological features. The spatial sensitivity of the EM instrument has been cited as a limiting factor for delineating features with sharp boundaries or features that lack a vertical extent (Constable et al. 1987).

Nevertheless, Dabas et al. (2016) present a potential solution to mitigate the potential resolution difficulties the quadrature-phase faces when detecting resistive features. Dabas et al.'s (2016) approach requires absolute calibration of the instrument, which is a comprehensive process. The instrument's idealised, theoretical responses are calculated. By calibrating the individual receiving coils' outputs in free space against a small conductive, but non-magnetic sphere, the instrument's idealised responses as a function of height and distance to the transmitting coil are calculated. These idealised responses are used to derive the magnetic field ratio from the instrument's output measurements, which have been compensated to account for instrument roll during data collection. The final step converts the quadrature-phase measurements to apparent resistivity to directly compare the results against earth resistance data. Compared to Simpson et al.'s (2009) survey over the castle (Figure 13), Dabas et al.'s (2016) results (Figure 14) provide a much finer resolution of the structural remains—especially considering Simpson et al.'s (2009) survey also utilised a similar quad-towed, sledge-based survey strategy as Dabas et al. (2016) employed.

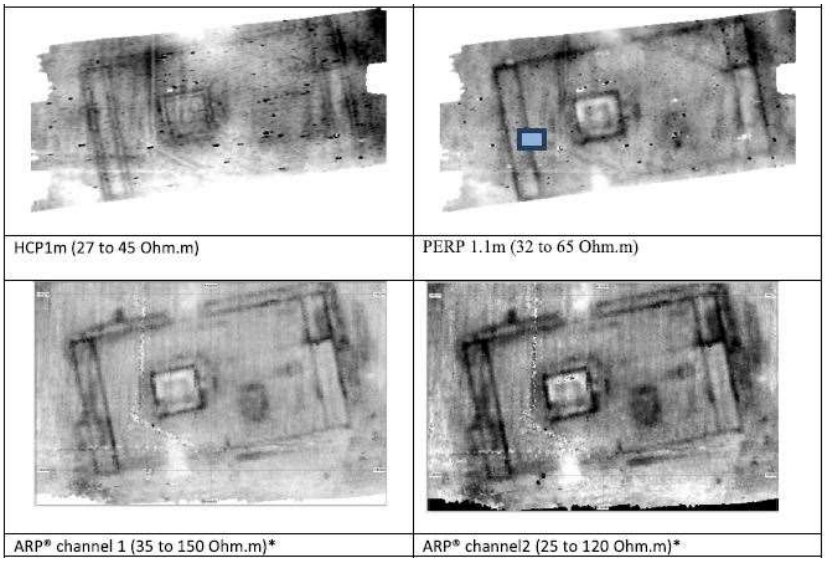

Figure 14: Comparison of EM quadrature-phase and earth resistance results over a Roman building in France. The EM results, in respective HCP and PERP orientations are presented in the top row, while the shallow and middle earth resistance soil volumes are bresented in the bottom row. From Dabas et al. (2016).

3. **Ferrous features:** Ferrous materials produce a strong response in both in-phase and quadrature-phase components, as they are highly magnetic and conductive materials. For example, De Smedt et al. (2014b) have digitised the discrete, ferrous anomalies at Stonehenge (Figure 15). As many of these features represent scattered metallic debris on or near the ground surface, they often occur in active anthropogenic landscapes.

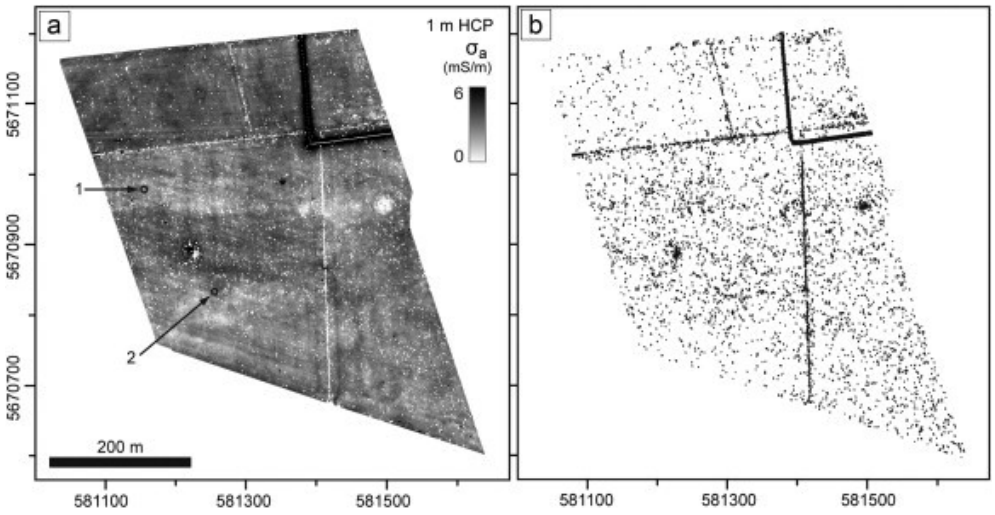

Figure 15: The ferrous anomalies (right) in an EM HCP quadrature-phase dataset over Stonehenge (left) have been digitised to illusrate the spread of scaterred metallic debris across the site. From De Smedt et al. (2014b).

Overall, these examples highlight the variability of EM responses. The variation of EM responses will be further explored in the following section on multimethod

strategies. A more accurate understanding of relationship between the EM responses and subsurface features will be explored by analysing the EM results against standard magnetic and earth resistance results.

2.5 Cross Analysing Earth Resistance, Magnetic and Electromagnetic Results: Case Studies of Multimethod Survey Strategies

Cross-analysing the results of different geophysical methods can be undertaken through a multi-method survey approach over a targeted area. Archaeological geophysicists have long appreciated the advantages of applying multiple survey techniques for the more comprehensive understanding of buried remains, but such a strategy was once considered a luxury, due to the slow and time-consuming rate at which multiple methods could be collected (Hesse 1999). As a result, due to the comparatively shorter history of application of EM methods to magnetic and earth resistance methods, there are limited sources available that present all three methods over the same survey area—particularly in Britain. A selection of available case studies will be presented below.

2.5.1 Multimethod Case Study: Boden Vean, Iron Age/Romano-British Site

One of the most detailed examples for a multimethod strategy utilising EM methods in Britain is presented by Linford (1998) at Boden Vean, Cornwall. The survey sought to assess a fogou, a subterranean dry-stone structure found in Iron Age/Romano-British settlements in Cornwall. Previous excavations on the site revealed a series of walls, which were suspected of forming a passage to the fogou. A magnetic survey was employed as the primary, wide-scale survey method, covering 4.5ha of the site. The magnetic results reveal a series of field enclosures, trackways, ditch-like anomalies, pits and other anomalies of modern origin. The detection of a circular enclosure-type anomaly corresponded with the anticipated position of the fogou (Figure 16). Earth resistance and electromagnetic induction surveys were targeted in the NW area of the site over the location of the fogou (Figure 16). The earth resistance survey used a twin probe array with 0.5m and 1.0m electrode separations to measure multiple exploration depths. The EM survey employed the Geonics EM38 instrument, using both HCP and VCP orientations.

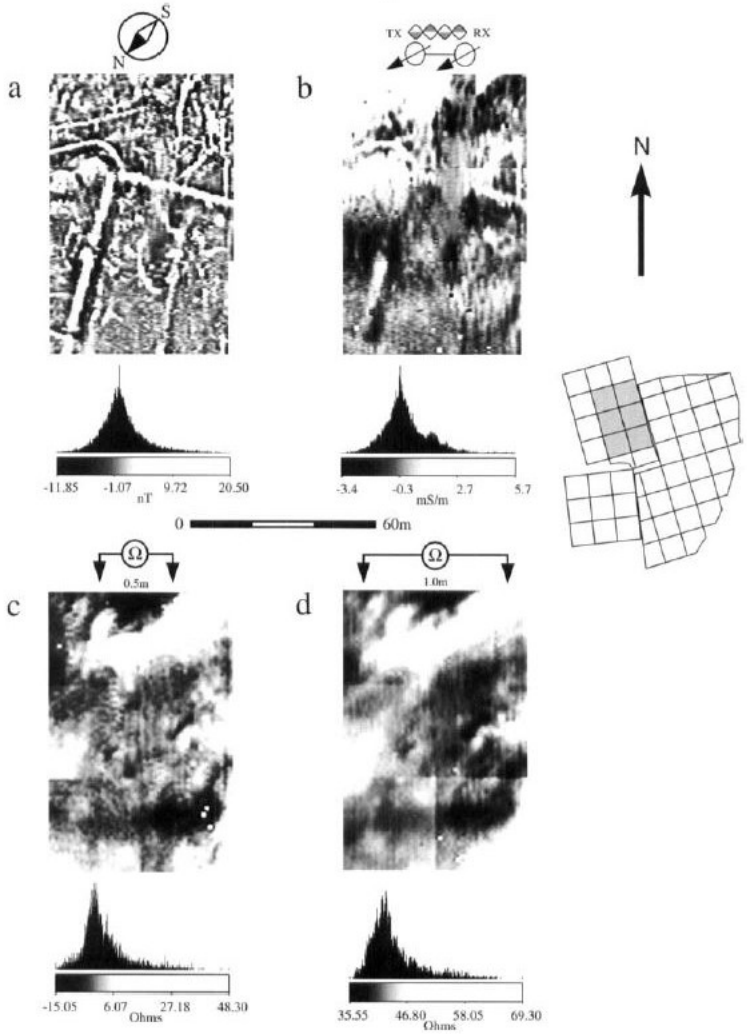

Figure 16: Comparison of the results from a multi-method geophysical survey over a fogou at Boden Vean from Linford (1998): (a) magnetic results (b) EM quadrature-phase results (c) earth resistance (a = 0.5m twin-probe) results (d) earth resistance (a = 1.0m twin-probe) results.

Linford (1998) expresses disappointment in the earth resistance results for failing to detect most of the significant magnetic anomalies. The EM quadrature-phase demonstrates better correlation with the magnetic results than the earth resistance does; the EM survey detects anomalies that are not present in the earth resistance results. Linford (1998) found these relationships between the EM results and the other methods “peculiar,” given the inverse properties of electrical conductivity and resistivity. As a result, Linford (1998) concludes that the quadrature-phase is responding to the magnetic properties at Boden Vean instead of the electrical conductivity properties: the phenomenon of “quadrature susceptibility.” Quadrature susceptibility describes the effect where the quadrature-phase responses are opposite in sign to the subsurface conductivity and considerably lower in magnitude to the in-phase responses. Because of relationship between the phases, a slight change in the in-phase will cause a

significant change in the quadrature-phase. In these conditions, the in-phase will be responding to highly magnetic properties. Laboratory testing confirmed the topsoil possessed a high magnetic susceptibility, due to an enrichment of iron oxides. A comparison of the magnetic results with the EM in-phase results shows good correlation between the two techniques (Figure 17).

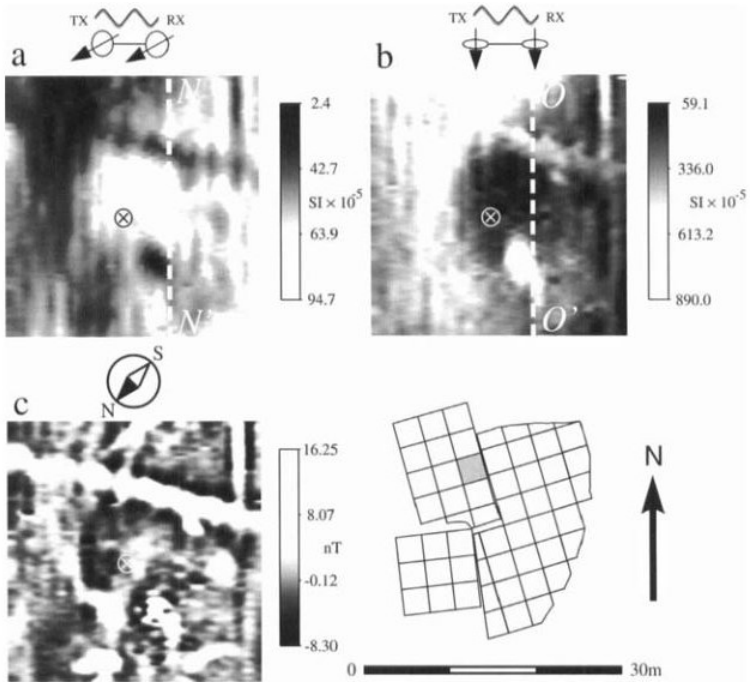

Figure 17: A targeted comparison of the EM in-phase and magnetic results over a fogou at Boden Vean: (a) in-phase VCP orientation and (b) in-phase HCP orientation against (c) magnetic results from (Linford 1998). The fogou location is marked at the circular symbol with an X.

Overall, the results of Linford (1998) establish that the quadrature-phase and in-phases may not always directly represent soil conductivity and magnetic susceptibility properties, respectively. Despite the unexpected quadrature-phase responses that were measured at Boden Vean, Linford (1998) was still able to comprehend and interpret his quadrature-phase results in the end, even if they did not directly represent true electrical conductivity.

2.5.2 Multimethod Case Study: Altinum, Roman City

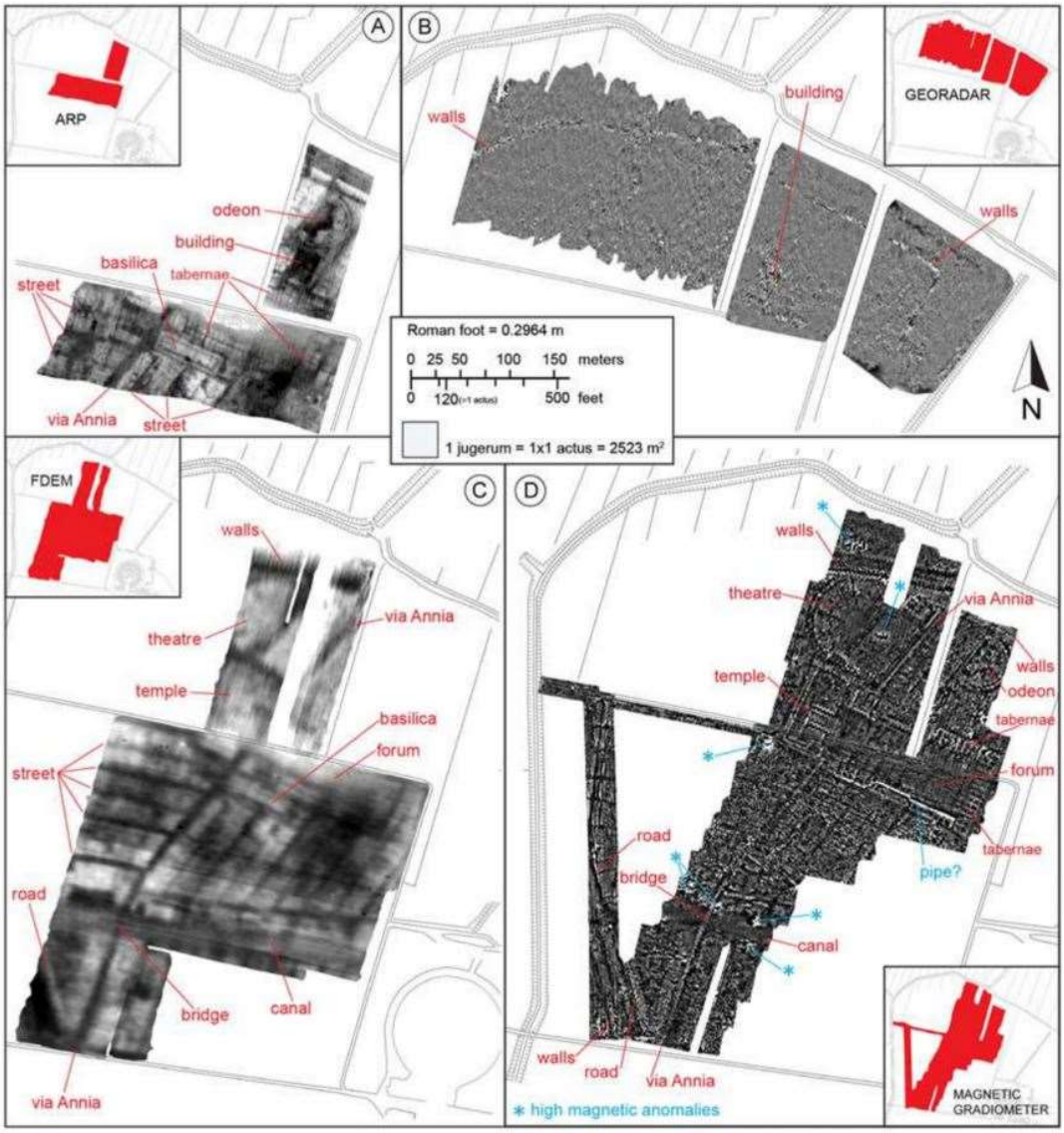

Figure 18: Comparison of the multimethod geophysical results over the Roman city of Altinum in Italy, from Mozzi et al. (2016): a) earth resistance results b) representative GPR time-slice c) EM quadrature-phase results converted to apparent resistivity d) magnetic results.

Mozzi et al. (2016) present a multimethod strategy over the Italian Roman city of Altinum. Geophysical survey of the site targeted the city's major public buildings, which had been identified through remote sensing. The different geophysical methods were collected over overlapping survey areas to compare and cross-validate the survey results. The magnetic survey was collected on a hand-pushed cart-based system in a grid using a sampling interval of 0.05 – 0.10m with traverses spaced 0.5m. The earth resistance survey was collected using the quad-towed, cart-based ARP© system, with rectangular and trapezoid electrode configurations. A sampling interval of 0.05 – 0.10m with traverses spaced 0.5m was also used for the earth resistance survey. The EM survey used the multi-

frequency GSSI EMP-400 instrument. After preliminary tests were conducted to establish the most effective operating frequency, the area was surveyed using instrument frequencies of 7 and 14 kHz. A sampling interval equating to 0.60m with traverses spaced 1.5m was employed for the EM survey. EM data were processed using bespoke software to correct for staggering issues before being converted to apparent resistivity.

Mozzi et al. (2016) were very satisfied by the magnetic results' delineation of the city's structural remains, canal feature, drainage and street networks. They cite the usage of trachyte slabs for the road pavement as contributing to a strong, remenant magnetic signal for the road features. Overall general impressions of the different methods' results show good correlation between many of the archaeological features, including roads, streets, structural remains and the canal. Targeted images of the overlapping survey areas between the different prospection methods allows cross-correlation between the magnetic, earth resistance and EM results (Figure 19).

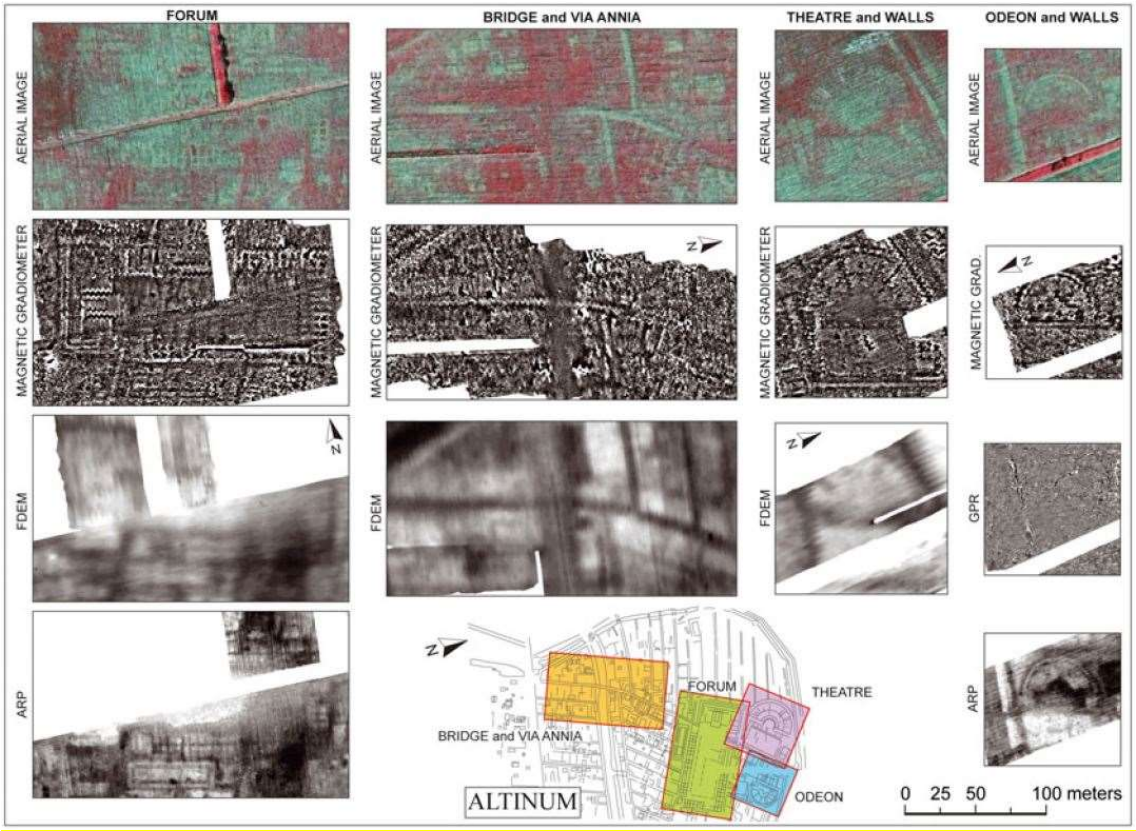

Figure 19: Targeted comparison of the multi-method geophysical and remote sensing results over corresponding areas at the Roman city of Altinum. From Mozzi et al. (2016).

In comparison to the EM and magnetic results, the earth resistance results provide detailed resolution of the internal structuring the buildings' remains. The less detailed results of the EM survey are unsurprising considering the EM strategy employed a much lower sampling density than the earth resistance survey. However, the EM survey has been more effective for providing a straightforward contextual view of the site, in contrast to the fine detail provided by the magnetic and earth resistance results. The EM survey's strength at this site, in comparison to the other methods, is for providing a clear, simplified plan of the street network. The street network is detected as low conductivity anomalies in the EM results, which agrees with the high resistivity responses in the earth resistance results. The simplicity of the street network plan in the EM results allows for the distinct segmented urban districts to be coherently understood; while the magnetic and earth resistance methods provide the fine detail of the building with these districts (Figure 20).

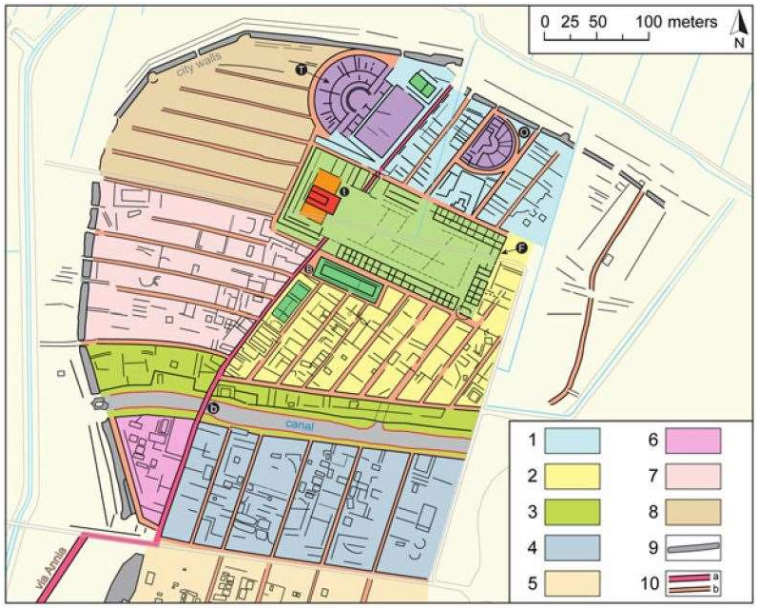

Figure 20: Integrated interpretation of the magnetic, earth resistance and EM results at the Roman city of Altinum. The different coloured areas represent a "tentative division in urban districts" from Mozzi et al. (2016).

The different methods employed at Altinum have contributed unique individual elements to produce a more holistic understanding of the plan and scale of the city. Still, Mozzi et al. (2016) conclude that further geophysical strategies at similar sites should "mainly focus on magnetic and [earth resistance] methods." This conclusion is in part due to the EM methods' not detecting many of the structural remains, which is contradictory to the author's assertion that this lack

of detection was due to the comparatively coarse sampling strategy, and not a reflection on the method's capability itself.

2.5.3 Multimethod Case Study: Whistling Elk, Earthlodge Village

The final example of a combined magnetic, earth resistance and EM approach is Ken Kvamme's (2001; 2003) investigations at the fortified earthlodge village of Whistling Elk, near Pierre, South Dakota in the United States. The site dates to *c.* AD 1300 and is a typical example of a fortified Plains Village site of that period. Fortified Plains villages include an outer ditch with palisade fortification to protect the settlement activity within. Earthlodges, the semi-subterranean, earth-covered housing structures characteristic of pre-contact Plains people, would have contained central hearth features, with pits situated immediately adjacent to the structure. Excavation of two earthlodges at Whistling Elk revealed burning and evidence indicating a rapid abandonment of the site, possibly due to enemy warfare. Excavations also recorded 0.8m – 1.5m of alluvial overburden with a 0.3m plough zone from the ground surface. In the presence of these deposits, Kvamme favoured earth resistance at this site, as the overburden depth nearly exceeded the detection range for the fluxgate gradiometer. Kvamme also believed GPR would be unsuitable at this site as the signal would be attenuated from the high conductivity of the alluvial overburden and the deposition of modern irrigation salts. Instead, an EM survey was employed to compare and correlate with the earth resistance and magnetic methods. The earth resistance survey utilised a wider 1.0m twin-probe configuration to see beneath the alluvial layer. The EM survey employed a Geonics EM38 in HCP, but despite the instrument's ability to measure both the quadrature-phase and in-phase, only the quadrature-phase is discussed by Kvamme (2001: 366-7). Figure 21 presents the results of the surveys.

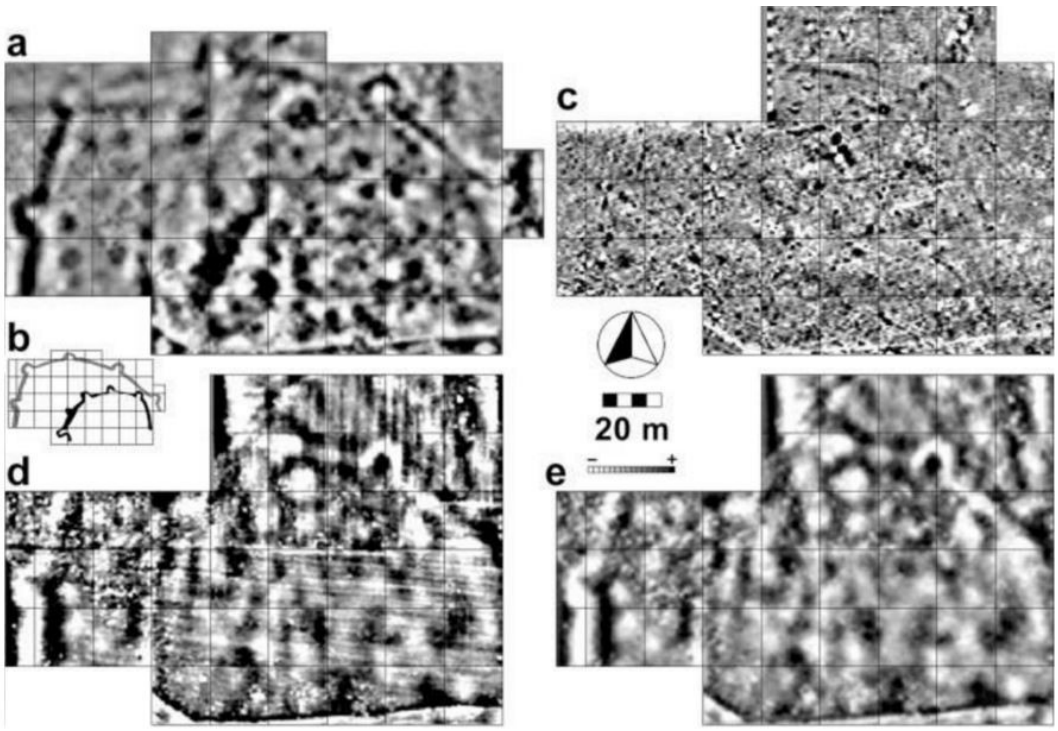

Figure 21: Multimethod geophysical results over the North American Great Plains fortified village of Whistling Elk: a) earth resistance results (high pass filtered) c) magnetic results d) EM quadrature-phase (high pass filtered) e) EM quadrature-phase (high pass filtered) with removal of plough zone signal through Fourier transform. From Kvamme (2003).

The earth resistance and EM methods were effective for detecting the ditched fortification feature and the earthlodge remains. In addition to these features, the EM results are also affected by ploughing activity across the site and showed overwhelming responses near a fence along the NW survey corner. Kvamme (2001) concludes the EM's sensitivity to the ploughing is due to the Geonics EM38's peak sensitivity lying at a depth of 0.4m, just below the end of the plough zone. The wider electrode separation of the earth resistance survey provided a depth of investigation effectively below the plough zone. Despite the ploughing, the earth resistance and EM results are inversely well-correlated (Figure 22). Where the earth resistance shows resistive earthlodge filling, the EM shows low conductivity anomalies. Where the earth resistance shows a resistive fortification anomaly, the EM shows a low conductivity anomaly. Indeed, statistical analysis of the ER and EM results reveal 95% variance between the different methods' datasets. However, the 5% still represents differences between the ER and EM results. Plotting the ER measurements against the corresponding EM measurements revealed the inverse relationship between resistivity and conductivity does not strictly hold at Whistling Elk (Figure 22).

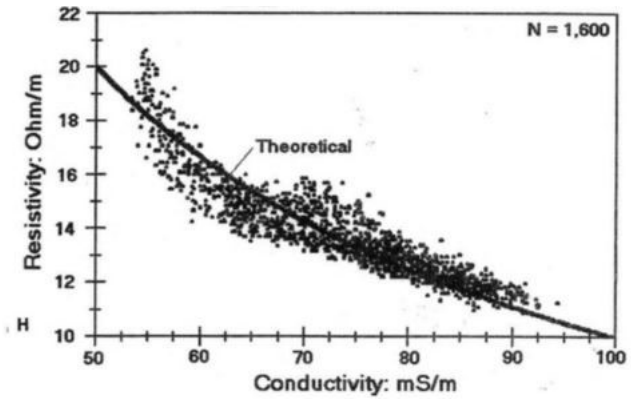

Figure 22: The theoretical inverse relationship between the EM quadrature-phase and earth resistance measurements does not strictly hold at Whistlking Elk. The relationship is illustrated by plotting the calculated apparent resistivity with the apparent electrical conductivity. From Kvamme (2001).

Kvamme (2001) ran a principal component analysis on the earth resistance and quadrature-phase datasets to better understand the variance between the separate results. The resulting second principal component image depicts linear features running parallel to the fortification ditch that are not explicit in either original ER or EM dataset. Kvamme (2001) hypothesises these anomalies may represent embankment features associated with the ditch's construction.

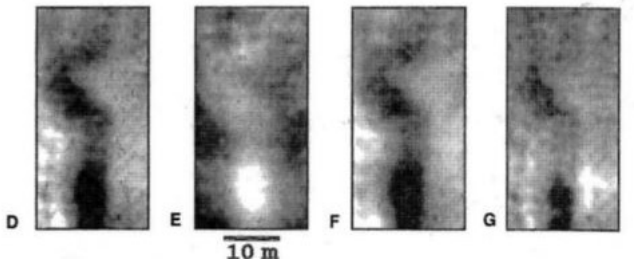

Figure 23: Principal component analysis on the earth resistance and EM quadrature-phase results over the fortification ditch at Whistling Elk: D) earth resistivity E) EM quadrature F) 1st principal component G) 2nd principal component. From Kvamme (2001).

The magnetic method was not effective for detecting many of the village's features. Surprisingly, this includes the fortification ditch, a type of feature that magnetometry is typically effective at detecting. The magnetic results only reveal the northern segment of the ditch and a bastion loop. A direct comparison of the different methods' results over an example earthlodge feature sheds light on the differences between the measurements (Figure 24):

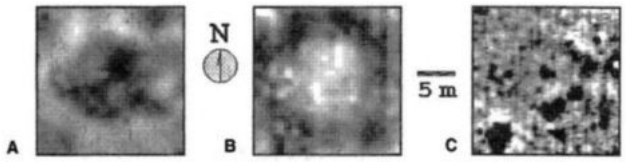

Figure 24: Differences between the (left-right) earth resistance, EM quadrature-phase and magnetic responses over an earthlodge feature at Whistling Elk. From Kvamme (2001).

The earth resistance and EM results both show the footprint and the filling debris of the earthlodge. This debris is detected as inverse anomalies in the respective datasets. The magnetic results, on the other hands, reveal internal features of the earthlodge relating to the hearth feature. Kvamme's (2001; 2003) EM and earth resistance results at Whistling Elk overall demonstrate many similarities, detecting inverted responses over many of the same features. In contrast, the magnetic results are considerably different. Therefore, the application of only a single prospection method at Whistling Elk would provide an incomplete understanding of the site.

2.5.4 Multimethod Case Study: Conclusions

Overall, the preceding examples illustrate how the analysis of the EM results in combination with magnetic and earth resistance methods can develop a greater understanding of the origin of EM responses and how these responses fit within a more comprehensive understanding of the site. Understanding the relationships between the different methods is therefore important for accurately understanding the EM results. The integration of different survey techniques can be effective for understanding and developing these relationships. The following section will explore how the different geophysical results can be understood in reference to one another.

2.6 Data Integration Techniques

Techniques for integrating individual datasets will be divided into two broad categories:

1. **Graphical combination**—where the visualisation stage is utilised for the integration of the individual datasets.

2. **Data combination**—where the individual datasets are integrated mathematically on the measurement level.

The following subsections will explore these two categories in greater detail.

2.6.1 Graphical Combination

An early example of graphical combination is found in Black and Johnson (1962), in their evaluation of magnetic methods for mapping historic sites in the United Sites. Black and Johnson (1962) employed a 1ft. x 1ft. sampling density with a proton magnetometer over a ditch-type stockade feature. Their integrated interpretation presented the magnetic results as a simple dot map, where each dot represents a high magnetic measurement. The dot map is overlain against a topographic survey of the site to visualise how the stockade feature correlates with the magnetic results (Figure 25). Linear alignments of high magnetic measurements are orientated within and parallel to the contour lines representing the stockade feature, confirming the magnetic enhancement of the stockade feature.

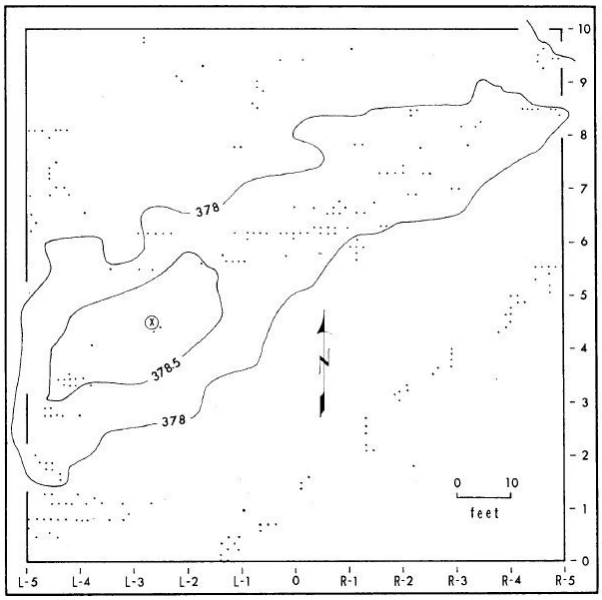

Figure 25: An early example of graphical integration accomplished through the overlay of magnetic results expressed as a dot point map with the trench stockade feature outlined by the topographic contours. From Black and Johnson (1962).

Graphical combination techniques have experienced further development since Black and Johnson's (1962) work, with many of the current graphical combination strategies originating from the development of visualising remote sensing imagery. The application of these graphical combination methods to archaeological geophysics datasets began when practitioners began integrating

geophysical results with remote sensing data to compare differences in scale (Kvamme 2006a). A straightforward method for graphical integration utilises a GIS environment to overlay the individual datasets, which are represented as individual layers. An example of a GIS approach is presented in Doneus and Neubauer (1998), who overlay the vectorised interpretation of rectified aerial photographic images over a magnetic greyscale image. Aerial photography was used to provide a landscape-scale understanding of the site's context while the magnetic survey could offer only a limited extent, due to its relatively slow rate of data collection. Interpretative layers drawn from the aerial photographs depict topographic, natural, and anthropogenic features, which help to provide a better understanding of the relationship of the archaeological magnetic anomalies within the greater natural and anthropogenic landscape (Doneus and Neubauer 1998; Figure 26).

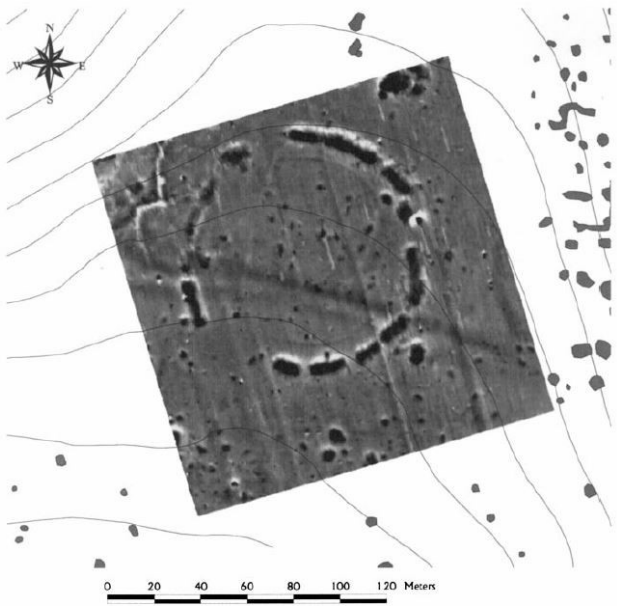

Figure 26: An example of graphical integration through the overlay of vectorised interpretation of rectified aerial photography with a greyscale image. From Doneus and Neubauer (1998).

Another graphical combination technique creates an image from the different datasets by ascribing them an individual image channel (Figure 27). The shade of the image provides an indication of which techniques are contributing to the signal in a given area (Neubauer and Eder-Hinterleitner 1997; Kvamme 2006b). For an RGB composite, the image is limited to three different geophysical methods, with the datasets assigned a unique red, green or blue channel. More than three techniques can be integrated by assigning additional methods a channel as a shade of red, green, or blue; however, if too many colours are used,

the resulting image can be difficult to interpret because the colours blend together to form a “muddy” image (Kvamme 2006b; Figure 27).

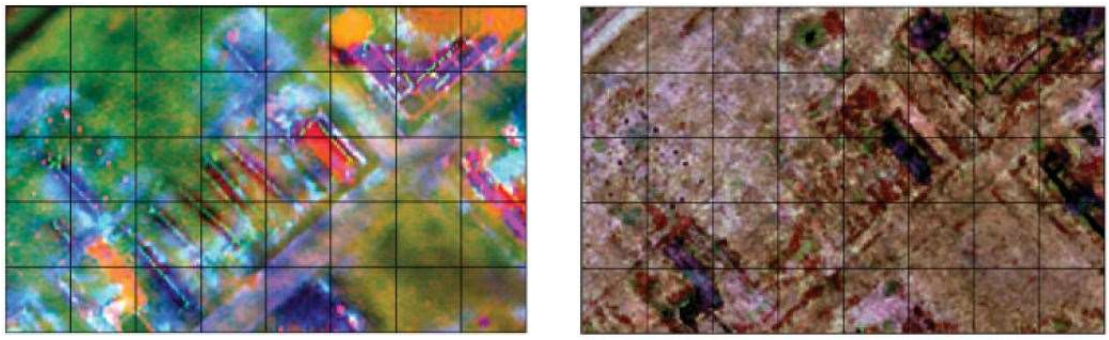

Figure 27: An example of graphical integration through image channels. Left: RGB composite of resistivity (red), EM conductivity (green), and magnetic susceptibility (blue) data. Right: composite of six datasets: EM conductivity (yellow), GPR (green), magnetometry (blue), magnetic susceptibility (cyan), resistivity (red), thermal infrared (purple). From Kvamme (2006b).

Watters (2006) presents an alternative approach to the traditional 2D graphical integration methods by using medical imaging software to create an integrated 3D visualisation of multiple datasets. Watters’ (2006) case studies visualises the three-dimensional extent of electrical imaging and ground penetrating radar (GPR) anomalies and uses the two-dimensional datasets to provide background or contextual information. ERT and GPR anomalies are converted to voxels, which are modelled and displayed as three-dimensional features (Figure 28). Watters (2006) also aims to reduce the subjective nature of anomaly visualisation by utilising manual and semi-automatic tools for designating the data voxels (i.e. the volume element of three-dimensional dataset) that will define the data as specific feature types. The data must still be segmented using user-defined thresh-holding, which is time consuming and requires knowledge of the parameters of the targeted anomalies, based on pre-conceived ideas of the types of features present.

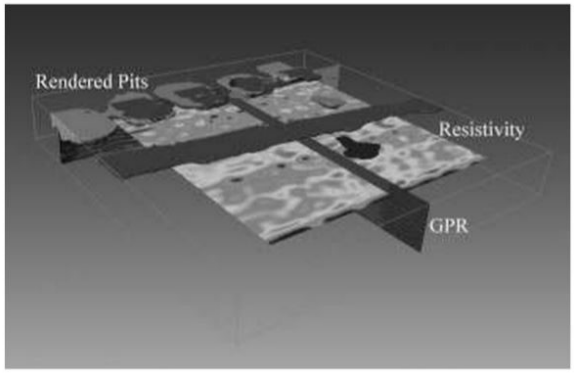

Figure 28: An example of graphical integration of two-dimensional datasets and three-dimensional interpretations. From Watters (2006).

While 2D overlays and RGB graphical approaches are relatively straightforward to implement, Watters' (2006) strategy is a more advanced approach to graphical combination. Overlaying greyscales with vectorised interpretations is one of the simplest graphical combination methods to both implement and interpret, but is limited to only displaying one greyscale at a time. RGB composites are most successfully executed when combining only two or three techniques. Still, the resulting composite images are more complex than the singular greyscales to interpret as they can take more time and understanding of colour combinations to adequately interpret and understand. The final limitation of graphical combinations is that they are only purely visual integrations; whereas mathematical combinations manipulate the data itself, and create new datasets to interpret, which may yield further information (Kvamme 2006b). Data combination techniques will be explored below.

2.6.2 Data Combination

Data combination techniques seek to integrate the different survey methods mathematically on the measurement level. One of the most basic methods of data combination is to perform mathematical operations on continuous datasets. This approach aims to present a comprehensive image of the archaeological features by combining collocated anomalies that are resolved between the different methods' results. Because the combination is done on the measured, uncategorised data, Kvamme (2006b) asserts data combination approaches are superior to graphical combination approaches for integrating results. The approach for arithmetic data combination is straightforward; the collected measurements are normalised and mathematical operators are applied between the datasets. For example, Neubauer and Eder-Hinterleitner (1997) employed a data combination approach at the Austrian Roman city of Carnuntum: first, the individual earth resistance and magnetic datasets were normalised to a range between 0 and 1. Basic arithmetic operations, including addition, subtraction, multiplication and division, were performed on the separate datasets to combine the results (Figure 29). The different arithmetic operations had different effects on the results. Addition of the datasets enhanced the wall anomalies because different aspects of the wall features were detected in the magnetic and earth resistance results; conversely, subtraction of the datasets removed the wall

anomalies. Because different aspects of the same features were detected in the magnetic and earth resistance results, the arithmetic combination of these datasets provided a more comprehensive image of the complete structural remains. Furthermore, by comparing the results of the different arithmetic operations, the nature of what the different methods to can be better characterised.

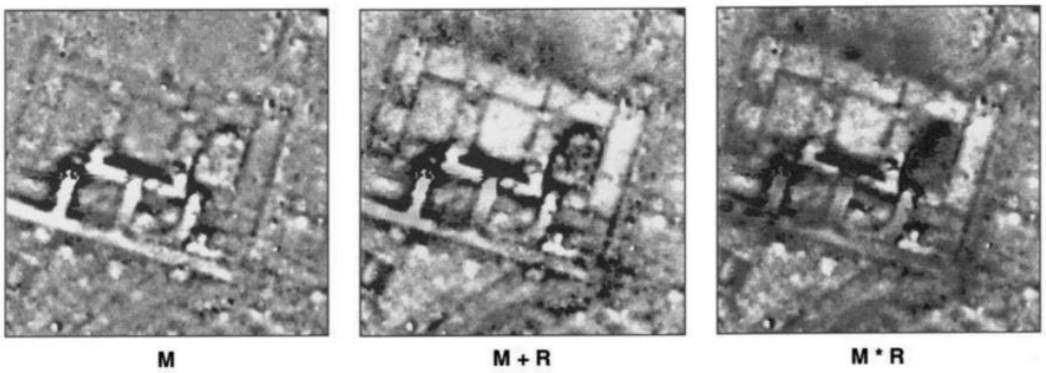

Figure 29: An example of an arithmetic data combination over a Roman villa in Austria. From left to right: magnetic data, sum of magnetic data and resistance data, product of magnetic and resistance data. From Neubauer and Eder-Hinterleitner (1997).

Another method for discrete data combination reduces the anomalous responses to binary values. To generate binary data, the geophysical data are clipped to a range within user-defined thresholds. Ideally the thresholds should target the expected range of archaeological anomalies and clip any extreme signals. New datasets for each method are generated by ascribing a value of either 0 or 1, indicating a presence or absence of a geophysical anomaly. By reducing the datasets to binary values, Boolean operators can be applied to the datasets to generate either “True” or “False” values. True indicates a cross-correlated anomaly, while False indicates an anomaly is absent or uncorrelated (Kvamme 2006b). The example figure below (Figure 30) compares the results of two Boolean unions employing different parameters: on the left is the result of a Boolean union where an anomaly is present in at least *one* of the six input datasets; the right shows the result of a Boolean union where the anomaly present in at least *two* of the datasets. The drastic differences between the two images indicates there is poor direct correlation between the individual anomalies across the datasets. This is not to say that the different methods are generally poorly correlated overall, but merely indicates the location or forms of the anomalous responses are different between the methods.

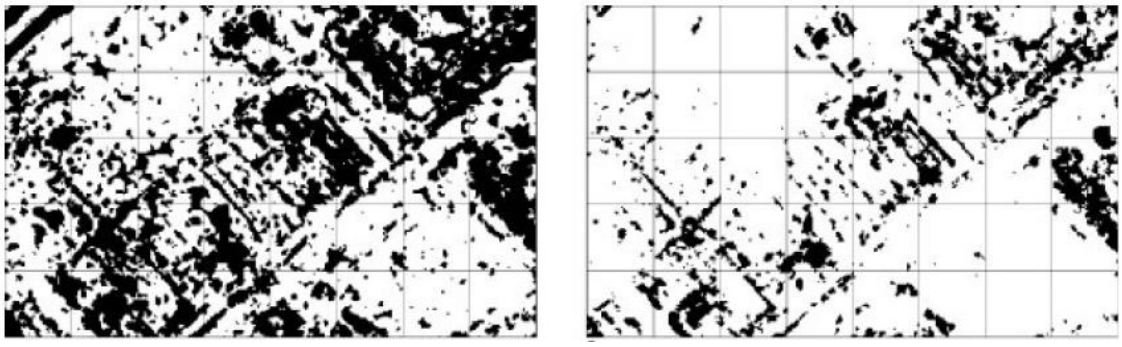

Figure 30: An example of a Boolean binary data combination approach. (left) Binary data combination showing the occurrence of an anomaly present in at least one of the six input datasets. (right) Binary data combination showing the anomalous responses present in at least two of the six input datasets. From Kvamme (2006b).

The strict dependency on the form and location of the anomalous response is one of the limitations of the binary combination approach. The approach is biased from the start of the process because the user must first define the thresholds for reducing the anomalies to binary values. The selection of appropriate thresholds is ultimately a subjective process. Consequently, weaker or less explicit archaeological features may be lost during the clipping, as this step works best on those responses that produce significant geophysical contrast. Binary combination also relies on the assumption of the infallibility of the geophysical anomaly. That is, that the geophysical anomaly is a direct representation of the feature generating it, which as discussed in the previous sections, is not necessarily true; measured anomalous responses are the result of a complex relationship between the depth, size, and physical properties of the buried feature; the background properties; and the measuring apparatus as well. The approach also strictly focuses on the archaeological signals themselves and disregards the contextual information of the background in which the remains lie. This contextual information can provide useful evidence regarding the nature of the natural and anthropogenic features of the site (Keay et al. 2009).

Unlike the binary data combination technique, data combination through principal component analysis (PCA) utilises the range of measurements within the input datasets. PCA is commonly used to combine multiband or hyperspectral remotely sensed images with the objective to reduce the dimensionality of the input dataset in a way that retains the most variation between the dataset's variables (Mather and Koch 2011). This is accomplished by calculating the "principal components,"

or the axes of most variance between the variables. These principal components will serve as the new axes to which the input dataset is transformed (see Jolliffe 1986 for a comprehensive discussion of PCA algorithms). Transforming the dataset onto these new axes can help enhance relationships between the dataset's variables and retain unique information that each variable provides. Published research on PCA for archaeological geophysics datasets is relatively limited. An example of PCA for combining earth resistance and EM was presented in Section 2.3., with Kvamme's (2001) second principal component revealing potential embankment anomalies not explicit in the individual results. Another example, by Linford (2004), presents the application of PCA on GPR time-slices to reduce the noise and enhance the archaeological response (Figure 31). Linford (2004) found the PCA was effective for improving the contrast of archaeological features, especially those with a comparatively weak signal.

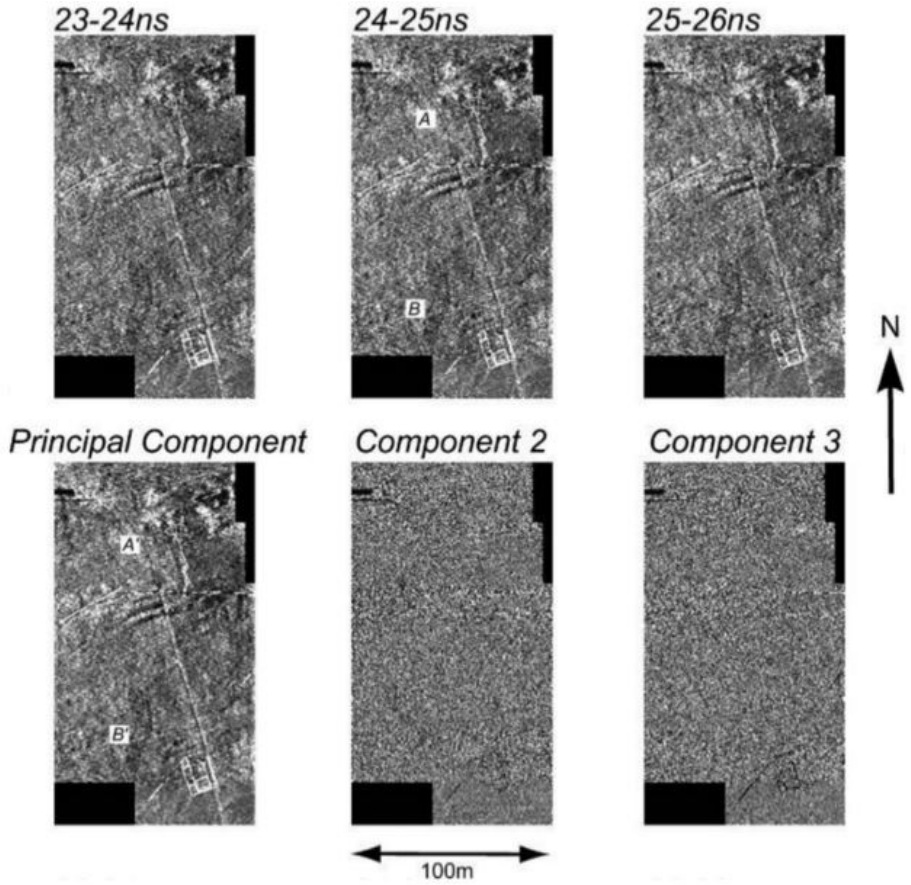

Figure 31: An example of combining GPR time-slices through principal component analysis to reduce data noise. From Linford (2004).

2.6.3 Data Integration Techniques Conclusions

The previous sections present a selection of the range of methods available for combing different geophysical survey results. The successful application of these combination techniques depends on what questions are being asked of the input results and what the desired output should be. The following chapter presents the research methodology and discusses which of these combination methods were selected and why.

Chapter 3 Research Methodology

3.1 Research Methodology: Electromagnetic Induction Experiments

To derive an accurate archaeological interpretation from the geophysical results, the nature of how the instrument's measurements represent buried archaeological features should be thoroughly understood and reasonably predictable. As discussed in the previous chapters, how the measured outputs from EM instruments relates to subsurface features and properties is not comprehensively understood, unlike earth resistance and magnetic methods, which are more predictable in behaviour. This issue is exacerbated by the variability of EM sensors, which employ a range of operating frequencies, coil separations and coil orientations, all of which will impact the measured response, as verified by the EM theory presented in Chapter 2. The experiments attempt to more accurately define how quantifiable external variables impact on the research instrument's measurements.

The GF Instruments CMD Mini Explorer has been utilised for all electromagnetic induction work as part of this thesis. The CMD Mini Explorer measures in-phase and quadrature-phase components simultaneously with ranges of +/-80 ppt (resolution to 10 ppm) and +/- 1000 mS/m (resolution to 0.1 mS/m), respectively. These measurements are accurate to within +/-4% over a ground conductivity of 40 mS/m, assuming the instrument is operating within a temperature range from -10° C to +50° C. For steady temperature changes, the instrument's temperature stability is less than 0.1 mS/m per °C change. The CMD has three receiving coils, R1, R2 and R3, at increasing distances from the transmitting coil to measure different bulk soil volumes. GF Instruments state these coils relate to the following exploration depths (Table 1). Table 1's estimates represent the depths where 75% of the cumulative sensitivity occurs for an idealised, homogeneous half-space under LIN conditions (Figure 32). In practice, the operation of this instrument is rarely in an idealised, homogeneous half-space. As a result, these depths should not be considered absolute.

Coil	R1 depth (m)	R2 depth (m)	R3 depth (m)
VCP	0.25	0.5	0.9
HCP	0.5	1.0	1.8

Table 1: GF Instruments' stated theoretical CMD Mini Explorer exploration depths.

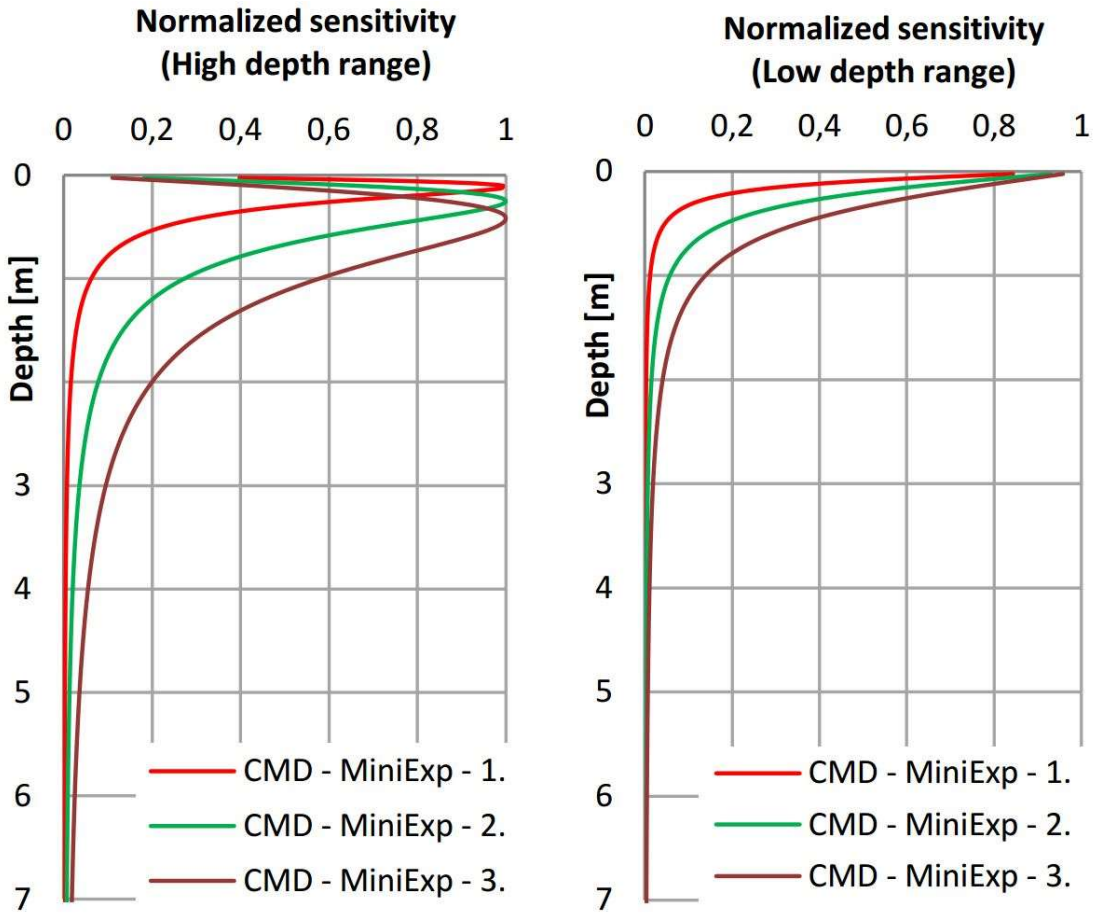

Figure 32: The two-dimensional sensitivty curves for the CMD Mini Explorer's HCP (left) and VCP (right) orientations. From GF Instruments (2016).

GF Instruments do not provide separate exploration depths for the respective in-phases and quadrature-phases, nor do they address this as a potential issue (GF Instruments 2016). The differences between the quadrature-phase's and in-phase's exploration depths is still poorly quantified, but McNeill (2013) states the in-phase has an exploration depth roughly 50% of the quadrature-phase. As a result, the different receiving coils' exploration depths will be referred to qualitatively as "shallow," "medium," and "deep" depth ranges for this thesis.

As discussed in Chapter 2, standard EM methodologies are poorly defined and vary between EM instrument and survey strategy. Developing an effective EM methodology was an important component of this thesis to ensure the accurate

combination of the EM results with other methods. In order to develop an effective EM methodology, a series of experiments were conducted to assess how typical EM instrument issues manifest in the CMD Mini Explorer. Instrument drift, calibration and elevation were targeted.

3.1.1 Research Methodology: Electromagnetic Induction Drift Experiments

The drift experiments sought to better understand the origin and behaviour of CMD Mini Explorer drift by answering the following questions:

1. How much time is required for the instrument to adjust to the ambient survey environment (i.e. “warm-up”) before commencing data collection? Recommended warm-up times vary within the literature, which implies that warm-up times are an instrument-specific problem (Delefortrie et al. 2014; Robinson et al. 2004). The length of warm-up should be long enough to allow for the instrument’s measurements to stabilise, but not be too long as to significantly interfere with available survey time. As warm-up drift was expected to have an impact on measurement stability, determining an appropriate warm up time was the initial focus of these drift experiments. The instrument was warmed to an indoor temperature of ≈21°C before running stationary on the University of Bradford’s amphitheatre, a modified landscape within the university’s main campus. Since these warm-up drift experiments were conducted in winter, there was an extreme temperature differential between the inside and outside temperatures. The instrument was laid on the ground surface over a reference point that was maintained across experiments. As this location was in a quiet corner of the amphitheatre and not subject to any disturbing works, returning to this position provided assessment of changes in absolute measurement versus different weather and soil conditions.

2. After an adequate warm-up time was established, the specific temporal nature of the instrument’s drift was targeted through a series of experiments in static and dynamic environments. These experiments sought to answer the following questions: does the CMD Mini Explorer demonstrate consistent drift behaviour? Furthermore, can drift be linked to any external factors, such as temperature or humidity?

a. **Drift in a Static Environment** - The University of Bradford's Phoenix SW geophysics laboratory provided a static, control environment that was not subject to weather changes and interference from external activity. Laboratory experiments were conducted at times when the room was not in active use, which meant room temperature and relative humidity remained stable. The instrument was placed on top of the room's central work stations. The effect of the surrounding ferromagnetic material was considered unimportant since these experiments were not concerned about absolute values, but the changes of instrument measurements with time. Experiments in the laboratory were important for understanding drift in the absence of unpredictable variables, such as fluctuating temperature and relative humidity.

b. **Drift in a Dynamic Environment** - The next stage of CMD Mini Explorer drift assessment subjected the instrument to field conditions in a dynamic, but controlled environment. By conducting the experiment in a controlled, yet changeable, environment, the change of measurements with temperature and relative humidity could be measured in the absence of any operator induced effects. The instrument was laid on the grass in the back garden of a mid-terrace house in Shipley. Throughout the experiment, the instrument experienced fluctuating ambient temperature and humidity, as well as varying amounts of direct sunlight and shade. Temperature and relative humidity were measured every 60 seconds with the sensor stationed as close to the instrument without causing interference. The instrument and temperature sensor were allowed to adjust to ambient outside conditions before the experiment began. Temperature and relative humidity measurements were cross-referenced against a nearby weather station's archive to confirm the accuracy of the temperature sensor.

Table 2 describes the individual drift experiments:

Experiment	Test Area	Name	Description	Length (min)
Warm Up Drift	Amphitheatre	HCP Drift Amp 3	Instrument allowed to warm to ambient inside temperature (≈23°C) for 25 minutes then left outside to cool to ambient air temperature.	30
Warm Up Drift	Amphitheatre	HCP Drift Amp 4	Instrument warmed to ambient office temperature (≈23.7°C—37%) then ran for 20 minutes outside.	20
Warm Up Drift	Amphitheatre	HCP Drift Amp 1	Instrument allowed to cool to ambient temperature for five mins, then ran for 15 mins.	15
Static Environment	Laboratory	HCP Drift Lab 1	Instrument left in lab for one hour after adjusting to ambient temperature for 30 mins.	60
Static Environment	Laboratory	VCP Drift Lab 1	Instrument left in lab for one hour after adjusting to ambient temperature for 90 mins.	60
Static Environment	Laboratory	HCP Drift Lab 2	Instrument left in lab for 30 mins adjusting to ambient temperature during the experiment.	30
Static Environment	Laboratory	HCP Drift Lab 3	Instrument left running in lab for one hour.	60
Static Environment	Laboratory	VCP Drift Lab 3	Instrument left running in lab for one hour.	60
Static Environment	Laboratory	VCP Drift Lab 5	Instrument left running in lab for four hours.	240
Dynamic Environment	Residential Garden	HCP Drift Garden	Instrument left to cool to ambient temperature for 15 minutes then left running outside in variable sun/shade, temperature and humidity for four hours	240
Dynamic Environment	Residential Garden	VCP Drift Garden	Instrument had been adjusting to ambient temperature for 255 minutes then left running outside in variable sun/shade, temperature and humidity for four hours.	240

Table 2: Summary of EM drift experiments.

3.1.2 Research Methodology: Electromagnetic Induction Instrument Calibration

GF Instruments have programmed automatic factory calibrations for the CMD Mini Explorer, which are performed at survey commencement and the completion of each traverse. The calibrations have been derived for the individual HCP and VCP orientations with the instrument at ground surface. The instrument recalibration experiments sought to answer the following questions:

1. How does the instrument's orientation affect the calibration at the end of the traverse? Is it better to recalibrate with the instrument pointing towards the direction of the next traverse or does it not make an impact on collected measurements?

    a. Instrument calibration orientation was initially explored over the reference amphitheatre control point used in the drift experiments. Calibration experiments were conducted with the instrument in a stationary position to avoid the unpredictable effects of dynamic instrument motion. The instrument's orientation was rotated 180° every minute to simulate zig-zag data collection where the instrument is rotated after recalibration at the end of the traverse, to walk down the next line. Temperature and humidity values were recorded as well in order to quantify any connection to the measured results.

Table 3 describes the individual calibration experiments:

Name	Description
HCP Cal Amp 1	Instrument recalibrated every minute for 10:00 minutes. At the 6:00 minute mark the instrument was rotated 180° and recalibrated. This rotation was performed every 1:00 minute to simulate the instrument rotation after recalibration at the end of traverses.
HCP Cal Amp 2	Instrument rotated 180° and recalibrated every 1:00 minute to simulate instrument rotation after recalibration at the end of traverses.

Table 3: Summary of the EM recalibration experiments.

3.1.3 Research Methodology: Electromagnetic Induction Instrument Elevation

The quadrature-phase component is an approximation for subsurface electrical conductivity properties under LIN conditions. LIN conditions are derived assuming the coils are at zero elevation, but in practice this criterion is strictly impossible to achieve as the instrument casing introduces a slight elevation of the coils off the ground surface. Instrument manufacturers must assume this elevation produces a negligible effect on the induction number when the instrument is operated on the ground surface, but becomes more important with increased elevation, for example, if the instrument were to be mounted on a cart-based system. Beamish (2011) presents how the impact of elevation can be

accounted for on an individual instrument-by-instrument basis. The focus of this experiment sought to answer the following question:

1. How does increased elevation affect the CMD Mini Explorer measurements? Can any changes be compensated for?

    a. Finding a suitable test area for the elevation experiment was difficult. Any subsurface inhomogeneity will affect the measured response as the instrument is raised; inhomogeneity induced measurement changes may be unrelated to any measurement changes due to the change in instrument height. A swimming pool was concluded to provide the most reasonable proxy for a homogeneous subsurface because the water is continually cycling and regularly checked to maintain standard water quality. Permission to access the University of Bradford's Unique Fitness and Lifestyle pool was granted when the pool was closed to public access. The experiment began with the instrument resting 15cm above the pool surface on a non-magnetic and non-conductive inflatable mat. This was the lowest height the instrument was able to safely rest at, without concern of water ingress. The mat was positioned as far into the centre of the pool as possible, to make use of the 1.75m water depth and not be effected by the metal railing running around the pool's perimeter. The instrument was raised to 30cm and 50cm heights by adding additional inflatable mats (Figure 33). Ten measurements for the respective HCP and VCP orientations were made at each height to average the minimal noise introduced by subtle currents in the pool. Average ambient air temperature was constant at 26°C with 54.5% relative humidity.

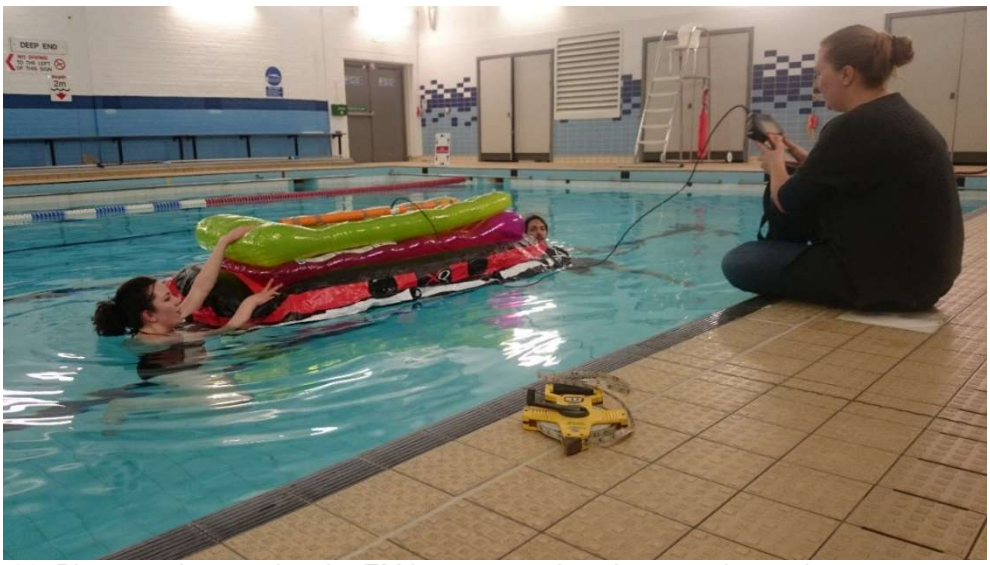

Figure 33: Photograph capturing the EM instrument elevation experiment. Image source: author.

3.2 Research Methodology: Fieldwork Methods

Most of the fieldwork data were collected as part of the University of Bradford's MSc Archaeological Prospection student training days. These days were a good a resource for utilising a range of geophysical methods at a variety of sites. However, because these fieldwork events were primarily aimed as training exercises for students, there is variability in the instruments used and survey strategies employed. The coverage of the different prospection techniques also varied by site, depending on the survey area's size, site traffic from other instruments, and time constraints. These constraints often limited EM survey to only HCP or VCP orientation. The course manager, Dr. Chris Gaffney, organised the selection of sites for the training days.

Project data have been stored on University of Bradford and cloud servers, which are regularly backed up. ArchaeoPY Modeller and CMD Regridder are stored in ArchaeoPY's GitHub Repository (https://github.com/ArchaeoPY/ArchaeoPY).

3.2.1 Research Methodology: Fieldwork Strategies

The following subsections discuss the specific instruments and survey strategies used for this thesis.

3.2.1.2 Fieldwork: Magnetic Systems

Fluxgate gradiometers have been solely utilised for the magnetic survey in this research. Geoscan Research FM256 and Bartington Instruments Grad-01-1000L fluxgate gradiometers were employed using handheld and cart-based survey strategies (Table 4).

Sensor	Sensor Comments	Strategy	Strategy Comments
Geoscan FM256	The Geoscan FM256 consists of two fluxgate sensors separated 0.5m. Data points are averaged measurements integrated over set time intervals.	Cart-based on Geoscan Research MSP25	The Geoscan MSP25 consists of a square array as a base platform, with a cradle at the back end to support the gradiometer. The Geoscan RM85 resistance meter triggers the FM256, based off the optical encoder wheel. FM256 data are stored in the instrument's datalogger.
Bartington Grad-01-1000L	The Bartington Grad-01-1000L consists of two fluxgate sensors separated 1.0m. Data points are averaged measurements integrated over set time intervals.	Handheld survey in Grad601-2 system	The Grad601-2 is Bartington's standard fluxgate gradiometer system with two 1000L sensors separated 1.0m.
		Mounted survey on hand-pulled, GPS-positioned CartEasyN cart	The bespoke CartEasyN cart consists of two-four 1000L sensors with the Bartington DL601 datalogger operating in NMEA mode. An RTK GPS mounted on the cart positions the measurements.

Table 4: Summary of the magnetic systems used for research.

3.2.1.3 Fieldwork: Earth Resistance Systems

Earth resistance survey utilised the Geoscan Research RM15 and Geoscan Research RM85 resistance meters. Both manual and cart-based survey strategies were employed (Table 5).

Sensor	Sensor Comments	Strategy	Strategy Comments
Geoscan RM15-D Advanced		Manual survey strategy	The Geoscan RM15-D Advanced with the Geoscan MPX15 multiplexer can collect eight electrode configurations per measurement sequence. Manual survey strategy requires the insertion and removal of electrodes at each point. Twin-probe, trapezoid and Wenner arrays were used with this system.
Geoscan RM85 Advanced	The Geoscan RM85 resistance meter collects measurements more rapidly than its RM15 predecessor, making it more effective for cart-based surveys. The RM85 does not require an MPX15 to collect eight different electrode configurations.	Cart-based on Geoscan Research MSP25	The Geoscan MSP25 consists of an a = 0.75m square array as the base platform. With the RM85 operating in "wheel mode," current is injected and potential difference is measured through the wheels. Data can be positioned using grid or GPS referencing.

Table 5: Table summarising the earth resistance systems used for research.

3.2.1.4 Fieldwork: Electromagnetic Induction Methods

Field survey used the GF Instruments CMD Mini Explorer in handheld, sledge-based and cart-based systems (Table 6).

Strategy	Strategy Comments
Handheld	Using GF Instruments' telescopic handle, data are collected in grids using time-based sampling. Data points are averaged measurements integrated over set time intervals. This research used sampling intervals between 0.2-0.4s, which roughly correlates to a 0.25m sampling interval.
Sledge-Based	The sledge created by Purvis (2013) holds the instrument in a central drain pipe with two outrigger drain pipes to provide stability. Blocks of foam within the central drain pipe help secure the instrument's orientation. The handset is connected to the sensor via a cable. Usually two operators are used with the sledge: one operator pulls the sledge while the other ensures the cable is kept taut and away from the sensor, as this can introduce noise. Data are continuously collected, either using grid or GPS positioning.
Cart-Based	The University of Bradford's cart is constructed of carbon-fibre tubing and suspends the EM sensor approximately 35cm above the ground surface, held in place by two braces. Measurements are continuously logged in the handset's real-time output mode using GPS positioning.

Table 6: Summary of the EM survey strategies for this research.

3.3.4 Fieldwork Sites

The archaeological backgrounds for the fieldwork sites were compiled from openly available sources. Where indicated, these sources include Google and Bing mapping; satellite imagery; Ordnance Survey mapping; published literary resources and unpublished grey literature. A Heritage Gateway (2016) search was undertaken for all sites to summarise recorded heritage assets. The origin of the database entries on Heritage Gateway (2016) is indicated in the in-text reference by the organisation's code (Table 7).

Code	Organisation
NHLE	The National Heritage List for England
SMR	Scheduled Monument Record
NT HBSMR	The National Trust's Historic Buildings, Sites and Monuments Record
YDNPA	The Yorkshire Dales National Park Authority
NY	The North Yorkshire County Council Historic Environment Record
AIP Record No.	Archaeology Data Service Entry

Table 7: Abbreviation codes for the archaeology databases on Heritage Gateway.

3.3.4.1 Fieldwork Site: Lister Park

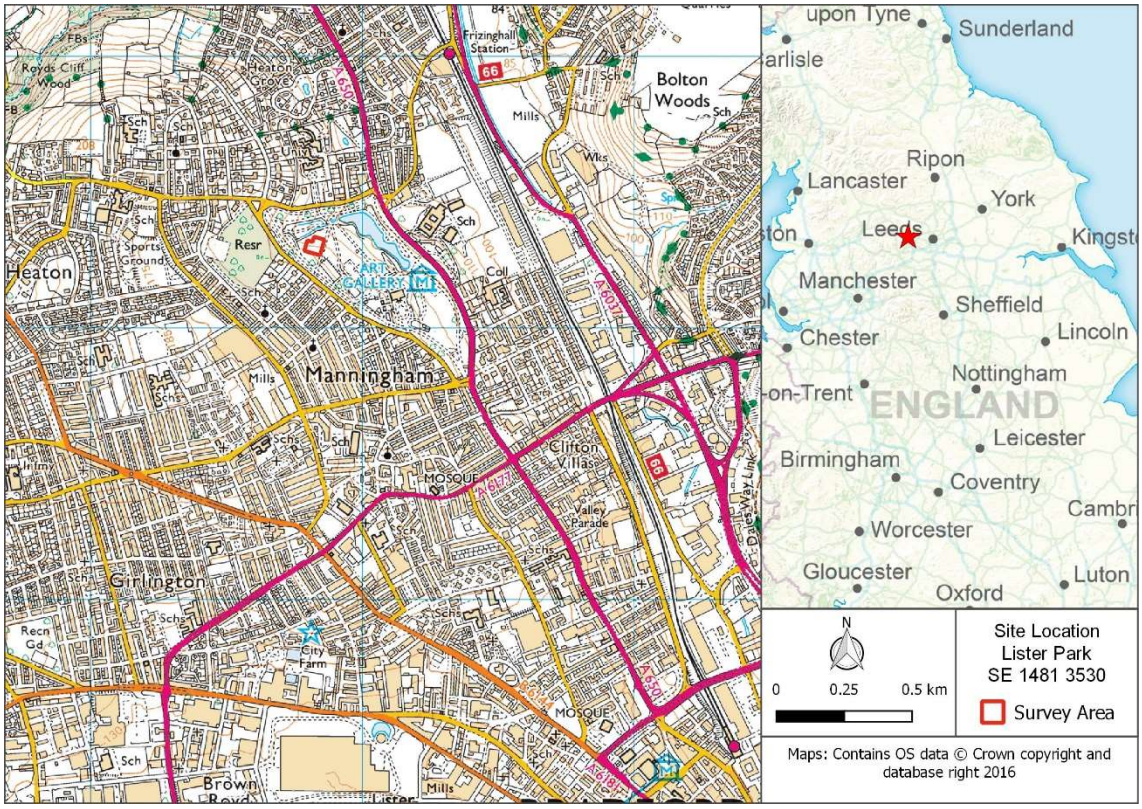

Figure 34: Lister Park site location.

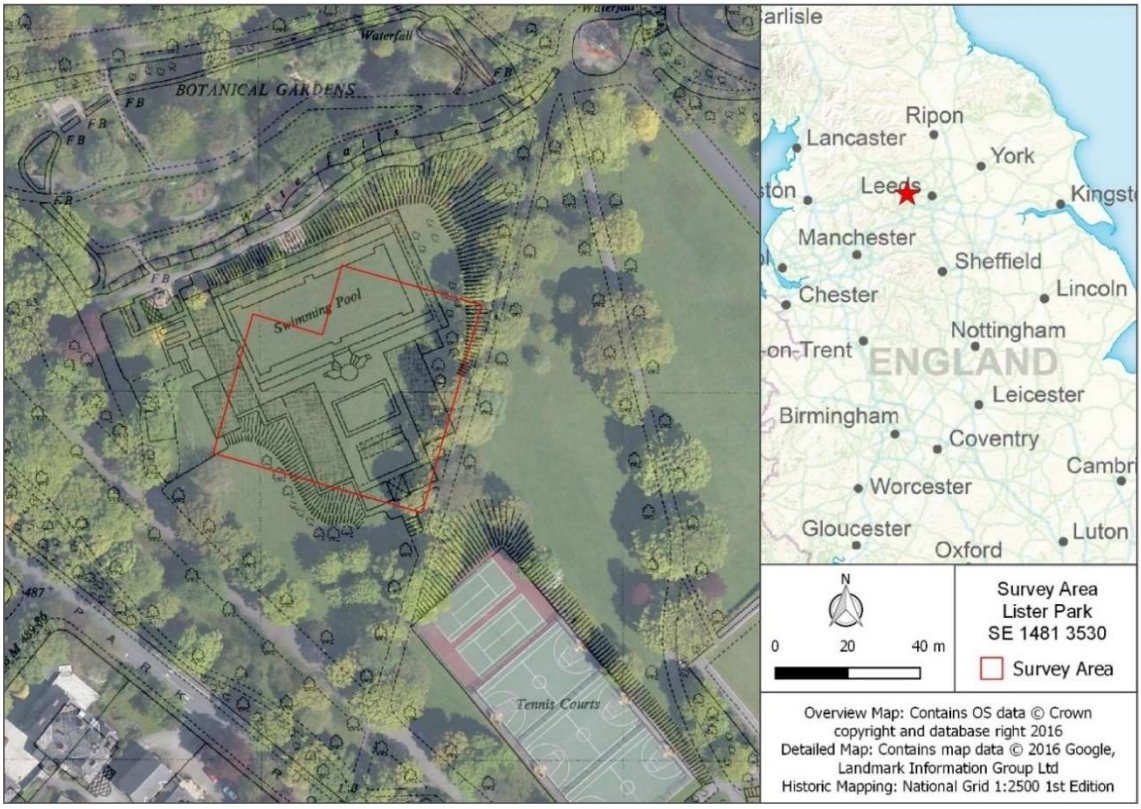

Figure 35: Lister Park survey area over 1960 Ordnance Survey National Grid 1:2500 1st Edition mapping.

Lister Park: Geographic and Archaeological Background

Lister Park is Grade II Listed Historic Park near Bradford's city centre (Figure 34). Established as a public park in 1870, the landscape, buildings and features of the park have changed through the past two centuries. The layout and elements of the park in its present form were not completed until the early 20th century when Cartwright Hall was constructed in 1904. During World War II the park was utilised for agricultural applications (NHLE No. 1001222). Survey work at Lister Park targeted the area containing the former lido, which was demolished in the 1960s. 1960 Ordnance Survey mapping (National Grid 1:2500 1st Edition) depicts the lido complex and its associated features (Figure 35).

Lister Park: Soils and Geology

Lister Park naturally consists of slowly permeable, seasonally wet loamy and clayey soils with impeded drainage (Soilscapes 2016). Underlying geology consists of sandstone bedrock (Elland Flags) with superficial alluvium of Devensian till (British Geological Survey 2016). However, the targeted survey area is a modified modern landscape and almost certainly contains disturbed soil deposits.

Lister Park: Survey Strategies

Method	Instrument	Survey Strategy	Sampling Interval	Traverse Interval
Magnetic	Geoscan FM256	Hand-pulled, cart mounted on Geoscan MSP25	0.25m	1.0m
Earth Resistance	Geoscan RM85	Cart based square array survey (*a* = 0.75m) with Geoscan MSP25	0.25m	1.0m
Electromagnetic Induction	CMD Mini-Explorer (HCP and VCP)	Hand-held, time based, grid positioned	0.3 seconds resampled to 0.25m	1.0m

Table 8: Lister Park survey strategies.

3.3.4.2 Fieldwork Site: Fountains Abbey

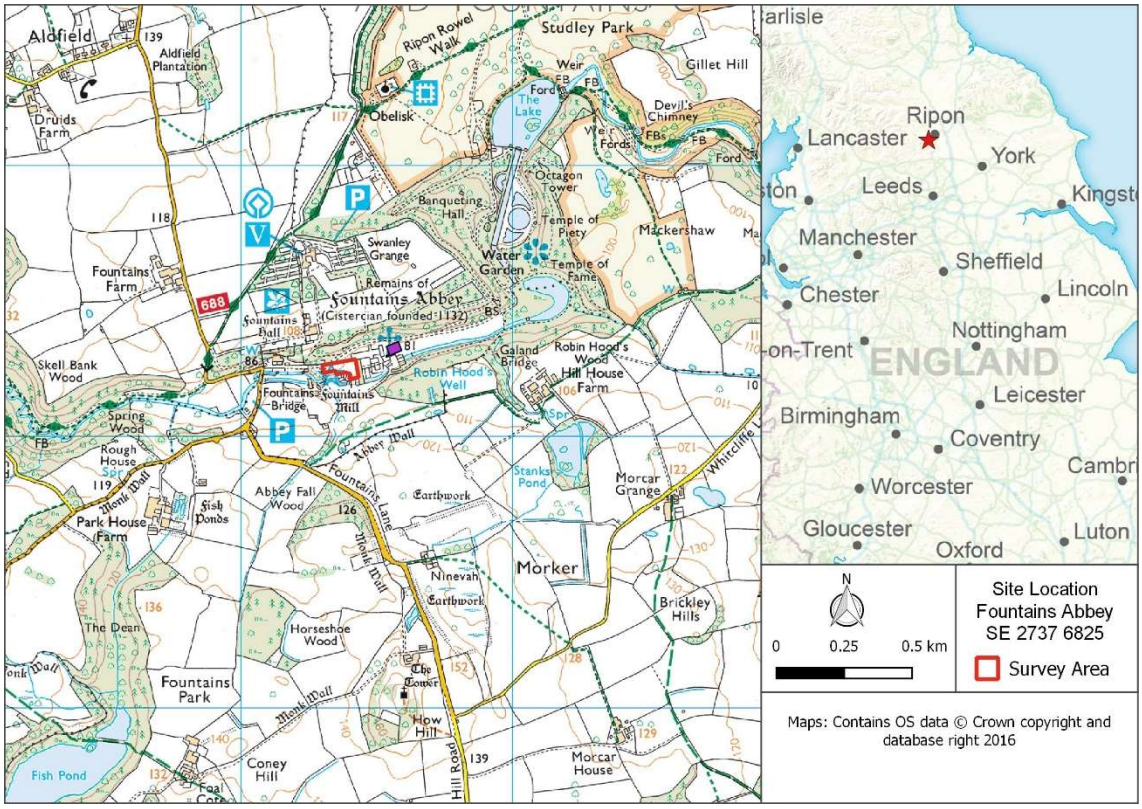

Figure 36: Fountains Abbey site location.

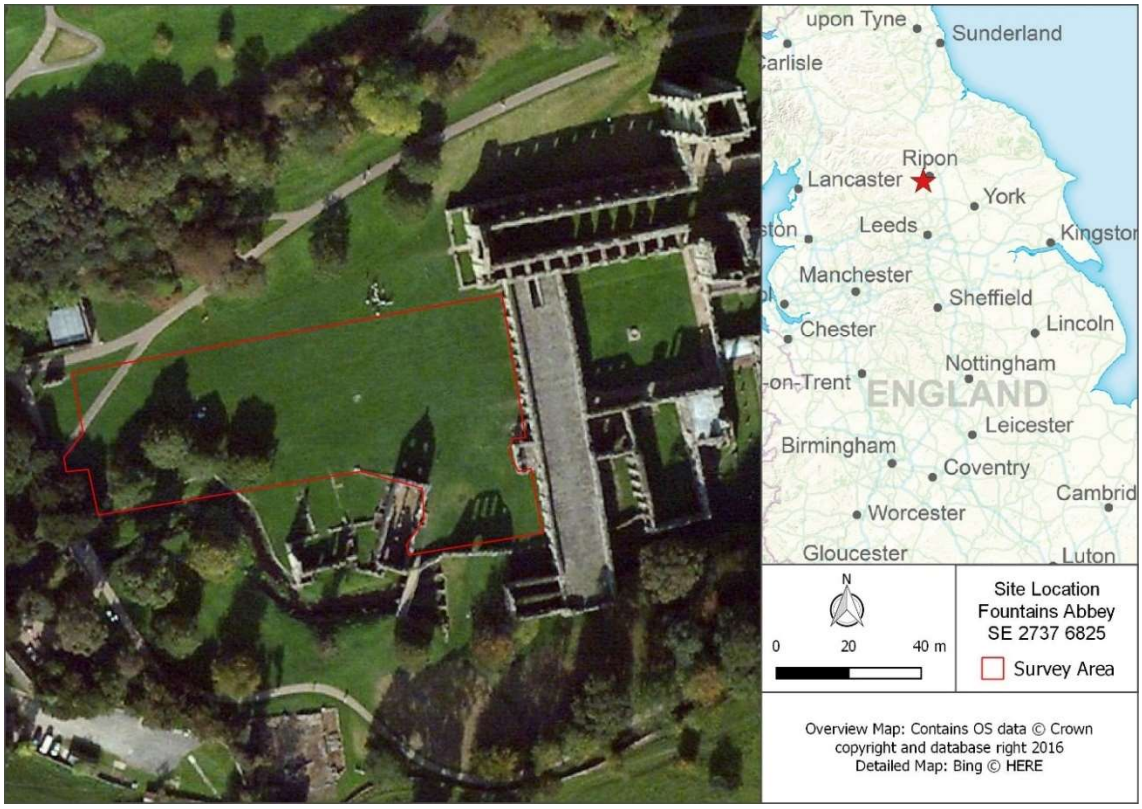

Figure 37: Fountains Abbey survey area.

Fountains Abbey: Geographic and Archaeological Background

Situated near present-day Ripon, North Yorkshire, Fountains Abbey was one of the largest and most powerful of the Cistercian abbeys in Medieval England (Figure 36). Established in the first half of the 12th century, the abbey landscape has experienced a dynamic evolution. Construction occurred in many phases, beginning with a timber monastery that formed the basis for the later stone church. Local sandstone was used as the primary construction material for the abbey complex. Major expansion of the church and associated buildings occurred through the mid-12th century and adhered to planning that reflected Cistercian ideologies. For example, entrance into the abbey from the east was considered a sacred approach and was reserved for members of the abbey. To control access into the site, the entrance of visitors was regulated from the west. In the 1160s, two guesthouses were constructed in the inner court, south-west of the nave, to host important visitors. These guesthouses were constructed to be self-contained units and situated away from the central abbey unit; separating the guests from the abbey's core. These guesthouses remain partially free-standing to present time (NT HBSMR 30432*2). A third, more substantial, guesthouse was also constructed, but only one pillar base remains extant to present day. Referred to as the "guest hall," this building was not included on the earliest plans of the ruins from the mid-18th century, suggesting the building was fully dismantled between the mid-16th and mid-18th centuries. The existence of the buried third guesthouse is known through the remenant pier base and faint crop marks of the building's features. A comprehensive twin-probe earth resistance survey by the University of York in the early 1990s revealed the full extent of the buildings, adjacent walls and structures, and a ditch created for a small-gauge railway for Victorian excavations in the 19th century. The focus of this research is the area over the buried guest hall (Figure 37).

Fountains Abbey: Soils and Geology

Fountains Abbey is situated within the valley of the river Skill, which contains slowly permeable, seasonally wet slightly acid base-rich and clayey soils with impeded drainage (Soilscapes 2016). Geology consists of Addlethorpe grit-sandstone bedrock, with superficial alluvium of clay, silt, sand, and gravel (British Geological Survey 2016). However, the survey area is within a landscape that has experienced a long occupational history, with many phases of construction

and modification of the natural environment. As a result, the underlying subsurface likely consists of disturbed soil deposits.

Fountains Abbey: Survey Strategies

Method	Instrument	Survey Strategy	Sampling Interval	Traverse Interval
Magnetic	Geoscan FM256	Hand-pulled, cart mounted on Geoscan MSP25	0.25m	1.0m
	Bartington 1000L	Hand-pulled, cart mounted on CartEasyN	10Hz resampled to 0.125m	0.5m
Earth Resistance	Geoscan RM15	Manual with parallel twin (*a* = 0.5m and *a* = 1.0m)	1.0m	1.0m
	Geoscan RM85	Cart based square array survey (*a* = 0.75m) with Geoscan MSP25	0.25m	1.0m
Electromagnetic Induction	CMD Mini-Explorer (VCP)	Sledge-pulled, time based, grid positioned	0.4s ≈ 0.25m (projected)	1.0m

Table 9: Fountains Abbey survey strategies.

3.3.4.3 Fieldwork Site: Markenfield Hall

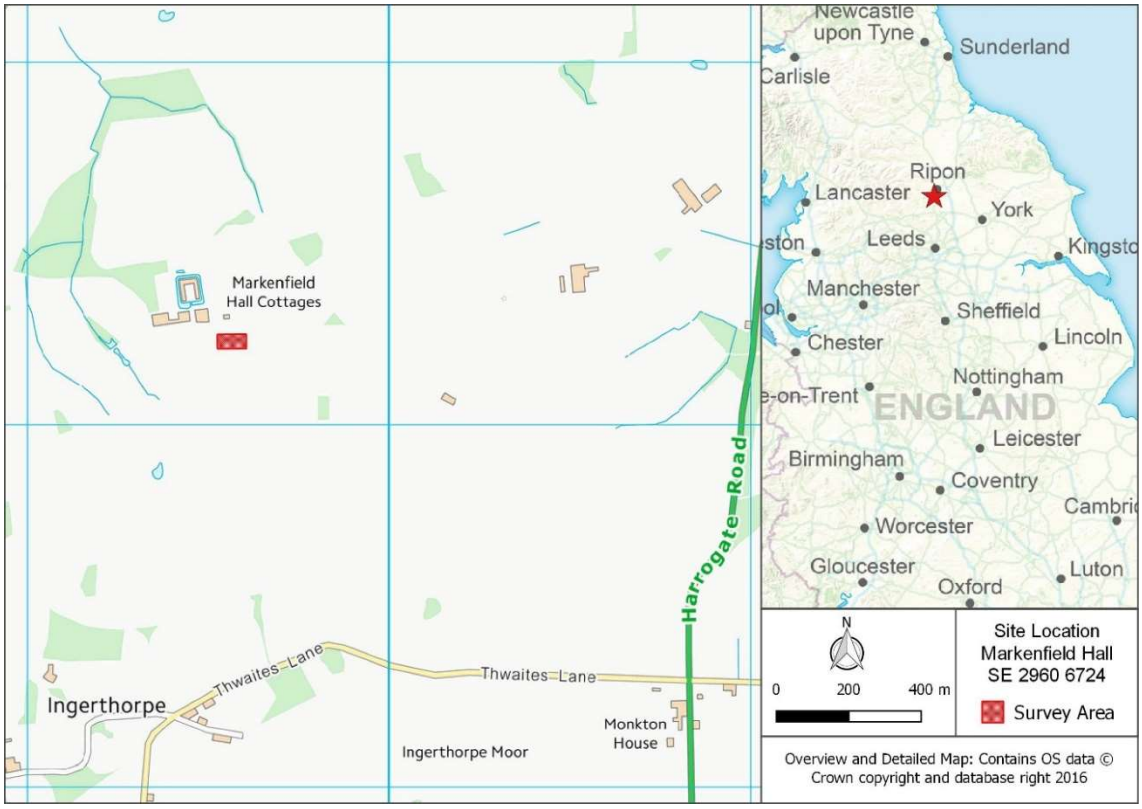

Figure 38: Markenfield Hall site location.

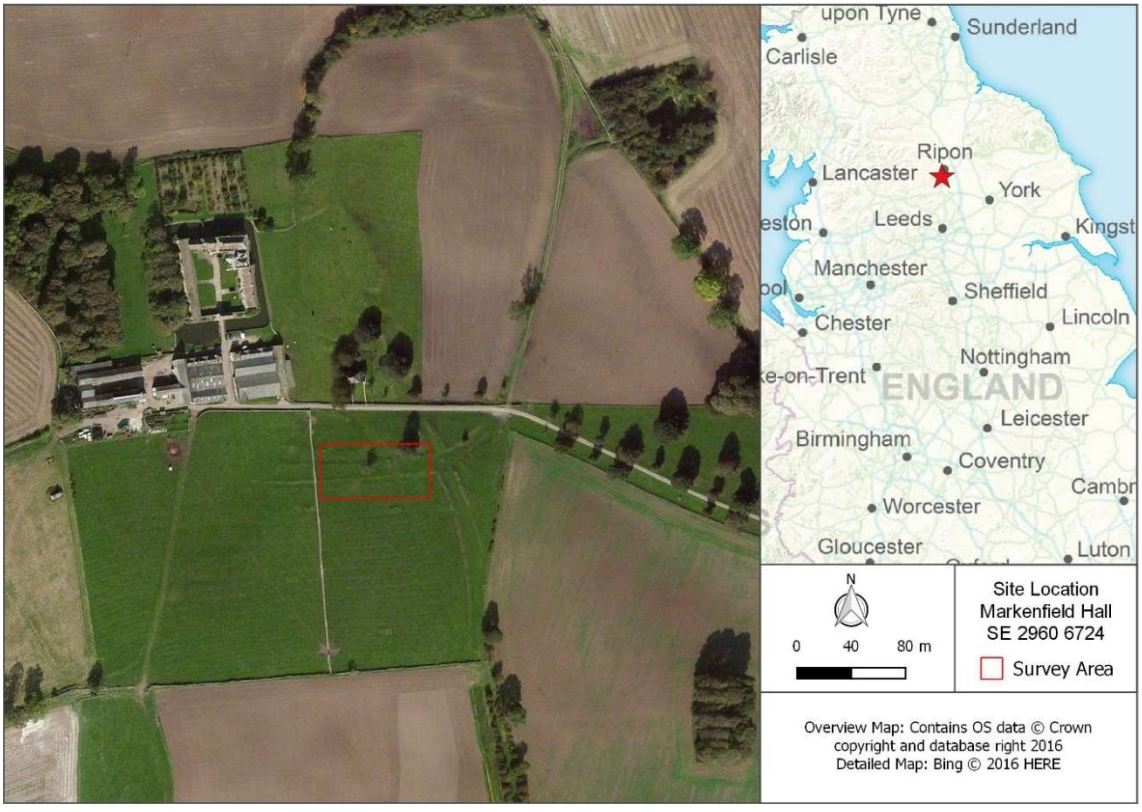

Figure 39: Markenfield Hall survey area.

Markenfield Hall: Geographic and Archaeological Background

This survey area relates to a field southeast to the Medieval manor house of Markenfield Hall, near Ripon, N. Yorkshire (Figure 38). The present house dates to the early 14th century when it was constructed by the Markenfield family. After a failed attempted uprising against Queen Elizabeth in the late 16th century, the family house was seized by the Crown on grounds of High Treason. The Crown later sold the house, after which the land has since been occupied by tenant farmers. The manor house of Markenfield Hall consists of a complex of buildings surrounded by a moat. An outer wall and ditch have been recorded surrounding the moat (AIP Record No. E.36.4327). A number of other earthwork features, including an enclosure (NY SMR No. MNY35812-3, 15493) and trackways (NY SMR No. MNY35815), have been identified in the surrounding landscape. These earthwork features are conjectured to be Medieval or post-Medieval in date and likely relate to livestock management. Ridge and furrow ploughing schemes have also been identified (NY SMR No. MNY35790, 35811), which indicates an agricultural usage of the land as well. Survey at Markenfield Hall targeted a field directly southeast of the manor house, which is colloquially known as the "Lumps and Bumps Field," owing to the extant earthwork features present (Figure 39). These earthworks are thought to reflect a Medieval settlement and agricultural activity associated with the manor house. A prominent trackway running through the survey area to the NE corner of the field runs into a historic trackway that leads to a post-Medieval limestone quarry (NY SMR No. MNY35796). Historic Ordnance Survey mapping (National Library of Scotland, 2016) does not record the trackway within the site, but these features are prominent on openly available satellite imagery (Bing, 2016) and LiDAR data (Environment Agency, 2016).

Markenfield Hall: Soils and Geology

The geology at Markenfield Hall consists of Dolostone sedimentary bedrock with clay, sandy and gravelly superficial deposits (British Geological Survey 2016). Soils consist of slowly permeable, seasonally wet, slightly acid but base-rich loamy and clayey soils with impeded drainage (Soilscapes 2016).

Markenfield Hall: Survey Strategies

Method	Instrument	Survey Strategy	Sampling Interval	Traverse Interval
Magnetic	Geoscan FM 256	Cart based on MSP25	0.25m	1.0m
Earth Resistance	Geoscan RM85	Cart based square array survey (*a* = 0.75m) with Geoscan MSP25	0.5m	1.0m
Electromagnetic Induction	CMD Mini-Explorer (HCP)	Hand-held, time based, grid positioned	0.3 seconds resampled to 0.25m	1.0m

Table 10: Markenfield Hall survey methods.

3.3.4.4 Fieldwork Site: Linton

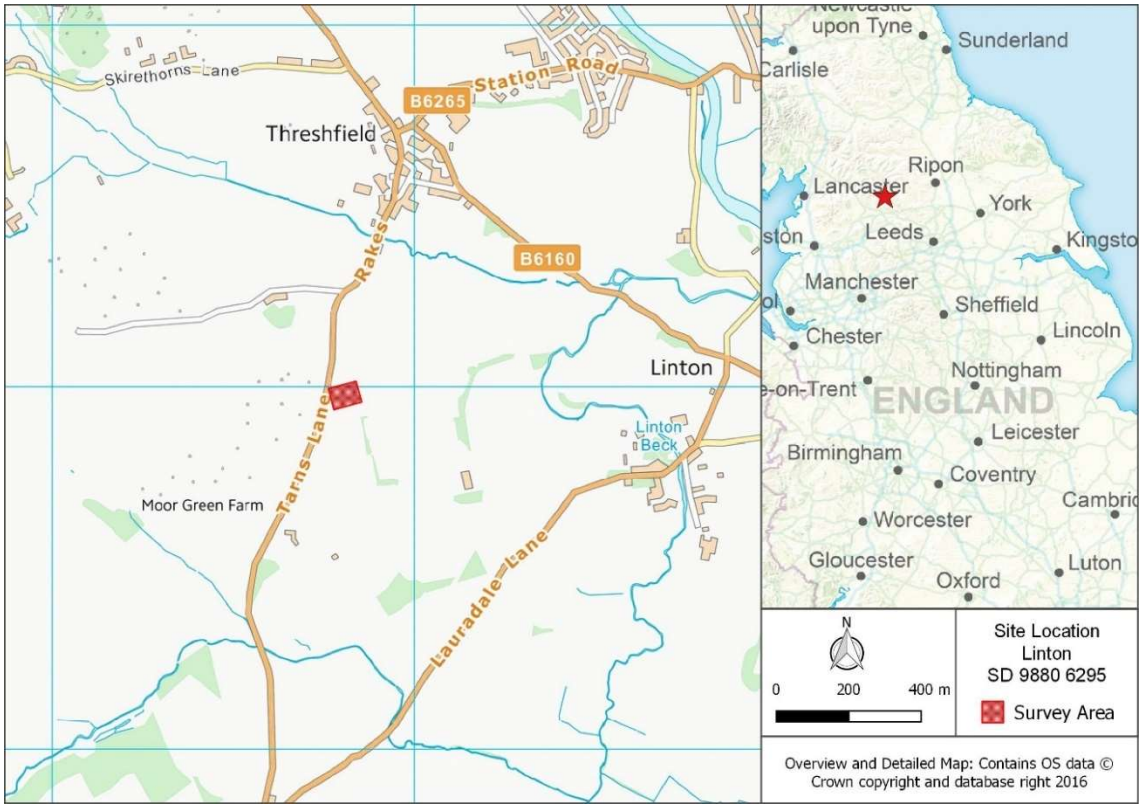

Figure 40: Linton site location.

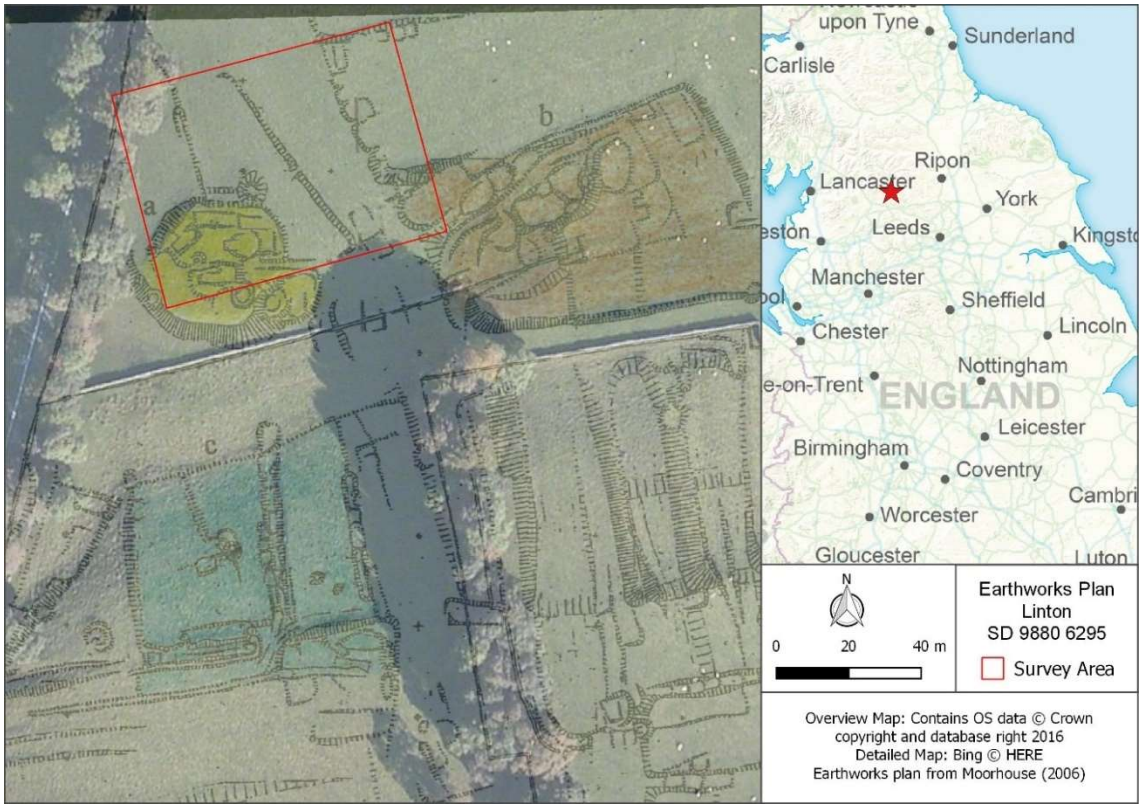

Figure 41: Linton survey area over a georeferenced image of Moorhouse's (2006) earthworks plan. Moorhouse (2006) has interpreted the area in yellow as containing Iron Age roundhouses and the area in orange as containing a timber Romano-British farm.

Linton: Geographic and Archaeological Background

The survey area at Linton, North Yorkshire lies east of Tarns lane, just south of the village of Linton (Figure 40). The survey area (Figure 41) lies within a rich archaeological landscape that has an extensive history of usage. Characteristic of this area are lynchets (YDNPA No. MYD38540) and field systems (YDNPA No. MYD4109, 38547) that traverse the landscape, running both parallel and perpendicular to topographic changes. Some of these features are Prehistoric in origin, but saw reuse and repurposing through the Medieval and post-Medieval periods. These features were likely utilised for animal husbandry and management (Richardson and Dennison, 2013; YDNPA No. MYD38547). The survey area at Linton targets a recorded enclosure of an unknown date (YDNPA No. MYD38537). The enclosures and earthworks within the survey area have been the previous subject to a walkover survey by Moorhouse (2006), who has mapped a plan of the extant earthworks features. Moorhouse's interpretation suggested the enclosure contained a settlement of Iron Age roundhouses, with a timber Romano-British farm directly to the east (Figure 41). There is no correlating evidence to support Moorhouse's (2006) interpretation; an archaeological survey directly west of the survey area concluded that if any prehistoric features are indeed present in the landscape, they would be difficult to identify given the continued usage and repurpose of these features throughout history. Furthermore, Medieval ploughing would have obscured or removed many of the prehistoric features. Directly east of the survey area, in the same field, a post-Medieval lime kiln was denoted on 1853 OS mapping; although the kiln was removed and only a hollow remains (YDNPA No. MYD2744). In addition to the lynchets and field systems, further recorded archaeological features in the survey area's greater landscape include a post-Medieval quarry (YDNPA No. MYD38542), Iron Age Barrow (YDNPA No. MYD4102), possible late Neolithic cairn (YDNPA No. MYD56026) and unspecified enclosures (YDNPA No. MYD38550).

Linton: Soils and Geology

The subsurface at Linton consists of freely draining lime-rich loamy soils (Soilscapes 2016). Geology consists of Bowland Shale Formation – Mudstone bedrock with superficial deposits consist of clay, silt, sand and gravel alluvium (British Geological Survey 2016).

Linton: Survey Strategies

Method	Instrument	Survey Strategy	Sampling Interval	Traverse Interval
Magnetic	Bartington 1000L	Manually collected with the Grad601-2 system	0.25m	1.0m
Earth Resistance	Geoscan RM15	Manual with Wenner and twin-probe arrays	1.0m	1.0m
Electromagnetic Induction	CMD Mini-Explorer (HCP)	Sledge-pulled, time based, grid positioned	0.3 seconds resampled to 0.25m	1.0m

Table 11: Linton survey methods.

3.3.4.5 Fieldwork Site: Menston

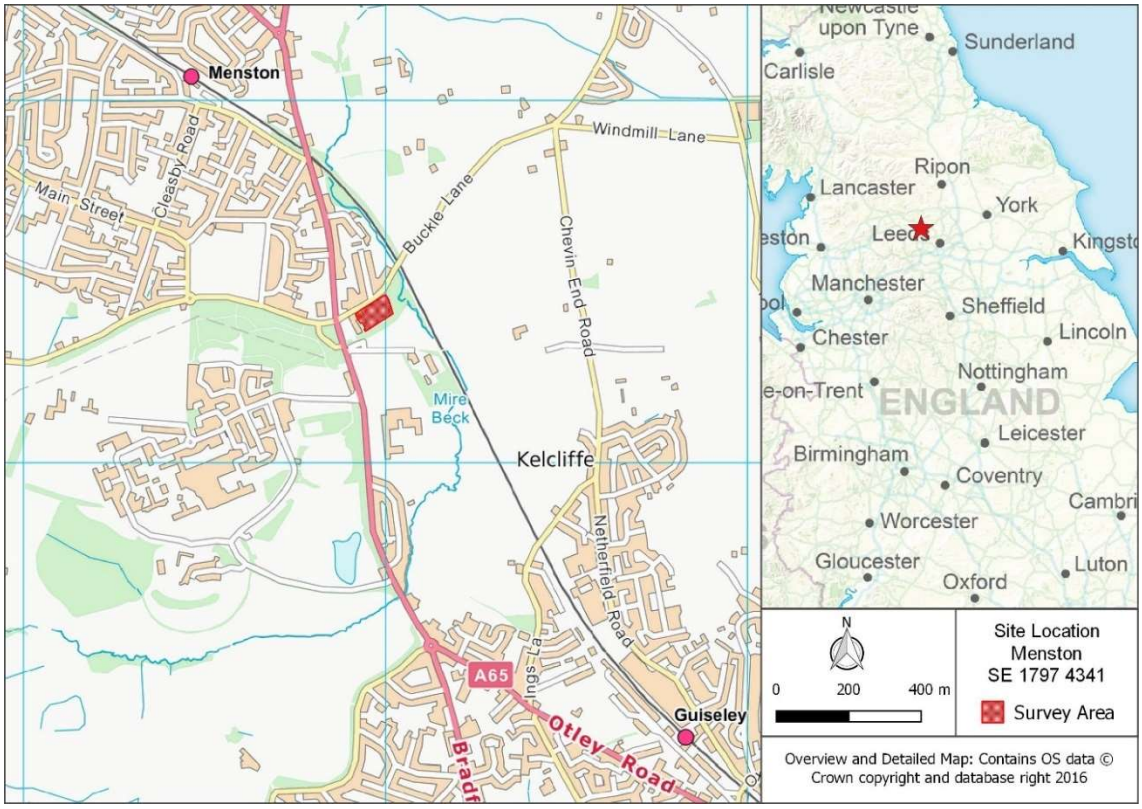

Figure 42: Menston site location.

Figure 43: Menston survey area with burial plan.

Menston: Geographic and Archaeological Background

The survey at Menston targeted the Buckle Lane Cemetery that served High Royds Hospital, a psychiatric care facility (Figure 42). Originally named the West Riding Lunatic Pauper Asylum, the facility was operational between 1890 and 1969. The hospital's complex currently has listed status (NHLE No. 1240191). At some point following the final internment in 1969, the Buckle Lane Cemetery was abandoned. A surviving burial plan shows the location of 1106 individual plots (Figure 43); although a memorial plaque on site indicates there are some 2861 burials on site. The discrepancy between the number of burial plots and recorded internments implies many plots contain multiple burials. While at time of survey, the burial plots lacked headstones and grave markers, burial plots would have been previously individually marked with a metal marker, which provided the row and burial number. A number of these markers have been found on site and left stacked within the chapel, but do not account for all of the burial plots. In 2011, the site was rediscovered and transformed through a community campaign. The basic integrity of the site was maintained, except for the gravel walkways, which were replaced with pavement.

Menston: Soils and Geology

Soils at Menston consist of slowly permeable seasonally wet slightly acid loamy and clayey soils with impeded drainage (Soilscapes 2016) over sandstone bedrock. No superficial deposits are recorded (British Geological Survey 2016).

Menston: Methods

Method	Instrument	Survey Strategy	Sampling Interval	Traverse Interval
Magnetic	Bartington 1000L	Hand-pulled, cart mounted on CartEasyN	10Hz resampled to 0.125m	0.75m
	Geoscan FM256	Handheld, grid positioned	0.25m	1.0m
Earth Resistance	Geoscan RM85	Manual trapezoid array	0.5m	1.0m
	Geoscan RM15	twin-probe array (a = 0.5m)	1.0m	1.0m
Electromagnetic	CMD Mini-Explorer (HCP and VCP orientations)	Sledge-pulled and handheld, time based, grid positioned	0.3 seconds resampled to 0.25m	0.5m and 1.0m

Table 12: Menston survey strategies.

3.3 Fieldwork Data Processing and Visualisation

The geophysical data were processed using a combination of bespoke and commercially available software. Earth resistance data were processed in Geoplot v.4.0 using a standard processing workflow; processing steps were limited to despiking, destaggering (if the data were collected cart-based), edge-matching (for twin-probe data) and a high-pass filter, to remove broad-scale background variations. CartEasyN magnetic data were processed using bespoke software written to handle GNSS positioned data; processing steps were limited to a zero-median traverse. The rest of the magnetic data were processed in Geoplot v.4.0; processing steps were limited to a zero-median traverse and destaggering, if required. An analytic signal was applied on magnetic datasets that exhibited overwhelming ferrous responses. The analytic signal code was developed as part of ArchaeoPY (Gaffney et al. 2015), for the application on vertical gradiometer data. Exact processing steps for the different sites can be found in Appendix 1.

The individual geophysical datasets are presented as greyscale images. The greyscale images have been georeferenced in a GIS environment to aid interpretation. Greyscale images have been interpreted in consideration with satellite imagery, historic mapping and LiDAR data. Magnetic data interpretation has been made using both greyscale images and XY traces. XY traces visualise in the anomaly magnitude and form, which can be informative for understanding the origin of the anomaly source (e.g. ferrous material, burning, etc).

3.4 Fieldwork Data Integration

The magnetic, earth resistance, EM quadrature-phase and EM in-phase datasets were integrated through graphical and data combination integration techniques. The suite of integration techniques were utilised to better understand the relationships between the different techniques, which would in turn aid in a better understanding of what the different techniques are individually responding to. This holistic understanding of the results both as individual datasets and in reference to one another was used to characterise the nature of the archaeological remains. However, before any integration techniques could be applied, the EM quadrature and in-phase datasets were combined to create two-

dimensional datasets that could be combined with the magnetic and earth resistance results.

3.4.1 Dimensionality Reduction to Produce Composite Quadrature-Phase and In-Phase Electromagnetic Induction Datasets

Using six individual EM datasets in combination against the magnetic and earth resistance methods would have overwhelmed the other methods' signals, creating a bias towards the EM results. To produce a balanced integration, the respective quadrature-phase and in-phase datasets were combined to produce one composite two-dimensional dataset per each phase. The dimensionality reduction of the EM data also had an additional benefit that for practical purposes, six unique datasets per survey can become an overwhelming amount of information to convey when presenting the results. The visualisation strategy for other geophysical methods that produce multiple exploration depths, such as GPR and ERT, often will present a single image or a few representative slices to encapsulate the overarching interpretation.

Different combination strategies were employed to assess which method would produce the best composite dataset. An arithmetic mean and PCA were performed on the EM datasets using bespoke software developed as part of ArchaeoPY. The software required the input data were structured in a gridded format. The functions used for the PCA cannot accept NaN or masked values. Dummy values would skew the results of the PCA; sites with incomplete grids were trimmed down to a useable size. The source code can be found in the ArchaeoPY repository (https://github.com/ArchaeoPY/ArchaeoPY), but the general algorithm follows below.

1. The gridded R1, R2 and R3 files from a survey are loaded.

2. The shape of one of the input datasets is obtained to reshape the datasets back into their original form after the mean and PCA transforms are performed.

3. The R1, R2 and R3 files are read into an array as flattened 1D strings of z-data. The array has three rows that contain all the z-data for the respective R1, R2 and R3 files.

4. Histograms of the R1, R2 and R3 results are visualised to illustrate the spread and range of the datasets.

5. The array data is sent to a function that computes the arithmetic mean and principal components.

6. Mean of Datasets—The arithmetic mean of the datasets is obtained using Python's built in mean function, which conforms to:

$$\bar{x} = \frac{1}{n}\sum_{i=1}^{n} x_i$$

Equation 4: Arithmetic mean.

where x_i is a dataset containing the values $x_1, \ldots x_n$ and n = the number of values. $\bar{x}$ = the mean of x_i.

7. Principal Component Analysis—The PCA is an implementation of Solem's (2012) algorithm, which is available as open source software (https://github.com/jesolem/PCV/blob/master/PCV/tools/pca.py).

The most representative composite datasets were then integrated with the earth resistance and magnetic results, using the graphical and data combination techniques discussed in the following subsections.

3.4.2 Fieldwork GIS Integration

The first integration of the results was undertaken in QGIS. Vector interpretations were drawn over the georeferenced greyscale images of the different methods. Digitising the interpretation in a GIS environment allowed for the utilisation of GIS analysis tools, which were used to visualise the geometric relationships between the vector interpretations. The most effective of these analysis tools was the geometric intersect tool, which produce a new shapefile of where the different methods experienced correlating anomaly interpretations. This intersection tool was utilised to answer the following questions, to quantify how the correlation of individual methods can be used to characterise the source target:

- Do the quadrature-phase and in-phase share correlating anomalies? Does this represent a blending of the in-phase and quadrature-phase signals?

- Where do the quadrature-phase and earth resistance datasets share correlating anomalies? Are the responses reasonable inverse proxies for one another?

- Where do the quadrature-phase and magnetic datasets share correlating anomalies? Are they correlated with a response in the in-phase? Is the quadrature-phase representing a magnetic response?

- Where do the in-phase and magnetic results share correlating anomalies?

- Are there any anomalies that are correlated across all of the geophysical datasets?

3.4.3 Fieldwork CMYK Graphical Integration

The geophysical results were also integrated by creating a TIFF image using a CMYK colour model. The CMYK model contains four colour channels: cyan, magenta, yellow and key, which allowed for each individual dataset to have its own colour channel. The CMYK combination code was written by the author and follows below. The input datasets must be in gridded format and resampled to the same sampling densities before they are loaded into the software.

1. The individual magnetic, earth resistance, EM quadrature-phase and EM in-phase files are loaded and read into an array.

2. The arrays are individually standardised then normalised to prepare for conversion into a pixel value:

$$x' = \frac{x - \min(x)}{\max(x) - \min(x)}$$

where x is the input value and x' is the normalised value

Equation 5: Data min-max normalisation.

$$x' = \frac{x - \bar{x}}{\sigma}$$

where x is the input value, $\bar{x}$ is the mean of the input dataset and σ is the standard deviation of the input dataset.

Equation 6: Data standardisation.

3. The arrays of the different methods are assigned one of the CMYK channels. Which method was used for what channel varied by site as different colour combinations worked better depending on the types of responses within the datasets.

4. The arrays are stacked to form a three-dimensional array, with each dataset slice representing the assigned colour channel.

5. The three-dimensional array is multiplied by 255 to assign the measurements a pixel value.

6. The three-dimensional array is then converted to an 8-bit unsigned integer for image creation.

7. Python Image Library's (PIL) "from-array-to-image" function is used to generate the CMYK image.

8. The CMYK image is resized to match the sampling density of the datasets using bicubic interpolation.

9. The image is scaled then saved as a TIFF.

The drawback of using CMYK images is that the CMYK colour model is not as commonly employed as the RGB colour model. For example, QGIS utilises the Geospatial Data Abstraction Library (GDAL) for transforming raster images during the georeferencing process. GDAL's support for CMYK values is limited and poorly documented. As a result, when CMYK images are georeferenced in GIS, the colour model is converted to an RGB model, before the transformation and creation of the geotiff. The CMYK to RGB conversion formula compresses the four CMYK bands into three RGB bands (Equation 7). The CMYK is a subtractive colour model; whereas the RGB is an additive colour model, meaning the CMYK images converted to an RGB model having a more vivid appearance.

$$R = (1 - C) * (1 - K)$$
$$G = (1 - M) * (1 - K)$$
$$B = (1 - Y) * (1 - K)$$

Equation 7: CMYK to RGB conversion formula.

Unlike QGIS, Esri's ArcMap supports CMYK images, but requires the figures be exported as PDFs to maintain the CMYK colour model. However, a specially calibrated printer is still required to print the CMYK image properly. Overall, the minor change in the intensity from CMYK to RGB images was considered negligible, in favour of the overall image effect.

3.4.4 Fieldwork Multi-Method Data Combination

The combination of the earth resistance, magnetic and EM datasets followed a similar workflow to one derived for combining the individual EM datasets. Since the mean and PCA algorithms cannot handle NaN or dummy values, only overlapping areas of all four methods are used. This required preparation of the datasets beforehand, to strip the non-collocated surveys areas from the input datasets. After the datasets were prepped, they followed the following workflow:

1. The individual magnetic, earth resistance, EM quadrature-phase and EM in-phase files are opened.

2. The shape of one of the input datasets is obtained to reshape the output datasets back into their original form after the mean and PCA transforms are performed.

3. The magnetic, earth resistance, EM quadrature-phase and EM in-phase files are read into an array as flattened 1D strings of z-data. The array has four rows that contain all the z-data for the respective methods.

4. The individual datasets are standardised following Equation 6.

5. Histograms of the individual methods are generated to visualise the spread and range of the different methods.

6. The array data is sent to a function that computes the arithmetic mean and principal components.

Chapter 4 Analysis of Fieldwork Results for an Archaeological Characterisation of the Geophysical Measurements

Chapter 4 presents the fieldwork results and the subsequent archaeological characterisation that was derived through the integration of the different survey methods. The integration of the results meets objective 3b, to establish the relationships between the different geophysical methods in order to develop a better understanding of what aspects of the environment the different techniques are specifically responding to.

To integrate the three-dimensional EM results with the two-dimensional earth resistance and magnetic data, a dimensionality reduction of the EM datasets was required. The respective EM quadrature-phase and in-phase datasets were combined to produce composite datasets that represented the information contained across the separate exploration depths. Owing to the site-specific variability of the EM results, the dimensionality reduction methodology varied between the sites. This was due in part to the variability in the instrument's responses, depending on the type and nature of the buried archaeology, which will be demonstrated in the following chapter. Methodology also varied depending on the processing steps applied to the input data, as the different processing algorithms will affect the values of the collected measurements and had to be compensated for individually.

This chapter is structured so that the standard magnetic or earth resistance results are presented at the beginning of each section, to establish a reference base map for the site. The EM results will be split into separate sections devoted to the quadrature-phase and in-phase individually. The dimensionality reduction strategy and the composite images will finish the respective quadrature-phase and in-phase sections. After the composite EM results are analysed, the integration methodology applied to combine the different geophysical datasets will be presented. Integration of the datasets will establish the relationship between the EM results with the standard earth resistance and magnetic datasets. Once the origin of the EM signal is thoroughly understood, the section will finish with the archaeological characterisation of the geophysical results from that site. This chapter will be used to answer research questions two and three.

4.1 Lister Park: Results and Characterisation

The survey at Lister Park in Bradford, West Yorkshire targeted the former lido complex; the position and extent of which is known from historic Ordnance Survey mapping (see section 3.3.4.1 for full background). The relevant features on the 1960 National Grid 1:2500 1st Edition map were digitised then categorised by comparing map data against photographic records (Figure 44). The geophysical results are interpreted in reference to this digitised plan.

Figure 44: The historic map of Lister Park digitised with colour-coded polygons to represent the different buildings with the lido complex.

4.1.1 Lister Park: Magnetic Results

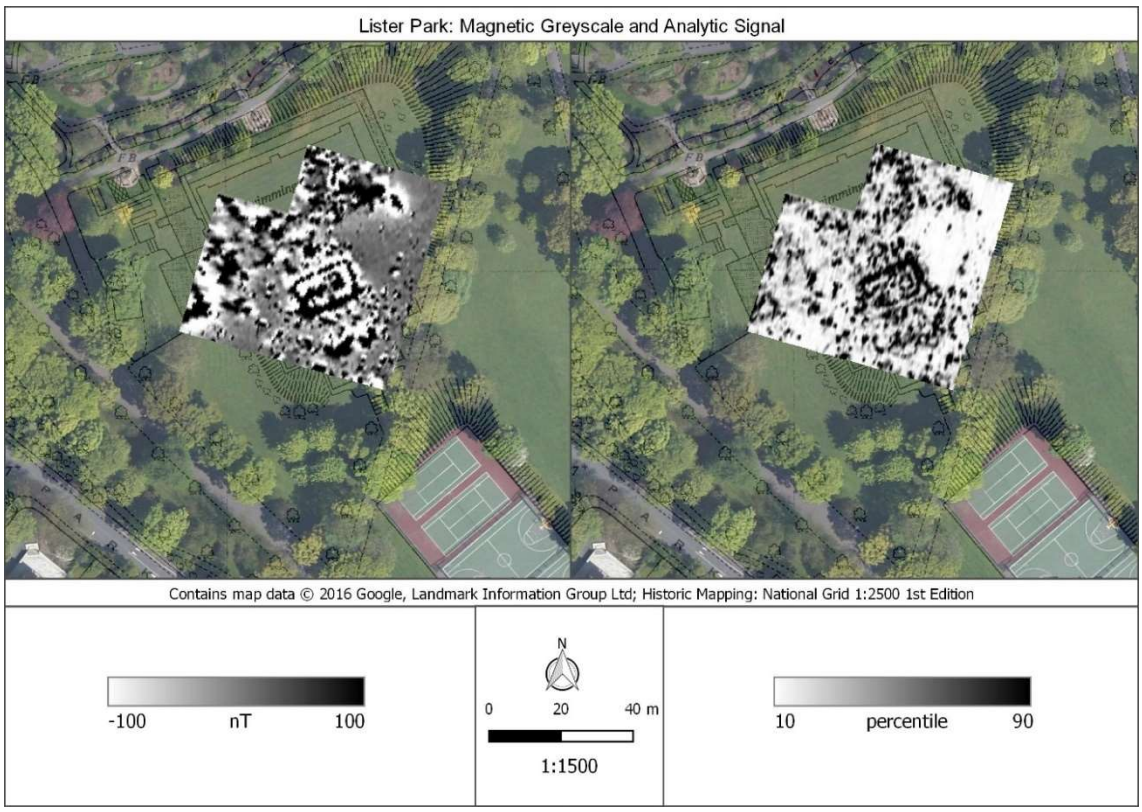

Figure 45: On the left, the Lister Park magnetic (cart-based Geoscan Research FM256) greyscale. An analytic signal (right) was applied to clarify the boundaries and extent of the detected material.

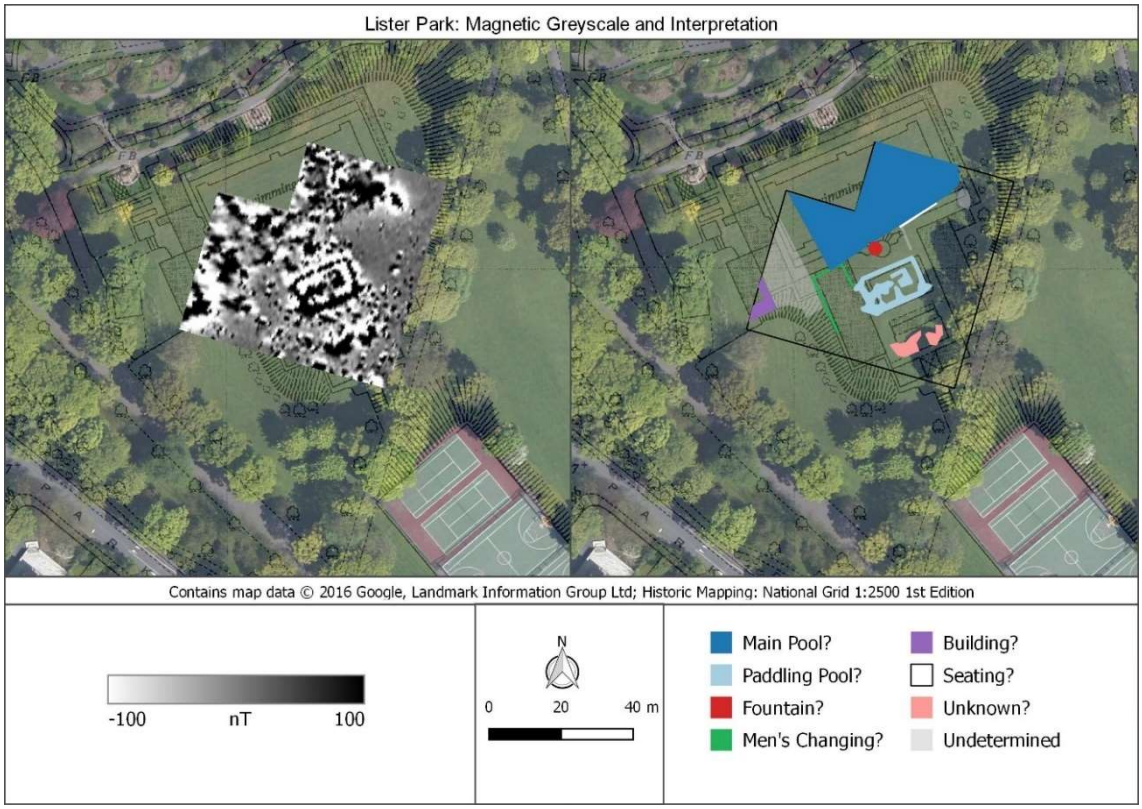

Figure 46: On the left, the Lister Park magnetic (cart-based Geoscan Research FM256) greyscale, with the resulting archaeological interpretation on the right.

The concentration of highly magnetic anomalies within the boundary of the main pool suggests that debris from demolition of the lido features has been infilled into the remnants of this feature (Figure 46); although, surprisingly the extent of this material does not comprise the entire footprint of the pool. In fact, the analytic signal results reveal a defined linear edge to the western extent of the pool fill, which does not correlate with the pool's edge in the historic mapping. Still, the lateral extent of the fill material should not be used strictly as an indication of volume of material, as the actual depth extent of the material cannot be accurately quantified through the two-dimensional results.

The magnetic results also delineate linear anomalies that correlate with the paddling pool's outline, an unnamed building and an unknown map feature. However, of equal importance in the magnetic results is the interpretation of the areas that lack magnetic anomalies. The magnetic results show comparatively quiet areas that correlate with the footprints of the women's and men's changing rooms. The boundaries of these buildings are defined by the strong responses from the debris material that has been deposited within adjacent structures. In this instance, it is the absence of anomalies and the boundaries of which they form that represent the former structures. Analysis of the correlating earth resistance and EM results help to shed light on the deposition of debris material and the preservation of the building features.

4.1.2 Lister Park: Earth Resistance Results

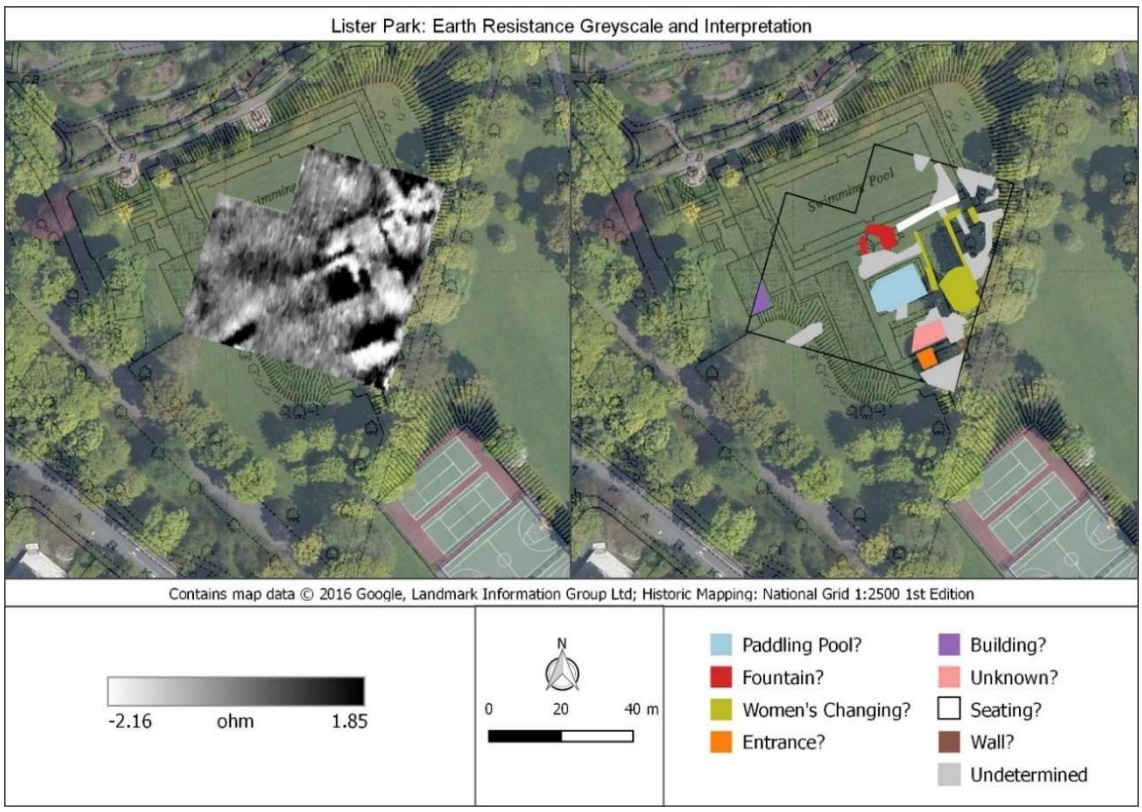

Figure 47: Lister Park earth resistance greyscale (averaged alpha & beta datasets) and integrated interpretation from the high-pass filtered and unfiltered results.

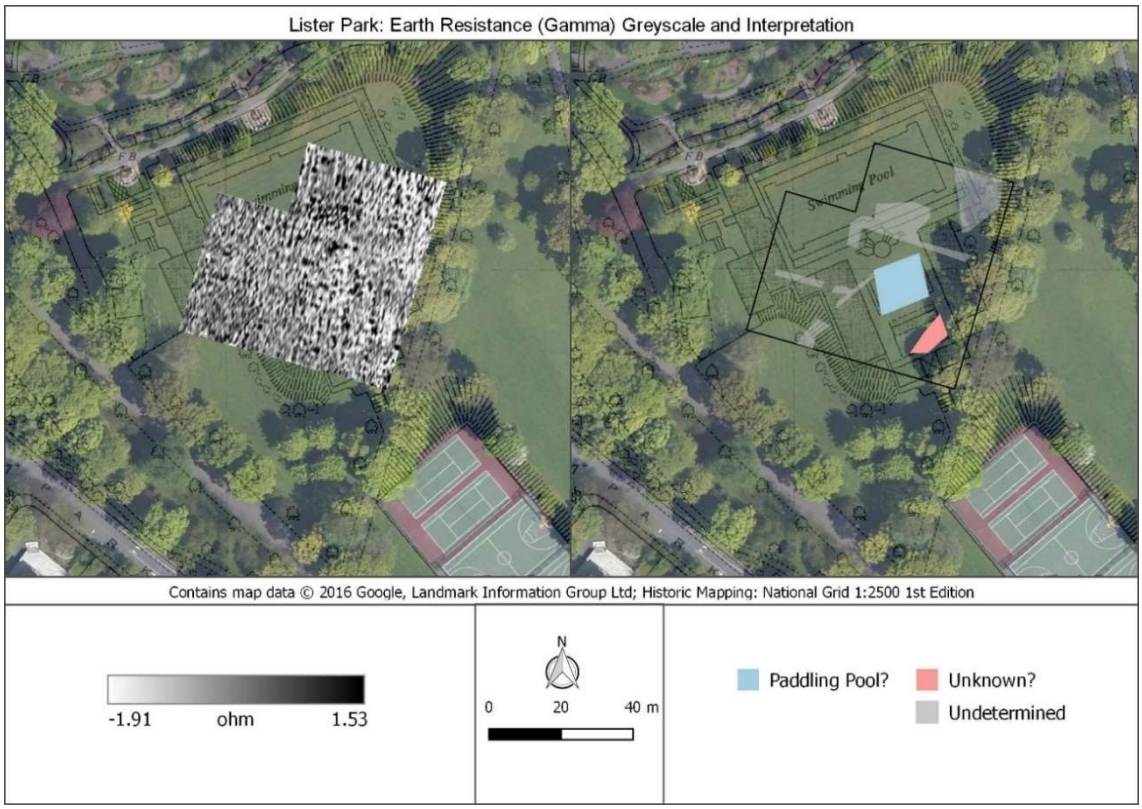

Figure 48: Lister Park earth resistance (gamma) greyscale and interpretation.

The earth resistance results at Lister Park primarily reflect the structural remains of the lido complex. Wall features are explicitly resolved in the averaged alpha and beta dataset as high-resistance linear anomalies, while the buildings' footprints are detected as low-resistance anomalies. The paddling pool is defined by a high-resistance rectilinear anomaly, but the main pool is not coherently defined at all (Figure 47). In contrast to the alpha and beta results, the gamma results are devoid of any clear anomalies that obviously relate to structural features. Considering that the square gamma configuration can be particularly effective for detecting structural edges, the Lister Park results are surprising (Figure 48). The calculated gamma (Equation 1) does not reveal any further structural features either (Figure 49). Given the similarities between the calculated and the measured gamma results, the lack of detection of the lido remains in both gamma datasets could be the effect of the orientation of the current electrodes relative to the orientation of the features.

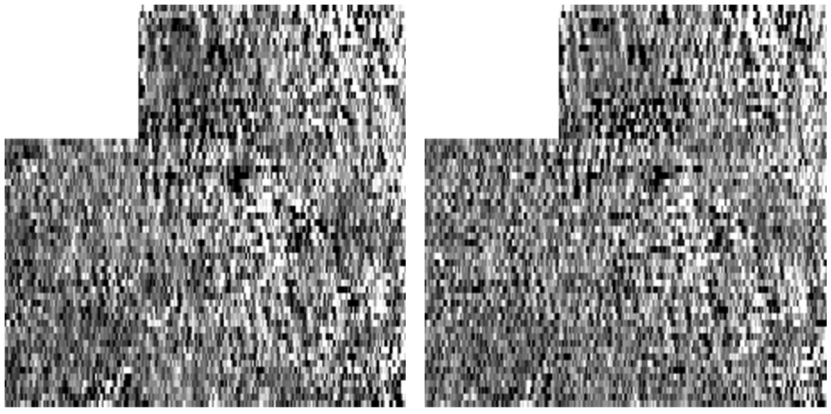

Figure 49: Comparison of the calculated gamma (left) and the measured gamma (right) at Lister Park.

The majority of the structural features detected in the earth resistance results occur in the eastern half of the survey area. In contrast, the western half of the site is relatively quiet. The western half of the survey area is significantly more elevated than the eastern half, which likely results from landscape modification following demolition of the lido complex. Assuming the square array's relatively shallow exploration depth, the thicker overburden in the western half of the site could inhibit the detection of structural remains in this area. However, if the earth resistance results were to be interpreted without comparison to the other methods, it would not be possible to prove whether this lack of detection is due to increased soil deposition or absence of features.

4.1.3 Lister Park: Electromagnetic Induction Quadrature-phase Results

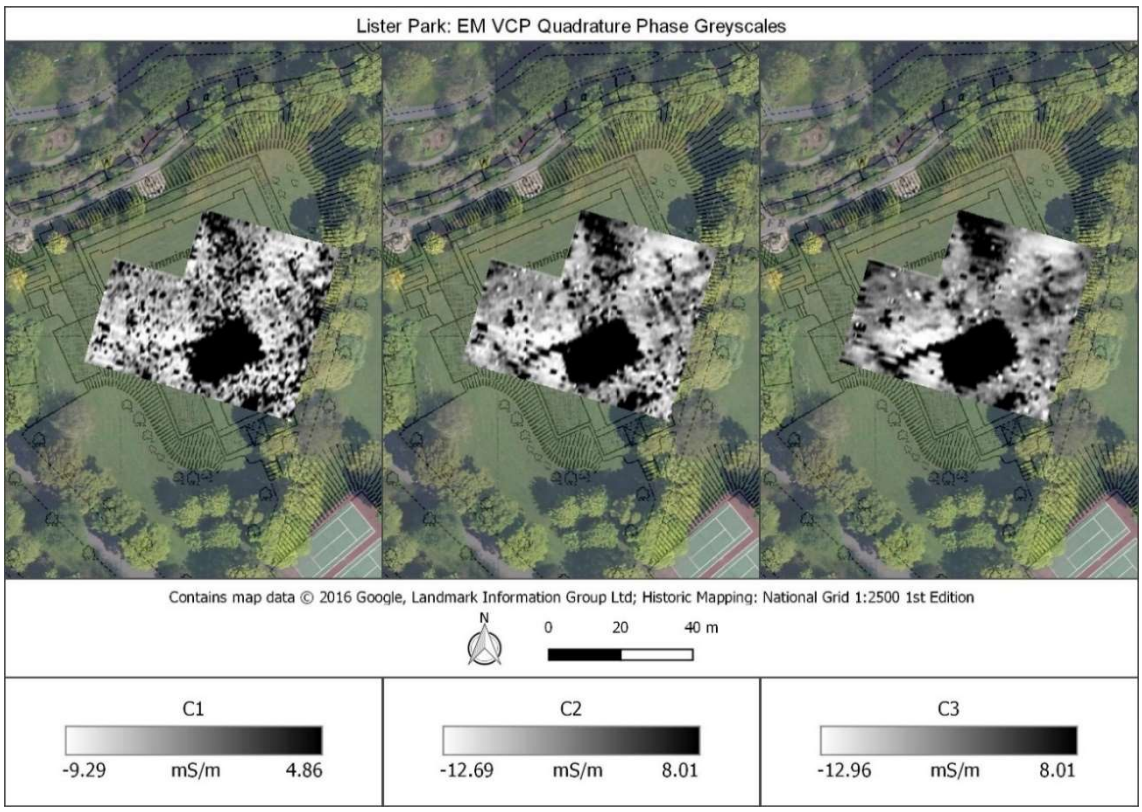

Figure 50: Lister Park electromagnetic induction (VCP quadrature-phase) greyscales.

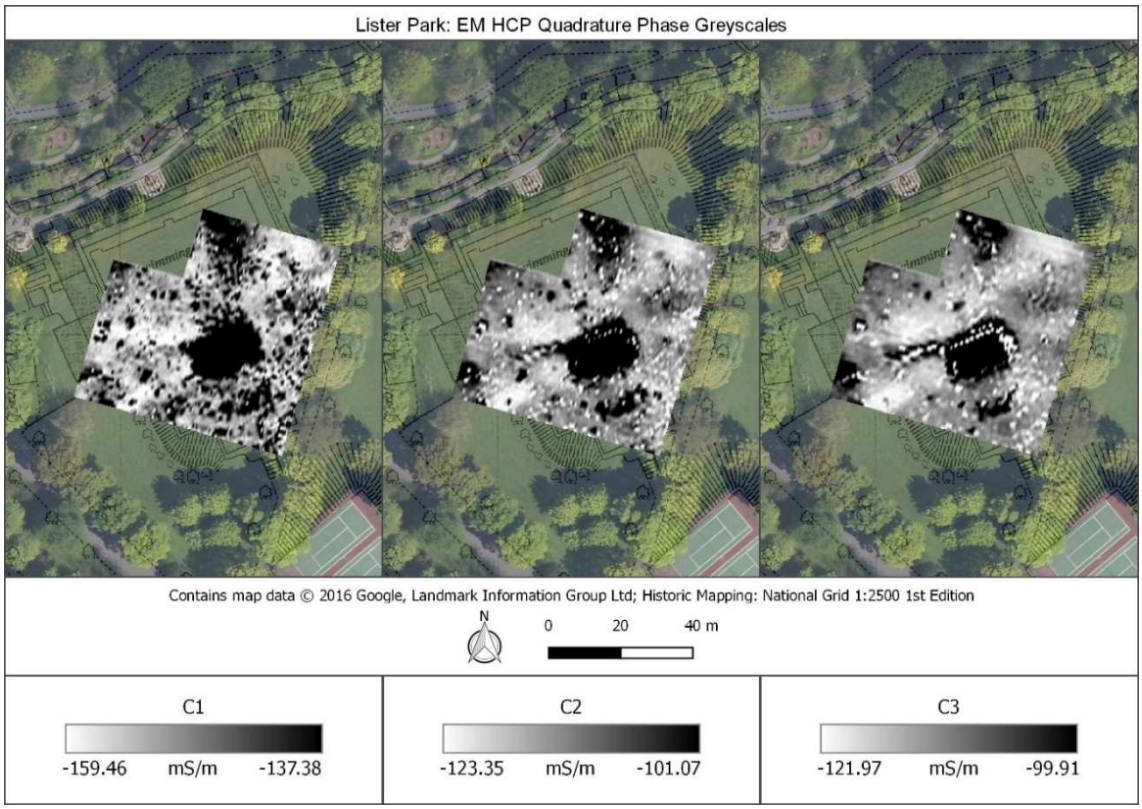

Figure 51: Lister Park electromagnetic induction (HCP quadrature-phase) greyscales.

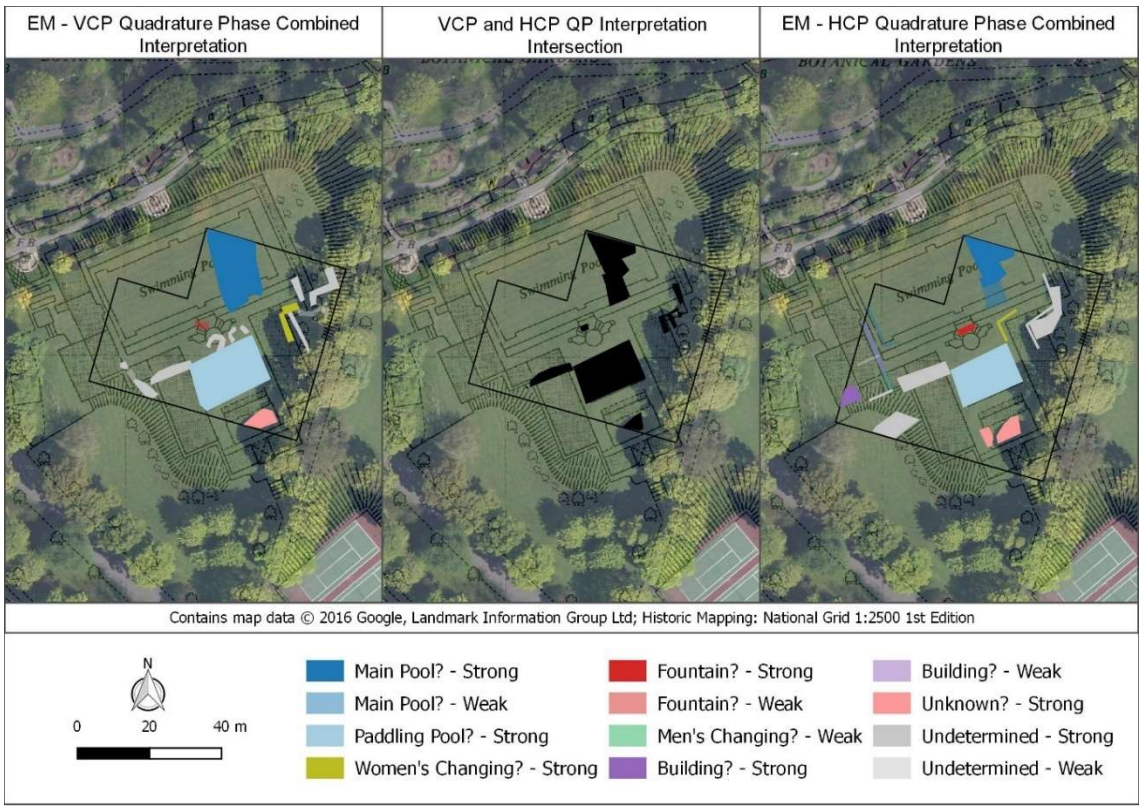

Figure 52: Interpretation of the VCP and HCP quadrature-phase orientations. “Strong” indicates the anomaly was detected in at least two of the datasets, while “weak” indicates the anomaly was detected only in one dataset. An intersection tool was performed on the respective interpretations to highlight common anomalies between the VCP and HCP orientations.

The EM quadrature-phase at Lister Park has responded well to the lido features. Near-surface debris has also been detected across the survey area as discrete point responses. In particular, the C1 datasets for both VCP and HCP configurations detects many of these responses, but the majority of these anomalies are not detected across the C2 and C3 results. For both HCP and VCP orientations, the quadrature-phase detects strong, high-contrast fill material within the pools. For the paddling pool, this material is spread within the entire footprint of the feature, but this is not the case in the main pool, where the response is concentrated at the eastern end.

For both HCP and VCP orientations, the resolution of the structural features, such as walls or feature edges, improves with increased depth. Both orientations also reveal a unique linear anomaly running westwards from the paddling pool that does not correlate with any structures on the historic mapping. This anomaly is most explicit in the deeper coils (C2 and C3) and therefore may be unrelated to the near-surface noise explicit in C1. A GIS geometric intersect tool was

performed on the HCP and VCP quadrature-phase interpretations to highlight common anomalies between the coil orientations (Figure 52).

The geometric intersection analysis of the HCP and VCP integrated interpretations demonstrates good correlation between the different coil orientations. Responses corresponding to the main pool, paddling pool, women's changing room, fountain and unknown feature resolved in both HCP and VCP results. However, the location of the responses correlating with these features are concentrated in different areas between the coil orientations. For instance, the HCP orientation detects a greater number of anomalies than the VCP orientation in the western half of the survey area; the HCP results reveal edges that correlate with the men's changing room and unnamed building in this area. Inversely, the VCP orientation performs better in the eastern half of the survey area than the HCP orientation, as the women's changing room and undetermined rectilinear anomalies are more explicitly defined.

The VCP and HCP orientations also differ in the response form of the paddling pool. In the VCP results, the paddling pool is distinctly resolved as a completely positive-contrast anomaly. In the HCP results, discrete negative-contrast peaks appear in alignment around the perimeter of the anomaly in C2 and C3. The distance between these peaks ranges from 1.5 – 2.0m. The spacing and patterning of these negative-contrast peaks corresponds with the dimensions of a hand railing evident in a historic photograph of the paddling pool (Figure 53). The detection of these responses suggests that when the railing was removed, the bases were left intact. The detection of the railing in only the HCP C2 and C3 datasets also informs the relative depth of the feature, as it must lie deeper than the VCP's detection range.

Figure 53: Historic photograph of Lister Park's paddling pool. Image source unknown.

Overall, at Lister Park, both VCP and HCP quadrature-phase orientations are detecting common features across the receiving coils. Therefore, combining the respective receiving coils' datasets through arithmetic processes into a composite image should be effective for conveying the sum of the results. From this point onwards, only the HCP quadrature-phase results will be discussed, as they will be used for integration with the other survey techniques. The HCP orientation reveals further information about the nature of the paddling pool feature (e.g. the railing) than the VCP results and is therefore more informative. In order to effectively combine the separate HCP datasets, a histogram of the results was create to visualise the spread and range of the different receiving coils (Figure 54).

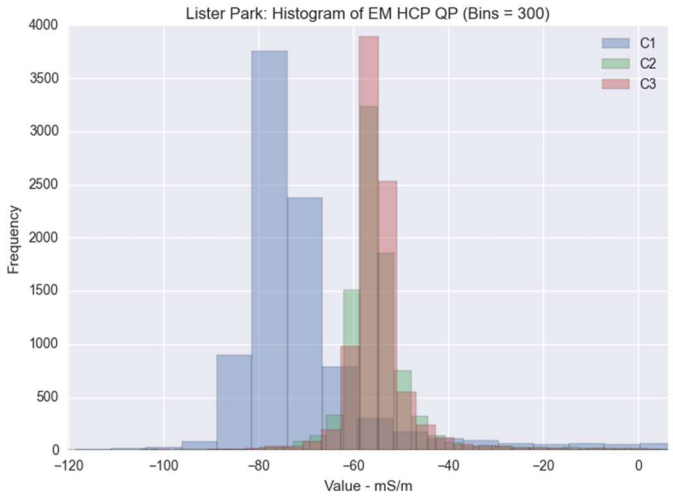

Figure 54: Histograms of Lister Park's EM HCP quadrature-phase results to visualise the differences between the individual coils' distribution and range.

The histograms reveal that the quadrature-phase coils are not evenly distributed around a common measurement value. C1 has a much wider distribution and greater dynamic range than C2 and C3. Thus, the C1 dataset will have a dominating contribution over C2 and C3 if a direct mean of the datasets is taken. To balance the contribution of the different coils, the respective datasets were normalised first. The resulting mean image represents the contributions of all the receiving coils. Figure 55 presents the results of the mean and a principal component analysis undertaken on the HCP quadrature-phase datasets.

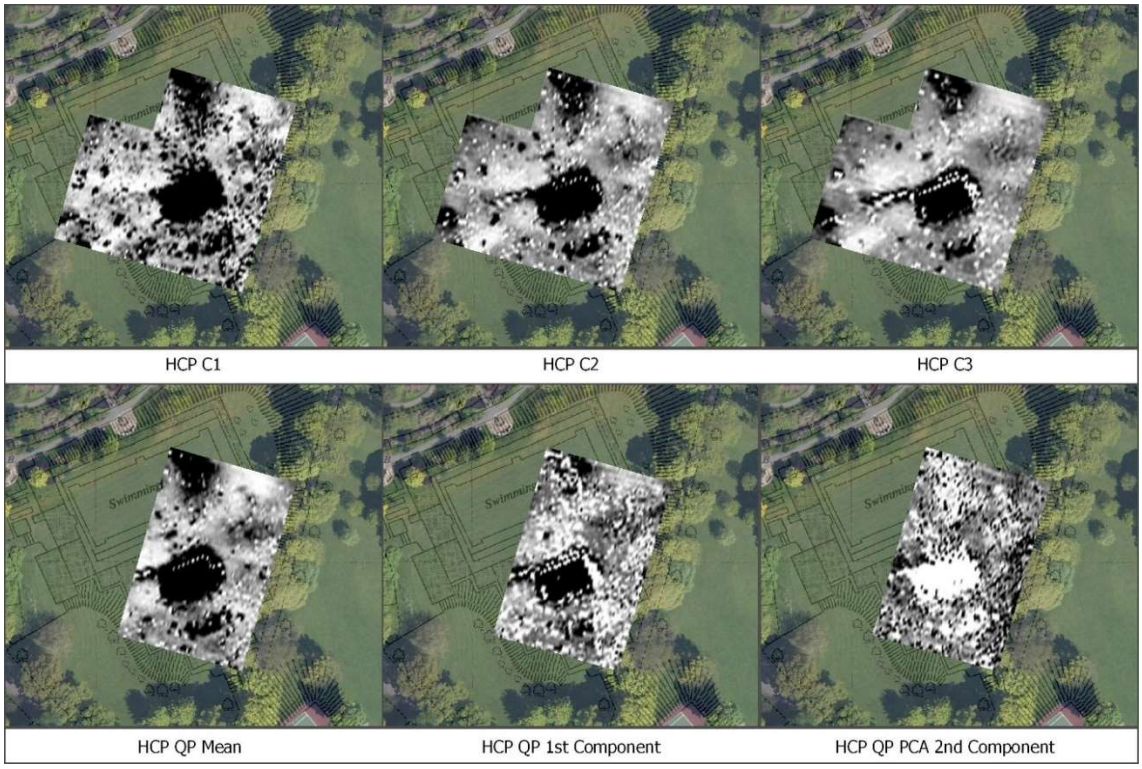

Figure 55: Comparison of the Lister Park HCP quadrature-phase coils against (lower row: left-right) the mean of the coils, first principal component and second principal component after the individual input datasets had been normalised. Map data: © Google 2016, © Landmark Information Group. Historic mapping: National Grid, 1:2500 1st Edition.

The mean image is a good representation of most of the key aspects of the individual HCP quadrature-phase datasets. The shapes of the paddling pool and unknown feature's responses are distinct in the mean image; most aspects of the railing feature in C2 and C3 are visible as well. Further rectilinear anomalies immediately east of the paddling pool are highlighted in the mean image, in contrast to their less distinct form in C1 and C2. And finally, the scattered discrete near-surface debris in C1 is represented in the mean image, but do not dominate and obscure the key features. In contrast, the principal component analysis produces outputs that are less effective as composite images, but still are

informative for highlighting specific aspects of the results. For example, the first and second principal components highlight the near-surface noise in the C1 and C2 results, which obscures the context of the other features. However, despite the noise, certain structural features are still discernible. In the first principal component, the fountain's anomaly is distinctly visible. The railing feature is also visible and a second alignment of negative peaks at the paddling pool's northern edge is visualised as well. Additional lido features can be identified in the second component result that are absent in both the mean and first component images. For example, a weak linear anomaly correlates with a wall of the women's changing room. This feature is not distinctly explicit in any of the individual quadrature-phase results, but its exact correlation with a structural feature suggests the anomaly represents an aspect of the quadrature-phase results and is not an erroneous measurement. The boundary of the walls and the seating associated with the main swimming pool are also more clearly defined in the second component results than they are in the individual datasets. Overall, the principal components highlight different aspects of the HCP quadrature-phase results; whereas the mean image provides an effective representation of the constituent parts. For interpretation purposes, the mean image is the most effective representation of the combined results, but the principal components offer insight into the similarities and differences between the different datasets.

4.1.4 Lister Park: Electromagnetic Induction In-Phase Results

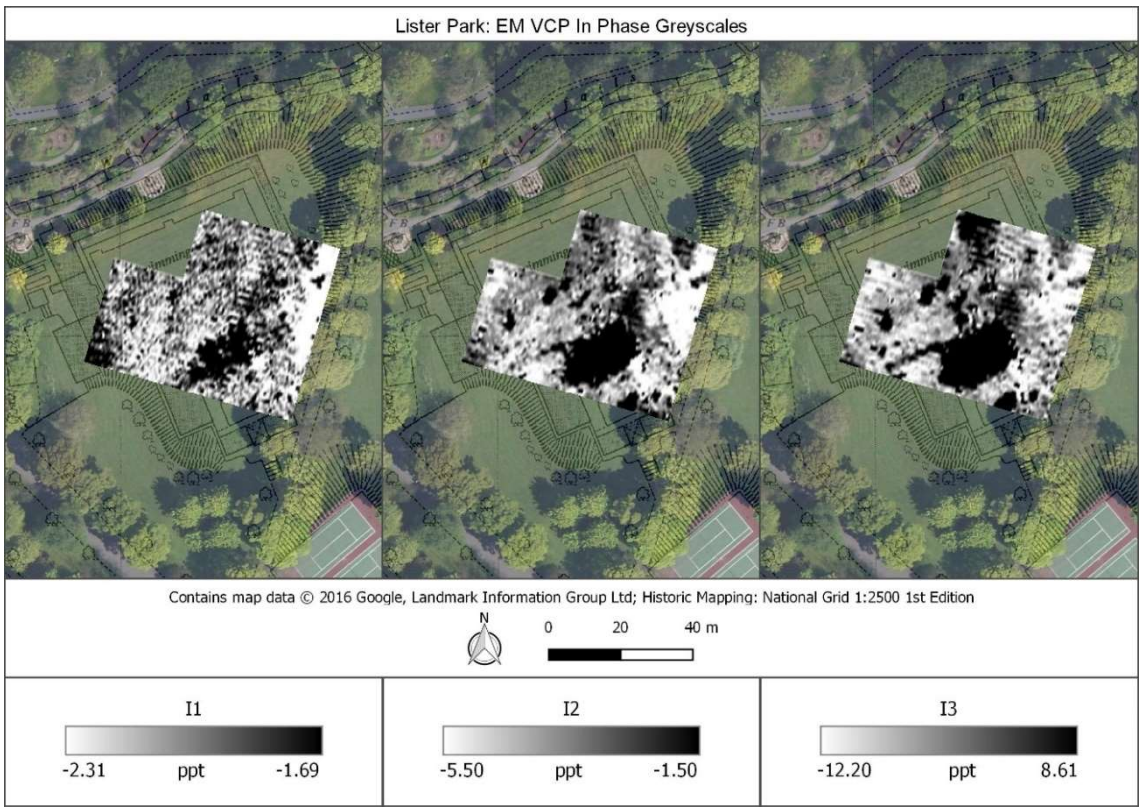

Figure 56: Lister Park electromagnetic induction (VCP in-phase) greyscales.

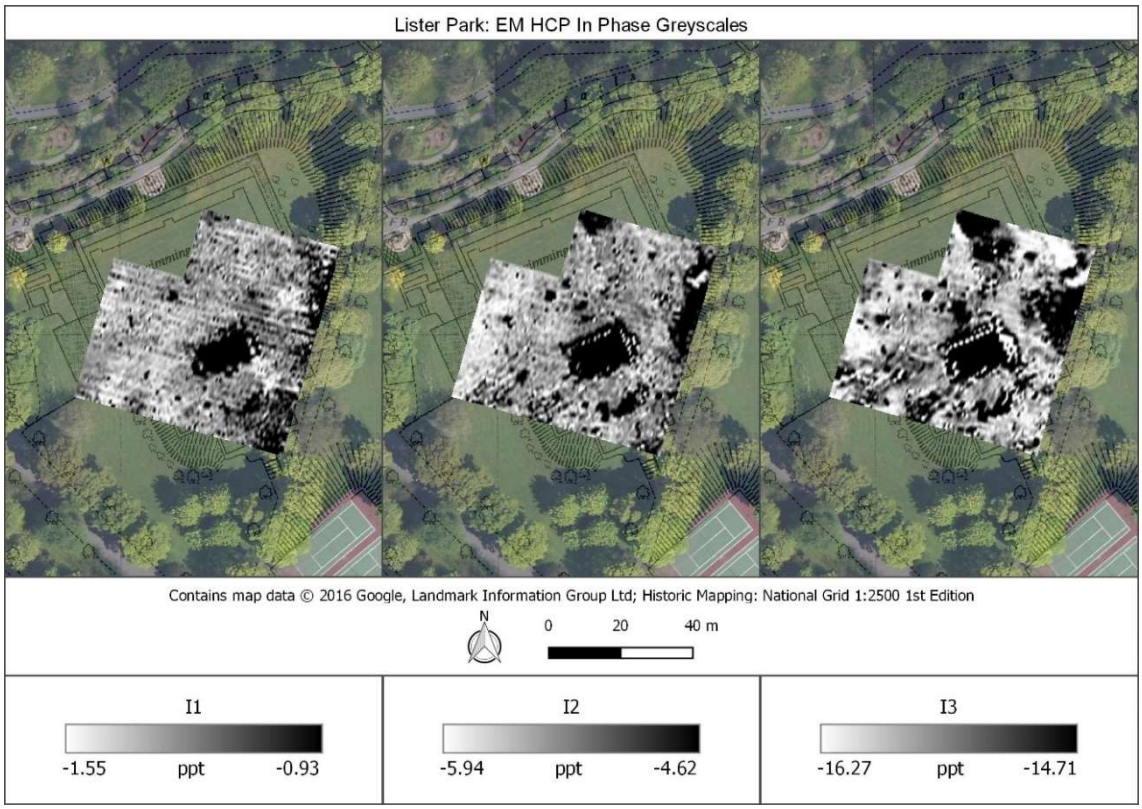

Figure 57: Lister Park electromagnetic induction (HCP in-phase) greyscales.

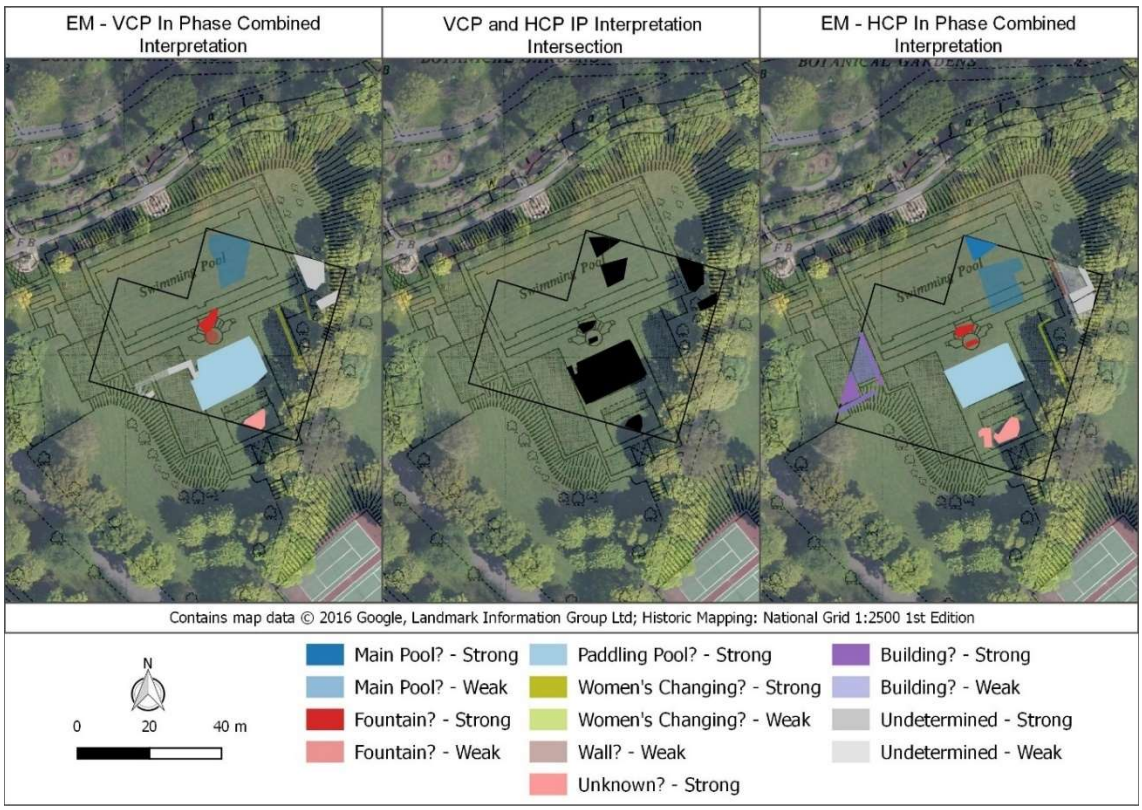

Figure 58: Interpretation of the VCP and HCP in-phase orientations. “Strong” indicates the anomaly was detected in at least two of the datasets, while “weak” indicates the anomaly was detected only in one dataset. An intersection tool was performed on the respective interpretations to highlight common anomalies between the VCP and HCP orientations.

The EM in-phase results at Lister Park primarily reflect structural features and fill material contained within these remains (Figure 56; Figure 57). Particularly in the eastern half of the site, anomalies correlating with the walls of the women’s changing room and edges of nearby buildings are explicit in the results. In the western half of the site, the HCP orientation detects further features than the VCP orientation by delineating walls and the edges of building features. Overall, for both orientations, the lido features, particularly the paddling pool, fountain and women’s changing room, are more wholly resolved in the larger coil separations. Thus, the differences in exploration depth and sensitivity are apparent between the VCP and HCP orientations. For example, the VCP orientation is more susceptible to near-surface noise, particularly in the I1 and I2 datasets. The paddling pool feature is discretely defined in the HCP results; whereas, in the VCP results, the anomalous form is broader than the mapped feature. Furthermore, the railing feature is not evident in the VCP results, while in the HCP results it is coherent in I2 and I3. Overall, at Lister Park, both VCP and HCP in-phase orientations are detecting common features across the receiving coils, but to a different degree of clarity depending on the depth to the feature. Only the

HCP results will be discussed in the further subsequent data combination sections, given their superior performance over the VCP orientation at Lister Park.

It was found in the HCP results, the deeper the exploration depth, the more features were being detected. Therefore, at Lister Park, an increased contribution from I3 is desirable when producing a composite in-phase image, than to have equal contributions from all soil volumes and obscure the responses of archaeological responses. Analysis of the histograms visualises the wider distribution and greater dynamic range of I3, in contrast to I1 and I2 (Figure 59).

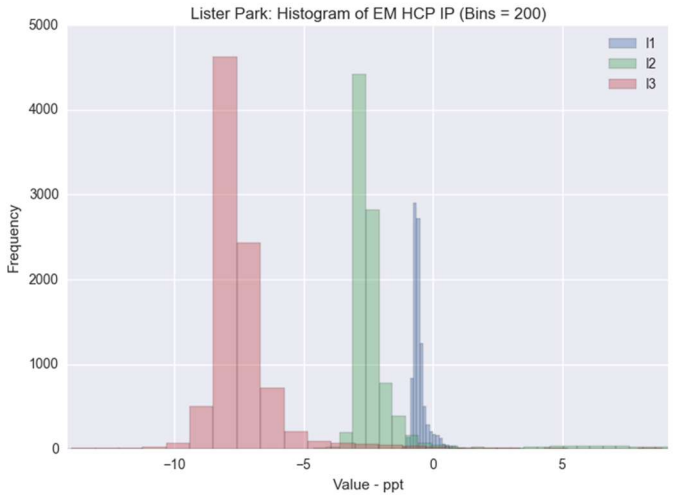

Figure 59: Histograms of Lister Park's HCP in-phase results, showing the differences between the individual coils' distribution and dynamic range.

Normalising the datasets before taking a mean of results produces a disappointing composite image. Because the shallower exploration depths are given equal contribution, the comprehensive information regarding the archaeological features is lost (Figure 60). For example, the equal contribution of I1 obscures the fountain anomaly and linear anomalies in the eastern half of the site. These features are more explicit in the mean image when the datasets are not normalised beforehand, because the larger coil separations that contain responses relating to archaeological features dominate the mean (Figure 60).

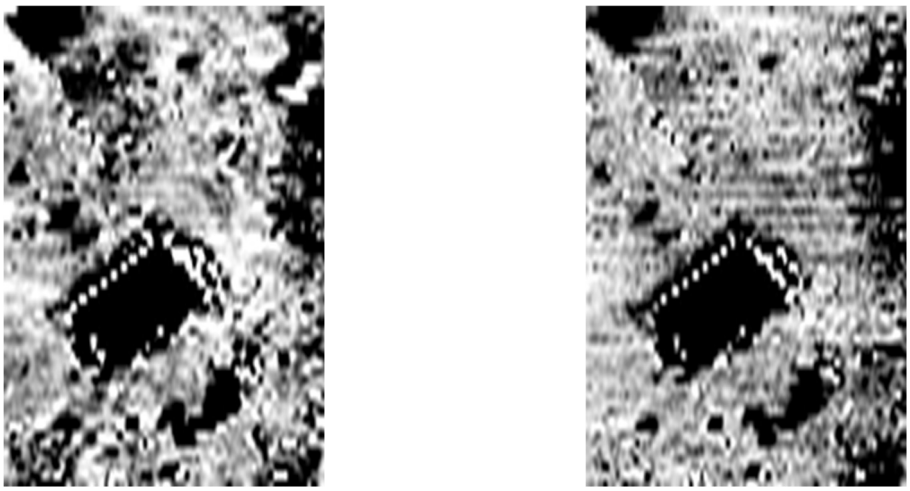

Figure 60: (left) Mean of Lister Park HCP in-phase datasets and (right) mean of normalised datasets.

The mean of the non-normalised datasets provides a more descriptive image of the buried features than the normalised results do. The first principal component is remarkably similar to the mean image, but improves the results slightly by reducing some of the striping between the lines and improving the definition of the women's changing room. On the other hand, the second principal component image is distinct from the mean and first principal component images. The second principal component instead represents the characterising anomalies of the I1 and I2 datasets: the near-surface noise and the amorphous area of high contrast at the eastern edge.

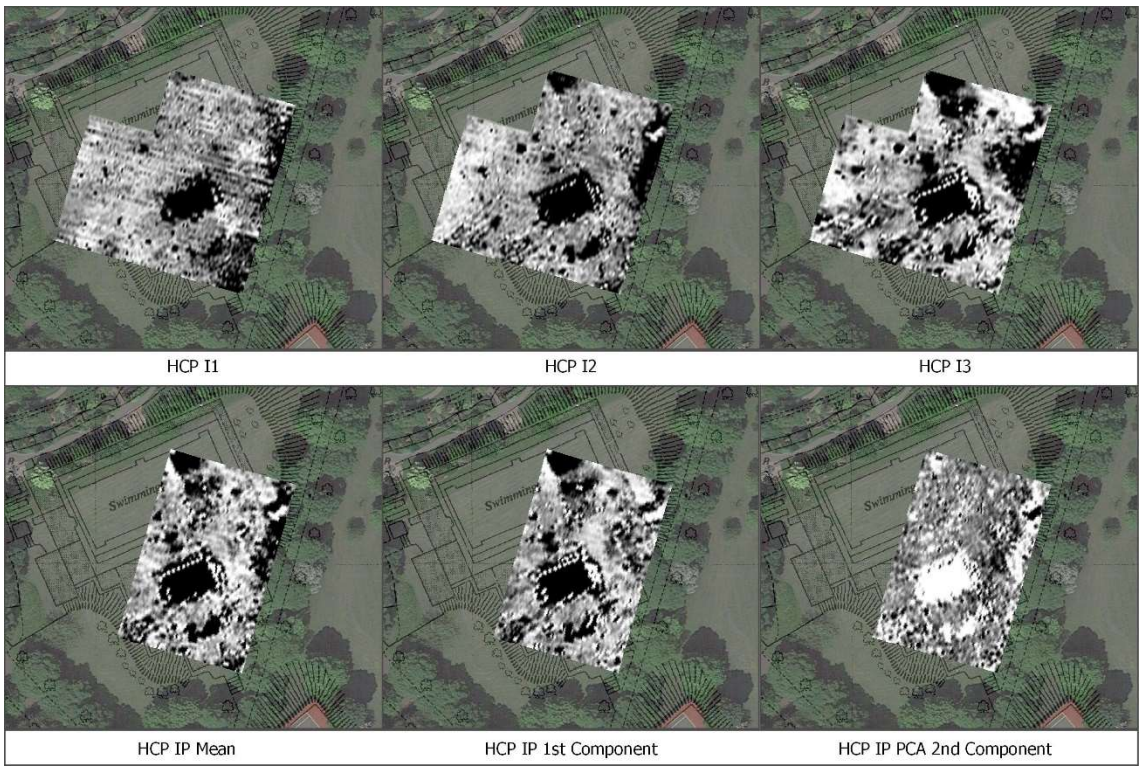

Figure 61: Comparison of the Lister Park HCP in-phase coils against (lower row: left-right) the mean of the coils, first principal component and second principal component. Map data: © Google 2016, © 2016 Infoterra Ltd & Bluesky. Historic mapping: National Grid, 1:2500 1st Edition.

Overall, the EM in-phase results demonstrate the method has been effective at Lister Park. The in-phase has detected anomalies relating to structural features, debris and near-surface noise. The following section will analyse the in-phase and quadrature-phase in relation to each other with the aim to better characterise the performance of the instrument on site.

4.1.5 Lister Park: Integration of EM Results and Composite Analysis

The EM quadrature-phase and in-phase will first be cross-analysed by comparing their correlating anomalies. Anomalies that correlate across the phases could indicate they are being generated from highly conductive and/or magnetic material—potentially ferromagnetic in origin and/or maintain a strong, defined presence through the soil column. Conversely, anomalies detected in only one phase would indicate the feature possesses distinct properties that are more associated to the specific phase it occurs in. Figure 62 presents the results of running an intersection analysis on the respective in-phase and quadrature-phase results of the VCP and HCP orientations.

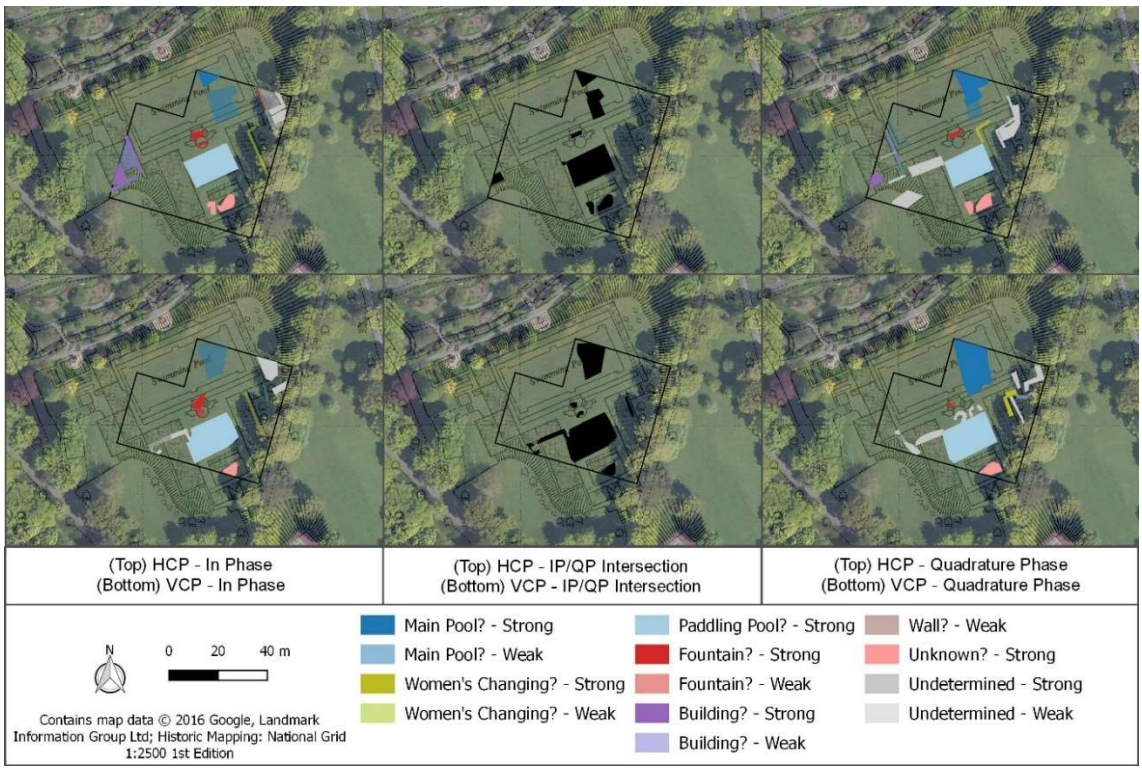

Figure 62: Lister Park EM interpretations. “Strong” indicates the anomaly was detected in at least two of the datasets, while “weak” indicates the anomaly was detected only in one dataset. GIS intersection tool has been run on the HCP and VCP interpretations of the respective in-phase and quadrature-phase to compare the overall similarities between the in-phase and quadrature-phase results.

Both HCP and VCP orientations demonstrate good correlation between their respective in-phases and quadrature-phases, resolving similar anomalies for the main pool, paddling pool, fountain, women's changing room, unnamed building, unknown and undetermined features. Furthermore, comparison of the HCP and VCP intersection results also demonstrates there is good correlation between the different coil orientations as well. The VCP orientation overall is more broad in its response form than the HCP orientation, which better matches the dimensions of the mapped feature. Considering the different exploration depths between the coil orientations and between the different phases, the remains of the lido features must lie relatively near surface and possess a defined presence with depth to produce comparable results between all the datasets. The only feature which is absent from the composite results is the linear anomaly extending westwards from the paddling pool, in the HCP in-phase results. The lack of detection is surprising, given the overall superior performance of the HCP orientation over the VCP orientation in the western half of the site. A closer look at the first principal component results reveals a portion of this feature is visible in the HCP in-phase PCA results, a feature which is not distinguishable in the

individual datasets (Figure 61). The strong correlation between the in-phase and quadrature-phase results suggests the instrument is responding to highly conductive and magnetic material—anticipated to be ferromagnetic in origin. Integration with the earth resistance and magnetic results in the following section will provide correlating evidence to support the nature of the material remains.

4.1.6 Lister Park: Integrated Interpretation and Archaeological Characterisation

The magnetic, earth resistance and EM results at Lister Park all reveal features relating to the lido complex. The magnetic and earth resistance results are distinct to one another and reveal the different methods have responded to different aspects of the same features. The EM results, on the other hand, share correlating anomalies to the magnetic and earth resistance results, which indicates the method is responding to similar aspects of the same features. Identifying where the different methods are responding to the same feature benefits from the Ordnance Survey maps of the buried features. The cross-comparison of the different results against the map features would suggest a binary Boolean combination strategy could be effective for quantifying where the individual results are detecting common features. However, the difficulty at Lister Park, is that structural remains are represented both as anomalies and defined by the absence of anomalies. The absence of anomalies defining structural remains is particularly evident in the magnetic results where some features, like the changing rooms, lack a magnetically enhanced fill. As a result, the changing rooms are not detected by correlating anomalies, but instead are defined by the lack of anomalies with the boundaries of the features defined by external activity. Therefore, a binary Boolean approach would not provide a comprehensive or accurate understanding of what techniques are seeing what features and where. Given the nature of the different results, arithmetic and image overlay integration strategies were applied instead.

The arithmetic mean of the results provides an accurate composite image of the different geophysical methods. The sum of the high-contrast anomalies produces a composite image that represents the key components of the different results (Figure 63). The earth resistance responses contribute to the linear walls of the women’s changing room, the southern edge of the main pool and the floors of the

entrance area; the magnetic responses contribute to the spread of material within the main pool, which in the composite image is bound by the defined walls from the earth resistance results; the EM results primarily contribute to the response of the paddling pool, particularly the railing along the perimeter.

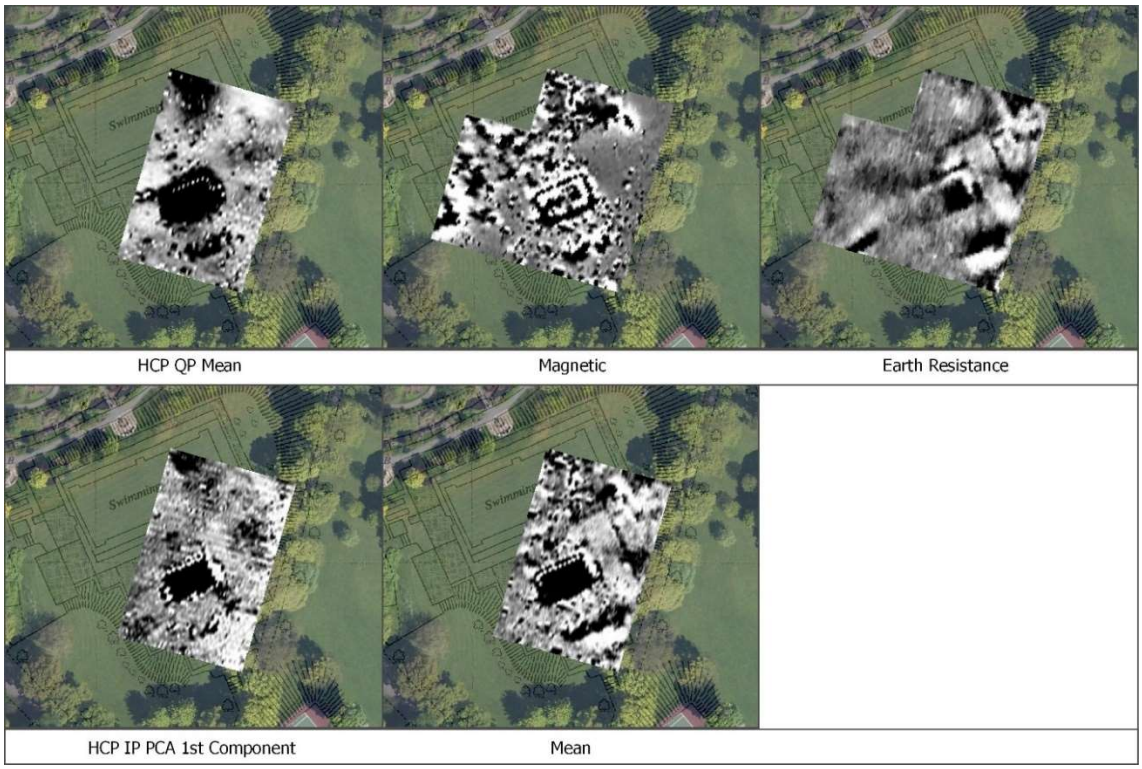

Figure 63: The mean of the geophysical methods at Lister Park after the individual input datasets had been standardised. Map data: © Google 2016, © 2016 Landmark Information Group. Historic mapping: National Grid, 1:2500 1st Edition.

Following the averaging of the results, a principal component analysis of the different methods was performed (Figure 64).

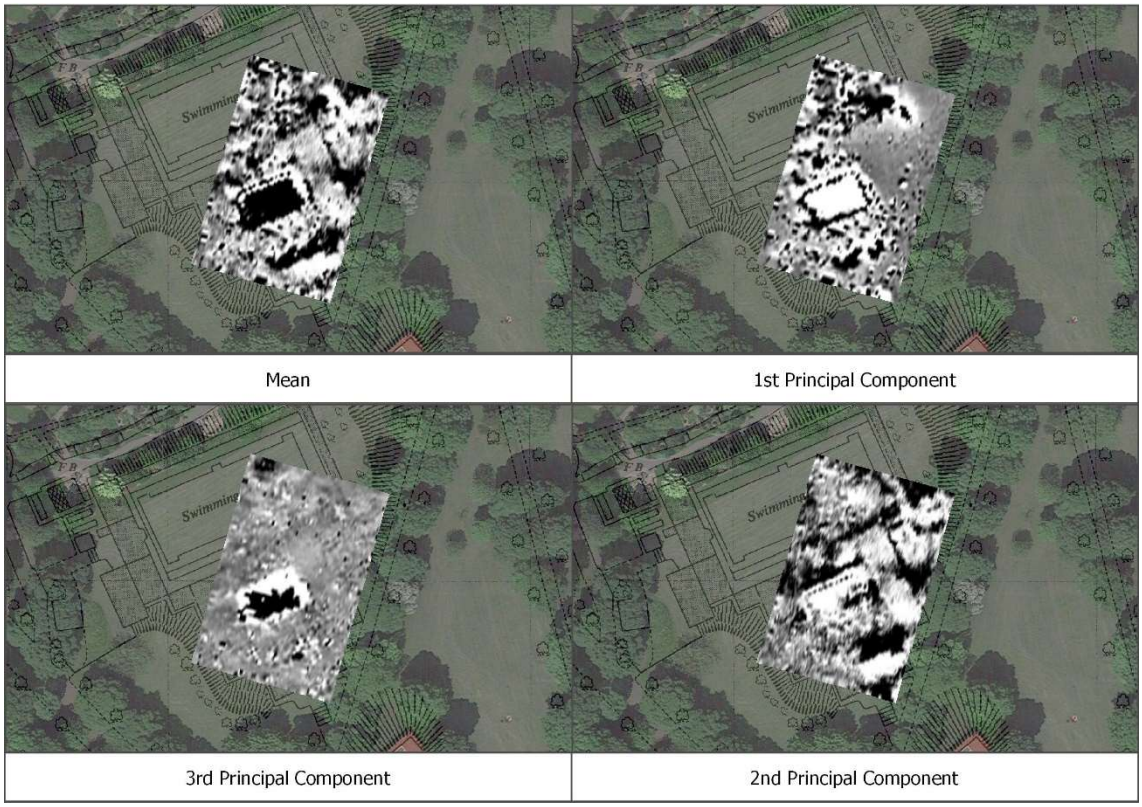

Figure 64: Comparison of the mean of the geophysical results at Lister Park with the first, second and third principal components of the standardised magnetic, earth resistance and EM results. Map data: © Google 2016, © 2016 Infoterra Ltd & Bluesky. Historic mapping: National Grid, 1:2500 1st Edition.

Overall, the principal components are less effective for representing the constituent datasets than the mean image is. Each of the first three principal components bears a distinct resemblance to a particular individual method (Figure 64). For example, the first principal component has a distinct resemblance to the magnetic results, while the second principal component to the walls and floors in the earth resistance results, and the third principal component to the paddling pool and near-surface noise in the EM results. The distinctness of the principal components can be understood through the correlation matrix (Table 13) and the histogram of the methods (Figure 65).

The histogram of the methods visualises why the individual results are poorly correlated. The magnetic method is centred around zero, but shows two positive and negative spikes in readings where the ferrous material produces overwhelming responses that swamp the limits of the instrument's dynamic range (Figure 65). Consequently, the 1st principal component highlights these very high contrast anomalies.

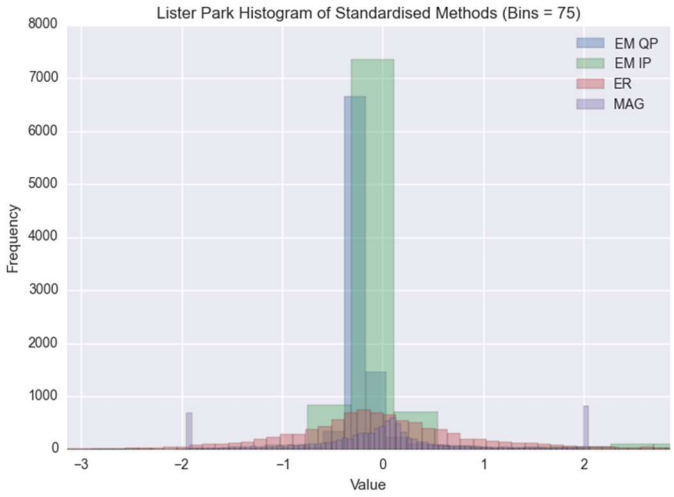

Figure 65: Histogram of the standardised geophysical methods at Lister Park.

The correlation matrix confirms that the magnetic method is the most uncorrelated to the other methods. Unsurprisingly, the EM in-phase and quadrature-phase share the most correlation. Surprisingly, the earth resistance method shows poor correlation to the in-phase and no correlation to the quadrature-phase. The magnetic method shows no correlation to the other methods. This poor correlation between the different methods would account for the distinctness between the principal components.

	EM QP	**EM IP**	**ER**	**MAG**
EM QP	1.00	0.56	0.05	0.03
EM IP	0.56	1.00	0.21	0.04
ER	0.05	0.21	1.00	0.01
MAG	0.03	0.04	0.01	1.00

Table 13: Lister Park correlation matrix of methods.

A graphical integration approach was undertaken by producing a CMYK image (Figure 66). The CMYK image was created using the following layers: C = magnetic dataset; M = normalised in-phase mean dataset; C = normalised quadrature-phase mean dataset; K = earth resistance dataset. The CMYK overlay image was created using the normalised mean EM datasets, as the PCA and un-normalised datasets produced too noisy an image.

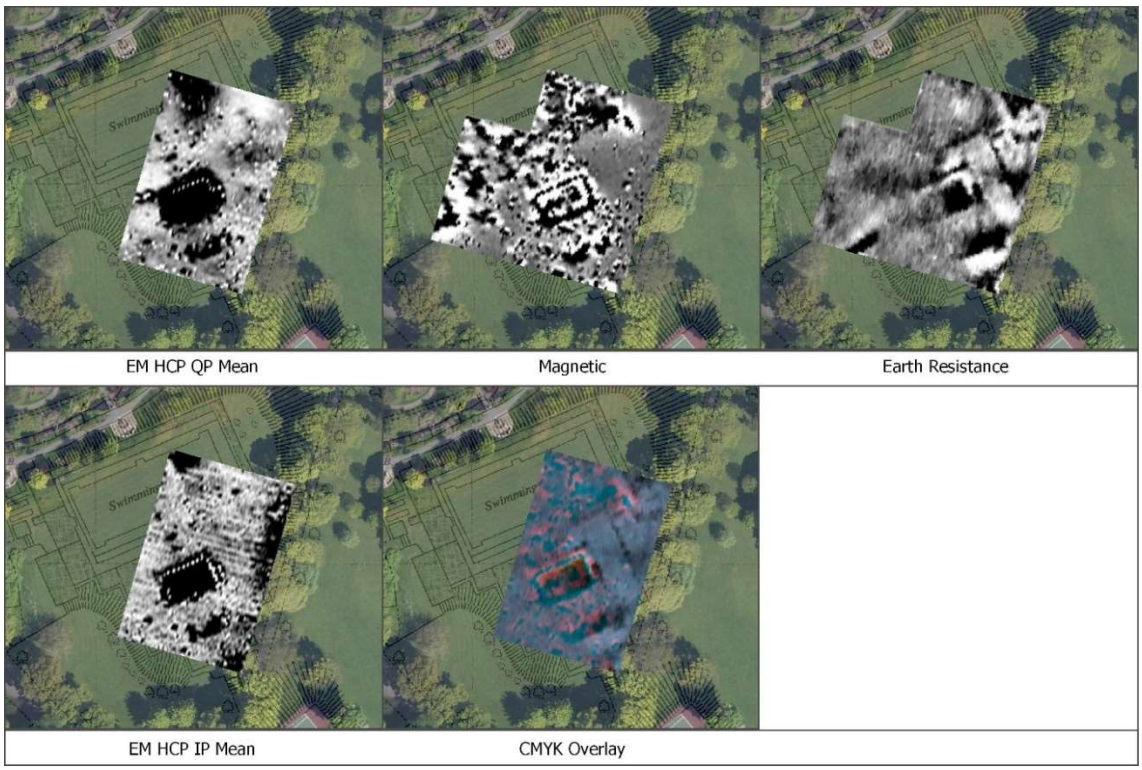

Figure 66: Lister Park CMYK overlay where C = magnetic data, M = in-phase data, Y = quadrature-phase data and K = earth resistance data. Map data: © Google 2016, © Landmark Information Group. Historic mapping: National Grid, 1:2500 1st Edition.

The overlay of the dipolar magnetic anomalies against the other methods combines to illuminate areas exhibiting strong magnetic properties (Figure 66). These strongly magnetic anomalies are bounded by the walls in the earth resistance data, which emphasises the distinctly empty footprint of the women's changing room and neighbouring buildings. Between the different methods, the features that are detected by all the techniques are limited to the paddling pool and the unknown feature directly south of the paddling pool. The analysis of these combination results will be presented below.

The combination of the different Lister Park datasets offers insights into the relationships of the different techniques to one another. The archaeological characterisation developed through this integrated interpretation will be explored using the features denoted in the historic mapping as common reference points (Figure 44).

- *Main Pool*—Anomalies associated with the location of the main pool have been detected by the magnetic and electromagnetic induction methods. The most explicit responses occur in the magnetic results, which reveal

the pool has been refilled with highly magnetic material. The mean of the methods confirms that these responses are confined within the edges of the main pool, demonstrated by the wall features contributed by the earth resistance results. However, the magnetic and EM results reveal what while the material occurs within the limits of the main pool, the extent of this material is not formed by the edges of the pool itself. An analytic signal of the magnetic results defines a denser concentration of this material in the eastern half of the pool, with a distinct western edge that is not formed by the boundary of the pool. This concentration correlates with a strong, positive contrast anomaly in the EM quadrature-phase and in-phase results, but this anomaly does not extend across the footprint of the main pool. In the quadrature-phase, this response is most explicit in the C3 soil volume of the VCP results and the C1 volume in the HCP results. Considering the depth sensitivities of these configurations, the approximate depth to this feature should be greater than 0.5 m. This depth range is beyond the theoretical depth of investigation for the square array, which supports the interpretation it was not detected by the earth resistance methods due to thick overburden.

- *Paddling Pool*—Anomalies associated with the footprint of the paddling pool have been detected by all the earth resistance and EM methods as a solid high-contrast response. The paddling pool feature is also detected in the magnetic results, but only the perimeter of the pool and two central features are defined. The analytic signal results do not indicate a dense concentration of magnetic anomalies within the paddling pool, but the detection of a solid fill in the other methods suggests there is refill debris, that must be poorly magnetic. The detection of this feature in the in-phase would therefore suggest the fill contains highly conductive materials, as this material could produce an overwhelming response that would lead to a blending of the different phases. However, the detection of the paddling pool in the earth resistance as a high resistance feature indicates the fill material is insulating as well. The quadrature-phase and the in-phase of the HCP EM survey have detected the bases of the railing enclosing the paddling pool as negative peaks. The railing feature is not detected in the VCP results. However, this is not indicative of a deeper feature as these

railings are visible in the HCP R1 separation, which theoretically should equate to a shallower depth than VCP R3. The graphical overlay of the results reveals correlation between the railing anomalies in the EM datasets with a block-like delineation of the NE, SE and SW edges in the magnetic results. This interpretation of the railing feature in the magnetic results would be difficult to identify as an archaeological feature without the supporting EM results, as the blocking also resembles cart-based staggering and/or interpolation issues.

- *Changing Rooms*—The earth resistance results clearly delineate the walls of the women's changing room, but the men's changing room is not detected. The EM quadrature-phase and in-phase results both reveal the footprint to the women's changing rooms. Wall features are also explicit in the in-phase datasets, but not the individual quadrature-phase results; although a wall feature is visible in the second principal component of the quadrature-phase. The magnetic results also show a comparatively quiet area, which shows this structure was not backfilled with material. In comparison, the men's changing room has not been as successfully detected. The footprint of the building is visible in the magnetic results, with the edges delineated by a scatter of magnetic anomalies. However, the EM in-phase results do not show any indication of this feature. The building is poorly resolved in the quadrature-phase as well, with only the westernmost edge only detected in HCP C3. Considering the earth resistance results did not detect any anomalies in this area either, this area may have increased soil deposition than the eastern area.

4.1.8 Lister Park: Conclusions

The geophysical investigations at Lister Park have been effective for mapping the remains of the lido complex. The individual datasets at Lister Park worked well within the integration strategies. Each individual method contributed unique information that has resulted in a more complete understanding not only of the buried archaeology, but of the surrounding soil matrix as well. The multiple exploration depths provided by the EM survey proved particularly useful at this site, due to the thicker overburden material over the western end of site. Evaluating the performance of the geophysical methods in relation to the natural

pedological and geological setting is difficult however, given the recent modern interference. However, all the methods responded well to the site conditions—despite areas of considerable mud during the survey events.

4.2 Fountains Abbey: Results and Characterisation

The following results from Fountains Abbey, near Ripon, North Yorkshire formed a portion of the investigations targeting the location of the remains of the former guest hall (refer to section 3.3.4.2 for a detailed site description). A single pillar base comprises the only extant remains of the building, with the rest of the building remains buried beneath the ground surface. The building's remains were previously recorded through a detailed twin-probe survey by the University of York in the early 1990s; further wall features were detected to the east of the hall as well, representing an unknown structure and the cellarer's yard immediately south-west of the nave. The following geophysical results expand on this previous survey by utilising different methods and multiple exploration depths.

4.2.1 Fountains Abbey: Earth Resistance Results

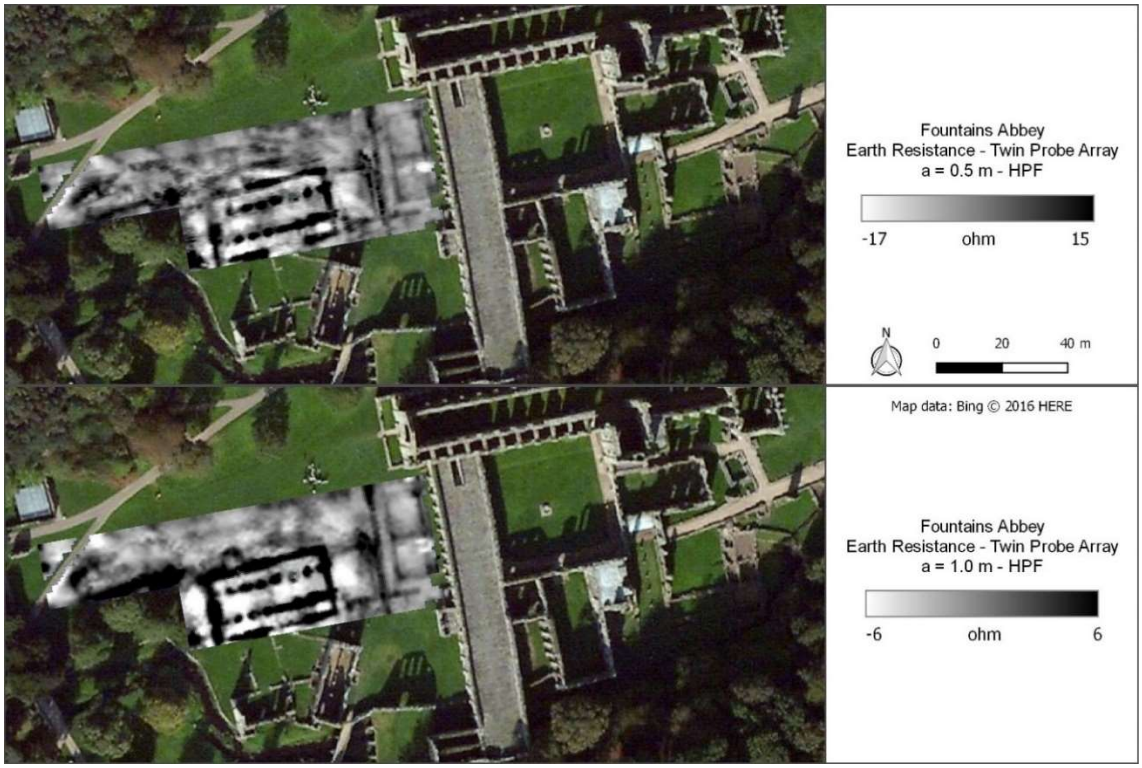

Figure 67: Fountains Abbey earth resistance (a = 0.5 m and a = 1.0 m twin-probe array) greyscales.

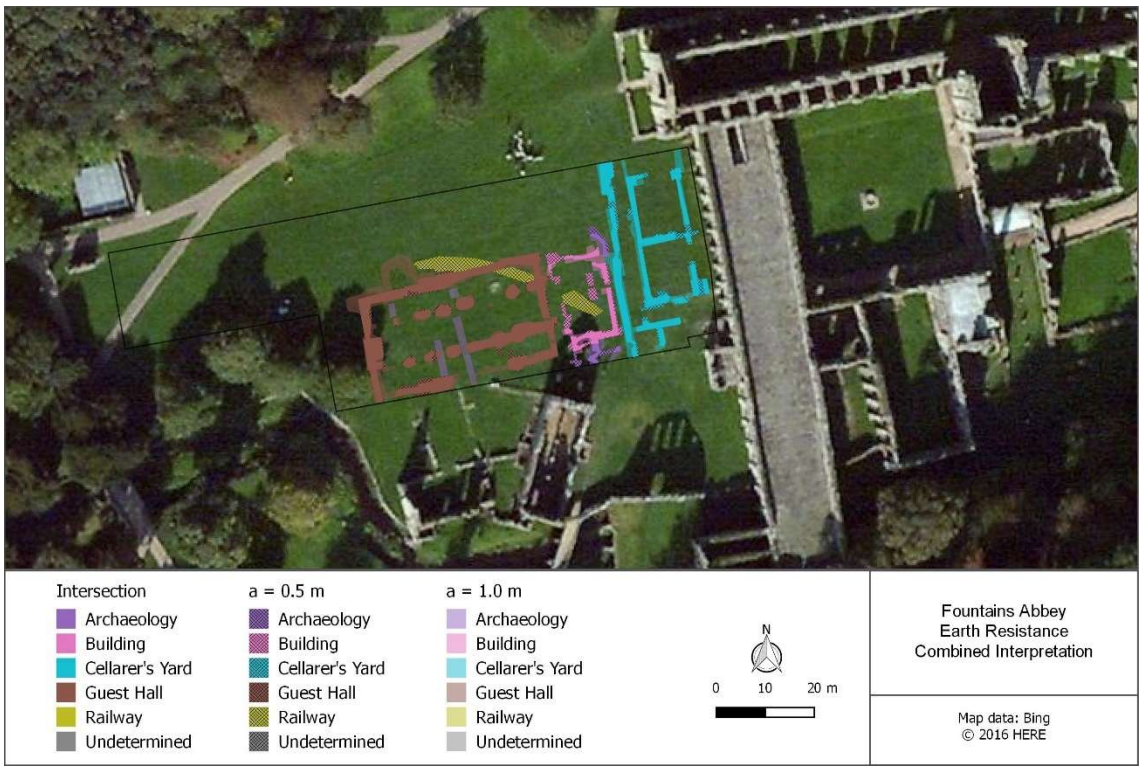

Figure 68: Fountains Abbey combined earth resistance (a =0.5 m and a= 1.0 m twin-probe arrays) interpretation. The interpretation has been simplified to highlight archaeological features.

The earth resistance survey has been effective for mapping the structural remains of the guest hall, cellarer's yard and the unknown structure. The composition of the extant pillar base indicates the guest hall was constructed from local sandstone, which, against the clayey soil, has produced strong, high-resistance anomalies that exhibit positive-contrast from the surrounding material (Figure 67). The adjacent unnamed building and the cellarer's yard also demonstrate positive-contrast from the background material. The basic footprints of the unnamed building and cellarer's yard are distinctly detected through both depths. In addition to these structural features, a railway line that was used to transport spoil during 19th century excavations has been detected as negative-contrast rectilinear anomaly. Surrounding these identifiable features, the near-surface soil matrix shows ambiguous areas of disturbed resistance. A specific origin for these anomalies cannot be determined, given the non-specific form of response.

The differences between the a = 0.5m and a = 1.0m separations reveal changes in the guest hall's structure with depth. Figure 68 presents a combined earth resistance interpretation, which makes a distinction between the anomalies resolved in each respective configuration and the anomalies resolved in both configurations. Anomalies that are resolved in both configurations indicate the

feature maintains a strong presence with depth, while anomalies resolved only in one configuration indicates a relatively shallow or deep feature, depending on which dataset it occurs in. For example, the main structural footprint of the guest hall is detected in both configurations, but a porch appears at the building's northern edge in the deeper results. The deeper results also reveal additional positive-contrast linear anomalies within the centre of the hall that are not detected in the shallower results. As these anomalies are not detected in the *a* = 0.5m results and only weakly detected in the *a* = 1.0m results, these anomalies hint at the potential for further structural remains beyond the depth sensitivity of the configurations used.

4.2.2 Fountains Abbey: Magnetic Results

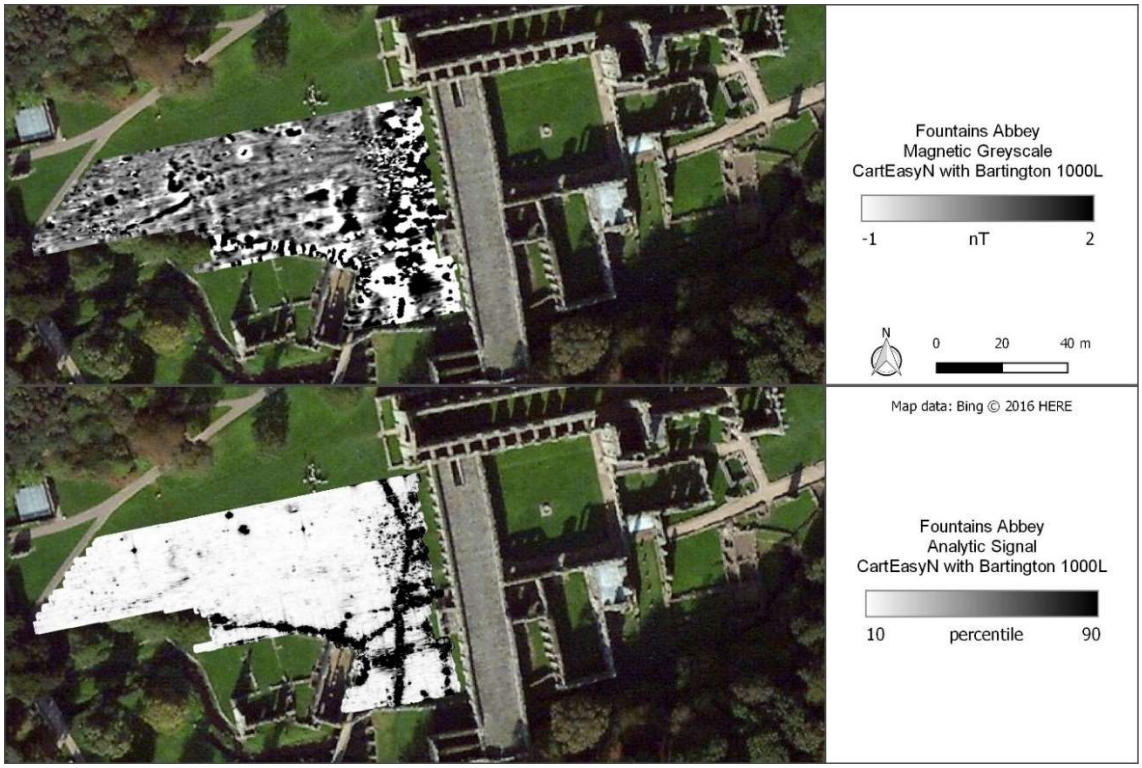

Figure 69: On the top, the Fountains Abbey magnetic greyscale (CartEasyN with Bartington 1000L). An analytic signal was applied to reduce the overwhelming signal of the services over the cellarer's yard (top).

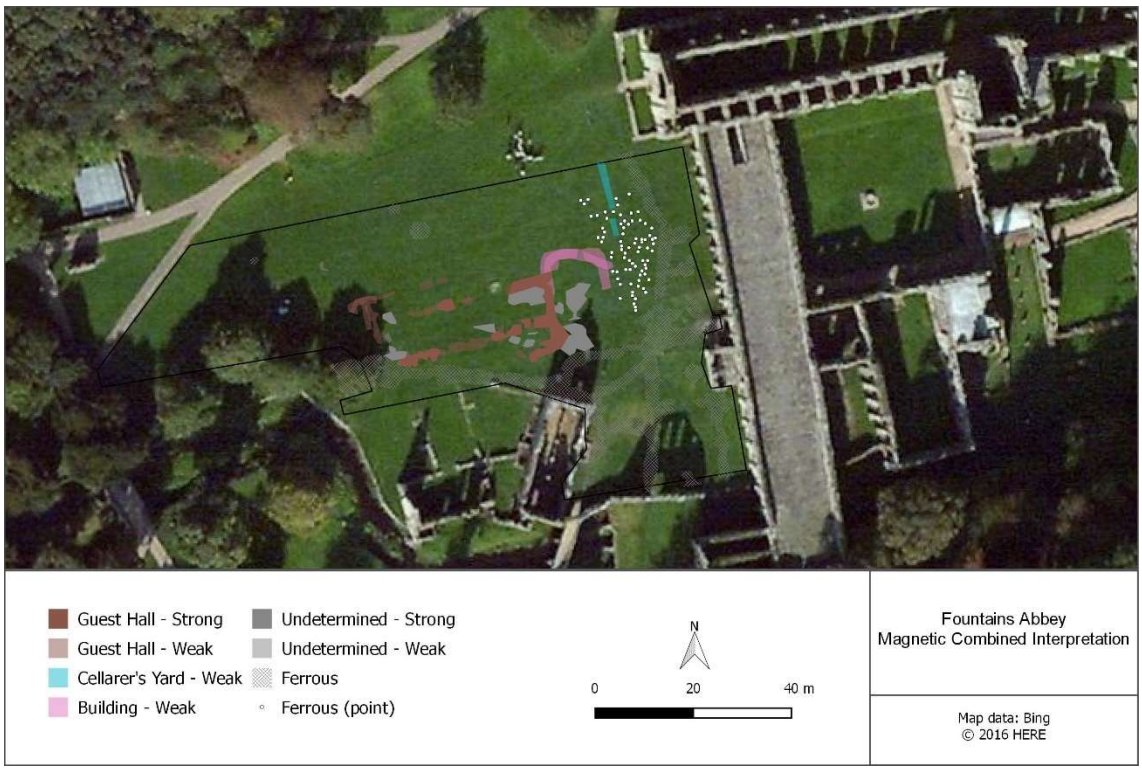

Figure 70: Fountains Abbey combined magnetic (CartEasyN with Bartington 1000L and Geoscan FM256) and analytic signal interpretation. “Strong” indicates a high-contrast magnitude of response, while “weak” indicates a low-contrast magnitude of response. The interpretation has been simplified to highlight archaeological features.

The magnetic method detects the guest hall remains as low-contrast and high-contrast negative magnetic anomalies (Figure 69). Given that sandstone is a weakly magnetic material, the detection of the guest hall in the magnetic results is impressive. The magnetic method is less successful for detecting the structural remains of the unnamed building, but magnetic enhancement bounded within the building’s area provides evidence for potential anthropogenic activity. A weak, negative magnetic linear anomaly runs parallel to the abbey’s extant walls and almost certainly reflects the cellarer yard’s westernmost wall. The results within the cellarer’s yard are dominated by the broad dipolar responses from the near-surface services, making interpretation of surrounding features within this area difficult. An analytic signal applied to the dataset effectively reduces these overwhelming service responses to a defined source target (Figure 69); the reduction of the broad ferrous-type responses helps reveal a concentration of discrete point anomalies bounded within the walls of the cellarer’s yard. These anomalies could potentially be linked to smelting activity within this area (Figure 70; Harris and Gaffney 2014). The railway line is not resolved in the magnetic results, suggesting the tracks were thoroughly dismantled and removed from the site.

4.2.3 Fountains Abbey: Electromagnetic Induction Quadrature-Phase Results

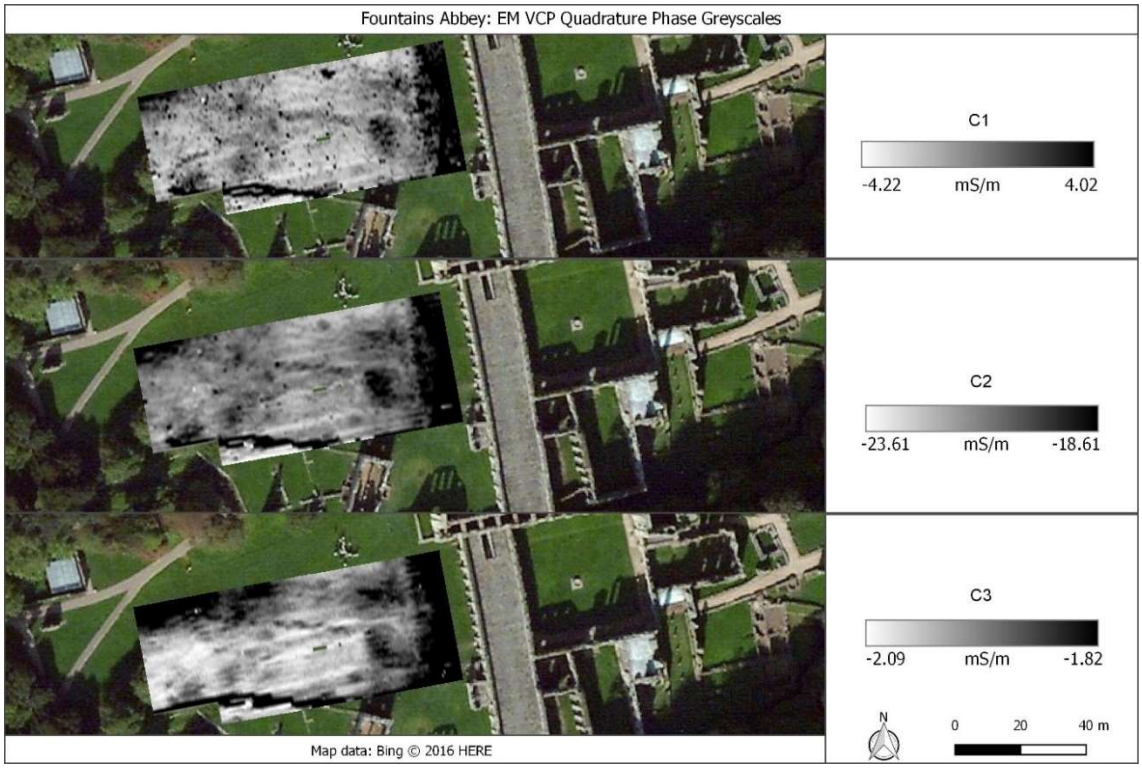

Figure 71: Fountains Abbey electromagnetic induction (VCP quadrature-phase) greyscales.

Figure 72: Fountains Abbey electromagnetic induction (combined VCP quadrature-phase) interpretation (top-bottom): C1, C2 and C3. The interpretation has been simplified to highlight archaeological features.

The EM quadrature-phase has detected both archaeological and modern features at Fountains Abbey. The modern features have produced strong responses in the measured EM signal, but the weaker archaeological anomalies adjacent to the modern service can still be distinguished from its high-contrast response. Similar to the Lister Park results, the C1 results are littered with discrete near-surface noise, likely caused by debris from the continual access and maintenance of the site. The anomalous forms of the archaeological features changes with depth. For example, the entirety of the guest hall structure becomes more explicit with increased exploration depth, with additional walls and structural features becoming apparent in C2 and C3. The building's southern wall and row of pillars are only very faintly visible in C1 and could easily be mistaken for erroneous data or line imbalances, if the presence of the guest hall had been previously unknown. However, the resolution of the guest hall improves with increased exploration depth, which may correlate with the decreased noise in the deeper coils as the guest hall remains are known to lie relatively near-surface. In all the receiving coils, the guest hall has been resolved by low-conductivity linear anomalies. The adjacent unnamed building to the guest hall demonstrates a similar resolution with depth, as the feature becomes more distinct in C2 and C3. Bounded within the walls of the building is an area of high conductivity, most explicit in C1 and C2. The occurrence of this amorphous response within the extent of the feature is indicative of potential anthropogenic activity, rather than a structural feature.

In contrast to the guest hall and the unnamed building, the westernmost wall of the cellarer's yard is more explicit in the shallower depth volumes than in the deeper volumes. Within the area of the cellarer's yard, the modern service produces a high-contrast response but does not overwhelm the nearby features. There is noticeable enhancement in the conductivity of the soil defined within the bounds of the yard's walls, particularly in C2. The other feature that also demonstrates a shallower depth presence is the railway bed, which is recognisably resolved as a high conductivity feature, most explicit in the C1 and C2 results.

Overall, all three exploration depths of the EM quadrature-phase have detected at least some aspects of all the archaeological features at Fountains Abbey.

Given the detection of these features across the separate datasets, a mean of the results should provide an effective composite image to represent the plan of the structural footprints. The individual quadrature-phase datasets were normalised before integration because different processing steps were undertaken on each dataset: a zero-median traverse was applied to C1 and C2, while a rolling-median was undertaken on C3. The normalisation centred the individual results and evened out the distribution of measurements (Figure 73). Figure 74 presents the mean image and the results of the principal component analysis.

Figure 73: Histograms of Fountains Abbey's EM VCP quadrature-phase results to visualise the differences between the individual coils' distribution and range for the normalised (right) and not normalised (left) results.

The resulting mean image of the quadrature-phase datasets provides an adequate representation of the key features in all depth volumes (Figure 74). The magnitude of the guest hall is not as distinct in the mean image as it is in the C3 results, but the form of the response is still coherent. The near-surface noise in C1 is minimised by the influence of the C2 and C3 datasets, which almost certainly improves with the resolution of the archaeological features. The outline of the unnamed building and the railway bed are clearly defined in the mean image, but the delineation of the cellarer's yard is less distinct.

The first and second principal components are less useful as representative composite images of the collective results because the guest hall feature is not discernible in either image (Figure 74). The railway bed and enhanced area within the unnamed building are still visible in the first component results, but the first component image highlights the discrete, near-surface responses—obscuring

the footprint off the guest hall. The second principal component highlights the modern service feature and depicts banding across the survey area, which likely represents a data collection or processing artefact, instead of a real feature. Overall, the PCA was ineffective at this site because the targeted archaeological features were obscured and no further information was revealed through the process.

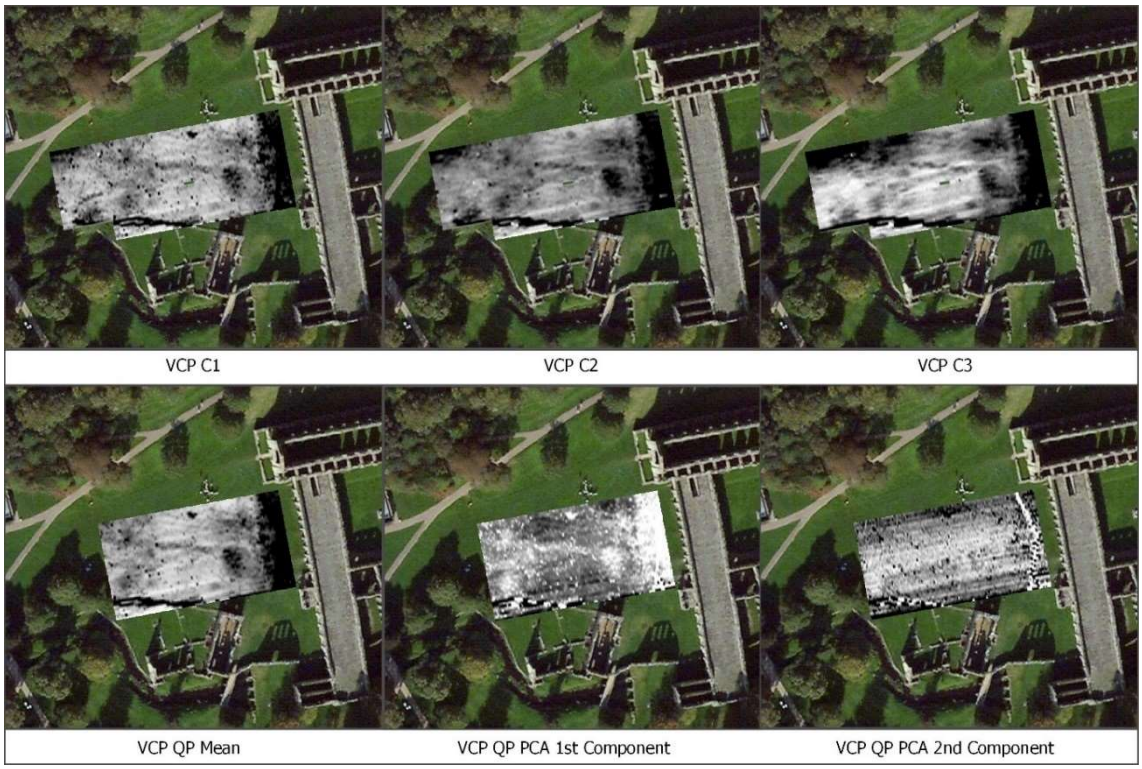

Figure 74: Comparison of the Fountains Abbey VCP quadrature-phase coils against (lower row: left-right) the mean of the datasets, first principal component and second principal component after the individual input datasets had been normalised. Satellite imagery Bing © HERE 2016.

4.2.4 Fountains Abbey: Electromagnetic Induction In-Phase Results

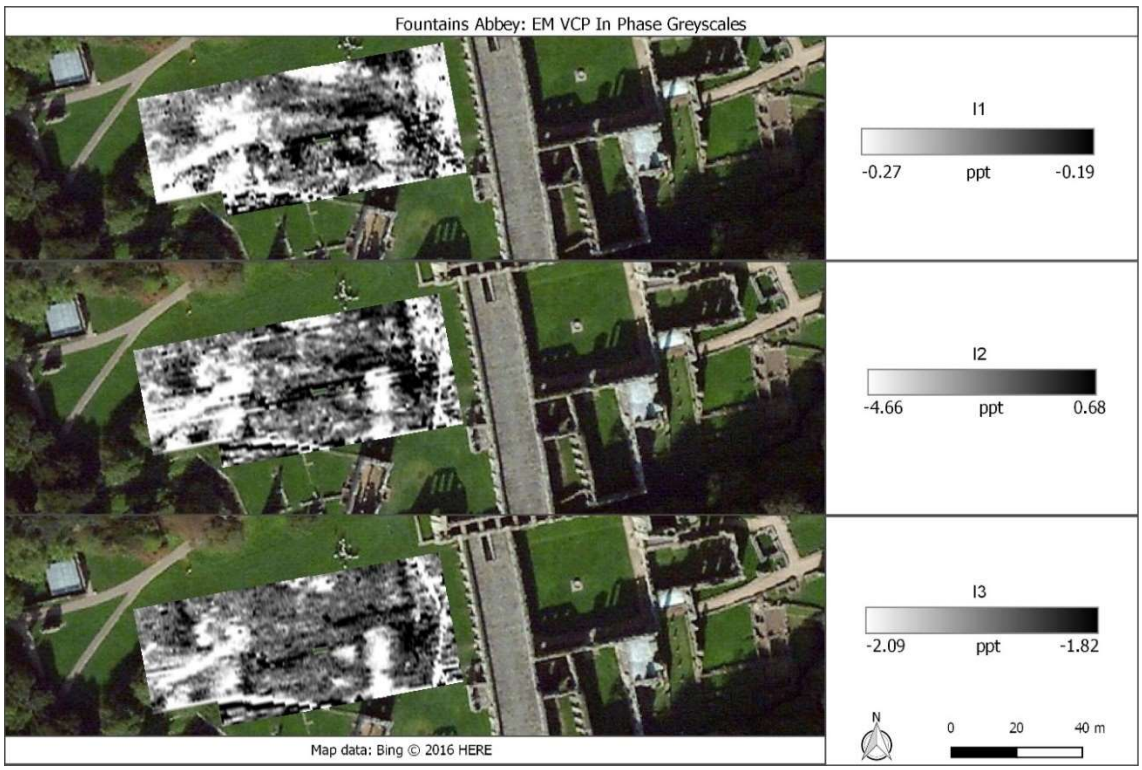

Figure 75: Fountains Abbey electromagnetic induction (VCP in-phase) greyscales.

Figure 76: Fountains Abbey electromagnetic induction (VCP combined in-phase) interpretation (top-bottom): I1, I2 and I3. The interpretation has been simplified to highlight archaeological features.

The EM in-phase has detected archaeological and modern features at Fountains Abbey (Figure 75). The structural features of the guest hall are not clearly resolved in the in-phase results and could only be coherently interpreted as a structural footprint in the I3 results (Figure 76); although given the incredibly weak magnitude of response, it would be difficult to interpret the guest hall's anomalous response in the in-phase as a building feature without prior knowledge of the building's existence. At the eastern edge of the survey area, a defined area of negative-contrast responses bounded within the extent of the cellarer's yard is apparent through I1 and I2. These responses are distinguishable from the defined response of the service feature, which becomes more apparent with increased depth. A similar type of negative-contrast response is defined within the area of the unnamed building. These responses maintain a strong presence with depth, unlike the cellarer's yard, which is most explicit in the shallowest soil volumes. The railway bed cannot be discerned within the in-phase results, suggesting the fill material has poor magnetic enhancement from the surrounding soil. A number of other distinct anomalies are visible in the in-phase results, but do not correlate with any known features and lack a distinct archaeological form or patterning to be ascribed a specific origin.

Overall, the archaeological features detected by the EM in-phase at Fountains Abbey are resolved only in the deeper soil volumes. Given that the footprint of the guest hall is only distinct in one of the in-phase datasets, the feature could easily be lost when combining the separate results. The individual in-phase datasets were first normalised before integration because different processing steps were undertaken on the different datasets: a zero-median traverse was applied to I1, while a rolling-median followed by a zero-median traverse were applied on I2 and I3. The rolling-median was applied to reduce the increased noise in the I2 and I3 results. These different processing steps had a different impact on the distribution and range of the different datasets (Figure 77), but the normalisation helped to rectify these the differences (Figure 78). Figure 79 presents the mean image and results of the principal component analysis.

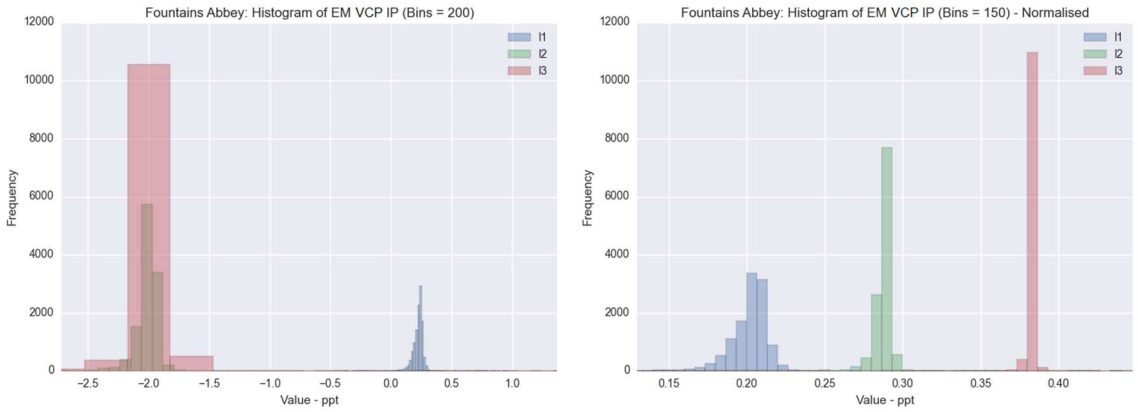

Figure 77: Histograms of Fountains Abbey's EM VCP in-phase results to visualise the differences between the individual coils' distribution and range for the normalised (right) and not normalised (left) results.

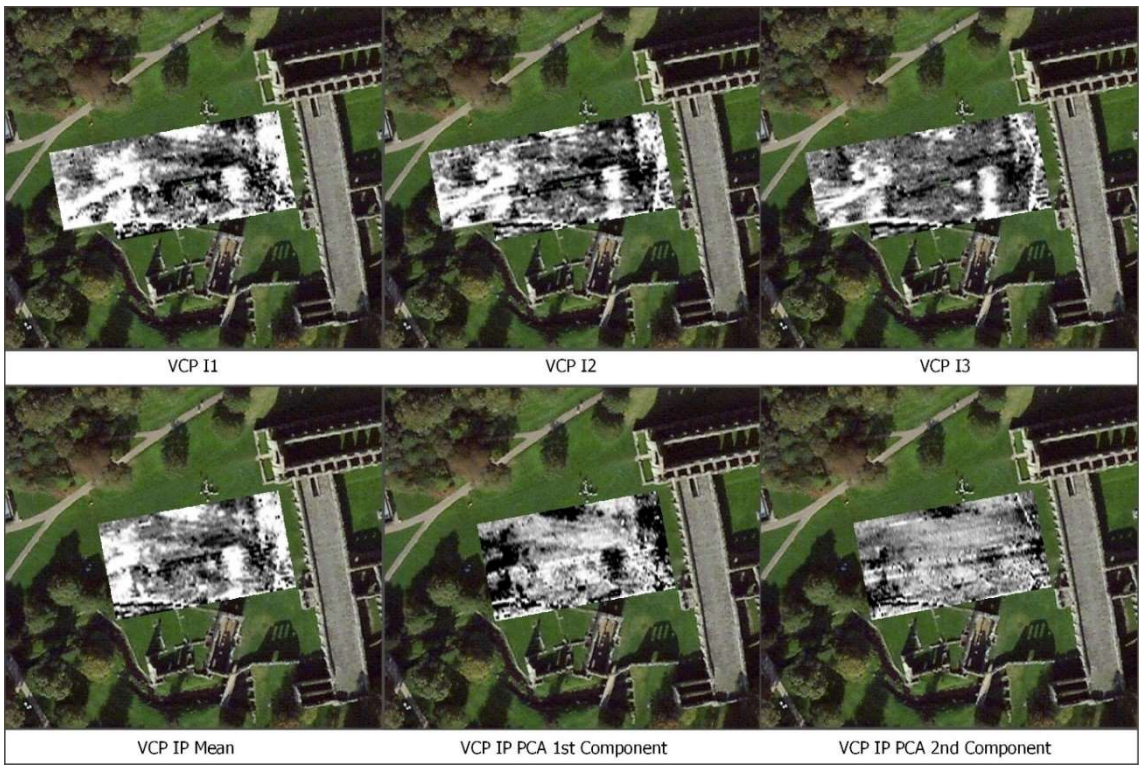

Figure 78: Comparison of the Fountains Abbey VCP in-phase coils against (lower row: left-right) the mean of the datasets, first principal component and second principal component after the individual input datasets had been normalised. Satellite imagery © Bing 2016.

The images of the in-phase's mean results and the first principal component are inverted in appearance. Both composite datasets represent the key features in the individual in-phase datasets, but do not offer any further interpretative information that could not already be derived from the individual results. The second principal component highlights the modern service features and striping along the traverse, likely an effect of data collection or processing. Overall, interpretation of the in-phase results in isolation is difficult given the relative

ambiguity and low-contrast nature of the responses, particularly in the I1 and I2 datasets. Interpretation of the in-phase alongside the quadrature-phase will follow below, in aim to better characterise the nature of the EM signal.

4.2.5 Fountains Abbey: Integration of EM Results and Composite Analysis

Figure 79 presents the results of a GIS geometry intersection of the quadrature-phase and in-phase interpretations. The intersect results reveal the majority of the main archaeological features are detected in both phases. Aspects of the guest hall, unnamed building and cellarer's yard are present in both datasets; although the quadrature-phase has been more successful overall for detecting the archaeological features. The low conductivity of the stone against the moist, clayey soil provided sufficient contrast from the surrounding soil of the building features in the quadrature-phase. The inferior performance of the in-phase at Fountains Abbey is not surprising given that the structural remains are comprised of weakly magnetic material. The former railway line is also distinctly coherent in the quadrature-phase results, but is absent from the in-phase results entirely. This preferential detection of the railway line indicates the quadrature-phase is responding entirely to the electrical conductivity properties of the feature, as it lacks detectable magnetic enhancement.

Comparison of the individual coils' quadrature-phase and in-phase interpretations (Figure 72; Figure 76) reveals most the structural elements are being detected in the deeper soil volumes. The structural footprint of the guest hall is only explicit in the I3 coil, but is discernible in C1, C2 and C3. The difference in detection demonstrates the differences between the depth sensitivities of the in-phase and the quadrature-phase; although the near-surface noise visible in the I1 and I2 results could obscure the signal of the guest hall in these datasets. Further comparison between the EM results with the other methods will provide a better indication of the relative depth extents of these features.

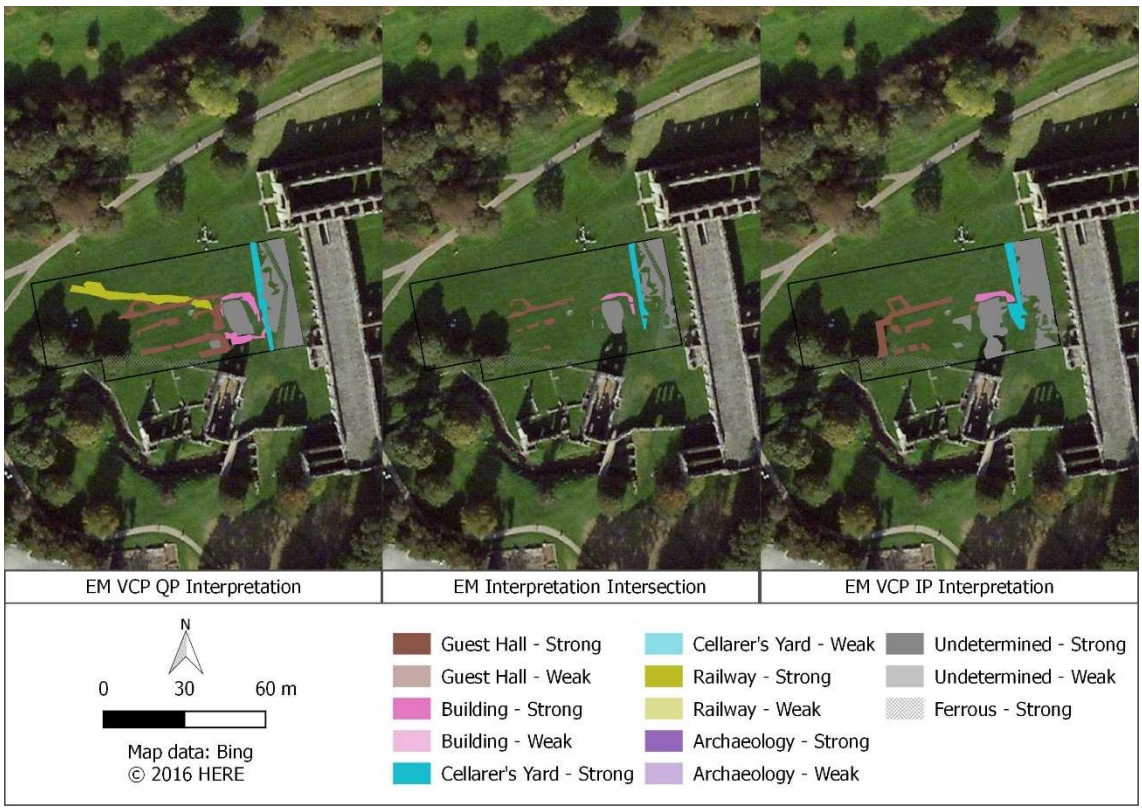

Figure 79: Fountains Abbey EM interpretations. “Strong” indicates the anomaly was detected in at least two of the datasets, while “weak” indicates the anomaly was detected only in one dataset. GIS intersection tool has been run on the in-phase and quadrature-phase interpretations to compare the overall similarities between the in-phase and quadrature-phase results.

4.2.6 Fountains Abbey: Integrated Interpretation and Archaeological Characterisation

The earth resistance and magnetic datasets from the cart-based Geoscan Research MSP25 survey are used instead of the twin-probe and CartEasyN data for the data integration, respectively, as they were collected in the same grids as the EM survey. The MSP25 earth resistance and magnetic datasets reveal the same features as the counterpart twin-probe and CartEasyN results (Figure 81).

The magnetic, earth resistance and EM methods all detect aspects of the structural remains of the guest hall, unnamed building and the cellarer’s yard. The quadrature-phase has been more effective for delineating the archaeological features than the in-phase. The magnitude and clarity of the quadrature-phase’s responses improves with increased depth, with C3 producing the most coherent visualisation of the guest hall feature, compared to C1, C2 and the quadrature-phase’s mean results. Of all the different geophysical methods, earth resistance has been the most effective for mapping the archaeological features. The structures are detected as distinct, high-contrast responses. Owing to the

magnitude of the contrast of the archaeological features to the background soil in the earth resistance results, this dataset dominates over the other methods in the CYMK overlay (Figure 80) and the mean results (Figure 81), despite the input datasets being standardised before combination. In the mean image, the responses of the guest hall and unnamed building are clearly representing the earth resistance dataset; whereas the magnetic and EM datasets are represented by the modern service in the south-west corner. Two discrete ferrous responses are present in the mean results, representing the magnetic dataset solely.

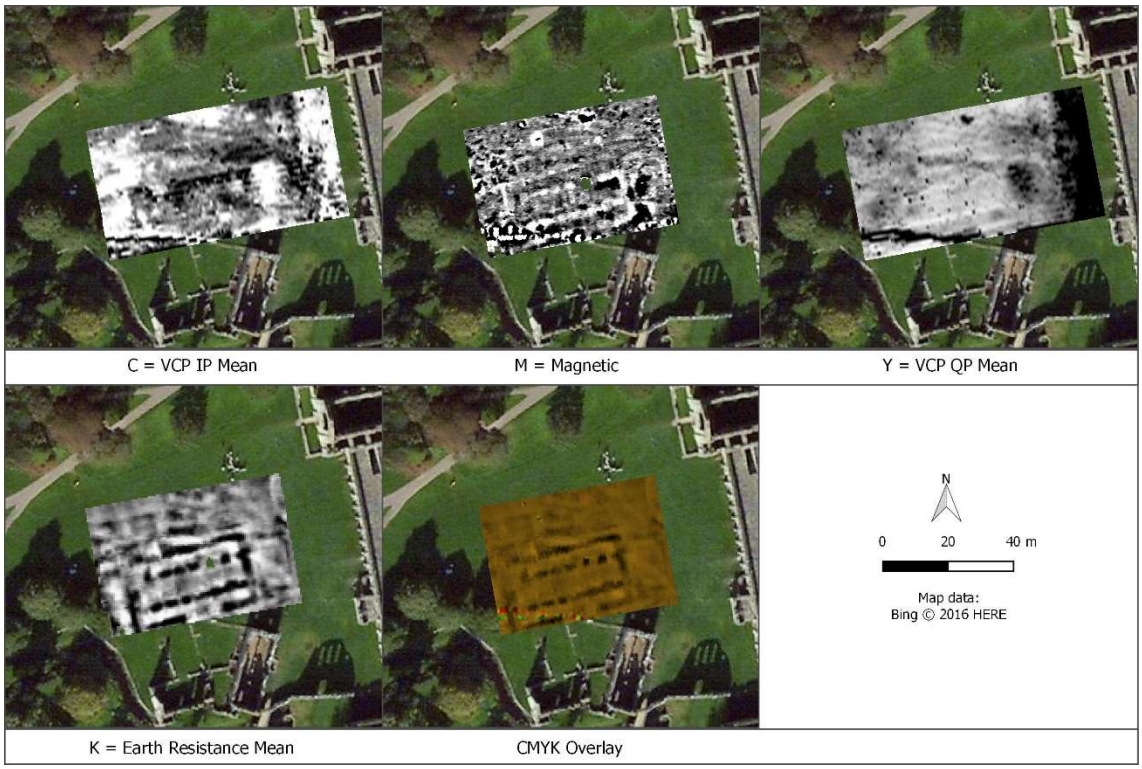

Figure 80: CMYK overlay of the standardised geophysical methods at Fountains Abbey.

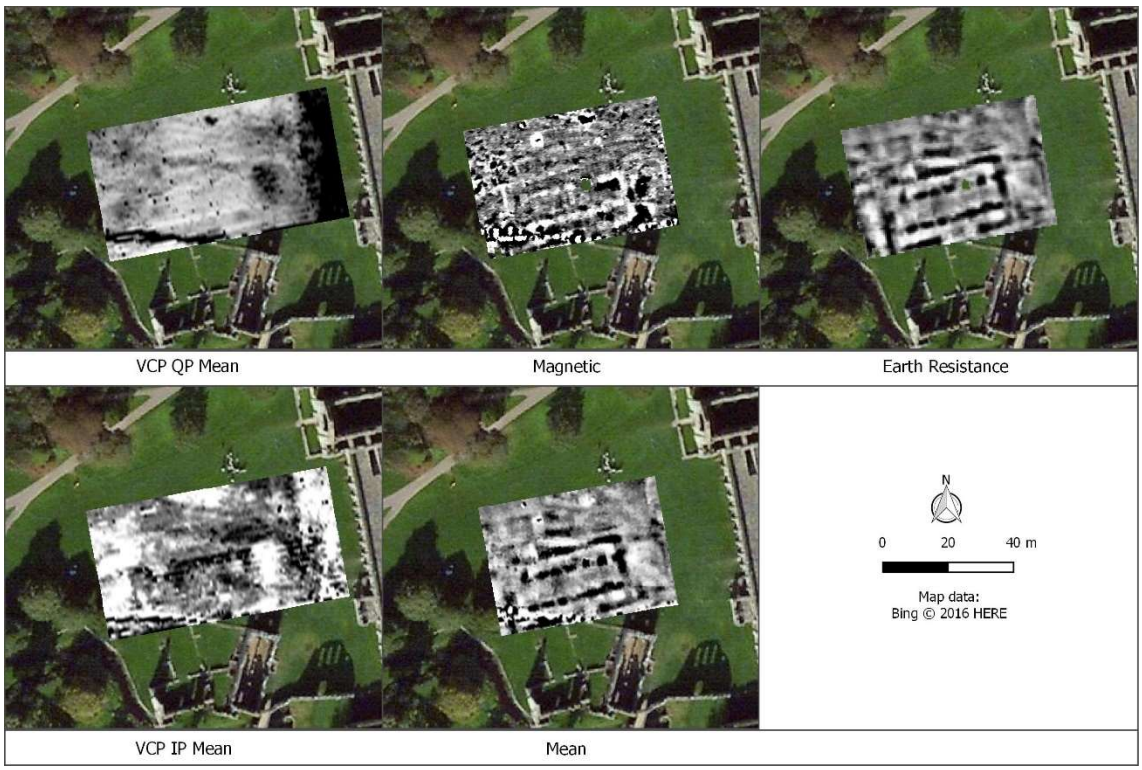

Figure 81: The mean of the standardised geophysical methods at Fountains Abbey.

Despite the bias of the mean results to the earth resistance dataset, the mean image is still an accurate representative image of the key structural aspects delineated in all the results, as all the methods have generally been successful for detecting the structural remains. However, the magnetic and EM results also offer additional interpretative value as they detect enhanced areas that may be resultant of anthropogenic activity. The PCA of the different datasets offers a holistic image of the collective geophysical results. The main structural features of the buildings are maintained the in the principal components, but they also represent the potential enhancement areas detected in the magnetic and EM datasets (Figure 82).

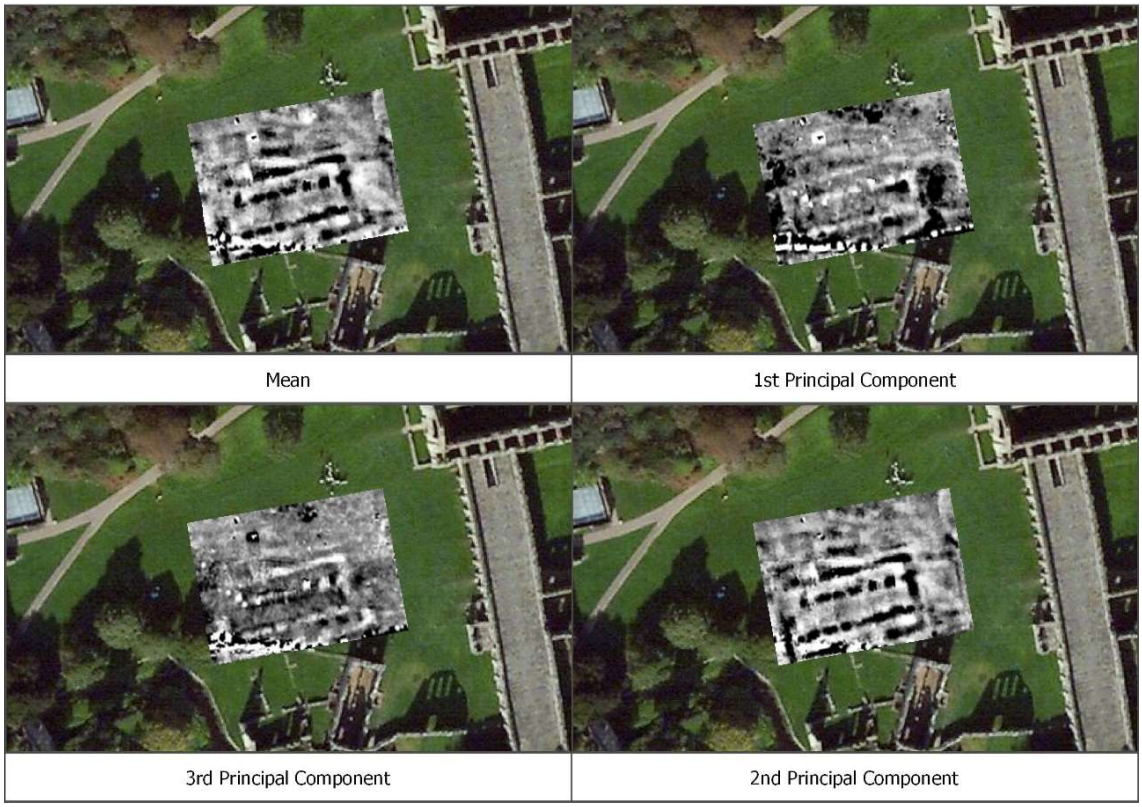

Figure 82: Comparison of the mean, first, second and third principal components of the standardised magnetic, earth resistance, EM in-phase and quadrature-phase datasets.

The first principal component (Figure 82) retains the basic structural outline of the guest hall and unnamed building, while displaying the areas of potential anthropogenic enhancement. The structural outlines of the buildings are the focus of the first and second principal components, as the near-surface soil variation surrounding the structure is not presented in these images. In the third component, the southern row of pillar bases is discernible as individual features. In all the individual datasets, the responses of the southern row of pillar bases are not individually defined; for example, in the earth resistance results, the pillars are resolved as a band of high resistance. No other new features are defined in the principal component results. Thus, the mean and PCA (Figure 82) has not been particularly useful for increased interpretative value, given the correlation between the different methods for detecting the same features. This is true of the CMYK overlay as well (Figure 81).

While these composite images provide good representations of the buried archaeological features, the three-dimensional variation in the structural changes is lost in the two-dimensional images. Understanding the three-dimensional variation of the features is particularly informative at Fountains Abbey, because

the earth resistance results hint to further features at deeper depths, which indicates these structures experienced separate building phases. The graphical and arithmetic combination of the different methods flattens the three-dimensional variation of the results into a two-dimensional planar view, where the relative depth—and thus inferred relative age—of the features is lost. To visualise the changes with depth, a union of the vectorised interpretations was performed to represent three gross soil volumes (Table 14). Figure 83 presents the results of the integrated GIS visualisation.

Dataset	Relative Depth
EM VCP I1	Shallow
EM VCP I2	Shallow
VCP C1	Shallow
TP a = 0.5 m	Middle
EM VCP I3	Middle
EM VCP C2	Middle
TP a = 1.0 m	Deep
EM VCP C3	Deep

Table 14: The relative depths of the different geophysical datasets.

The structural footprints of the guest hall, unnamed building and the cellarer's yard are fully defined in the middle and deep soil volumes, but the resolution of the structural features varies depending on the depth. For instance, the porch feature on the guest hall becomes explicit in the middle soil volume, which is the contribution from VCP I3. Internal structuring is visible with the unnamed building, but only in the middle soil volume, which is a contribution from the *a* = 0.5 m twin-probe dataset. The potential additional structure is only resolved in the deepest soil volume, which is the contribution from the *a* = 1.0 m twin-probe dataset. This feature exceeds the depth sensitivities of the other instruments and configurations. Only certain aspects of these features are detected in the shallowest soil volume, where the results primarily reflect anomalies potentially indicative of anthropogenic enhancement and the railway feature.

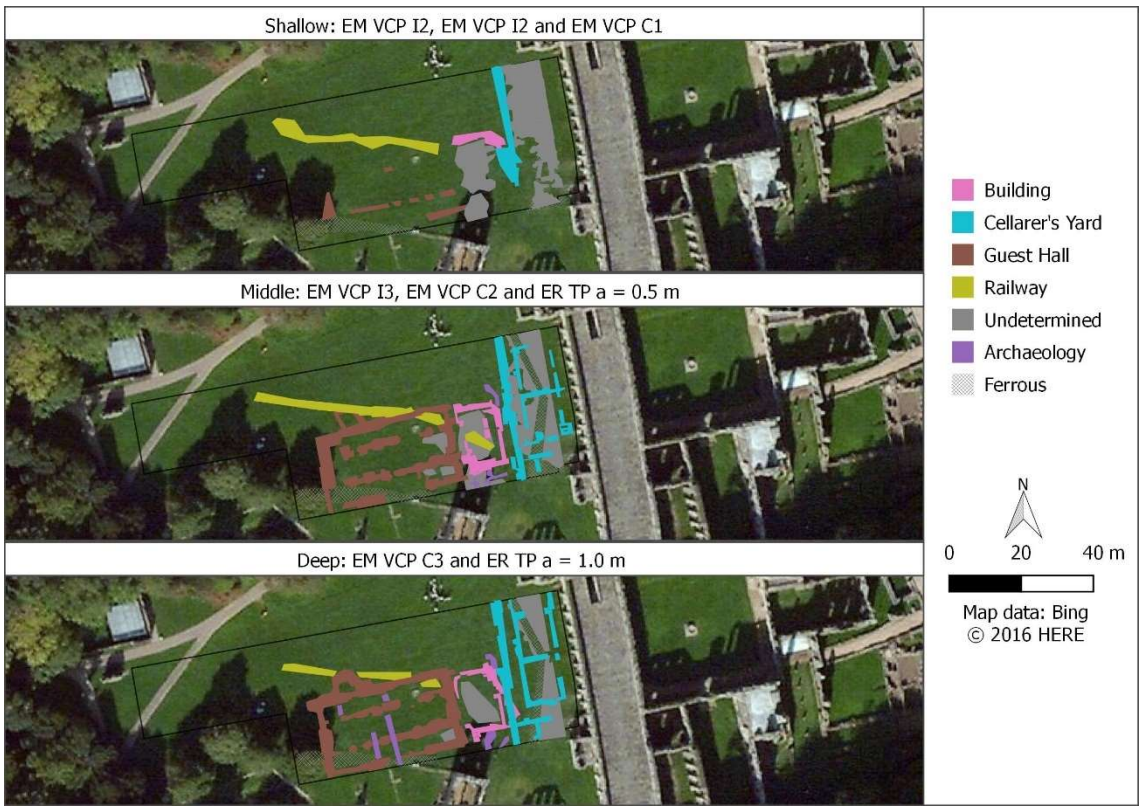

Figure 83: Relative depths (top-bottom: shallow, middle, deep) of the archaeological features, as detected by the different geophysical methods (Table 14).

The different methods at Fountains Abbey have all responded well to the buried archaeological remains, detecting different aspects of the same features. How the different methods relate to one another will be analysed below, using the common features detected as a reference point.

- *Guest Hall*—Anomalies associated with the guest hall have been detected by all the geophysical methods. The most explicit responses occur in the earth resistance results, where the feature is detected as strong, positive-contrast anomalies. The quadrature-phase detects the same footprint of this feature, but as a negative-contrast anomaly; the inverse response between the earth resistance and quadrature-phase results indicates the quadrature-phase is responding to the electrical conductivity properties of the guest hall. In contrast to the earth resistance and quadrature-phase results, the guest hall produces less explicit responses in the magnetic and in-phase results—almost certainly owing to the weakly magnetic properties of the sandstone building materials. In the magnetic results, the walls and the pillars of the building are detected as negative-contrast responses; whereas in the in-phase results, the structural elements are

detected as positive-contrast responses. The outline of the guest hall is only distinctly visible in the I3 configuration. The different exploration depths of the respective geophysical methods are particularly informative at Fountains Abbey because the structural configuration of the guest hall changes with depth. The core structure of the guest hall feature is detected through the soil column, with additional features detected in the deeper results.

- *Unnamed Building*—Anomalies associated with different structural aspects of the structure adjacent to the guest hall have been detected by all the geophysical methods. The most coherent responses from this structure occur within the earth resistance and quadrature-phase results. Within the bounds of the walls, the magnetic, EM in-phase and quadrature-phase results resolve ambiguous high-contrast responses, while the earth resistance results reveal further internal structuring and the railway line traversing NW-SE through the building. The lack of correlation between the earth resistance and EM quadrature-phase datasets suggests the quadrature-phase is responding more to the magnetic properties of the source feature, than its electrical conductivity properties—especially considering the high-contrast magnitude of response in the magnetic and in-phase results. In the EM quadrature-phase results, the railway line appears to terminate at this area of high-contrast responses, but photographic and documentary sources confirm this railway ran all the way to the main abbey complex. Still, the correlation between this area of enhancement with the railway feature suggests a potential correlation between the two features.

- *Cellarer's Yard*—Only the earth resistance results reveal the full structural outline of the cellarer's yard, but responses potentially associated with the usage of this area are detected in the other methods. The analytic signal of the magnetic results reveals a concentration of highly magnetic point sources bounded within the westernmost wall of the cellarer's yard. These point responses are not resolved in the EM results, but both the quadrature-phase and in-phase show the area bounded with the cellarer's yard dominated by amorphous high-contrast responses, particularly in the

shallower soil volumes. These responses are distinct from the response from the service, which is defined as a linear feature. The difference in the quadrature-phase's responses from the earth resistance results indicates the quadrature-phase may be responding more to the magnetic material in this area, instead of the electrical conductivity properties. As these features are limited by the extent of the cellarer's yard's western wall, these responses potentially represent anthropogenic activity. The point response could represent smelting debris from the usage of this area.

- An important and impressive outcome of the survey has been the successful delineation of the resistive structures in the EM quadrature-phase results because EM methods have been criticised as being ineffective for detecting resistive structures. Considering the "overall picture" of the subsurface (i.e. the guest hall, the associated building, the cellarer's yard), the EM quadrature-phase has been the most effective technique because it has detected all aspects of the features, which are represented separately in the magnetic and earth resistance results. For example, the earth resistance demonstrates excellent contrast for the building features and highlights the structural remains, but does not detect the enhancement and activity zones; whereas the magnetic method has effective for detecting the enhanced areas that potentially indicate anthropogenic activity, but has been less effective for detecting structures remains and the railway bed. The EM was able to detect all these various aspects, albeit to a poorer resolution than the earth resistance, but the general footprint of the structures can still be discerned.

4.2.7 Fountains Abbey: Conclusions

The geophysical investigations were successful at Fountains Abbey. All the methods responded well to the survey area's environment, which is naturally clayey and wet in situ. All of the geophysical methods applied to Fountains Abbey were successful for detecting basic structural elements of the buried archaeological remains. The earth resistance and EM quadrature-phase methods have been the most effective for delineating the structural outlines of the buried remains; while the magnetic and EM in-phase methods were more informative on areas of potential increased anthropogenic activity. Of importance at Fountains

Abbey, however, are the vertical changes of features with depth. The integration strategies were therefore less effective at this site, since most of the outputs were two-dimensional in nature and could not convey how the features change with depth. The GIS-based approach was the only integration strategy that was able to capture the variable depth information.

4.3 Markenfield Hall: Results and Characterisation

The investigations at Markenfield Hall, near Ripon, North Yorkshire, targeted the location of a potential deserted medieval village in the “Lumps and Bumps” field, located immediately adjacent to the south-east of the manor house itself. No mapping of the earthwork features in the “Lumps and Bumps” field at Markenfield Hall is available nor has this area been explored through intrusive investigation. However, as the surviving earthworks have distinguishable relief from the level of the ground surface (Figure 84), satellite imagery and LiDAR data can be used to cross-reference the extant features to the geophysical results. Furthermore, the LiDAR data indicates topographic relief: darker, shaded areas are indicative of depression features while ridge and embankments appear as lighter features (Figure 85). This information will be useful when interpreting the results to distinguish between the ditch-like and embankment-like features.

Figure 84: Markenfield Hall survey area with comparison to survey considerations at time of survey. Satellite imagery © 2016 Google © 2016 Infoterra Ltd & Bluesky.

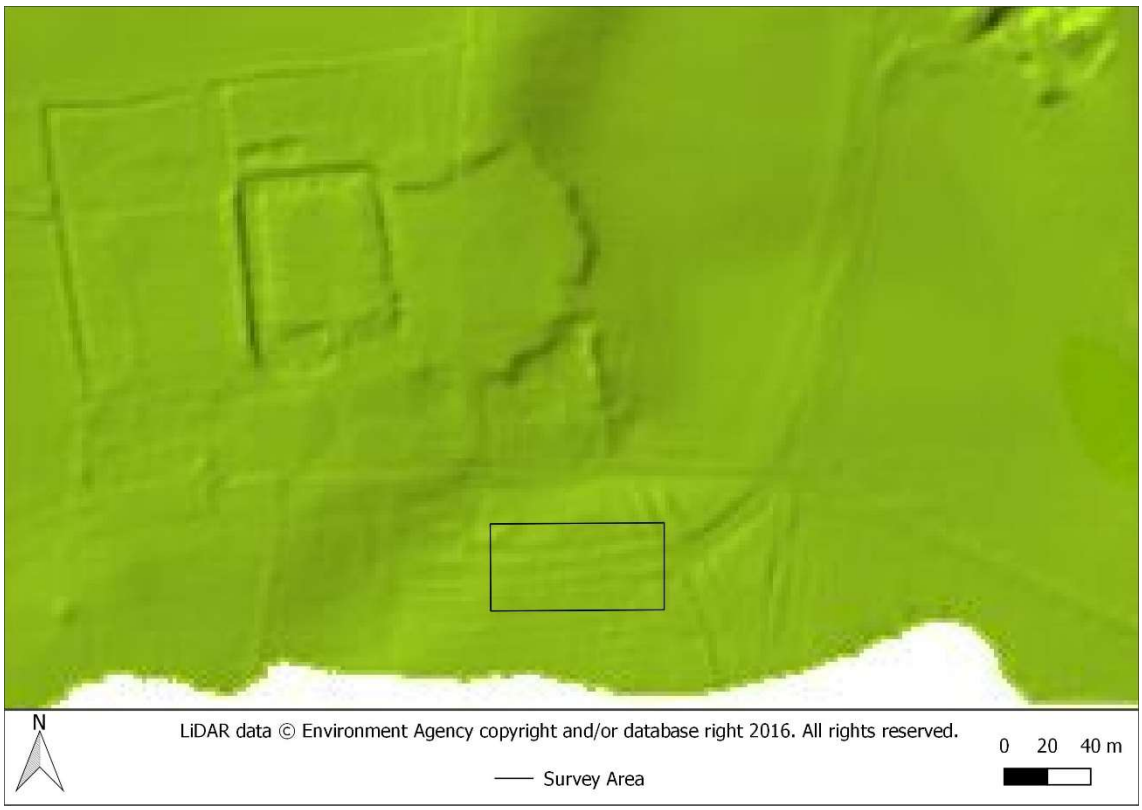

Figure 85: The survey area at Markenfield Hall over 2m DTM LiDAR data.

4.3.1 Markenfield Hall: Earth Resistance Results

The earth resistance survey has been effective for mapping the trackway features at Markenfield Hall. The averaged alpha and beta (Figure 86) and gamma (Figure 87) results reveal an intersecting pattern of linear anomalies, most which can be correlated with features discernible in the satellite imagery (Figure 84) and LiDAR data (Figure 85). The clarity of the trackway features in the remote sensing imagery allows for direct comparison between the anomalous response and the source feature. For instance, low resistance anomalies correlate with the ditch-like features in the remote sensing imagery; many of these features have companion high resistance anomalies, which have been interpreted as an embankment-type feature. A disturbed area of variable resistance in the north-western corner of the field correlates with an earthwork mound, which is extant on the ground surface (Figure 84). A E-W running linear anomaly near the south-west corner of the survey area does not correlate with any discernible trackway features, but is parallel to the evident ridge and furrow cropmarks in the southern half of the field. The earth resistance results do not provide any evidence that would indicate settlement structures or associated settlement activity.

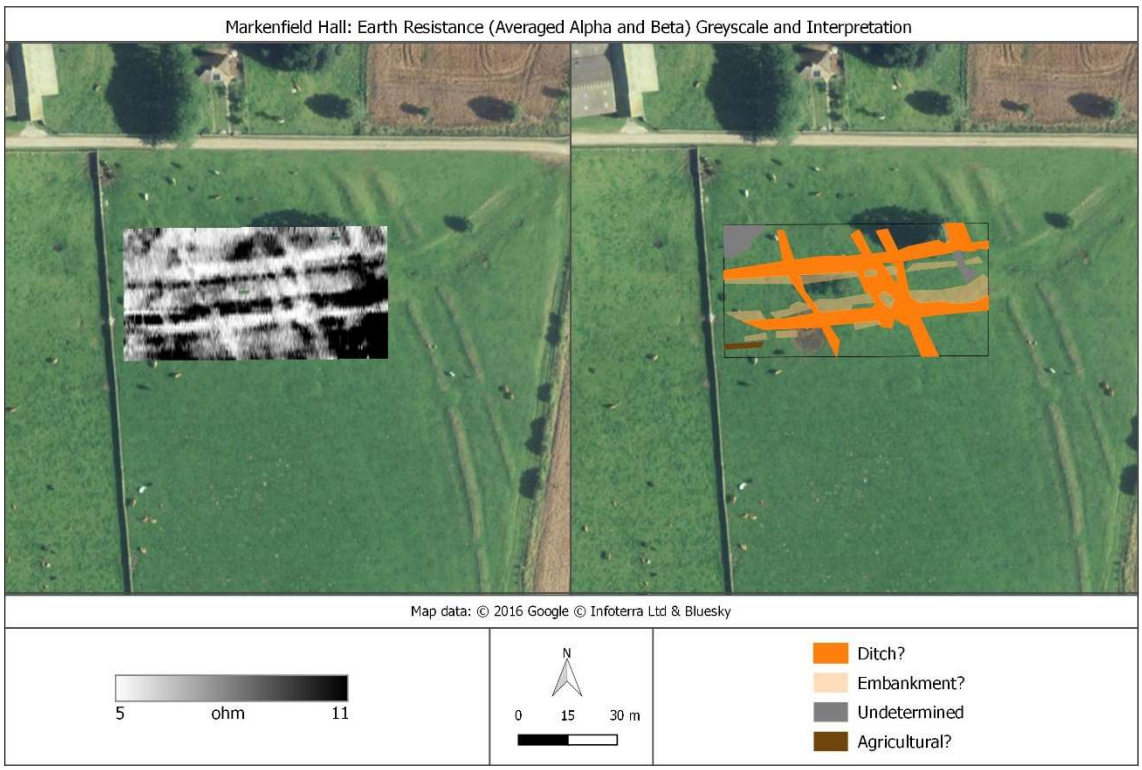

Figure 86: Markenfield Hall earth resistance (square array—averaged alpha and beta configurations) greyscale and interpretation.

Figure 87: Markenfield Hall earth resistance (gamma) greyscale and interpretation.

4.3.2 Markenfield Hall: Magnetic Results

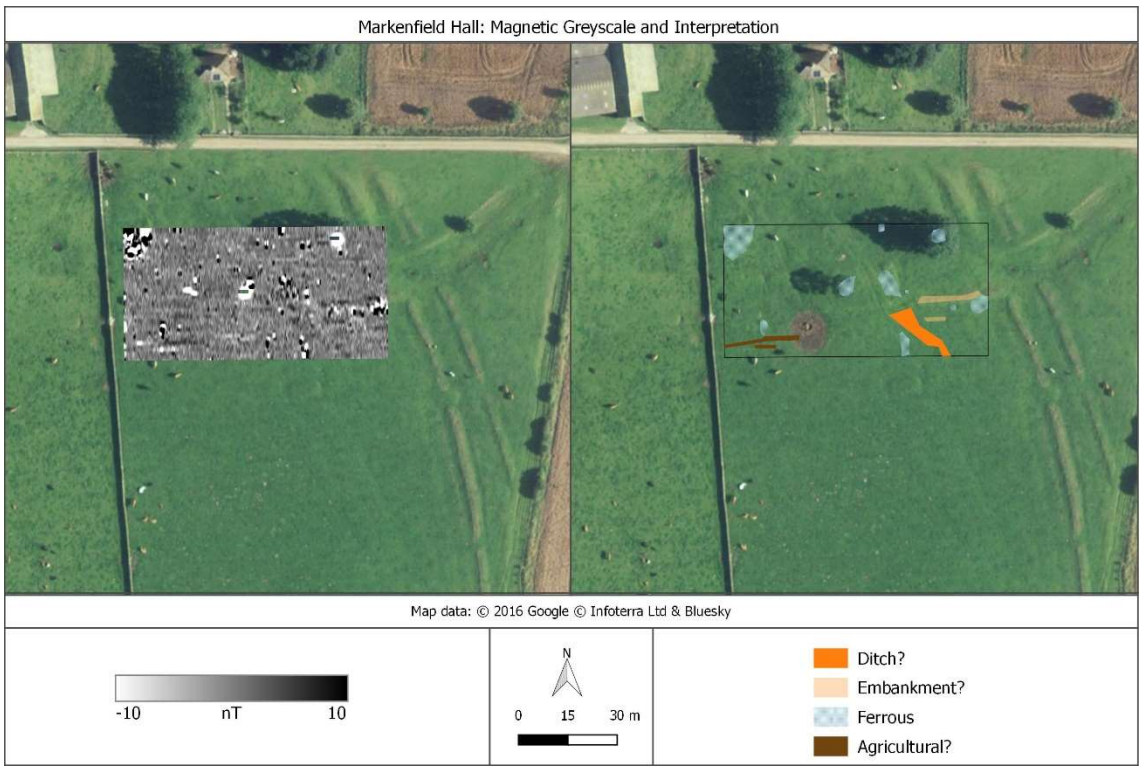

Figure 88: Markenfield Hall magnetic greyscale and interpretation.

The magnetic method has not been effective for mapping the trackway features overall (Figure 88). The absence of anomalies recognisably associated with the ditch or embankment features signifies the topsoil is poorly magnetically enhanced, as the fill of the trackway features does not exhibit strong magnetic contrast. Also hindering data interpretation are the responses running in-line with the direction of traverse, which are difficult to distinguish as a real or erroneous feature, given their resemblance to an artefact originating from abrupt movement of the sensor or some other operational effect.

The most distinct anomalies in the magnetic results are the dipolar ferrous responses. These ferrous responses likely reflect modern activity on site. The area of ferrous disturbance in the north-west corner of the field correlates with a mound visible on the ground surface (Figure 84). This mound may have been built-up from a concentrated deposition of modern material, potentially a feeding trough or other feature related to livestock management; as such features are visible in the satellite imagery. Further areas of ferrous disturbance have also been interpreted, many of which correlate with modern trackway lines visible in the remote sensing imagery. Considering the overall poor magnetic

enhancement of the site, the magnetic results do not indicate any settlement activity or associated features.

4.3.3 Markenfield Hall: Electromagnetic Induction Quadrature-Phase Results

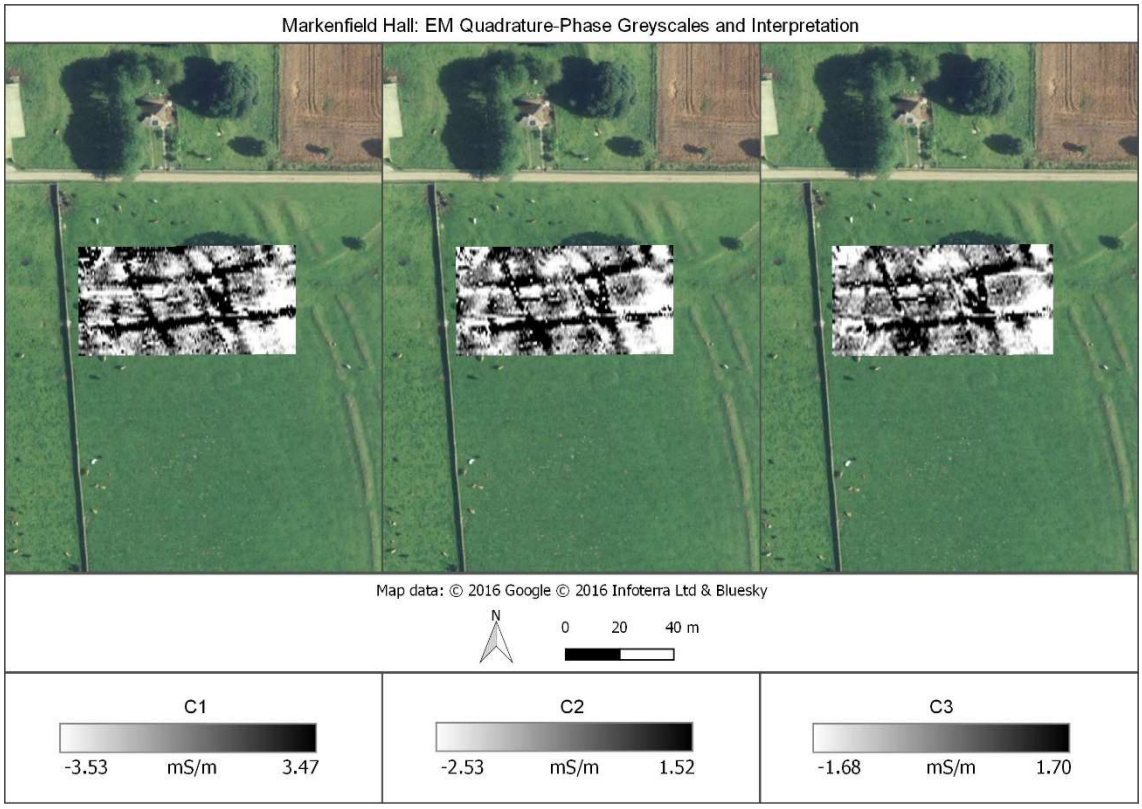

Figure 89: Markenfield Hall electromagnetic induction (HCP quadrature-phase) greyscales.

The EM quadrature-phase has been effective for mapping the trackway features at Markenfield Hall (Figure 89). Broad, high-conductivity rectilinear anomalies traversing across the survey area correlate with ditch-like features, while the corresponding low-conductivity rectilinear anomalies correlate with embankment-like features (Figure 90). The N-S running ditch-like anomalies in the centre of the survey area are detected directly over the modern trackway lines visible in the satellite imagery. The combined quadrature-phase interpretation shows that most of the trackway features are detected through the soil column, with the forms of the anomalous responses remaining relatively consistent between the datasets (Figure 90).

A low-conductivity rectangular anomaly is detected in C2 and C3 at the western terminus of the southernmost east-west running trackway. This feature is not detected in C1; in fact, the trackway anomaly appears to extend through the

location of this feature. Given the deeper depth extent of the rectangular feature, a modern origin is unlikely as it would be anticipated to make an impact on the near-surface topsoil, and affect the extension of the trackway feature, as it does in C2 and C3. Given its intersection with the trackway anomalies in the deeper soil volumes, it may be related to these features. Still, its specific origin can only be inferred—particularly because the anomaly does not correlate with any visible earthworks in the remote sensing; however, it is likely archaeological in origin.

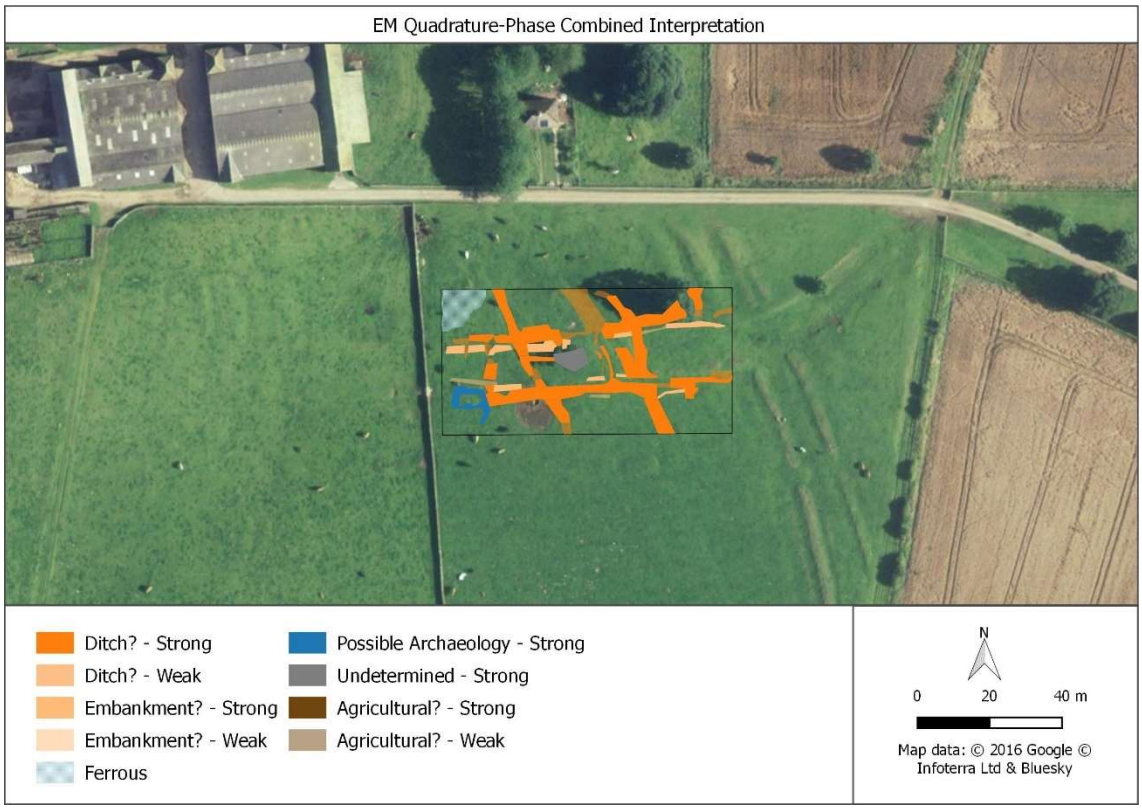

Figure 90: Markenfield Hall electromagnetic induction (HCP quadrature-phase) integrated interpretation. **"**Strong" indicates the anomaly is present in two or more datasets. "Weak" indicates the anomaly is present in only one dataset.

The mean, first principal component and second principal component images are exhaustive representations of the relevant features in the individual datasets, and exhibit little difference between one another. Overall, these composite images do not offer additional interpretative information over the single datasets, as most of the relevant features are discernible in every individual dataset.

Figure 91: Comparison of the Markenfield Hall quadrature-phase coils against (lower row: left-right) the mean of the coils, first principal component and second principal component after the datasets were normalised. Map data: © 2016 Google © 2016 Infoterra Ltd & Bluesky

4.3.4 Markenfield Hall: Electromagnetic Induction In-Phase Results

The EM in-phase has been less than adequate for detecting most of the trackway features (Figure 92). Anomalies associated with the trackways (Figure 93) can be discerned in the deeper coils, but the I1 results have been particularly sensitive to near-surface noise and magnetic enhancement. Overall, anomalies representing the embankment features are more difficult to differentiate from the surrounding data noise than those anomalies representing the ditch-like features; this preferential detection of the ditch-like features is likely a result of the greater physical extent of these features, compared to the embankment features.

The N-S running ditch-like features are the most explicit anomalies in the in-phase results and are detected as strong, positive-contrast anomalies. These areas of ferrous disturbance can be coherently identified in the in-phase results. All the discrete areas of ferrous disturbance occur within the trackway features, except for in the north-west corner, where the responses correlate with an extant mound on the ground surface. The ferrous responses likely represent the deposition of mixed modern material.

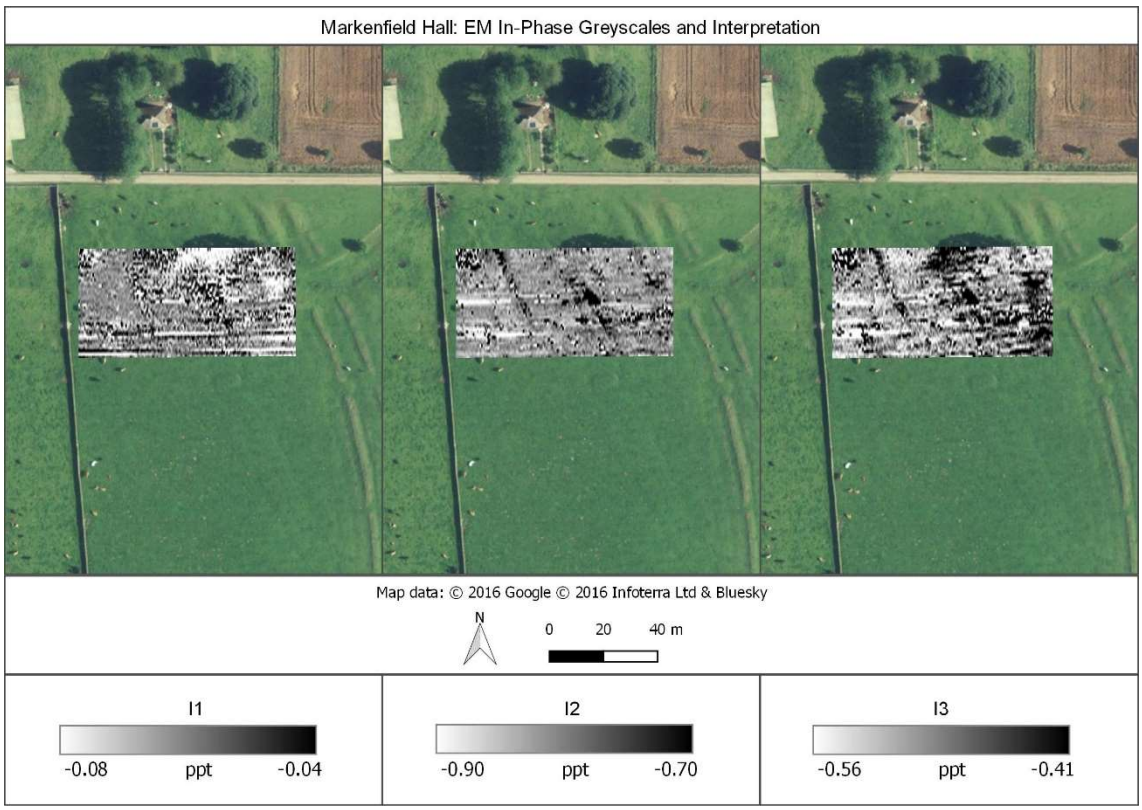

Figure 92: Markenfield Hall electromagnetic induction (HCP in-phase) greyscales.

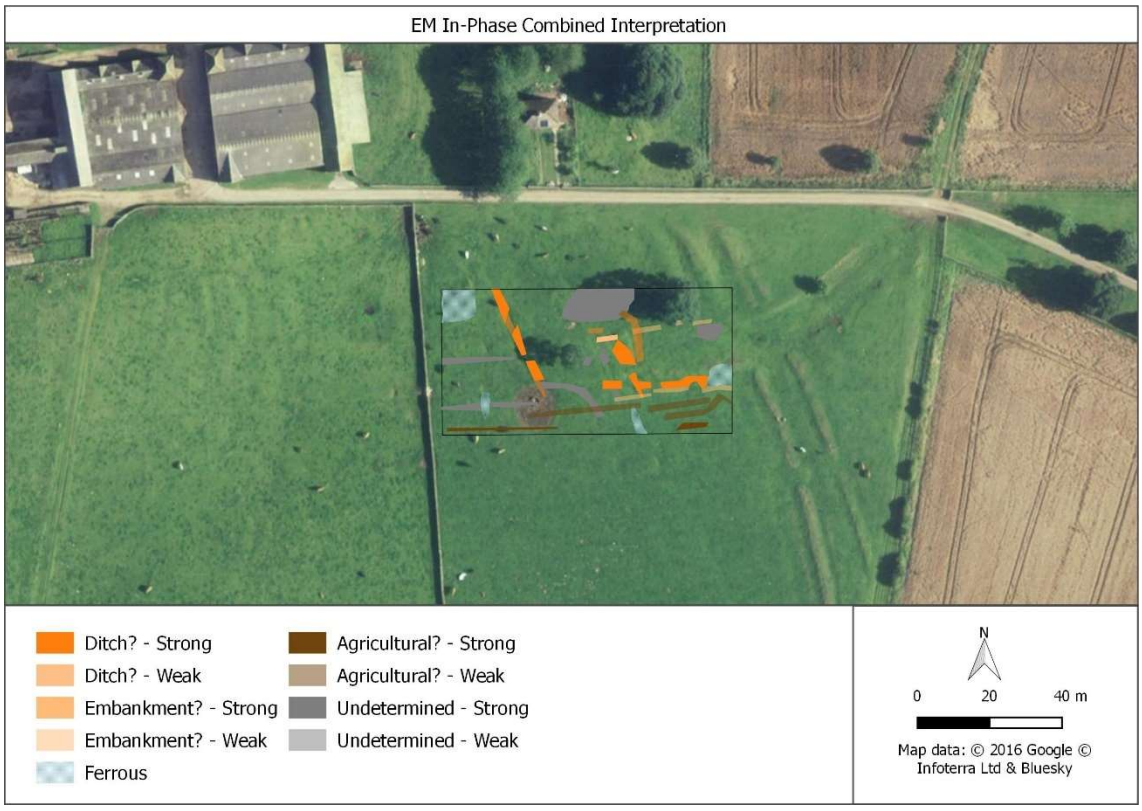

Figure 93: Markenfield Hall electromagnetic induction (HCP in-phase) integrated interpretation.

A series of positive, parallel linear anomalies have been detected near the southern end of site and likely represent a former ridge and furrow ploughing

scheme. These agricultural anomalies can be confidently interpreted in the deeper datasets, but data noise and banding in I1 makes distinguishing these features from erroneous responses difficult in the shallower depths. The banding along the line in I1 cannot be confidently interpreted as an actual response, despite the trackway features running in-line with the direction of a traverse, because these responses also have the appearance and magnitude of an instrument or operator induced effect.

The mean of the datasets and the first and second principal components retain this banding in the composite images (Figure 94); although the form of the N-S running trackways is enhanced in the mean image, which makes the features more distinct than how they are resolved in the individual in-phase datasets.

Figure 94: Comparison of the Markenfield Hall in-phase coils against (lower row: left-right) the mean of the coils, first principal component and second principal component after the datasets were normalised. Map data: © 2016 Google © 2016 Infoterra Ltd & Bluesky

The first and second principal component datasets are less useful as composite images (Figure 94), as the response form of the trackway features is obscured by the noise and magnetic enhancement contributed from I1 and I3. Overall the in-phase results are not useful for comprehensively mapping the trackway features. The areas of magnetic enhancement in I1 and I2 are indicative of

potential anthropogenic activity, but distinguishing an origin from modern or archaeological activity is difficult. Overall, the contexts for many of the in-phase responses are poorly understood when interpreting the results without the consideration of complementary geophysical techniques. The following joint interpretation of the in-phase and quadrature-phase results will aid in a more developed understanding of these features.

4.3.5 Markenfield Hall: Integration of EM Results and Composite Analysis

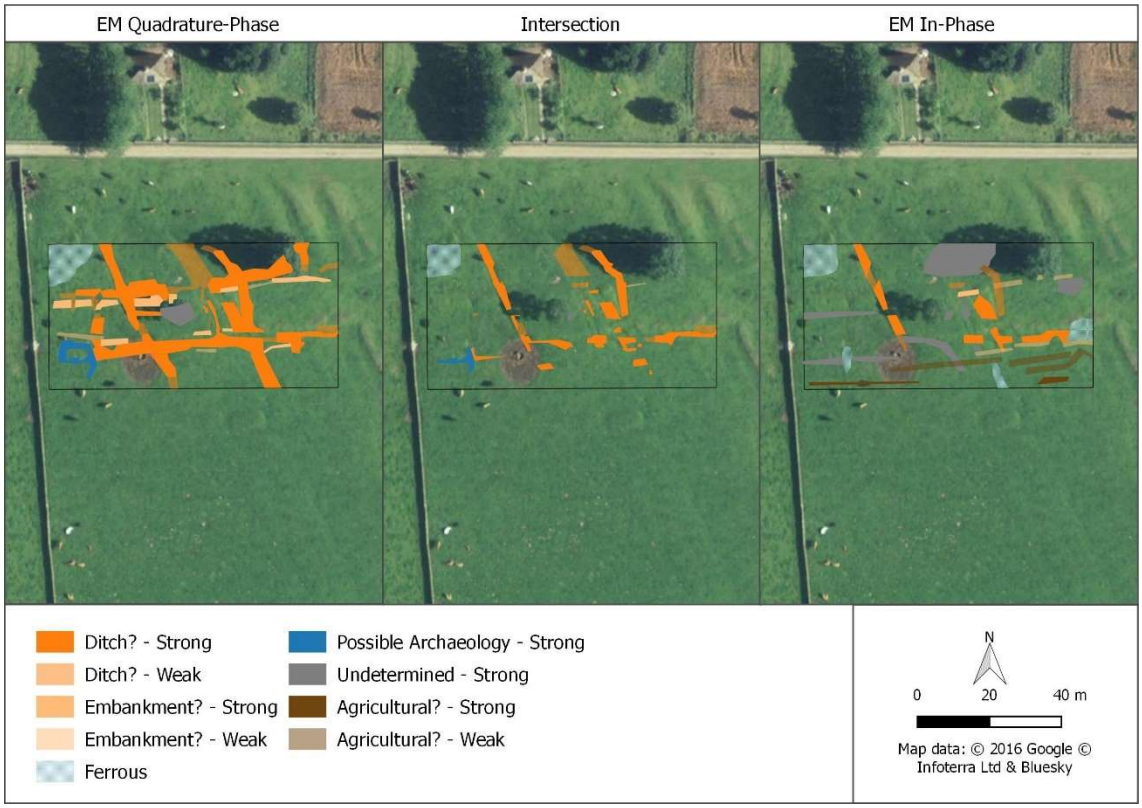

Figure 95: Intersection of the respective EM quadrature-phase and in-phase interpretations, highlighting common features between the datasets. “Strong” indicates the anomaly is detected in two or more of the coils; “weak” indicates the anomaly is only detected in one of the coils.

The E-W running trackways evident in the remote sensing imagery are explicit in the quadrature-phase results, but are not distinctly resolved in the in-phase (Figure 95). The poor detection of the E-W trackways in the in-phase results indicates these features exhibit poor magnetic enhancement; their detection in the quadrature-phase therefore will arise from differences in the electrical conductivity properties between the feature and the surrounding soil matrix. In comparison to the E-W running trackways, the N-S trackways have the same magnitude and form of response as these features in the quadrature-phase; however, the in-phase is able to detect the N-S running trackways. The in-phase’s preferential detection of the N-S running ditch-like features over the E-W running

features could be accounted for by the modern usage of the site for livestock management. Further comparison of these datasets in consideration with the earth resistance and magnetic results will aid comprehensive description of the magnetic and electrical conductivity properties of these features.

4.4.6 Markenfield Hall: Integrated Interpretation and Archaeological Characterisation

The majority of the detected features occur in the earth resistance and EM quadrature-phase datasets at Markenfield Hall. In contrast, the magnetic results are relatively quiet, primarily revealing a scattered detection of ferrous responses. The EM in-phase results have been more successful than the magnetic results for detecting the trackway features, but suffer from increased noise. Given these properties of the individual datasets, the CMYK overlay bears little difference from the individual earth resistance dataset (Figure 96). There is poor correlation across all the geophysical methods at Markenfield Hall. Most of the common anomalies between the datasets occur in the areas of ferrous disturbance (Figure 96), which is confirmed in the GIS analysis (Figure 97).

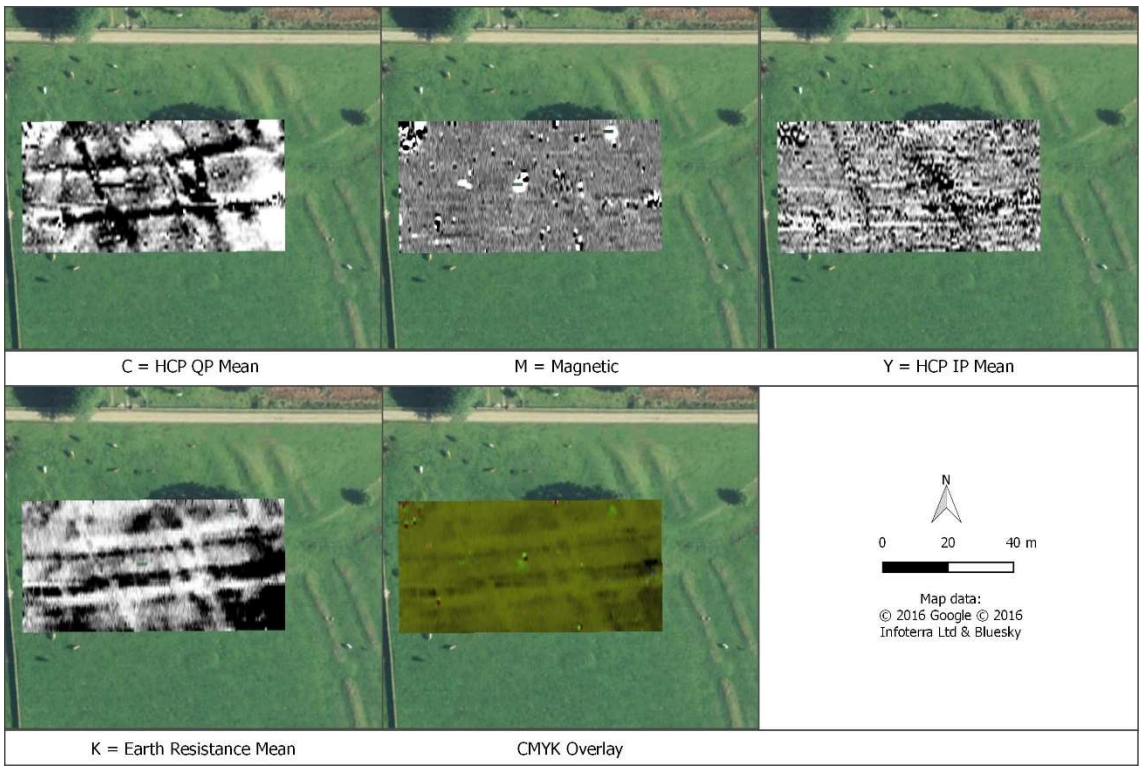

Figure 96: CMYK overlay of the Markenfield Hall geophysical results.

The ferrous disturbance in the north-west corner of the survey area is distinct in all the geophysical datasets; this cross-correlation supports the interpretation of significant deposition of modern debris very near-surface (Figure 97). The intersection of the different methods also confirms that the earth resistance and EM quadrature-phase datasets share the majority of their anomalous responses—particularly for the ditch-like features (Figure 97).

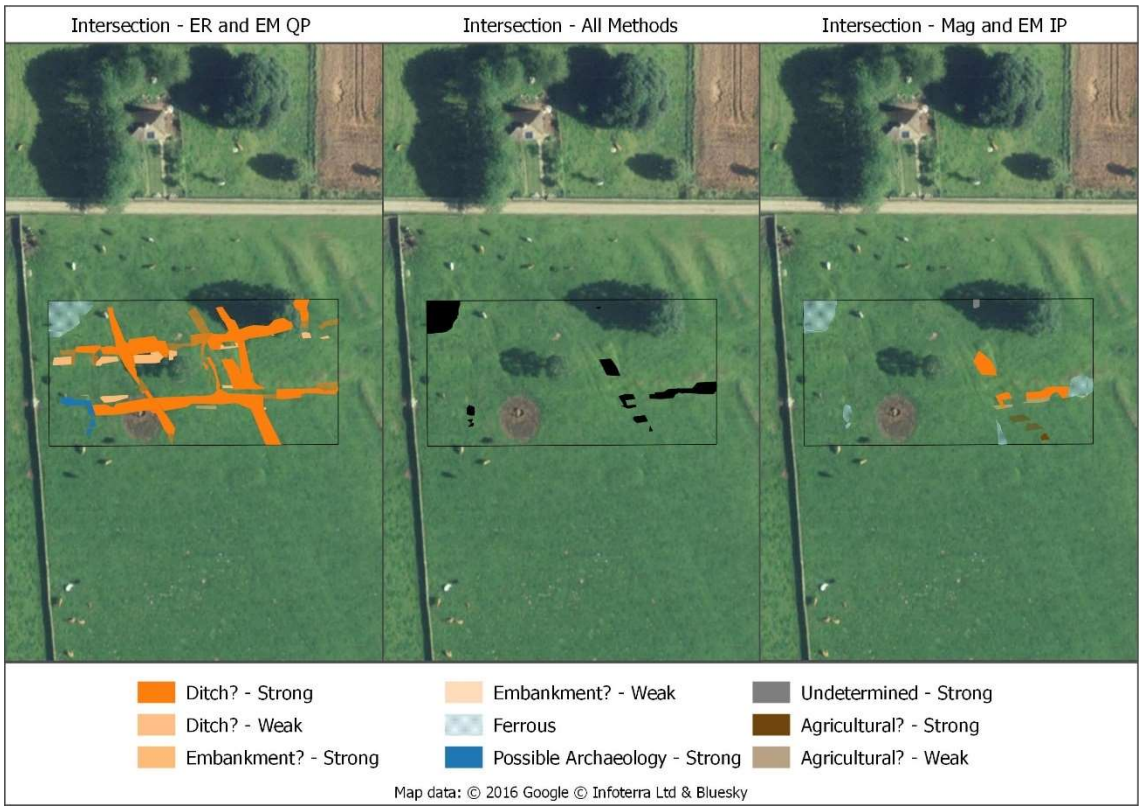

Figure 97: Intersection of the interpretations of all the geophysical methods.

Given the similarities between the EM quadrature-phase and earth resistance datasets, the input datasets were standardised for further data combination. The intersecting trackway features, although slightly diminished in magnitude, can be interpreted in the mean results (Figure 98), primarily representing the contribution from the quadrature-phase and earth resistance datasets. Areas where the different geophysical methods correlate include an area of disturbance in the northwest corner of the field; a ferrous-type response is contributed by the magnetic and EM datasets, while this area appears as a discrete disturbance in the earth resistance results. This area is the primary contribution of the magnetic results, because the low magnetic enhancement of the trackway features has a resulted in a quiet magnetic dataset.

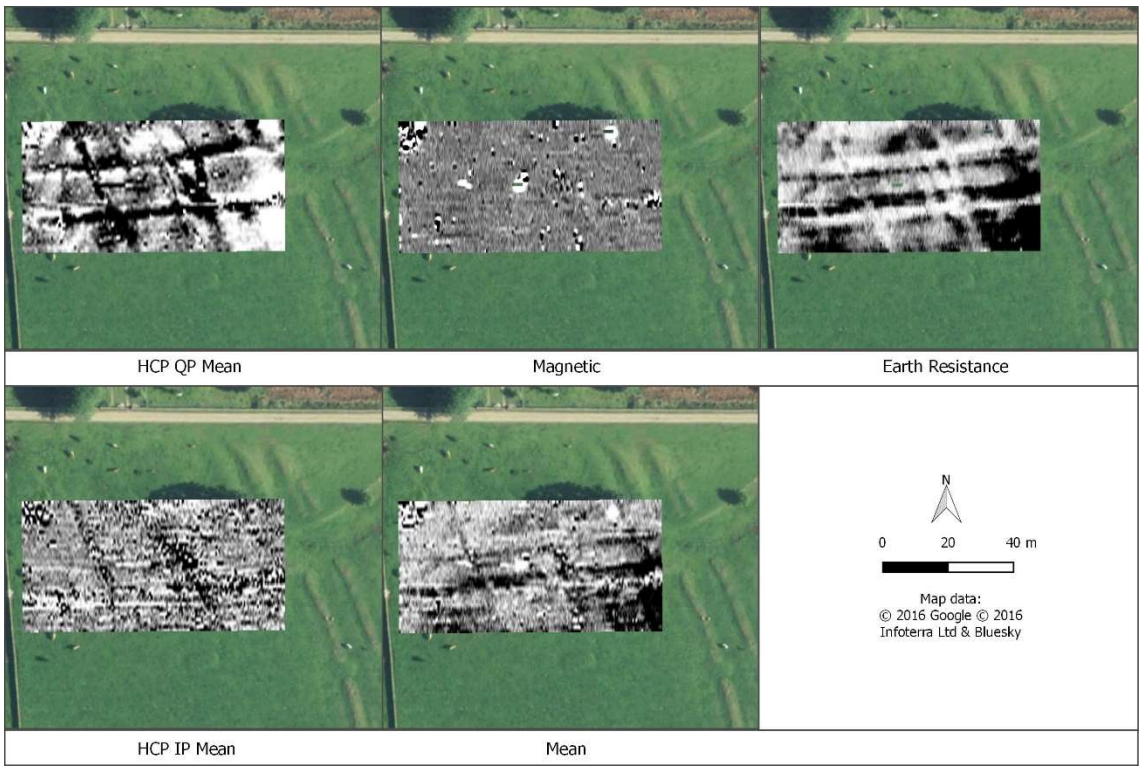

Figure 98: The mean of the geophysical methods at Markenfield Hall after the individual input datasets had been standardised.

While the mean image is a good representation of the different aspects of the individual methods, the first principal component provides a more useful composite image for mapping the trackway and embankment features (Figure 98). The contribution of the magnetic and in-phase results is less explicit in the first-principal component image, but aspects of these datasets are still visible. The second and third principal components highlight the ferrous anomalies. The ridge and furrow responses are most explicit in the second principal component dataset, further enhanced in this image than they are in the individual results. Aspects of the possible archaeological rectangular feature can be discerned in the second and third principal components, but have a more ferrous-type response at the eastern end. The nature of this response indicates contribution from the magnetic results, which could suggest parts of this feature are generated from a modern source. This reduces the confidence in interpretation of this anomaly as an archaeological feature.

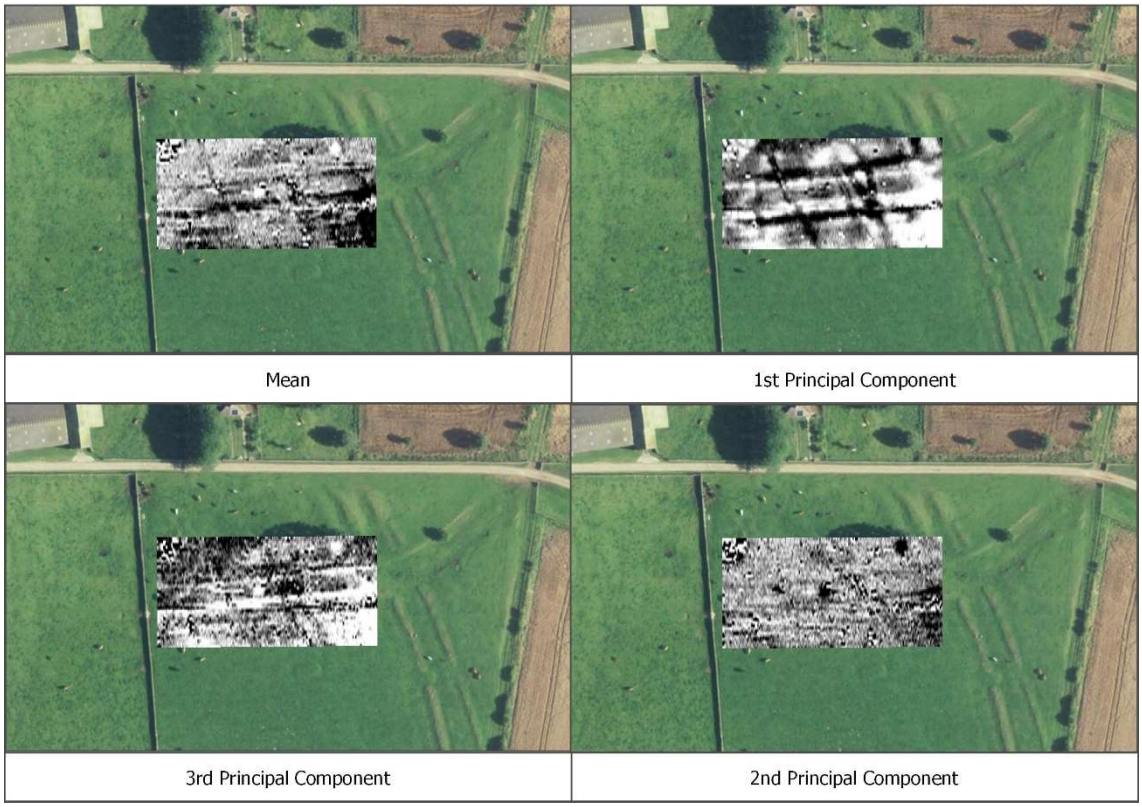

Figure 99: Comparison of the mean of the geophysical results at Markenfield Hall with the first, second and third principal components of the standardised magnetic, earth resistance and EM datasets. Map data: © 2016 Google © 2016 Infoterra Ltd & Bluesky

The earth resistance and EM quadrature-phase results have been the most effective methods for mapping the trackway and embankment features. In both methods, the features are resolved as intersecting linear anomalies, but are detected opposite in sign. The resolution of these trackway features as low resistance, high conductivity anomalies provides evidence that the features are comprised of loosened soil; their detection is a result of preferential moisture holding within the features in contrast to the surrounding soil matrix. Linear features that are comprised of loose soil fill are generally ditch-like in nature. The evidence for these features on the ground surface and in the satellite imagery suggests the features have been formed from anthropogenic modification. Incidentally, the proximity of these features to the medieval manor house and anticipated use related to settlement activity would normally indicate the soils should be magnetically enhanced. Magnetic methods are generally quite effective for detecting ditch-like features when the fill material is magnetically enhanced. However, at this site, both the magnetic and the in-phase results demonstrate poor magnetic enhancement. It is therefore possible this survey area falls outside the limits of the settlement area and does not correlate with

active anthropogenic occupation. These trackway features may therefore represent a transitory zone between Markenfield Hall and the potential associated medieval village. Further geophysical survey in the rest of the field and adjacent areas would be helpful for mapping the extent of these trackway features to further contextualise the archaeological landscape of this area.

4.3.7 Markenfield Hall: Conclusions

The geophysical methods have produced mixed results over the survey area at Markenfield Hall. The earth resistance and EM quadrature-phase methods have been successful for detecting the trackway and embankment features; while the magnetic and in-phase methods struggled to detect the weak magnetic contrast of these features. The potential archaeological reasons for the poor magnetic contrast of these features is discussed above in section 4.3.7. Environmental factors, although possible, are a less likely cause for the poor magnetic response. None of the recorded soil or geological information indicates a subsurface that is explicitly unsuitable for magnetic survey. While results of magnetic survey over dolostone geology is poorly documented, dolostone falls within the category of carbonate sedimentary rocks, which includes limestone. Magnetic responses over limestone geology have been evaluated as good (David et al. 2008).

4.4 Linton: Results and Characterisation

The work at Linton targeted the area surrounding a complex of circular earthworks within an elevated ridge. The earthworks are part of a greater archaeological landscape that has been utilised for multi-occupation agricultural activity and livestock management (see section 3.3.4.4 for further detail). The site has been previously mapped through a walkover survey by Moorhouse (2006), who interpreted the earthworks as potential Iron Age roundhouses. The following results will consider his work as a frame of reference, using the integrated geophysical results to derive a more certain characterisation of these features.

4.4.1 Linton: Magnetic Results

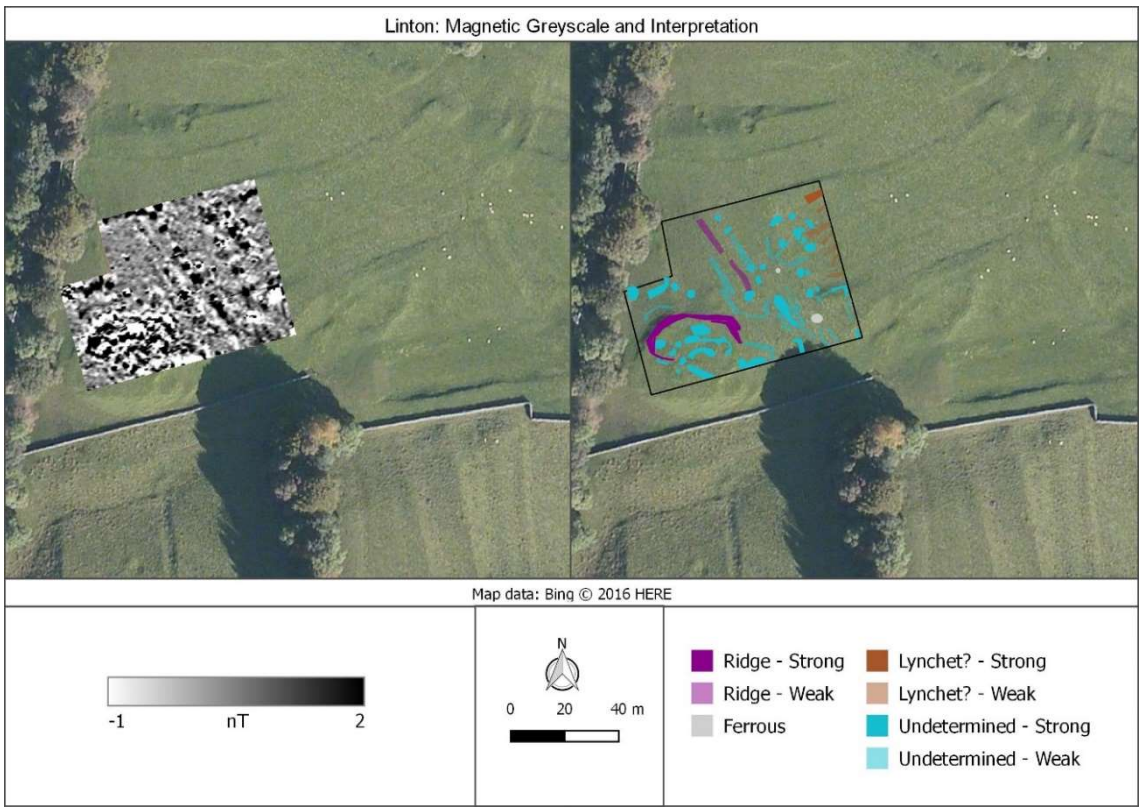

Figure 100: Linton magnetic greyscale and interpretation (Bartington Grad601-2). "Strong" indicates a high-contrast response while "weak" indicates a low-contrast response. Anomalies interpreted as "ridge" correlate with features drawn on the earthworks plan of the site (Moorhouse, 2006).

The magnetic method has been effective for detecting the earthwork features at Linton. Many of the magnetic anomalies correlate with features visible in the satellite imagery and drawn on Moorhouse's (2006) plan of the site (Figure 100). The earthwork features at the southwestern corner of the site, which Moorhouse (2006) has interpreted as a complex of Iron Age roundhouses, are resolved in the magnetic results as series of concentric hemispheric rings. These anomalies do not have an apparent form that would suggest a roundhouse origin; although given the magnitude of response, magnetic enhancement of this area through anthropogenic activity is probable.

Other distinct features in the magnetic results include a N-S running linear feature, which has been interpreted as a "ridge" feature from Moorhouse's (2006) plans. Flanking this feature are further linear anomalies that could be indicative of natural topographic changes. An alignment of strong, pit-like anomalies has also been identified running parallel with these features. While the alignment of the pit-like anomalies could be indicative of an anthropogenic origin, the presence

of superficial sand and gravel deposits recorded within this area means a natural origin cannot be entirely ruled out; hence, these features have been classified as Undetermined.

Lynchet features, visible in the satellite imagery running east-west, are detected in the magnetic results primarily as weak, parallel linear anomalies. A number of other anomalies are detected in the magnetic results that do not correlate with any features denoted in Moorhouse's (2006) plan or correlate with features visible in the satellite imagery; as these anomalies lack a coherent patterning to indicate a specific archaeological origin, they have been classified as Undetermined.

4.4.2 Linton: Earth Resistance Results

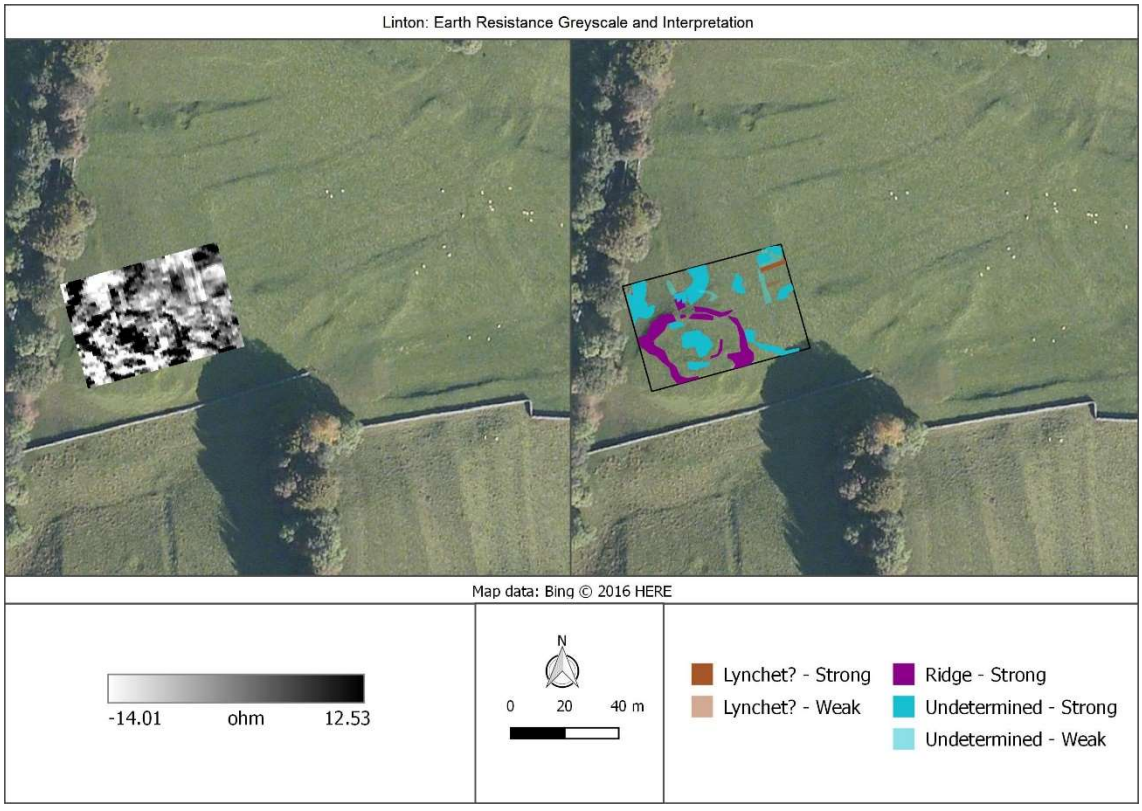

Figure 101: Linton earth resistance greyscales and interpretation (combined Wenner and twin-probe arrays).

The earth resistance results clearly resolve a high-resistance sub-circular anomaly in the southwest corner of the field. The northern and eastern extents of this feature correlate with ridges visible in the satellite imagery and on the ground surface. The western edge of this anomaly does not extend to the edge of the earthwork feature, but does correlate with other potential archaeological features denoted in Moorhouse's (2006) drawings. The earth resistance results do not

reveal any internal structuring within the enclosure that would support the presence of a settlement area; however, the sampling strategy employed was relatively coarse (1m x 1m) and may be too large to detect discrete features, such as pits.

Outside of the circular earthwork feature, the other earth resistance anomalies are ambiguous in origin; although a couple of weak, linear anomalies are in alignment with the lynchet features in the satellite imagery. Overall, the ambiguous anomalies lack a distinct form and correlating evidence that would be informative for ascribing a specific archaeological, agricultural or natural origin. Thus, these anomalies have been classified as Undetermined.

4.4.3 Linton: Electromagnetic Induction Quadrature-Phase Results

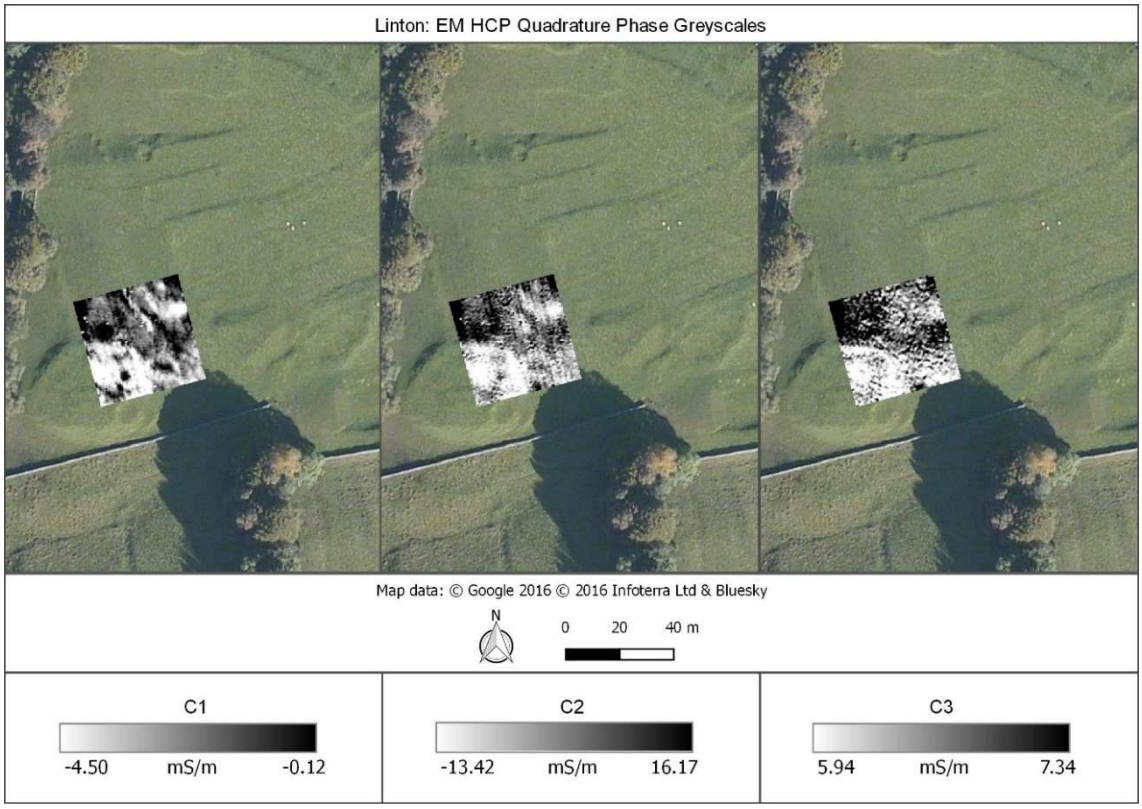

Figure 102: Linton electromagnetic induction (HCP quadrature-phase) greyscales.

Figure 103: Linton electromagnetic induction (HCP quadrature-phase) interpretation. “Strong” signifies the anomalies occurs in two or more datasets while “weak” signifies the response only occurs in one dataset.

The EM quadrature-phase reveals anomalies that correspond with the earthworks visible in the satellite imagery and Moorhouse’s (2006) plans. The C1 configuration has provided the clearest and most detailed delineation of these features, resolving the circular earthworks feature as an area of lower conductivity. Two distinct high conductivity anomalies are detected within this feature, circular and curvilinear in form. The circular anomaly is collocated with a house feature drawn by Moorhouse (2006). A NW-SE running linear negative-contrast anomaly correlates with the ridge drawn on Moorhouse’s (2006) plans; although in the quadrature-phase results, distinct high conductivity anomalies flank this feature. The clarity of these anomalous responses is reduced in the increasing soil depths, with the C2 and C3 datasets demonstrating increased noise. The increased noise with greater depth is opposite in behaviour to the previous sites, where the shallower EM datasets exhibited increased noise over the deeper datasets. Figure 103 visualises how only a few of the distinct anomalous responses are detected through all the soil volumes; thus, when the mean of the datasets is taken, the increased noise in C2 and C3 obscures many of the unique anomalies in C1 (Figure 104). In contrast to the mean results, the

first principal component is a more effective composite image as it not only retains the unique anomalies in the C1 dataset, but further enhances these responses, which aids in visualising new features. The second principal component primarily represents the noise in the C2 and C3 results.

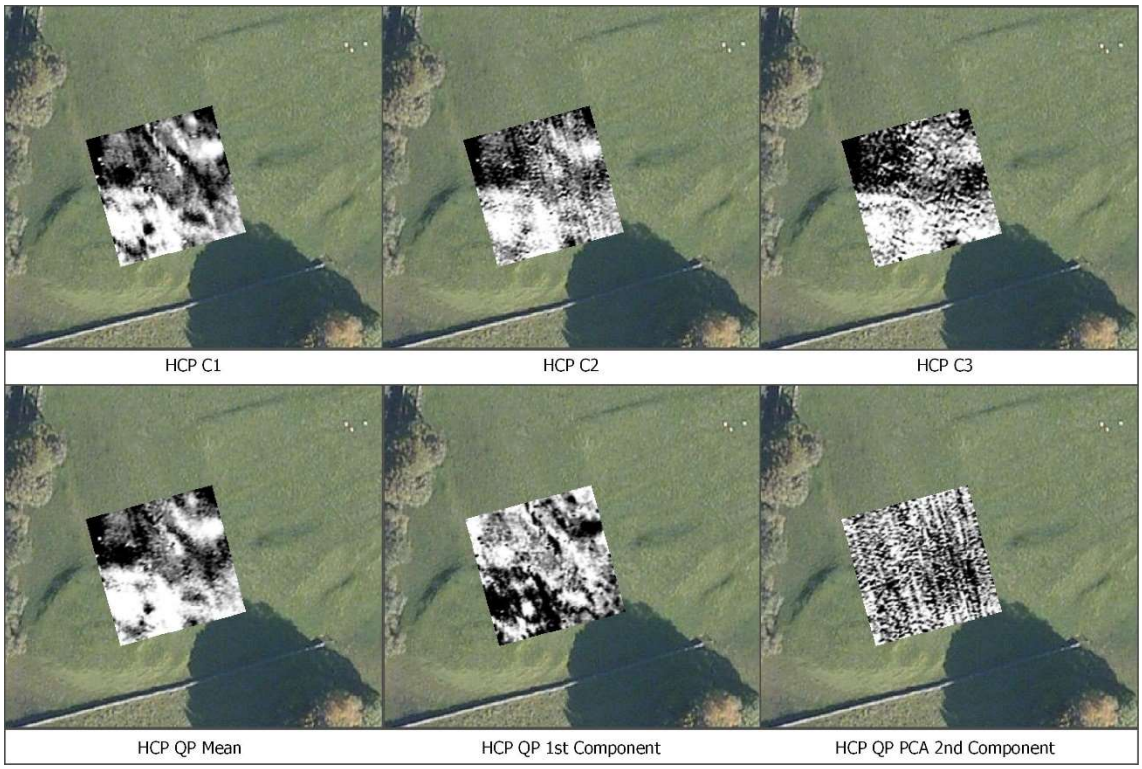

Figure 104: Comparison of the (bottom row: left-right) mean, first principal component and second principal component of the individual (top row: left-right) C1, C2 and C3 datasets.

4.4.4 Linton: Electromagnetic Induction In-Phase Results

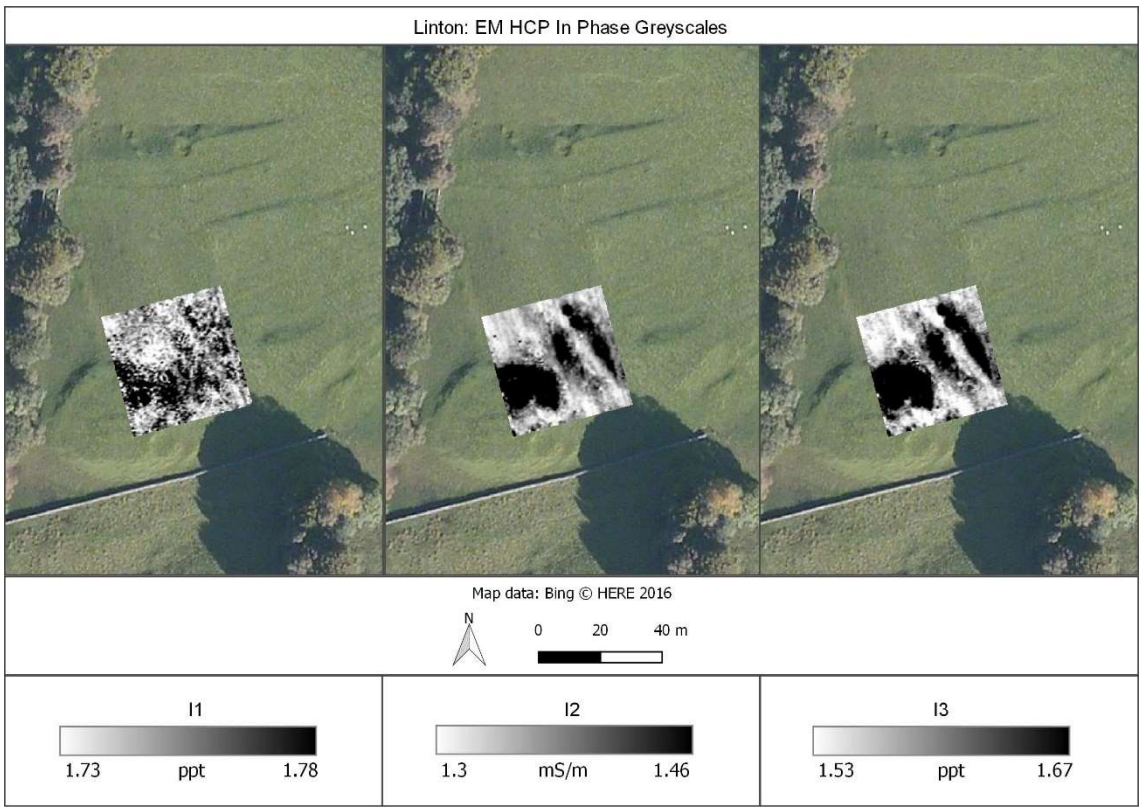

Figure 105: Linton electromagnetic induction (HCP in-phase) greyscales.

Figure 106: Electromagnetic induction (HCP in-phase) integrated interpretation. “Strong” indicates the anomaly was present in two or more datasets, while “weak” indicates the anomaly was only present in one.

The EM in-phase results have resolved anomalies relating to the earthwork features at Linton, but the resolution of these features is distinct with depth (Figure 105). The I2 and I3 datasets are very similar, but I1, in contrast, is unique. I1 is more susceptible to increased noise than the deeper soil volumes, but distinct linear and curvilinear anomalies can still be distinguished in the results. Circular and curvilinear anomalies are detected over the earthwork features in the I1 results; whereas the I2 and I3 resolve a broad area of strong magnetic enhancement. Further areas of broad magnetic enhancement in the I2 and I3 results occur on either side of the circular ridge, which may be a result of anthropogenic activity or a natural topographic effect (Figure 106). Owing to the similarities between the I2 and I3 datasets, the in-phase's mean results almost entirely represent these datasets (Figure 107). In contrast, the first and second principal components offer unique representations of the in-phase results, which are not visually reminiscent of any individual dataset (Figure 107). The first principal component primarily reflects the broad, magnetic enhancement areas in I2 and I3. In contrast, the second principal component reveals features that are not explicit in any of the individual datasets (Figure 105), such as several isolated circular anomalies.

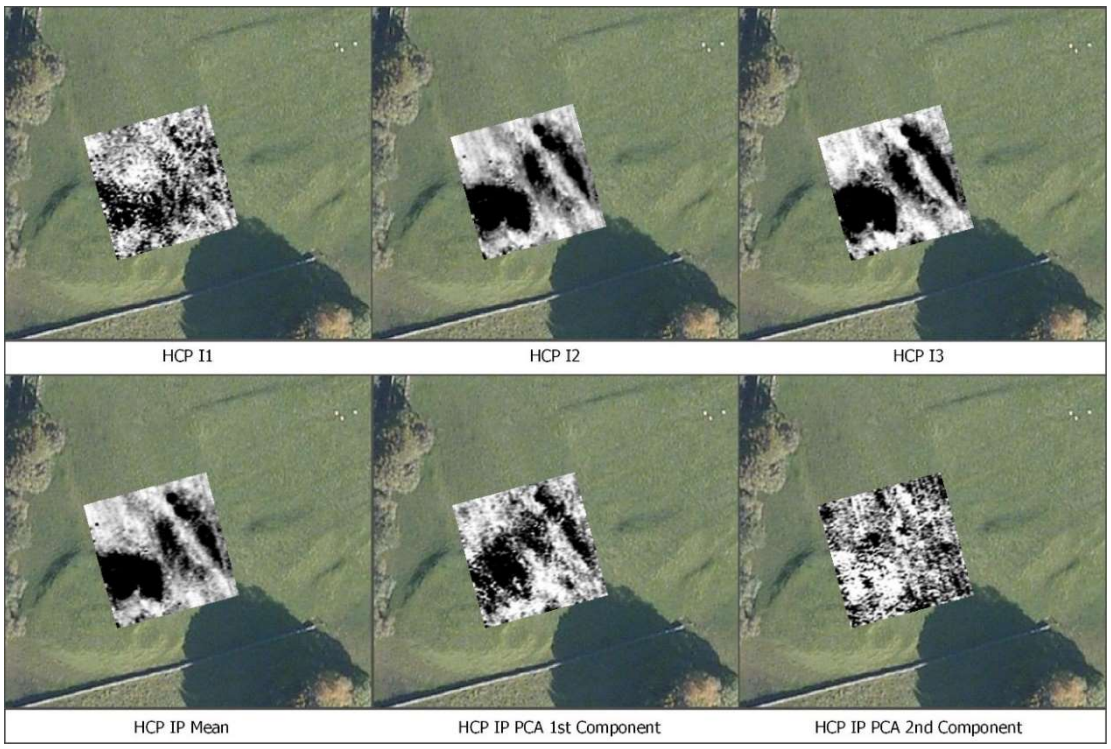

Figure 107: Comparison of the (bottom row: left-right) mean, first principal component and second principal component of the normalised individual (top row: left-right) I1, I2 and I3 datasets.

4.4.5 Linton: Integration of EM Results and Composite Analysis

The shallowest soil volumes measured by both phases have a more defined detection of the individual features than the larger soil volumes do, which indicates the features lie near surface and have a limited depth extent. Overlaying the combined EM quadrature-phase interpretation over the greyscale of the mean in-phase results visualises how the EM phases are responding to different features. The defined curvilinear and circular anomalies within the quadrature-phase fit within the broad contextual responses in the in-phase. Given the distinctness between the in-phase and quadrature-phase results, comparing the EM results against the earth resistance and magnetic methods could provide further evidence for what different features these techniques are measuring.

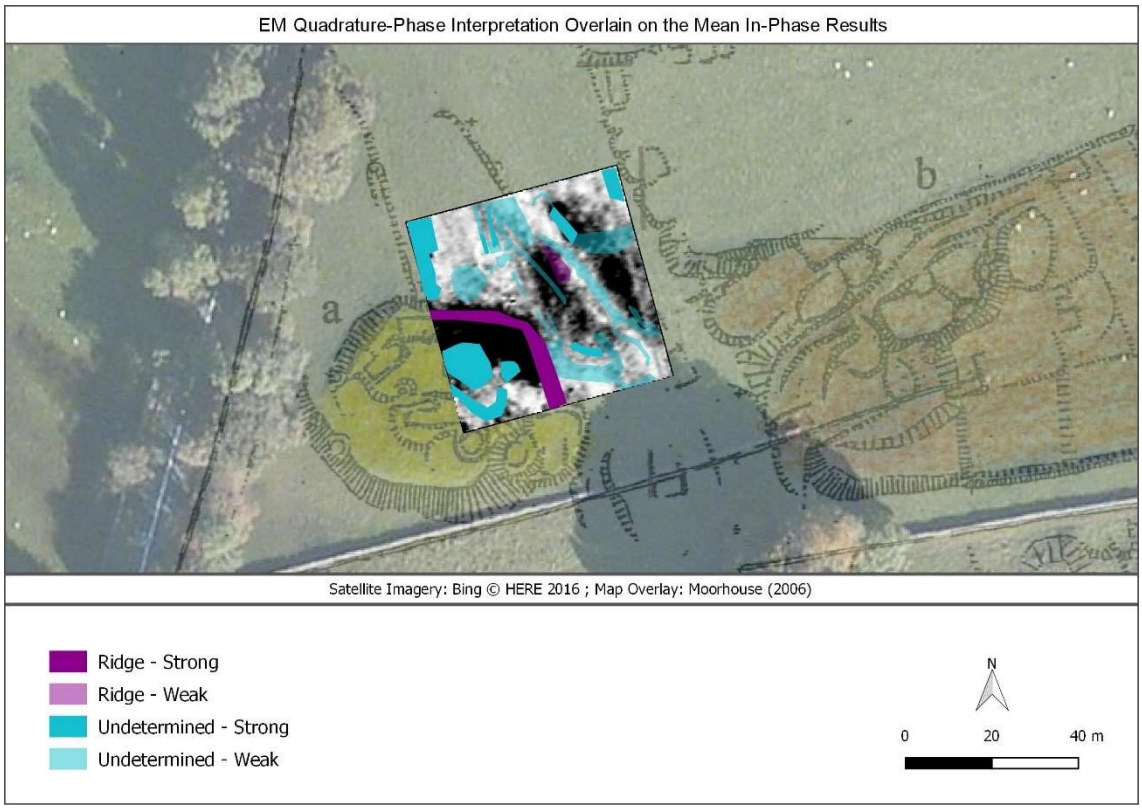

Figure 108: The combined QM quadrature-phase interpretation overlain the mean in-phase results.

4.4.6 Linton: Integrated Interpretation and Archaeological Characterisation

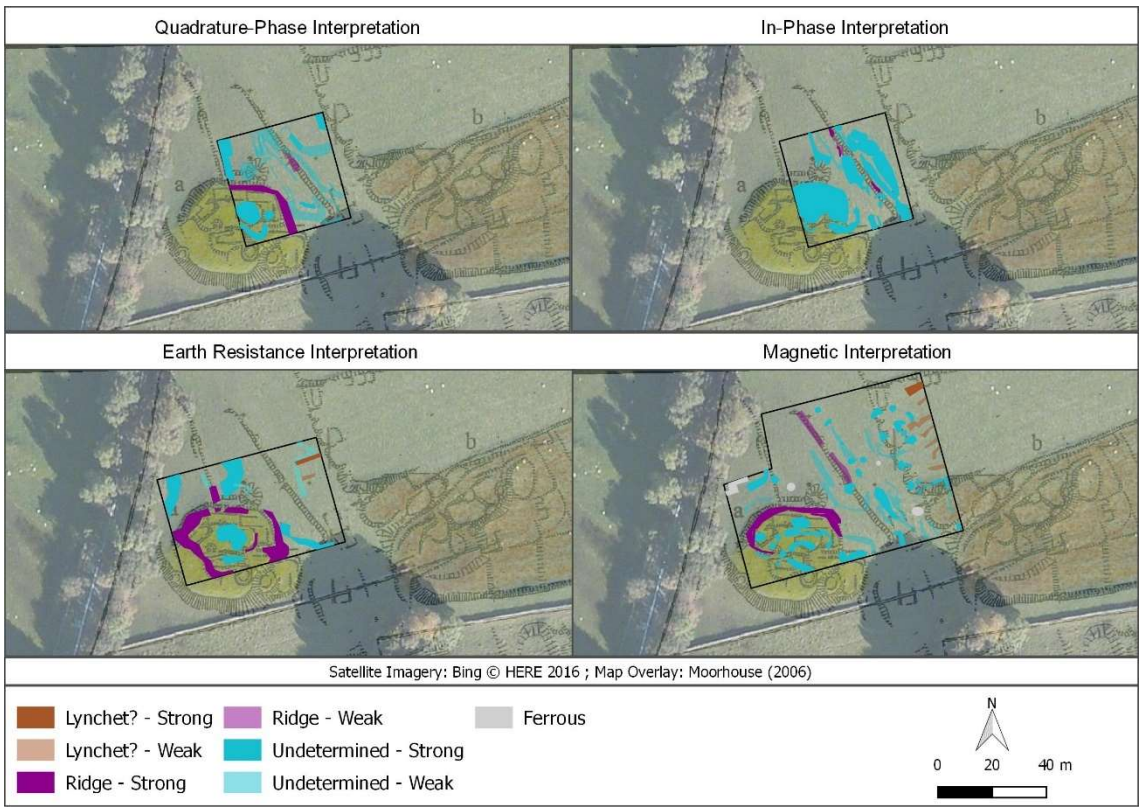

Figure 109: The interpretations of the EM, earth resistance and magnetic methods at Linton.

The circular earthwork in the southwest corner of the survey area is the most coherent feature between the different methods' results (Figure 109). The extent of this feature is consistent between the different methods and coincides with the drawings in Moorhouse's (2006) plans. However, where the different methods vary is the delineation of the internal structuring of this feature. The EM quadrature-phase and earth resistance results show a similar circular feature within the enclosure, flanked by rectilinear anomalies. The first principal component of the different methods (Figure 110) enhances the internal features within the circular earthwork, represented in the earth resistance and quadrature-phase results.

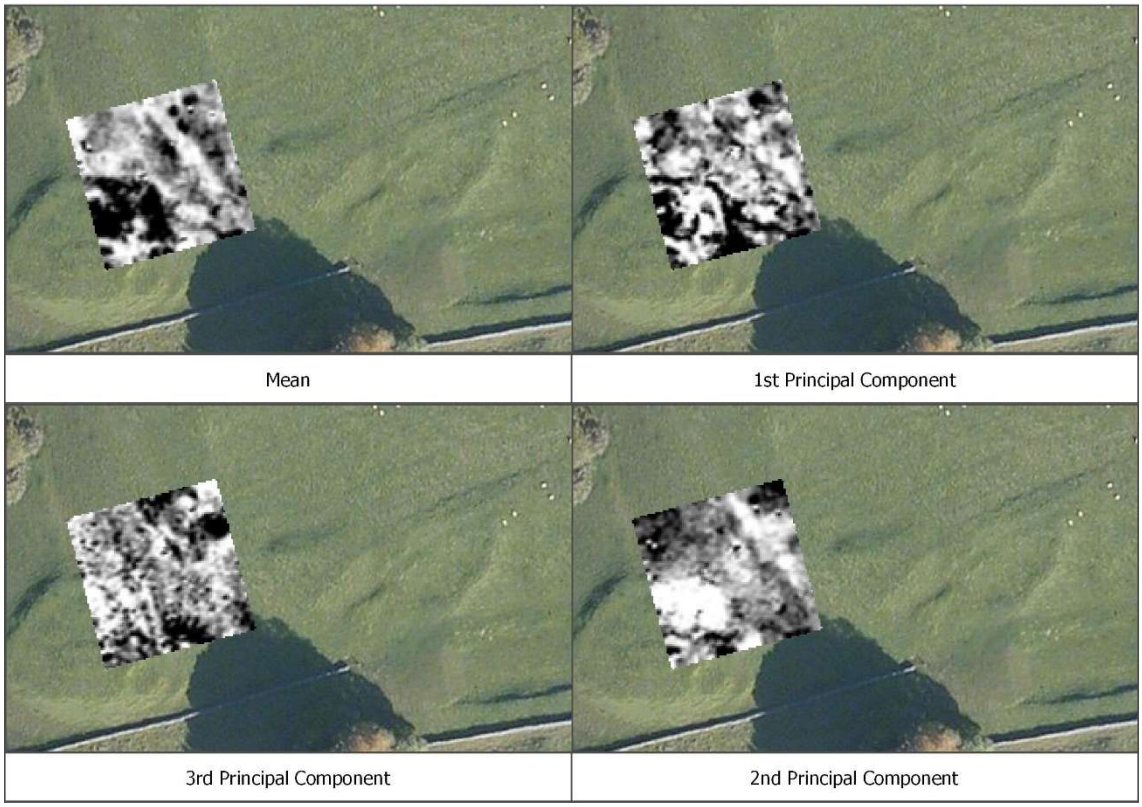

Figure 110: The mean, first principal component, second principal component and third principal component of the EM, earth resistance and magnetic results.

The CMYK overlay visualises how the broad area of enhancement resolved within the in-phase results (i.e. the magenta colour) is bounded by the internal rectilinear anomalies and outer extent of the earthwork feature, as delineated in the earth resistance and quadrature-phase results (Figure 111). The juxtaposition of these responses suggests the vivid pink area within the greater circular earthwork feature experienced increased anthropogenic activity and usage, compared to the other areas.

The CMYK overlay also emphasises two vivid pink anomalies in the northeast corner of the survey area, which correlate with pit-like anomalies in the magnetic results. These pit-like features cannot be separated from the broad, enhancement areas in I2 and I3, but correlate with two high-contrast positive anomalies in I1; although they are still difficult to discern in the individual I1 results due to apparent data noise. The correlation with the magnetic results and the strong responses in the composite images provides further evidence to support a potential anthropogenic origin for these anomalies—distinct from the ridge topographic changes. The limit of this material could relate to the magnetic

enhancement of the soil through animal waste—as the enclosure could reflect livestock management.

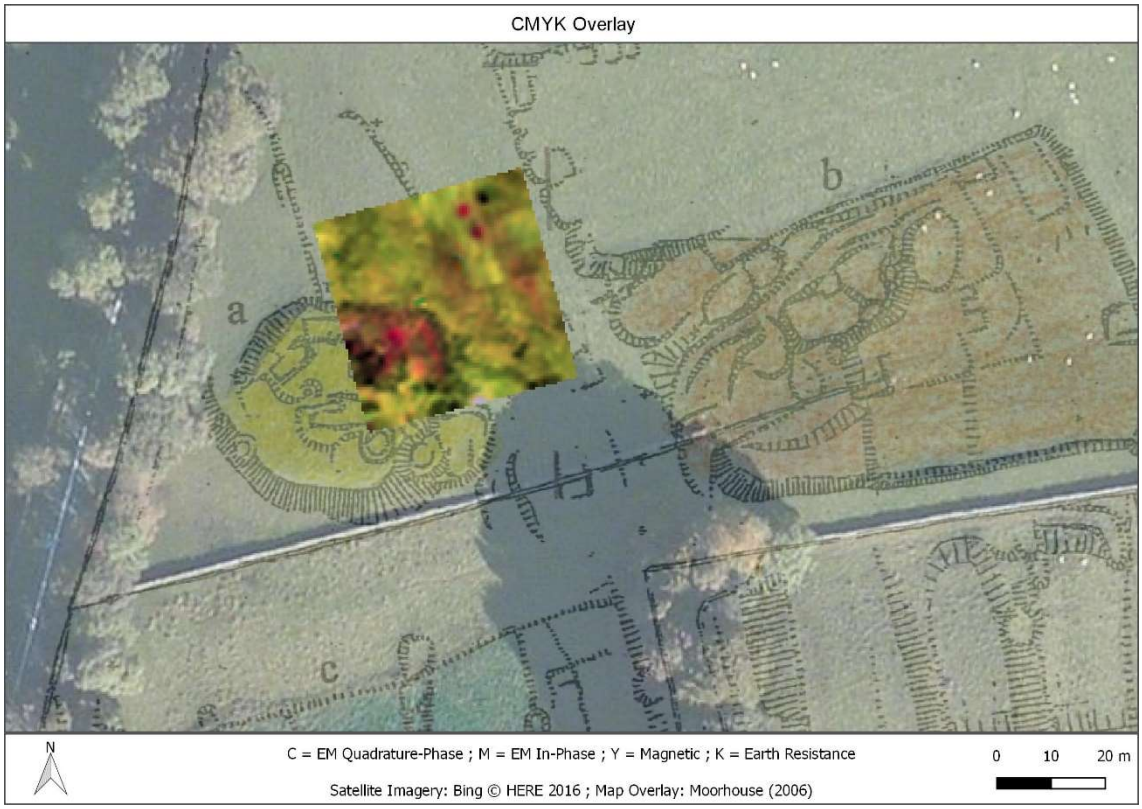

Figure 111: CMYK overlay of the different methods. The mean dataset for the in-phase was used while the first principal component for the quadrature-phase was used.

Interpretation into the origins of the other features outside of the circular earthworks complex is less certain given the poor correlation between the datasets (Figure 112). The in-phase results offer broad contextual information while the magnetic, earth resistance and quadrature-phase results offer detailed information. While the anomalies between the datasets are detected within the vicinity of another, the archaeological correlation between the responses is difficult to ascertain. Given the long history of archaeological activity within this landscape, the detected anomalies may represent multiple phases of anthropogenic activity—which would futher complicate the archaeological interpretation.

Figure 112: Geometric intersection of the features present in the EM, magnetic, and earth resistance datasets at Linton.

4.4.7 Linton: Conclusions

The geophysical methods have been effective at Linton, but have produced unique and complex results. The CMYK image has been the most effective integration technique at the site, providing a coherent relationship between the different methods over the circular earthwork complex in the south-west corner. While some of the anomalies within this area correlate with features drawn in Moorhouse's (2006) plans, none of methods provide clear evidence for any Iron Age roundhouses or other settlement activity. Outside of the circular earthwork complex, the correlation between the different methods is harder to ascertain. The results of this work demonstrate that the geophysical success of a survey does not necessarily guarantee meeting the archaeological objectives of the investigation. A detailed topographic survey could help elucidate the origins of these anomalies, since the topographic relief in this area varied greatly.

4.5 Menston: Results and Characterisation

The work in Menston, West Yorkshire comprised the Buckle Lane Cemetery, which once served as the cemetery for the nearby High Royds Hospital, formerly the West Riding Pauper Lunatic Asylum. The arrangement of the burial plots is

known from a historic plan of the site; metal markers, denoting the row and plot number of the individual graves, were discovered on site and support the adherence to this plan. The plan will be used as a common reference point to directly compare the results of the different methods.

4.5.1 Menston: Magnetic Results

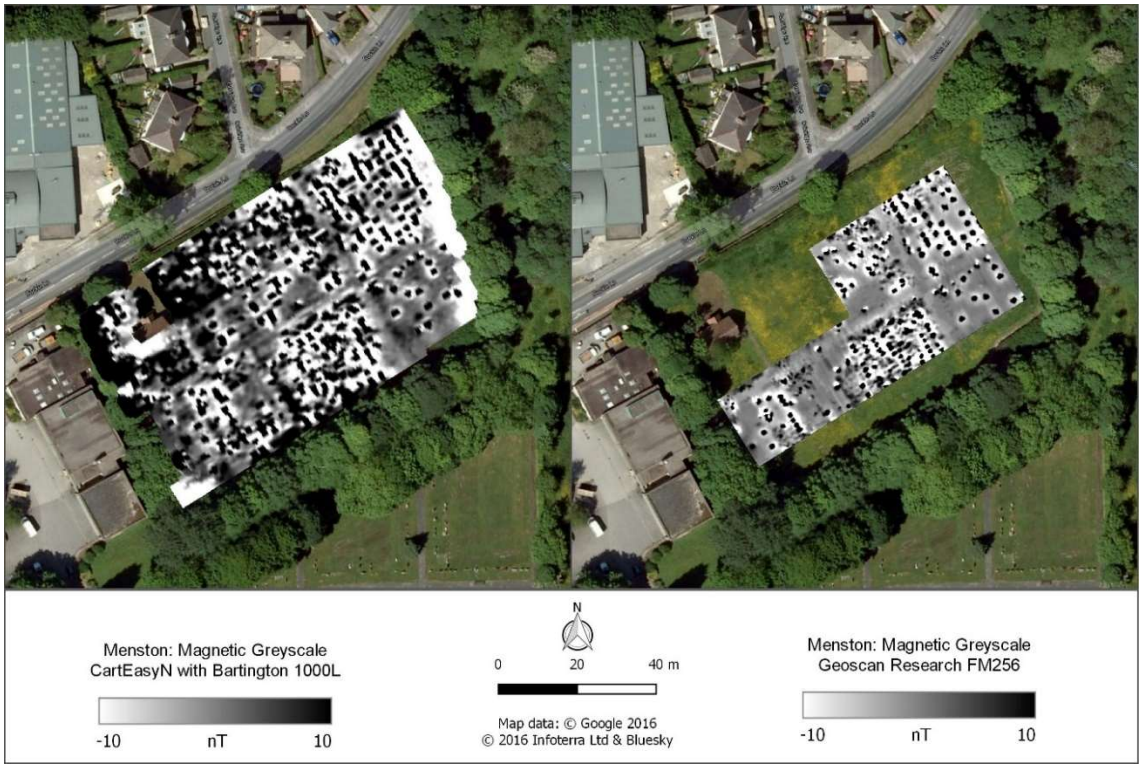

Figure 113: Menston magnetic greyscales comparing GPS-positioned (left) and grid-positioned (right) results.

Figure 113 shows the results of two separate magnetic surveys at Menston using GPS (CartEasyN with Bartington 1000L) and gridded (Geoscan Research FM256) survey strategies. The magnetic results are primarily responding to the buried iron plot markers, which are resolved as high-contrast magnetic points with a negative magnetic halo. An analytic signal was performed to help distinguish the individual marker anomalies by reducing the broad dipolar response back to the origin source (Figure 114). The analytic signal's reduction to point source was most successful on those individual anomalies that exhibited a distinct bipolar response. Marker anomalies that lacked the typical, high-contrast bipolar response were lost through the filtering process. Thus, both the filtered and unfiltered datasets were essential to make a comprehensive interpretation.

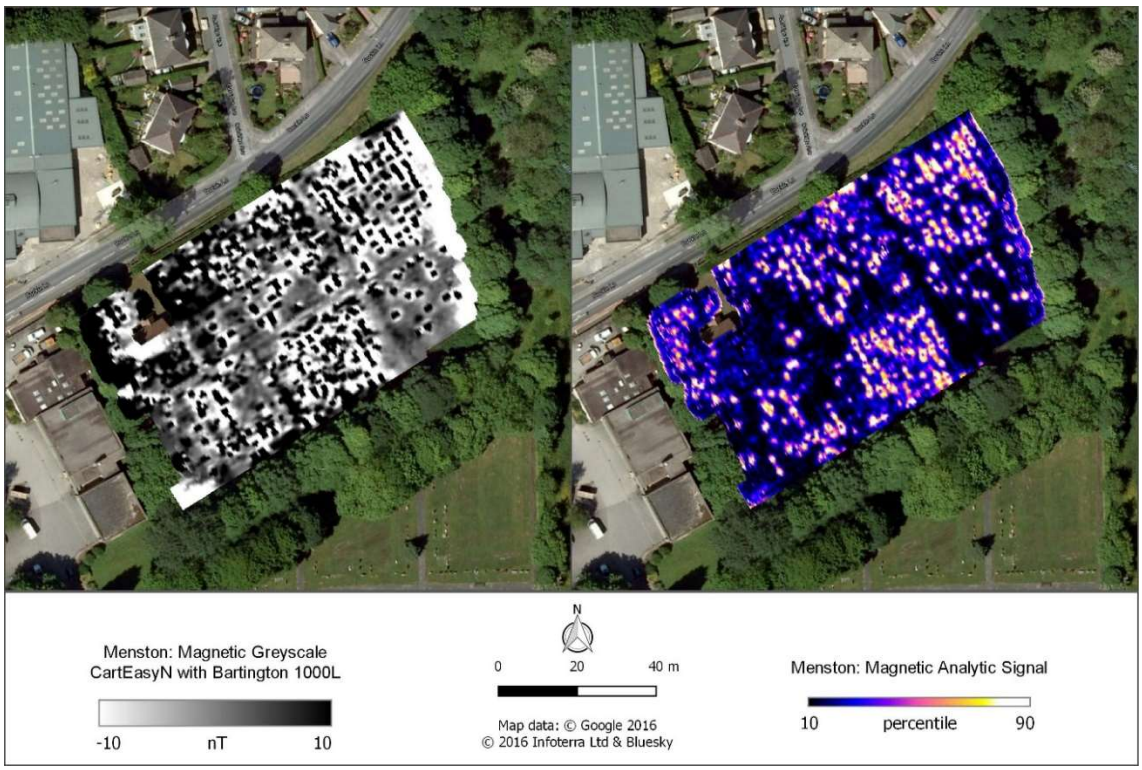

Figure 114: Menston magnetic greyscale (left) and analytic signal results (right) from the CartEasyN with 1000L system.

Figure 115: Menston combined magnetic interpretation of the GPS-positioned and gridded results. “Strong” denotes a high-contrast response, while “weak” denotes a low-contrast response.

The combined magnetic interpretation (Figure 115) highlights the concentration of the marker anomalies; the alignment of which fits within the ordered arrangement of the burial plots in the historic plan. In regards to the other features detected in the magnetic results, the paths are weakly resolved as negative-contrast and positive-contrast anomalies. Amorphous areas of weak magnetic enhancement can be discerned within some of the burial sections as well. These areas of weak magnetic enhancement have been classified as Undetermined, as the origin of these response is ambiguous, although is likely caused by an associated burial process.

4.5.2 Menston: Earth Resistance Results

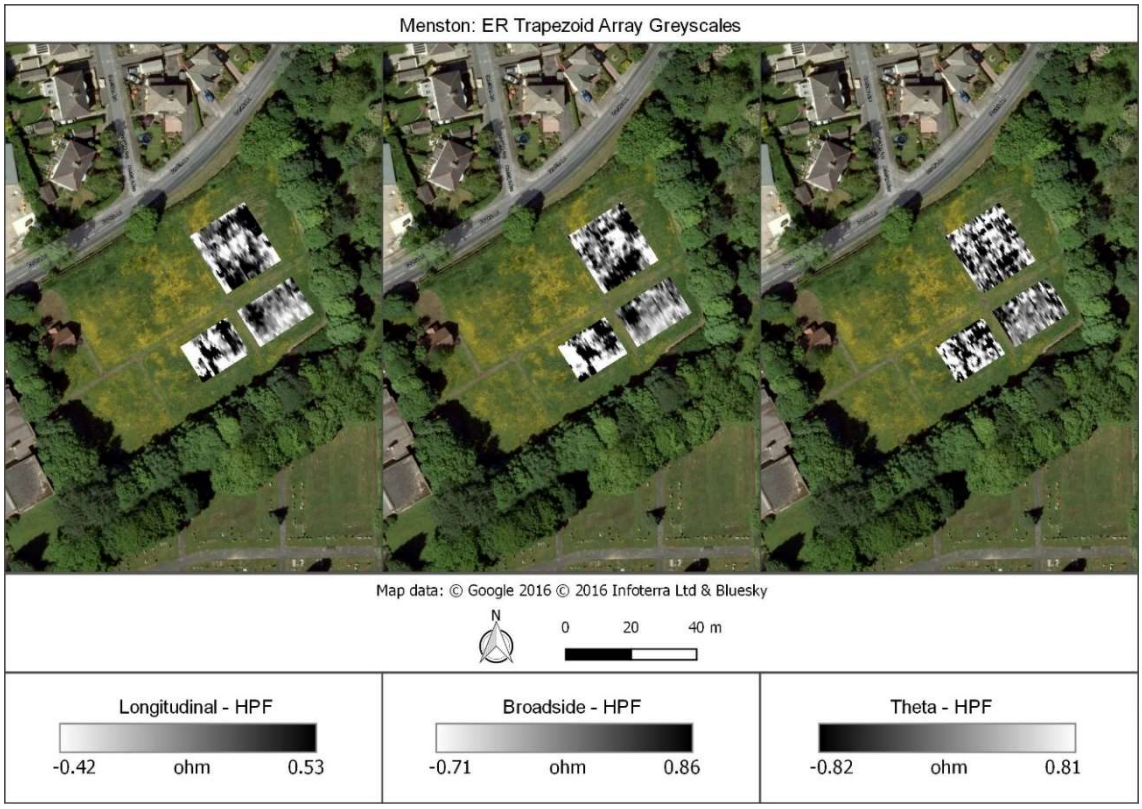

Figure 116: Menston earth resistance (trapezoid array) greyscales.

Figure 117: Menston earth resistance (twin-probe array – a = 0.5 m) greyscale.

Both the trapezoid array (Figure 116) and the twin-probe (Figure 117) earth resistance results are presented because the different arrays offer unique and complementary interpretation information. Both datasets reveal broad areas of variation, but individual grave features can be identified among these areas under close examination of the results. In the trapezoid array results, discrete positive-contrast and negative-contrast rectangular anomalies have been classified as grave features because their position correlates with individual burial plots denoted in the historic mapping (Figure 118). Similar types of high-contrast discrete anomalies have been interpreted as potential grave features in the twin-probe results as well, but the trapezoid array was more successful than the twin-probe array for detecting the individual burial features (Figure 117). The greater success of the trapezoid array may be a result of its unique electrode configuration, as the form of the array produced current paths that would have intersected the grave features at an acute angle. As these burial features are small, tightly spaced features, the trapezoid array's additional benefit of measuring different current paths simultaneously allows three different views of the features to be collected.

The anomalies classified as Undetermined have a less distinct response than those anomalies marked as grave or path features, which makes interpreting a specific origin for the feature more difficult. The broad areas of varying resistance are bounded by the path features, the most explicit of which occurs in the central southern plot alignment. The extent of these broad areas is more indicative of anthropogenic activity, rather than floral or faunal bioturbations.

Figure 118: Menston combined earth resistance interpretation of the trapezoid and twin-probe results. “Strong” denotes a high-contrast response, while “weak” denotes a low-contrast response.

4.5.3 Menston: Electromagnetic Induction Quadrature-Phase Results

Several rounds of EM survey have been conducted at Menston over the past few years. This thesis will present the results from surveys undertaken in 2012 and 2014, which employed different instrument operation strategies, different grid locations and different directions of survey. Both rounds of survey collected data in VCP and HCP orientations; however, due to the poor data quality of the 2012 HCP results, only the VCP results from 2012 will be presented.

The 2012 VCP survey collected data with the instrument in a handheld apparatus using the time-based setting. Data were collected in 20m x 20m grids, with the orientation of the traverses on a NW-SE alignment. An effective sampling density of 0.25m x 0.5m was collected by the 2012 survey, with the operator updating the reference position every 1m. The 2014 survey utilised the entire survey area as a single grid, with the user updating the position every 20m. Traverses were separated every 1m, providing an effective spatial resolution of 0.25m x 1.0m. Since the 2014 survey used a sledge-based system, traverses were orientated on a NE-SW alignment. This alignment was designed to collect data along the longest possible lines to improve survey efficiency.

The 2012 and 2014 surveys collected data in overlapping areas, allowing an assessment on the link between the nature of the response with the survey strategy employed to be made. All the quadrature-phase datasets at Menston detect numerous discrete point anomalies that almost certainly represent the plot markers (Figure 119). These point anomalies are detected through the Cl, C2 and C3 datasets. However, the separate surveys differ in how the plot markers are resolved. For example, in the 2012 VCP (NW-SE) results, as the coil separation increases, the individual marker responses become bipolar in form, with positive and negative peaks representing a single feature; for the 2014 VCP and HCP (NE-SW) results, the sign of the response also changes with depth, but in contrast to the 2012 VCP (NW-SE) results, the maker anomalies flip entirely from a positive peak to a negative response. This reversal in polarity is more prominent in the HCP configuration than in the VCP configuration, which is expected given the differences in their spatial sensitivities (see Figure 32).

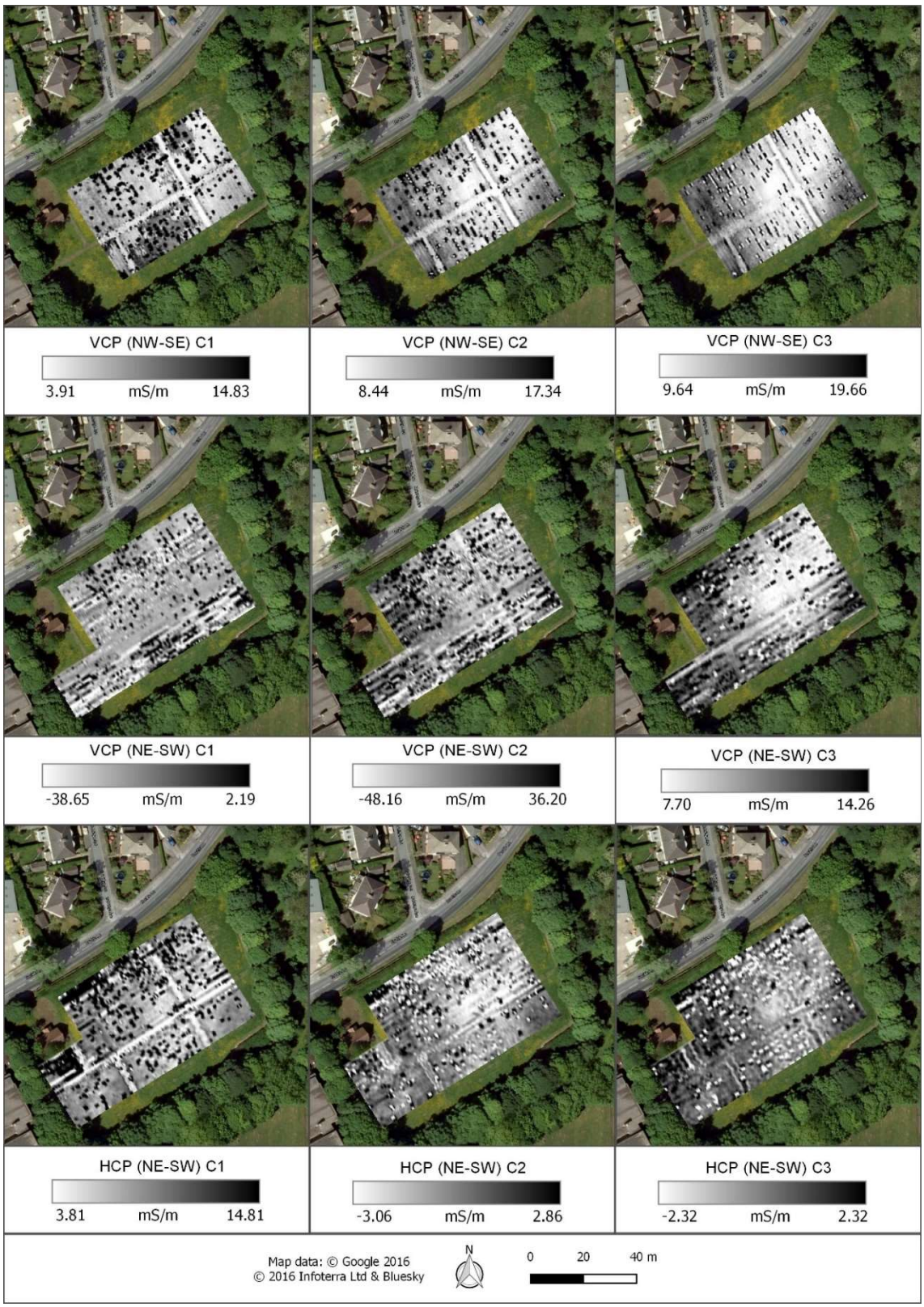

Figure 119: The quadrature-phase results from three separate EM surveys at Menston. The top row was collected in 2012 in a handheld apparatus. Traverses were orientated along a NW-SE alignment. The two bottom rows were collected in 2012 in a sledge-based system. Traverses were orientated along a NE-SW alignment. The 2012 survey has a higher spatial resolution than the 2014 surveys, owing to the traverse intervals of 0.5m and 1.0m, respectively.

Despite these differences, the separate surveys also show similarities in how the markers are resolved. In each separate survey, the individual marker responses

elongate along the survey line. The elongation becomes more pronounced as the exploration depth increases, which likely reflects the greater bulk soil volume being measured. In addition to this response elongation, the 2014 VCP (NE-SW) C1 and C2 results also suffer from significant response blurring along the lines, particularly in the southern half of the survey area. As this same effect is not seen in the counterpart 2014 HCP (NE-SW) results, the blurring may be caused by highly magnetic or conductive near-surface material at a shallower depth to the HCP's sensitivity range. Brisk survey pacing and positional accuracies also certainly exacerbated this effect.

Besides the plot markers, the path features are also detected in the quadrature-phase results. The path features are detected in every quadrature-phase dataset except for2014 VCP (NE-SW) C1. This lack of detection in 2014 VCP (NE-SW) C1 is surprising considering the features were detected in the 2012 VCP (NW-SE) C1 results. Therefore, the lack of detection in the 2014 VCP (NE-SW) C1 results could reflect changes in the soils' properties, as the surveys were undertaken several years apart. Landscape modification was ongoing during the 2012 survey, but the amount of works between the surveys is poorly documented.

The final note-worthy anomalies in the Menston quadrature-phase results are the discrete areas of positive-contrast enhancement. The 2012 VCP (NW-SE) C1 dataset provides the most coherent resolution of such enhancement, bounded within the path features in the southern half of the survey area and near the northwest corner of the site. The lack of detection of this enhancement in the C2 and C3 results demonstrates these responses are caused by relatively near-surface material of a non-ferrous origin. These responses are less distinct in the subsequent 2014 VCP (NE-SW) survey, with the northern area weaker in magnitude than the previous results.

Of the three surveys, the 2012 VCP (NW-SE) has the clearest resolution of the plot markers, path features and the enhanced areas. This is not unexpected considering it has double the sampling density as the 2014 VCP (NE-SW) results. However, there are still positional inaccuracies in the 2012 VCP (NW-SE) results, evident in the areas of enhancement in C1, where staggering issues could not be corrected. This may be a result of updating the position every 1m. A smaller

update interval will have less margin of error for inaccurate button presses; whereas with the 20m window, any positional errors are better distributed along the line. The use of 20m sized grids also has a significant effect on the VCP (NW-SE) in-phase results (Figure 121).

The 2014 HCP (NE-SW) datasets were selected for the integration of the quadrature-phase results (Figure 120). The PCA is more effective than the arithmetic mean for producing a composite image that conveys the important information within the Menston quadrature-phase results. In the results of the arithmetic mean, the burial plot markers are represented by bipolar and monopolar responses. The negative peaking of the scattered bipolar responses makes the data appear noisier, obscuring many of the marker responses. In contrast, the first principal component results show the plot markers as distinct negative-contrast point anomalies. As a result, individual marker anomalies are easier to distinguish, which allows for the overall regular patterning of the markers to be discerned. The pathways are also fully delineated in the first component results; although are less distinct than the path features in the second and third components.

Figure 120: Data combination of the 2014 HCP quadrature-phase dataset. Map data: Bing © 2016 HERE.

4.5.4 Menston: Electromagnetic Induction In-Phase Results

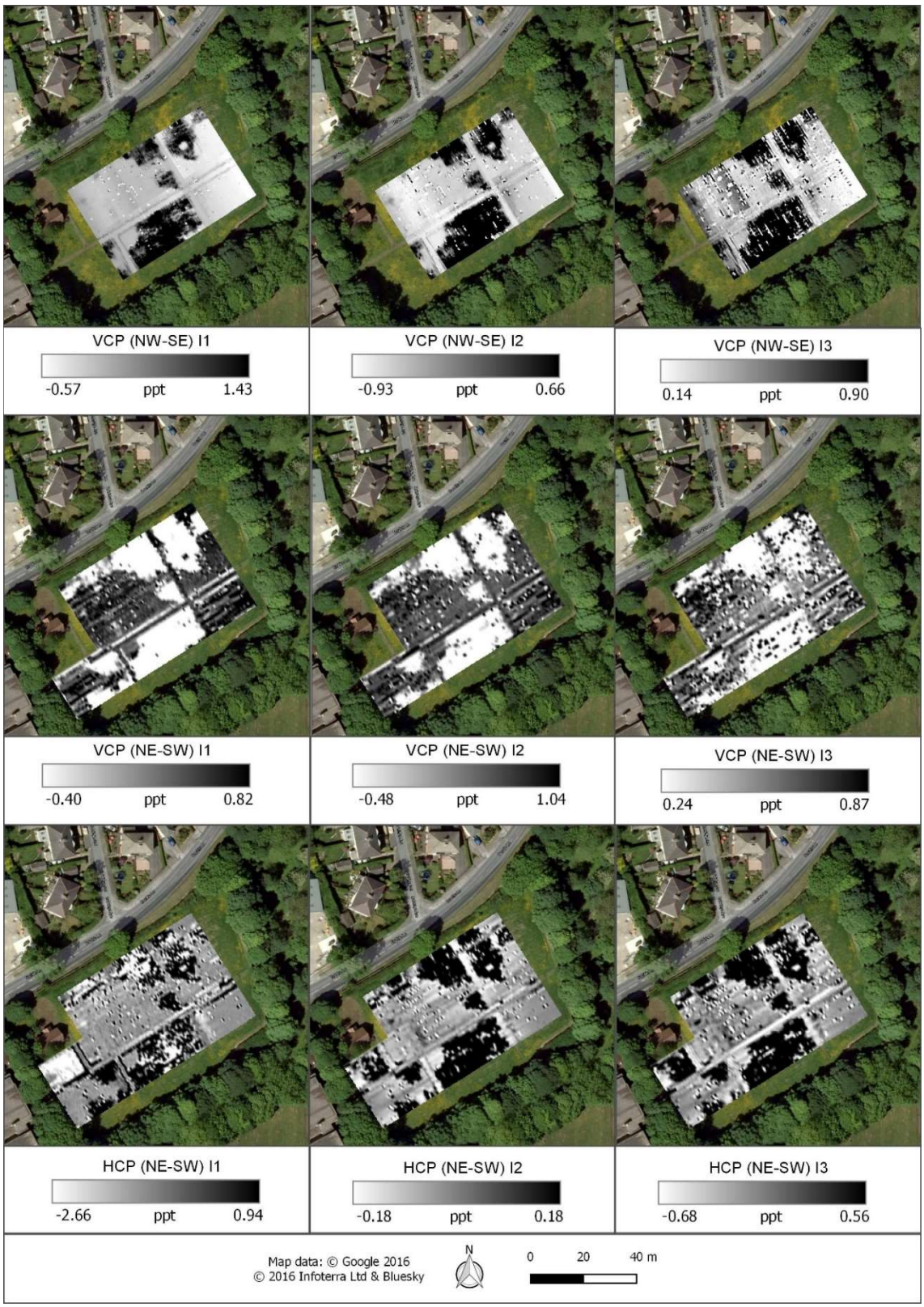

Figure 121: The in-phase results from three separate EM surveys at Menston. The top row was collected in 2012 in a handheld apparatus. Traverses were orientated along a NW-SE alignment. The two bottom rows were collected in 2012 in a sledge-based system. Traverses were orientated along a NE-SW alignment. The 2012 survey has a higher spatial resolution than the 2014 surveys, owing to the traverse intervals of 0.5m and 1.0m, respectively.

Striping along the lines is evident in the 2014 VCP and HCP results and almost certainly has been introduced from a combination of pacing issues and uneven ground terrain due to the presence of mole and other animal activity. The EM in-phase has responded well to the features at Menston. Isolated, high-contrast point responses reflect the plot markers in all the datasets, but the greatest number are detected in the deeper results. The edges of the pathways are also clearly delineated in the in-phase results. Bounded within the path features are areas of high-contrast enhancement, visible across the in-phase datasets. The responses of these enhancement areas are distinct from the marker responses, as the plot markers can be differentiated against the enhancement, particularly in the I2 and I3 datasets. The spread and strength of these areas remain consistent between the 2012 and 2014 site visits.

The most evident difference between the separate in-phase datasets is opposite polarity of the 2014 VCP results to the polarities of the 2012 VCP and 2014 HCP results. In the 2014 VCP results, the enhancement areas are detected as negative enhancement from a relatively high background; whereas for the other results, the datasets present the opposite image. The 2014 VCP results are dominated by positive measurements very near surface; whereas the counterpart HCP datasets tend towards negative values (Figure 122). While the histograms visualise the range and the spread of the respective datasets, the origin for the behaviour of the 2014 VCP results is poorly understood—especially since the 2012 VCP results do not exhibit the same polarity.

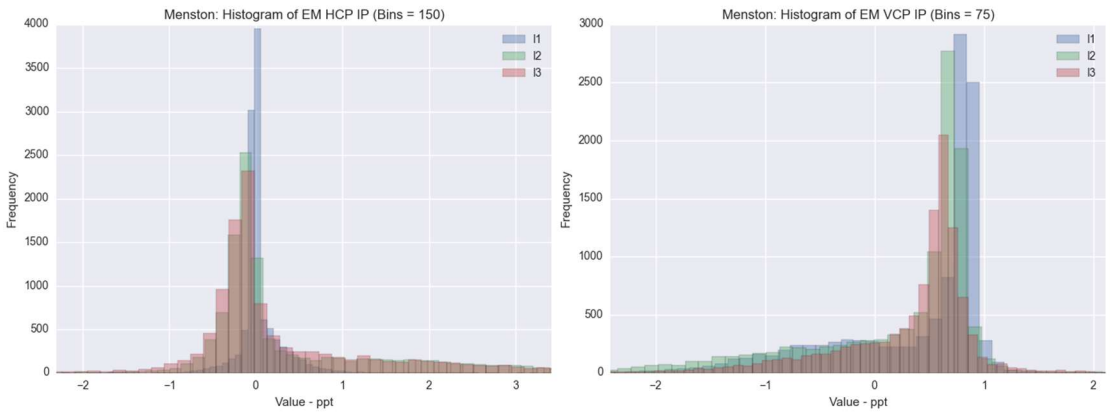

Figure 122: Histograms of the Menston 2014 HCP (left) and VCP (right) in-phase results. The datasets have not been subjected to further processing beyond gridding of the xyz data.

The 2014 HCP (NE-SW) datasets were selected for the integration of the in-phase results (Figure 123). For the purposes of producing a composite image, the arithmetic mean and first component results are effective. However, for the purposes of deriving further interpretative value from the input datasets, the mean and PCA results are not particularly useful. No further information can be derived that is not already present in the individual datastes.

Figure 123: Data combination of the 2014 HCP in-phase datasets. Map data: Bing © 2016 HERE.

4.5.5 Menston: Integration of EM Results and Composite Analysis

Considering the collective quadrature-phase and in-phase results, the EM results provide a comprehensive interpretation of the features at Menston. Both phases detect the plot markers and path features as high-contrast responses in all the datasets (Figure 124). The biggest difference between the performances of the quadrature-phase and the in-phase is the detection of the discrete areas of enhancement. The 2012 VCP results are the only quadrature-phase datasets that correlate with the enhanced areas that dominate the in-phase results. The differences in the detection of these features confirms that the enhancement represents strong magnetic enhancement, but does not have distinctly conductive properties. Analysis against the corresponding magnetic and earth

resistance results will provide further information to better characterise the origin of these responses.

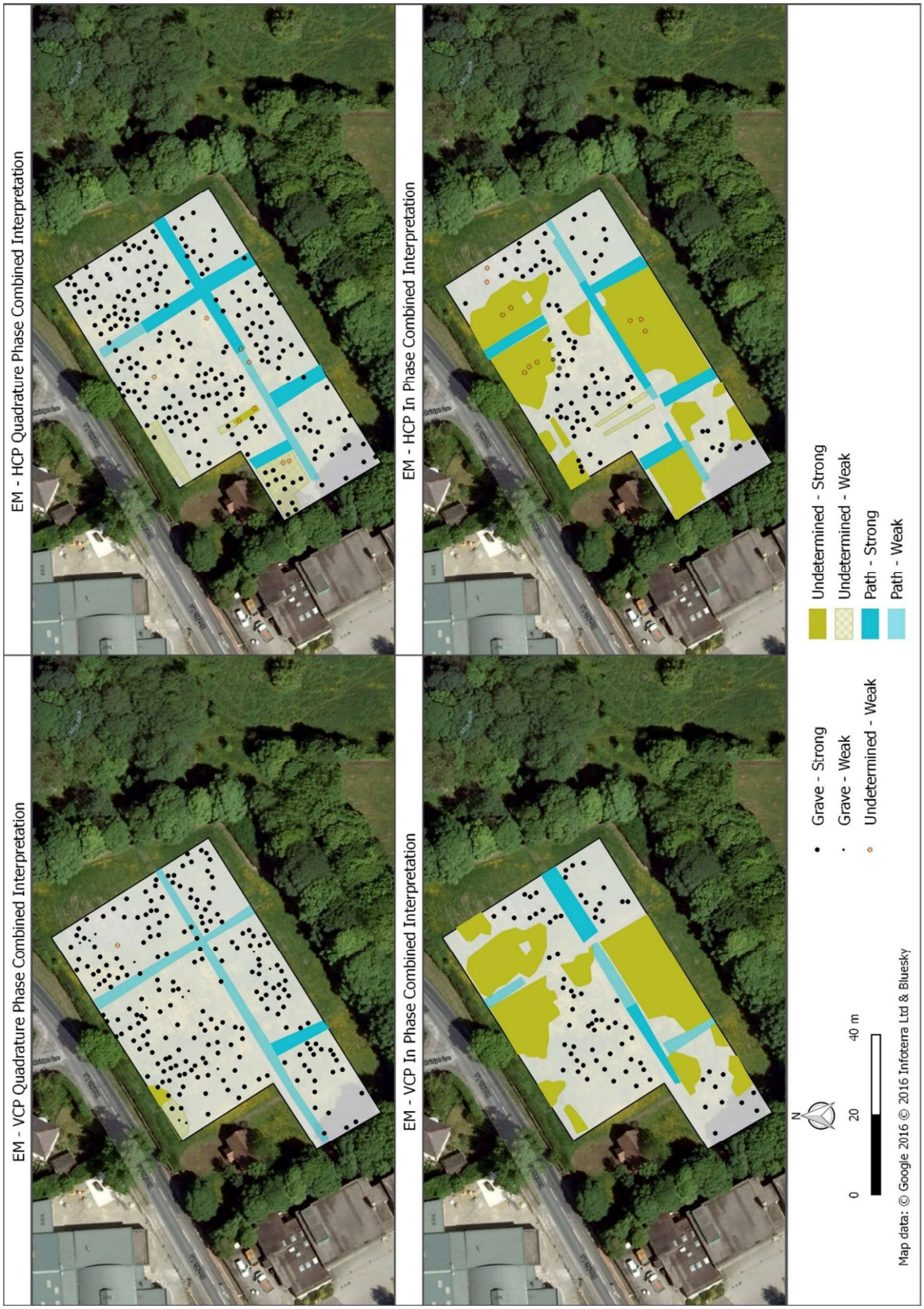

Figure 124: Menston 2014 HCP and VCP EM interpretations.

4.5.6 Menston: Integrated Interpretation and Archaeological Characterisation

The individual survey areas of the magnetic, earth resistance and EM methods varied in location and extent, leaving relatively limited areas of overlapping results. Therefore, the graphical and data combination strategies employed at the other sites would not be suitable and an alternative integration strategy had to be derived. Menston is a unique site in that there are records of what is buried beneath surface. Since mapping the grave features was the primary objective of the survey, an interpretative strategy targeted at the discrete anomalies relating to the burials was devised. This strategy and results have been published in Gaffney et al. (2015).

Similar to a Boolean binary data combination, the Gaffney et al. (2015) strategy interpreted grave features on a presence or absence basis against the historic burial plan. An analytic signal was performed on the magnetic dataset to simplify the bipolar responses and reduce the signal back to its origin. Following the analytic signal, a peak finding algorithm was run to automatically map the centre of mass of these marker responses. Through GIS analysis tools, these centres of masses were binned into the burial plots on a Boolean True/False basis. This same workflow was performed on the EM quadrature-phase data, on the basis that the EM results were primarily reflecting the same marker responses. The earth resistance results had a different workflow as the technique was not responding to the plot markers as the magnetic and EM methods. Instead, the discrete individual anomalies associated with the burial features were targeted, but were manually digitised. After the methods' responses had been binned into the individual associated burial plots, the GIS geometry intersect tool was utilised to determine where the different methods correlated. This GIS-based analysis was initially developed to determine where any magnetic and EM anomalies did not correlate; since both methods were believed to be responding to the same features. However, as the GIS analysis proved effective for determining the relation between the magnetic and EM methods, the intersection analysis was applied to understand on all of the datasets, to confirm which technique was most successful for detecting grave features.

Figure 125 shows the results of the intersection analysis of the binned geophysical responses. Further analysis of these results provides the following statistics (Harris et al. 2015a):

- The most overlap between the different methods occurs, unsurprisingly, between the magnetic and EM results with 61% of EM anomalies correlating with a magnetic anomaly.
- Following that, 9% of EM anomalies occur with an earth resistance anomaly.
- The earth resistance technique has the highest numbers of uncorrelated anomalies.

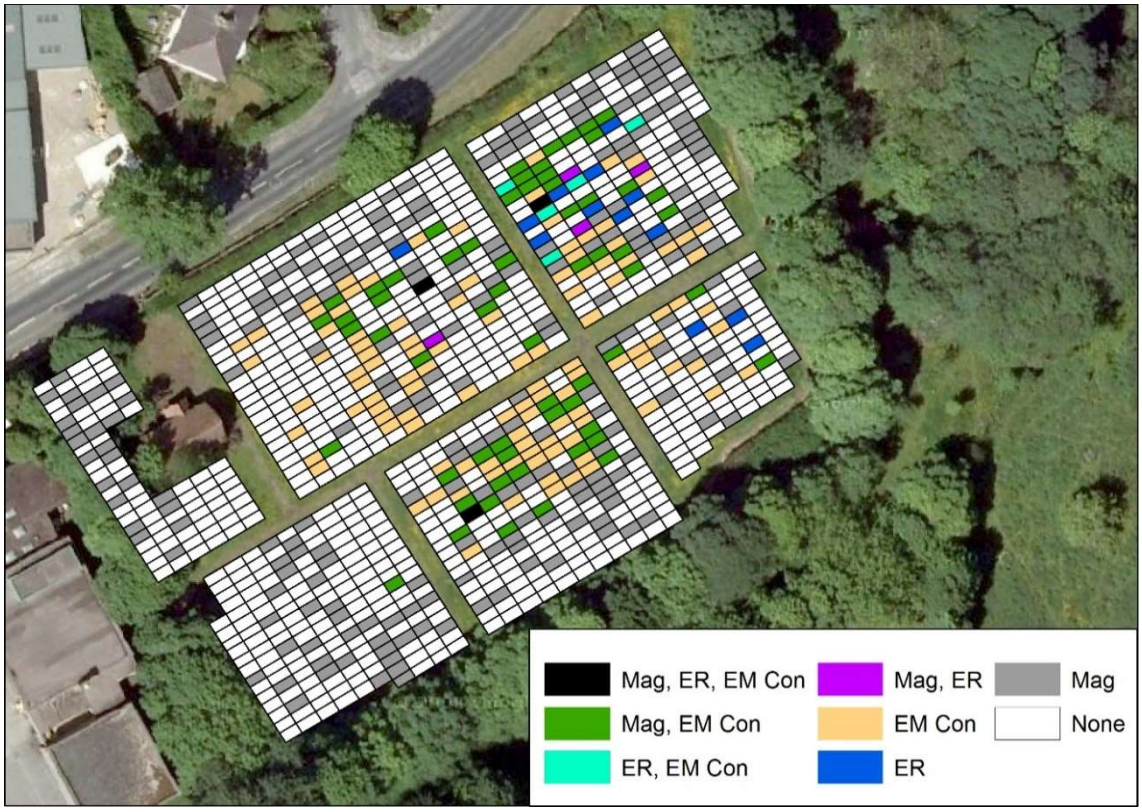

Figure 125: GIS analysis of the co-occurrence of the different methods' anomalies at Menston. From Gaffney et al. (2015). Map data: © 2016 Google © 2016 Infoterra Ltd & Bluesky.

The lack of correlation between the earth resistance results and other methods was unsurprising given the former's inability to detect the individual plot markers. The analysis suggests the earth resistance results are primarily reflecting the grave cuts or another aspect of the grave feature. Given the close proximity of the burial plots and the bulk nature of earth resistance measurements, it is

therefore unsurprising the technique showed less discrete anomalies than the other methods. Instead, what was surprising was the lack of association of 39% of the EM anomalies, considering that the EM results appear to primarily reflect the burial markers. The discrepancies between the magnetic and EM results are therefore likely attributable to the anomalies' dependencies on the technique, instrument, survey strategy, data processing and unpredictable environmental factors; instead of the electromagnetic induction results reflecting some other distinct burial feature. While the interpretation strategy presented by Gaffney et al. (2015) proved effective for understanding the distribution and correlation of binned geophysical responses, the geophysical results offer further information that cannot be addressed through the intersection of binary interpretations.

University of Bradford researchers have suggested the potential for possible quicklime deposition over the burials, as cemetery records suggest multiple bodies would have had to been laid in single plots. Quicklime is the common name for calcium oxide (CaO), which is formed through the calcination of calcium carbonate ($CaCO_3$) at temperatures in excess of 800° C. The use of quicklime and hydrated lime ($Ca(OH)_2$) on burials throughout the archaeological record has been attributed to the management of odours produced through body decomposition (Schotsmans et al. 2015). Controlled studies of the effects of quicklime and hydrated lime on burials reveals the lime creates a cast over the remains, producing a void when the body decomposes. While the EM quadrature-phase results primarily respond to the markers, path feature and natural soil variations, the 2012 VCP C1 dataset also shows enhancement over the south-central block and in the north-eastern corner. This area of enhancement is identical to high-contrast areas of enhancement identifiable in all the in-phase datasets. However, the 2014 EM quadrature-phase results do not resolve these responses.

Evidence for these defined areas of enhancement are less clear in the other methods. In the earth resistance results, the defined areas of enhancement correlate with broad areas of varying resistance in the earth resistance data (Figure 117). It is difficult to distinguish the enhancement areas in the magnetic data due to the overshadowing bi-polar responses of the grave markers; however, the Geoscan Research FM256 data shows weak magnetic

enhancement correlating in these areas (Figure 113). The preferential detection of the enhancement areas within the EM in-phase and magnetic results indicates the presence of a material or substance that is magnetically enhanced. Since quick-lime is fired material, it could demonstrate magnetic enhancement in these methods. The detection of this material in the 2012 EM results, but not in the 2014 EM surveys could also indicate a quick-lime origin as calcium oxide is a poor electrical conductor in a solid state, but exhibits greater conductivity in a molten or liquid state. The lack of detection in between the years could indicate different soil moisture conditions, which could lend to a variable detection of this material. While invasive procedures would be required to confirm the presence of quick lime, the combined geophysical results do not negate the potential for it and suggest, at the least, that some external material has been deposited in these areas.

4.5.7 Menston: Conclusions

The success of the geophysical investigations at Menston can be attributed to the presence of the burial plot markers. The magnetic and EM results do not provide clear evidence for grave features in the absence of a burial plot marker. Therefore, the identification of graves where the plot marker has been disturbed or removed is difficult. The trapezoid earth resistance results provide the most convincing evidence for the grave feature itself, but unfortunately the survey was limited to a small area of the site. Further trapezoid earth resistance survey across the site could be useful for detecting additional grave features. Overall, the GIS integration strategy was effective for targeting the grave features, but unsuitable for understanding the enhancement areas.

Chapter 5 Assessment of EM Instrument Behaviour Through Comparison of Experimental Results with Field Survey

The results of the EM experiments will be presented and analysed against the fieldwork results to determine how external variables effect the output measurements. The results of this chapter will be used to answer research questions one and two. The experiments are presented in order of collection as the successive experiments built upon the results of the previous ones. For this reason, the warm-up drift results will be presented first, as determining an adequate instrument warm-up time is the starting point for an accurate instrument set up.

5.1 Warm-Up Drift: Stabilisation of Instrument Before Survey

The warm-up drift experiment was designed to establish an adequate length of time to allow the instrument's measurements to stabilise to when introduced to the ambient survey temperature. Three iterations of the experiment were performed during different weeks to ensure the accuracy of the results. Before each experiment iteration commenced, the instrument was left outside of its case to warm to an ambient office temperature around 20-21°C. After 30 minutes of warming to office temperature, the instrument was brought out into the amphitheatre, in much cooler temperatures. As this experiment was conducted during winter when the ambient outside temperature ranged from 4-6°C, the difference between inside and outside temperatures presents an extreme temperature difference.

For all iterations of the warm-up experiment, the in-phase experienced a greater amount of change than the quadrature-phase when exposed to this sudden temperature difference. Figure 126 and Figure 127 demonstrate the significant change in in-phase measurements when exposed to a temperature difference of 17°C and 15°C, respectively.

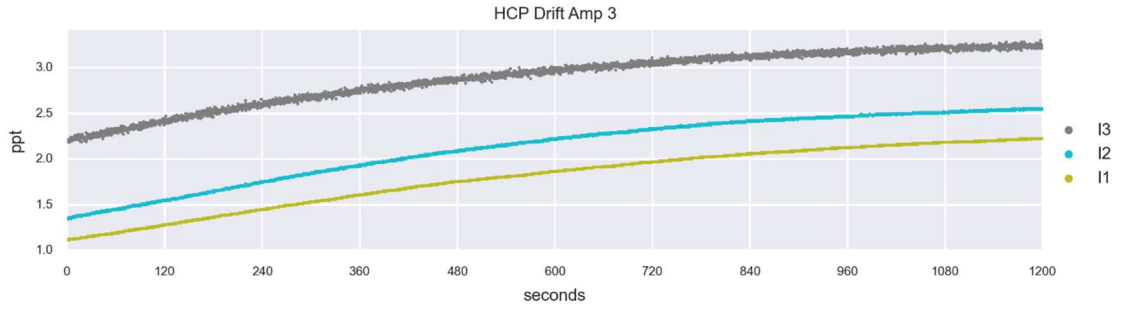

Figure 126: Drift of the in-phase's measurement values over a 20 minute period as the instrument cools to ambient survey temperature (4°C) in the amphitheatre.

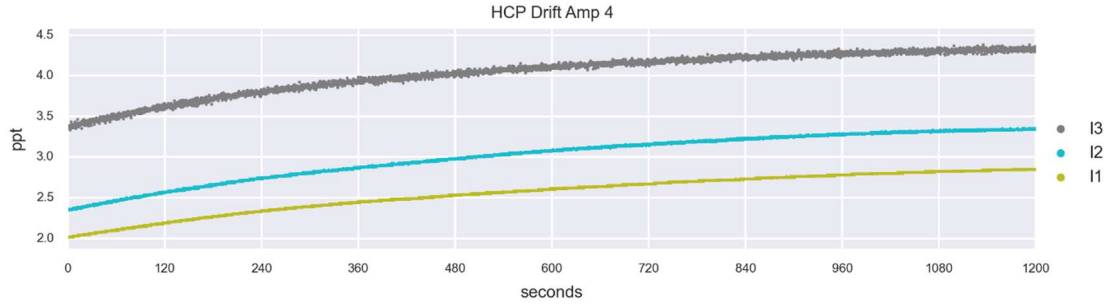

Figure 127: Drift of the in-phase's measurement values over a 20 minute period as the instrument cools to ambient survey temperature (6°C) in the amphitheatre.

Despite the noticeable drift in measurement values as the instrument cooled to ambient field temperature, the behaviour of the in-phase's warm-up drift remained consistent across the different experiment iterations, as evidenced in the above figures. The main difference between the in-phase drift in Figure 126 and Figure 127 is the absolute value of the measurements themselves. Overall, across the warm-up drift iterations, the in-phase demonstrated a quadratic tendency towards drift (Figure 128).

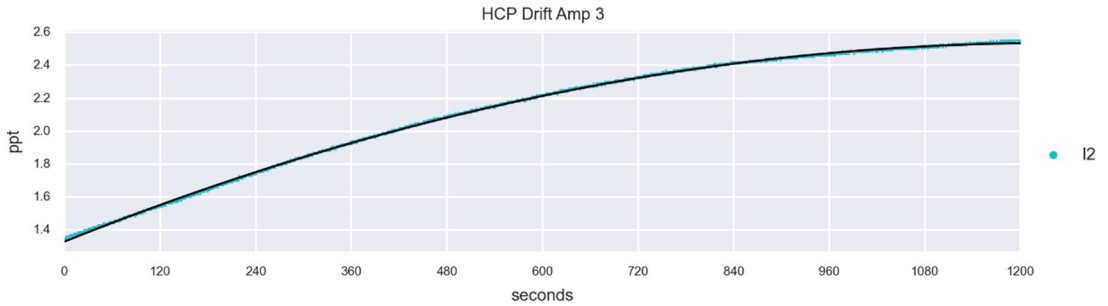

Figure 128: The in-phase experienced a quadratic tendency to drift as the instrument cooled to ambient survey temperature. For I2, R^2 = 1.0 for a second-degree polynomial fit.

Another consistency in the in-phase results across the warm-up drift experiments was the smaller the coil separation, the greater the amount of measurement change (Figure 129).

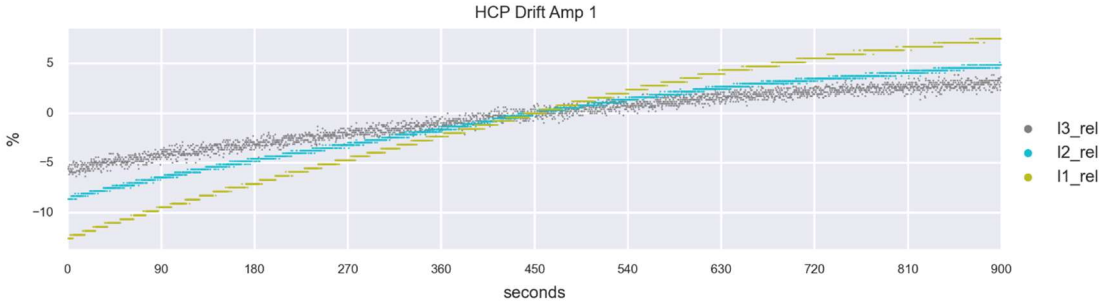

Figure 129: In the warm-up drift experiments, the smaller the coil separation, the greater the relative change in in-phase measurement values as the instrument cooled to ambient survey temperature.

In contrast to the in-phase, the quadrature-phase's C2 and C3 configurations exhibited warm-up drift to a lesser degree (Figure 130; Figure 131).

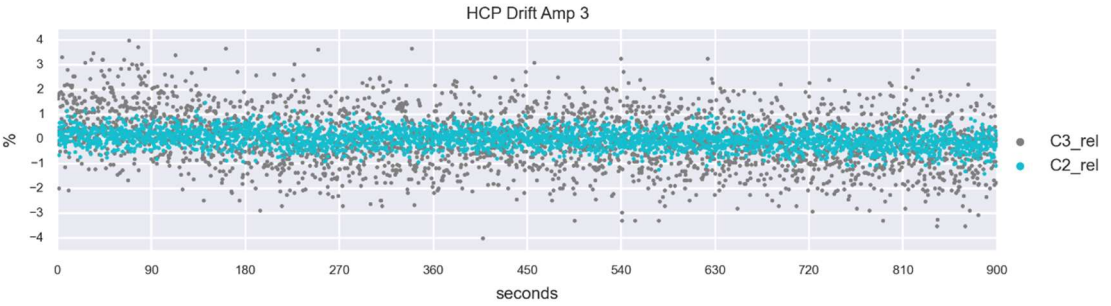

Figure 130: The relative drift in C2 and C3 configurations as the instrument cooled to ambient survey temperature.

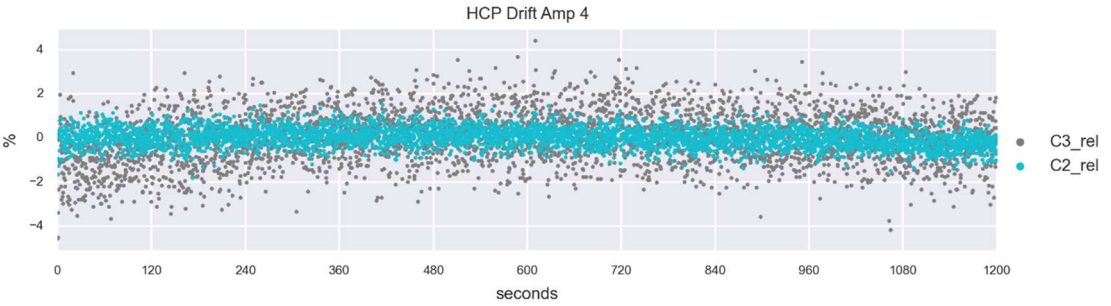

Figure 131: The relative drift in the C2 and C3 configurations as the instrument cooled to ambient survey temperature.

As seen with the in-phase, the C2 and C3 datasets also have best fits with second-degree polynomial functions (Figure 132).

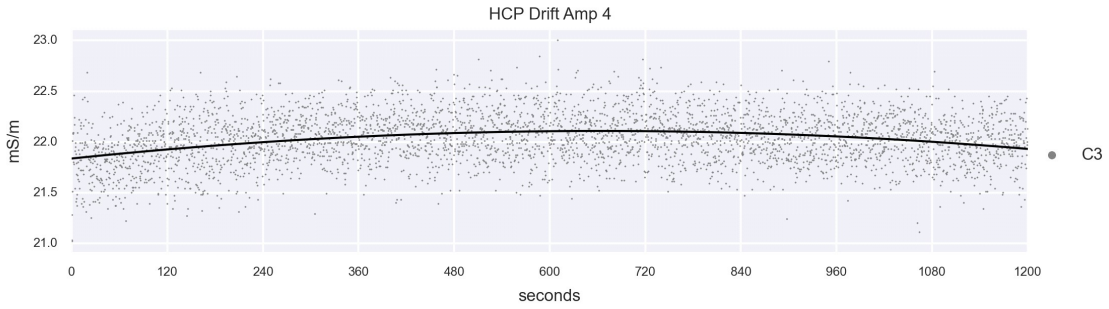

Figure 132: The quadratic tendency of the C3 configuration to drift as the instrument cooled to ambient survey temperature.

In contrast to the consistent behaviour observed across the in-phase datasets, C1 exhibited unique behaviour to C2 and C3, experiencing a drift much greater to the latter configurations. For example, Figure 133 shows the relative stability of C2 and C3 in contrast to the extreme increase in values measured in C1.

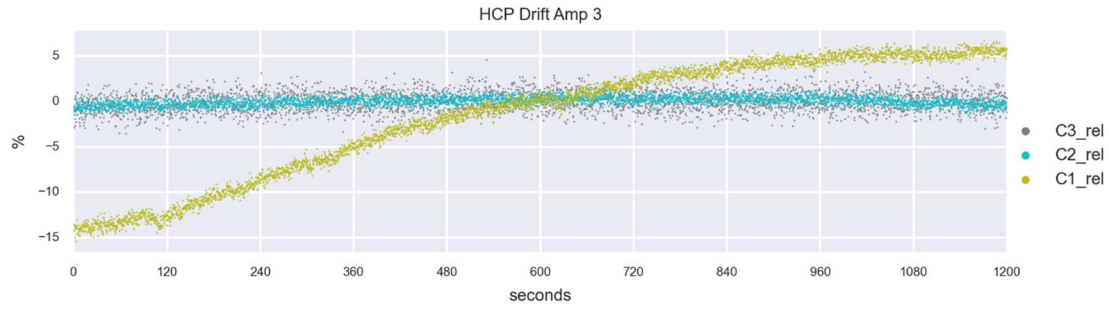

Figure 133: The significant drift of C1 in contrast to the relative stability of C2 and C3 as the instrument cools to ambient air temperature in the HCP Drift Amp 3 experiment.

In two of the three warm-up drift experiment iterations, the baseline C1 measurements experienced an abrupt, rapid drop in measurement values. These sudden drops occurred in a relatively short space of time and occurred at similar times (Figure 134).

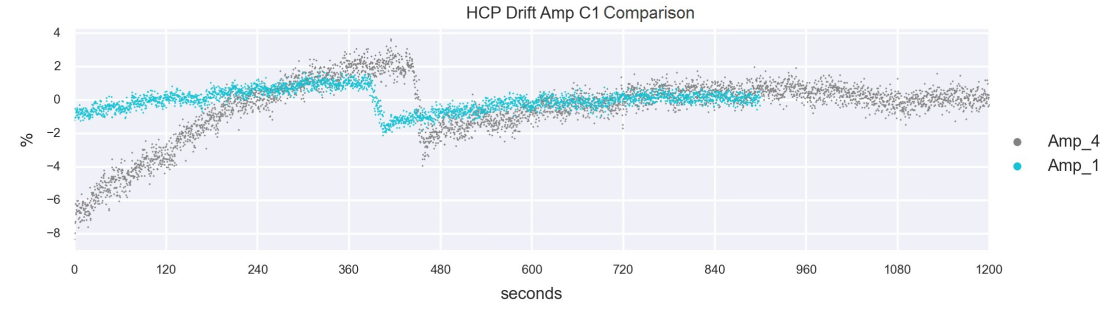

Figure 134: The sudden, rapid drops in C1 measurement values observed in the HCP Drift Amp 1 and 4 experiments as the instrument cools to ambient survey temperature.

These abrupt drops occur independently of any changes in the other configurations, including the in-phase configurations. Even more puzzling is this drop does not correlate with any environmental effect or instrument movement. The cause of this sudden drop is unaccounted for by these experiments, but is not an entirely unknown phenomenon. For example, Delefortrie et al. (2014) found increased measurement instability and noise in the HCP coils upon immediately powering on their DUALEM 21S. Hence, this abrupt drop in measurement values could potentially result from a contribution of electronic instability and the rapid change between the different temperatures.

Overall, the in-phase configurations, as well as C2 and C3 experienced predictable, quadratic changes in measurement values as the instrument cooled to ambient survey temperature. The results show that for extreme temperature differences, the instrument should be left for at least 30 minutes to adjust to ambient temperature. Best practice would also recommend checking the measurement values of all three coils and ensure the values stabilise before surveying.

The warm-up drift experiment quantified the change in measurements as the instrument adjusted to ambient temperature. However, the short-term and long-term stability of instrument measurements over time, after the instrument had adjusted to ambient survey temperature, were not explored in this experiment. The following experiments explore the behaviour of the instrument in a controlled, static environment to target the stability of the instrument measurements over time in the absence of any changing environmental conditions.

5.2 Drift in Static Environment: Stability of the EM Instrument in the Absence of Changing Conditions

With the adequate warm-up time established from the preceding experiment, the instrument was given sufficient time to adjust to ambient laboratory temperature and humidity; warm-up drift should not contribute to these results. For both short and long experiment time periods, the quadrature-phase demonstrated relatively consistent stability (Figure 135; Figure 136, respectively). Although the

measurements are relatively noisy, likely a result of the highly magnetic laboratory environment, the trend of the instrument measurements is stable.

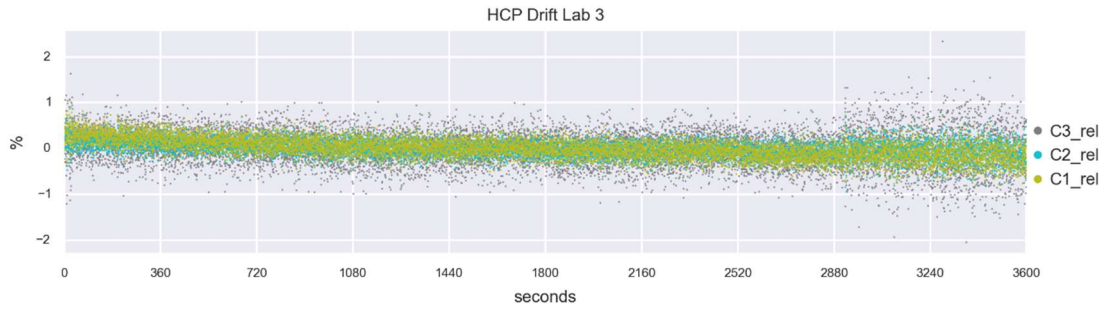

Figure 135: The relative stability of the HCP quadrature-phase over a 60-minute period in a controlled, static environment.

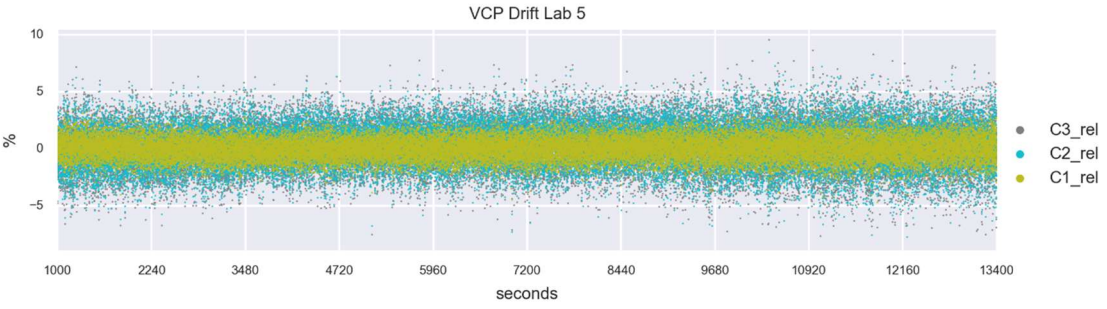

Figure 136: The relative stability of the VCP quadrature-phase over a 204-minute period in a controlled, static environment.

For example, in the HCP Drift Lab 3 experiment, despite minor variations in the room's temperature and relative humidity, the instrument's measurements remained stable across the 60-minute experiment period.

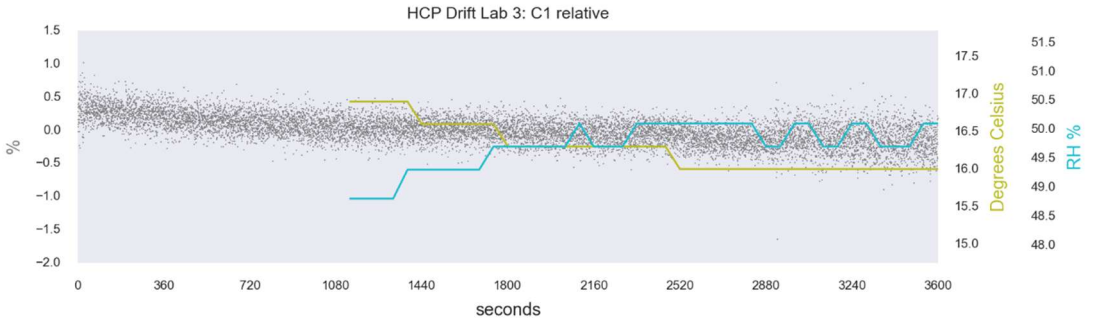

Figure 137: The relative stability of the quadrature-phase measurements across a 60-minute period despite minor variations in temperature and relative humidity. The first 1100 seconds of temperature and relative humidity measurements are ommitted due to a sensor error.

In contrast to the quadrature-phase, the in-phase experienced a greater degree of drift over time, but at a relatively low rate of measurement change, on average a less than 3% change across the experiment (Figure 138; Figure 139).

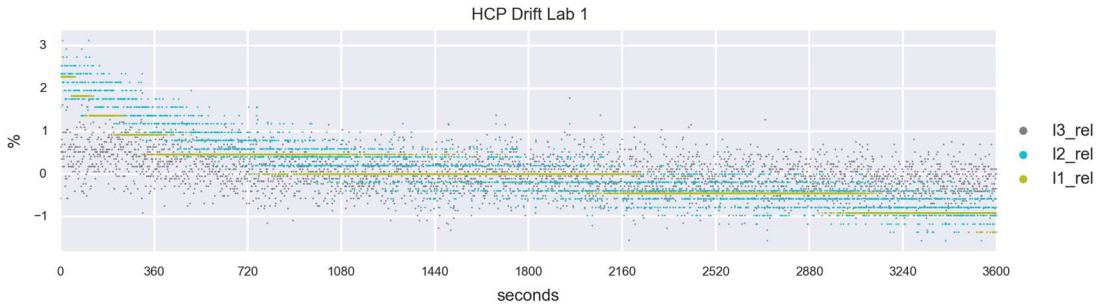

Figure 138: HCP Drift Lab 1 experiment showing the relative in-phase drift over a 60-minute period in a controlled, static environment.

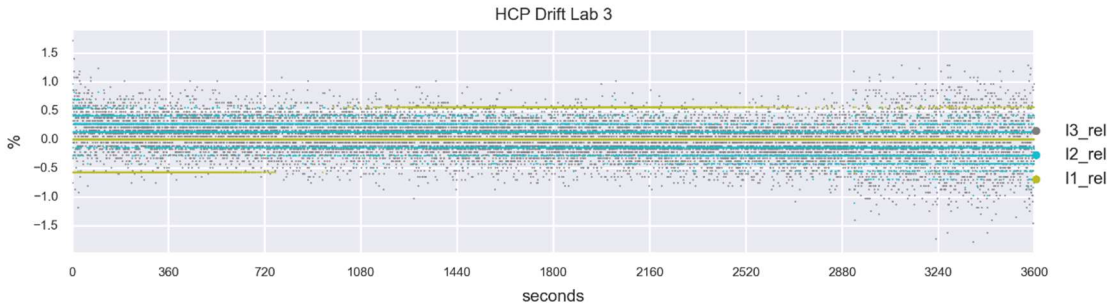

Figure 139: HCP Drift Lab 3 experiment showing the relative stability of the in-phase over a 60-minute period.

The greater magnitude of drift in the in-phase over the quadrature-phase is corroborated in the warm-up drift experiment. Another similarity to the warm-up drift experiment is the behaviour of I1 when compared to I2 and I3. For example, across the four-hour VCP Drift Lab 5 experiment, I1 demonstrates a cubic tendency to drift (Figure 140), whereas I2 and I3 have best fits with quadratic trendlines (e.g. Figure 141). The uniqueness of the smallest coil separation in contrast to the other separations was evident in C1 in the warm-up drift experiment.

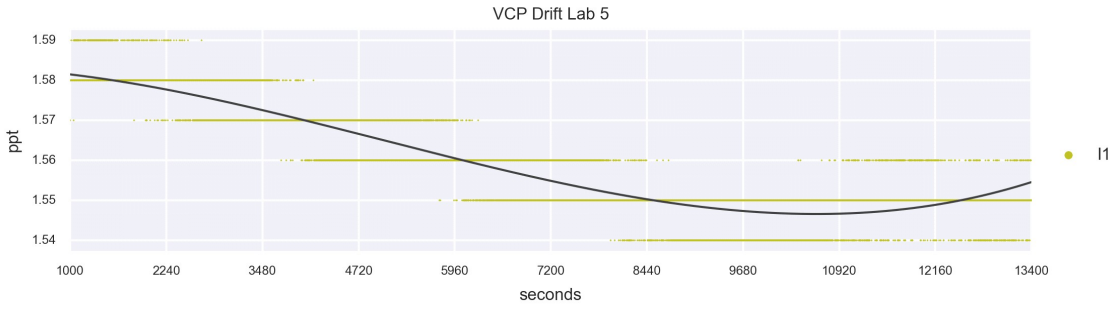

Figure 140: VCP Drift Lab 5 experiment showing the quadratic drift in I1 measurements over a 206-minute period in a controlled environment. Measurements are fit with a third-order polynomial function, with $R^2 = 0.92$.

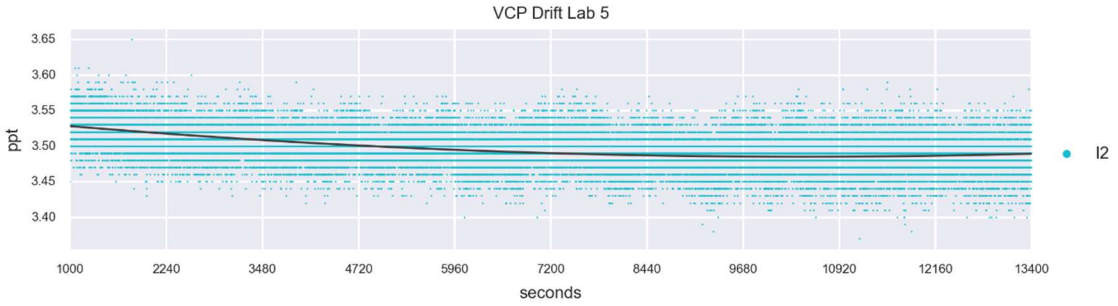

Figure 141: VCP Drift Lab 5 experiment showing the quadratic drift in I2 measurements over a 206-minute period in a controlled environment. Measurements are fit with a second-order polynomial function, with $R^2 = 0.29$.

This drift in the in-phase is not correlated with any subtle temperature or humidity changes when plotted against these measured variables (Figure 142; Figure 143), which suggests the change in measurements may reflect an unspecific instrument instability.

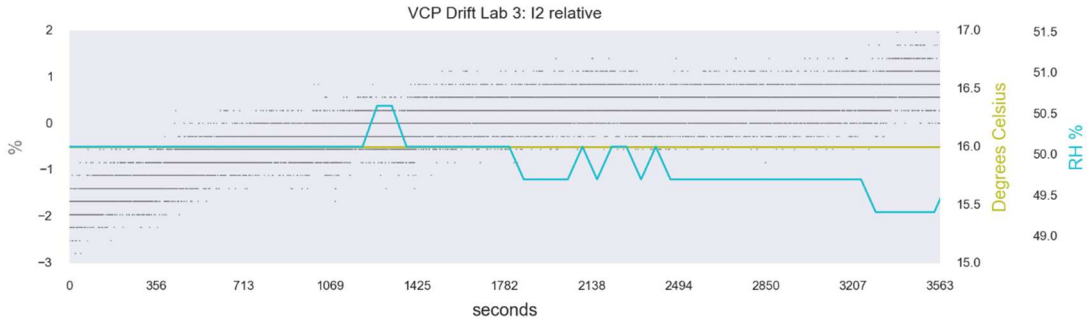

Figure 142: VCP Drift Lab 3 experiment showing the relative drift in the I2 measurements, versus the relative stability of the temperature and relative humidity in a controlled environment.

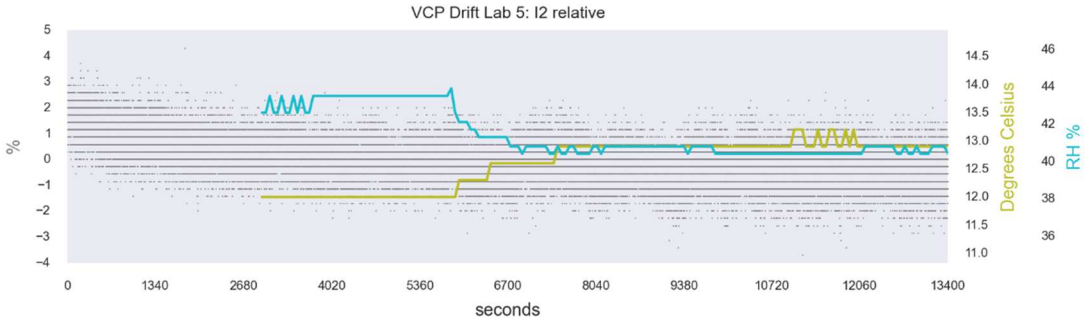

Figure 143: VCP Drift Lab 5 experiment showing the relative drift in the I2 measurements, versus the relative stability of the temperature and relative humidity in a controlled environment. The first 2800 seconds of temperature and relative humidity measurements are omitted due to a sensor error.

Overall, in the controlled laboratory conditions, the instrument maintained relative stability over the experiment time—except for the VCP Drift Lab 3 experiment. Directly following the HCP Drift Lab 3 experiment, the instrument was rotated 90° to collect measurements in VCP orientation. Compared to the HCP orientation, the VCP quadrature-phase experienced significant change across the hour-long experiment period (Figure 144; Figure 145). The evident drift across all the coils in both phases is unexpected considering the experiment directly followed the HCP Drift Lab 3 experiment, with negligible change in room temperature and relative humidity. In the absence of other external variables, the rotation of the instrument into VCP orientation could have introduced some unknown instability in the instrument. Alternatively, the rotation of the instrument could have introduced a warm-up drift type effect, as the underside of the sensor would have been resting on the wooden work surface and potentially introduced a temperature differential across the instrument. Sudduth et al. (2001) suggest temperature differentials across the sensor were potential source of drifts for their Geonics EM38. While this explanation does sound plausible, in the warm-up drift experiment (section 5.1), barring C1, the changes in measurement values were not as great as seen in VCP Drift Lab 3, which is important considering the instrument experienced more extreme temperature changes in the warm-up drift experiment. Furthermore, in the warm-up drift experiment, significant drift was limited to the in-phase and C1; whereas in VCP Drift Lab 3, it is evident across all coils.

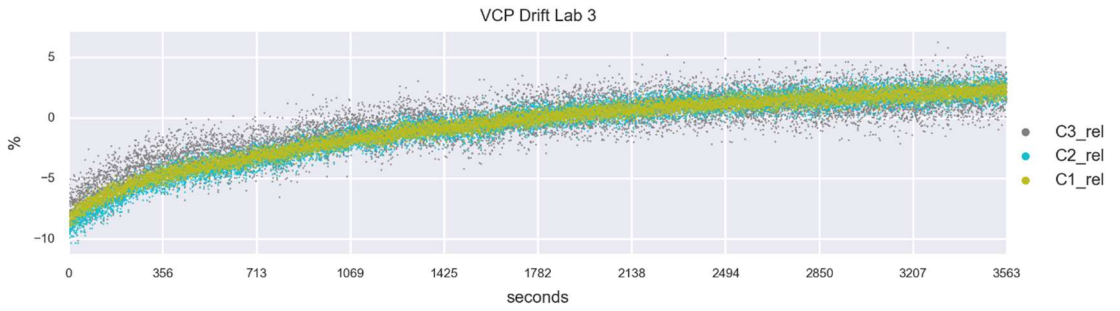

Figure 144: VCP Drift Lab 3 experiment showing the relative quadrature-phase drift across a 60-minute period in a temperature and humidity controlled environment.

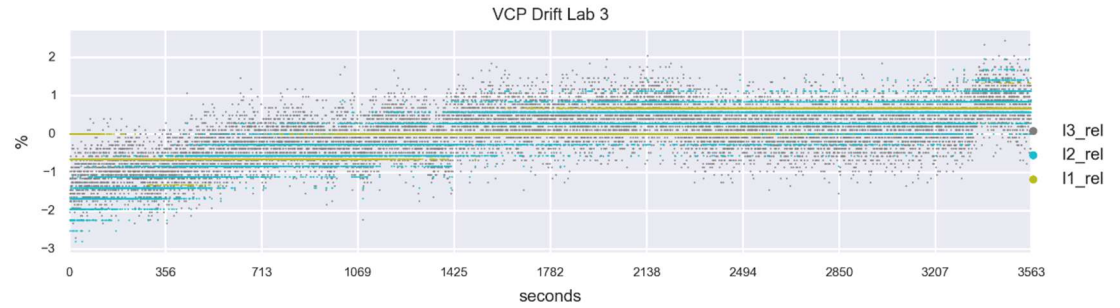

Figure 145: VCP Drift Lab 3 experiment showing the relative in-phase drift across a 60-minute period in a temperature and humidity controlled environment.

The significant drift witnessed in the VCP Drift Lab 3 is limited to that experiment. Overall, in a constant temperature and humidity and environment, the instrument measurements remain relatively stable across both short (i.e. one hour) and long (i.e. four hour) time periods. These results indicate that any *significant* instrument drift is likely to be caused by external variables and general instrument instability has a limited effect on measurement outputs. With this information, the instrument's performance in a variable temperature and humidity was tested next in a dynamic environment.

5.3 Drift in a Dynamic Environment: Stability of the EM Instrument in the Presence of Changing Conditions

The drift experiments in a dynamic environment were designed to mimic changeable temperature, humidity and sunlight conditions—similar to what would be experienced in a field survey. The instrument ran stationary in a fixed position, in order to measure instrument drift without measuring the impact of instrument movement or operation. The instrument was given sufficient time to adjust to ambient outside temperature before running, using the warm-up time derived

from the previous experiments. The HCP configuration ran first, sampling every 0.3 seconds over a four-hour period. Both the quadrature-phase (Figure 146) and in-phase (Figure 147) experience change in measurements over time.

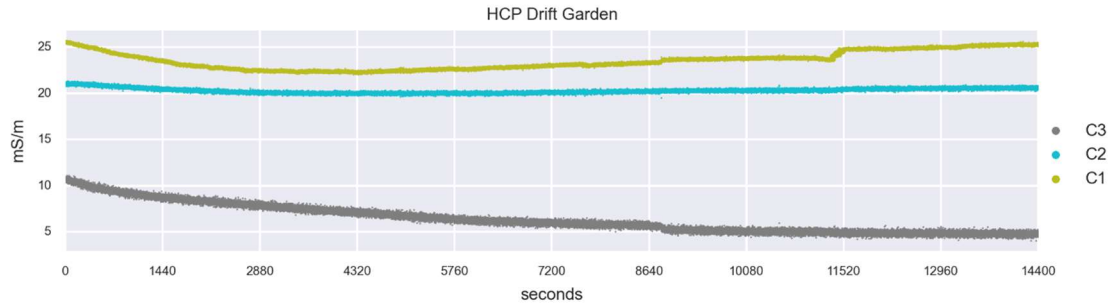

Figure 146: HCP Drift Garden experiment showing the change in quadrature-phase measurements over a four-hour period in a variable temperature and humidity environment.

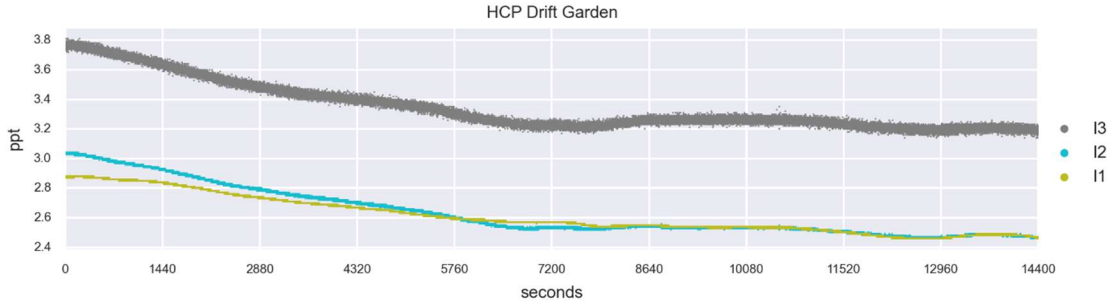

Figure 147: HCP Drift Garden experiment showing the in-phase measurements over a four-hour period in a variable temperature and humidity environment.

The changes in the instrument's output measurements generally exhibited poor direct correlation to changes in temperature and relatively humidity, for both quadrature-phase and in-phase configurations (Figure 151; Figure 149).

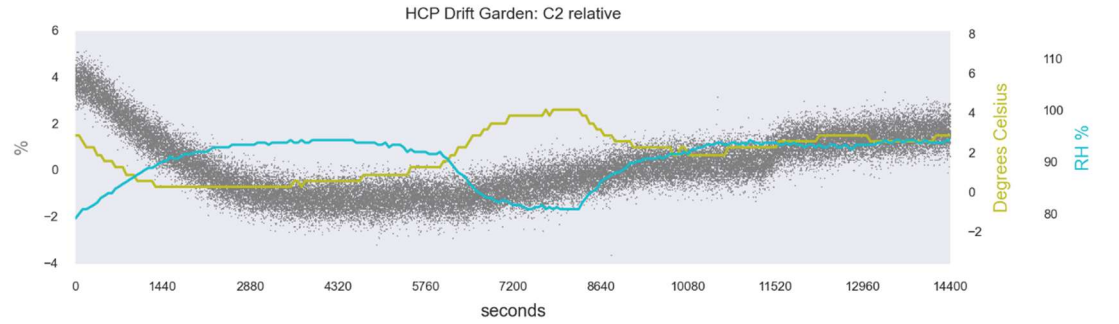

Figure 148: HCP Drift Garden experiment showing the relative change in C2 measurements, temperature and relative humidity across a four-hour period in a dynamic environment.

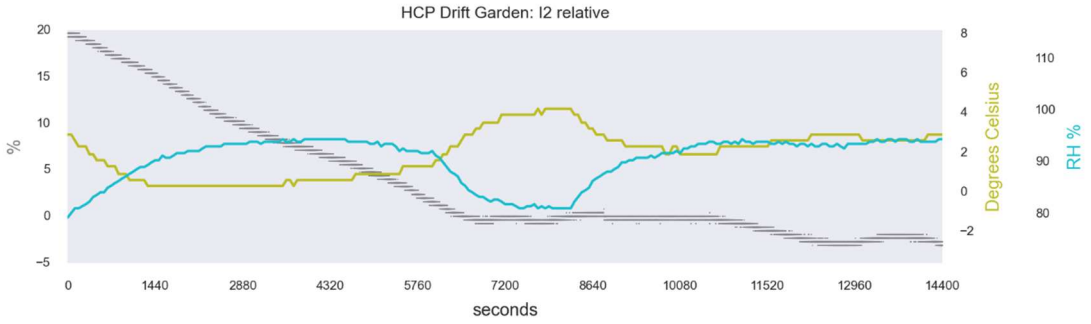

Figure 149: HCP Drift Garden experiment showing the relative change in I2 measurements, temperature and relative humidity across a four-hour period in a dynamic environment.

In addition to the drift observed throughout the experiment duration, the C1 and C3 configurations experienced abrupt, rapid jumps in measured values (Figure 150; Figure 151)—similar to those of C1 in the warm-up drift experiment. The occurrence of these abrupt changes is not correlated across the coils.

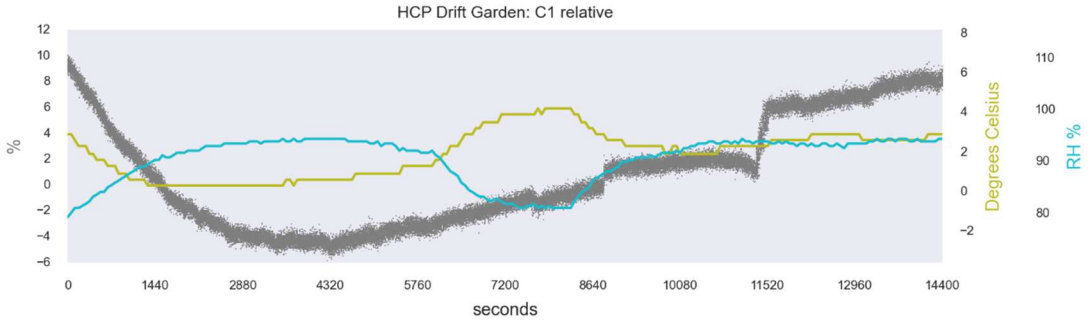

Figure 150: Abrupt change in C1 measurements around three and a quarter hours in the HCP Drift Garden experiment, uncorrelated with changes in temperature and relative humidity.

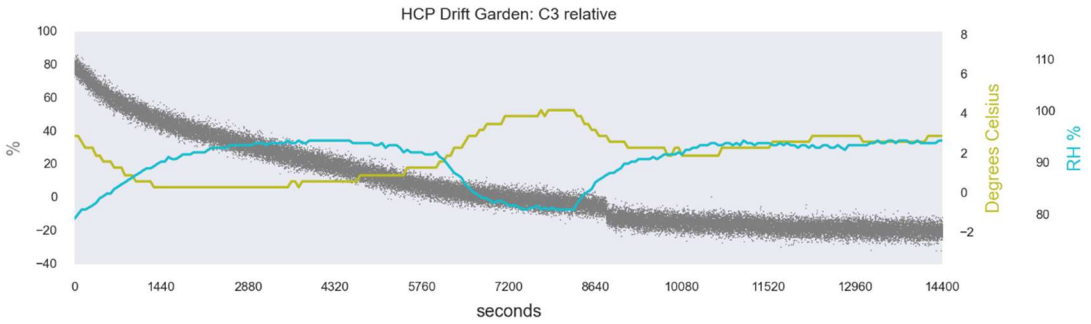

Figure 151: Abrupt changes in the C3 measurements just after two and half hours in the HCP Drift Garden experiment, uncorrelated with changes in temperature and relative humidity.

The VCP orientation of the experiment is less useful for understanding temporal instrument drift as the sensor was abruptly knocked by an animal around 4204 seconds into the experiment. The effect of this accidental knocking was apparent in all phases and coils, but how the accidental knocking effected the

measurements was not consistent between the phases or the coils. For the in-phase, the effect was most dramatic in the I2 coil (Figure 152).

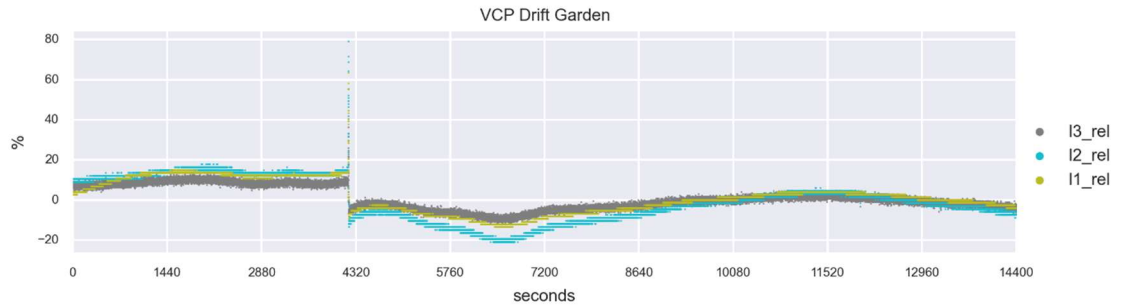

Figure 152: VCP Drift Garden experiment showing the relative in-phase measurements over a four-hour period in a variable temperature and humidity environment.

For the quadrature-phase, the effect was most dramatic in the C3 coil (Figure 153).

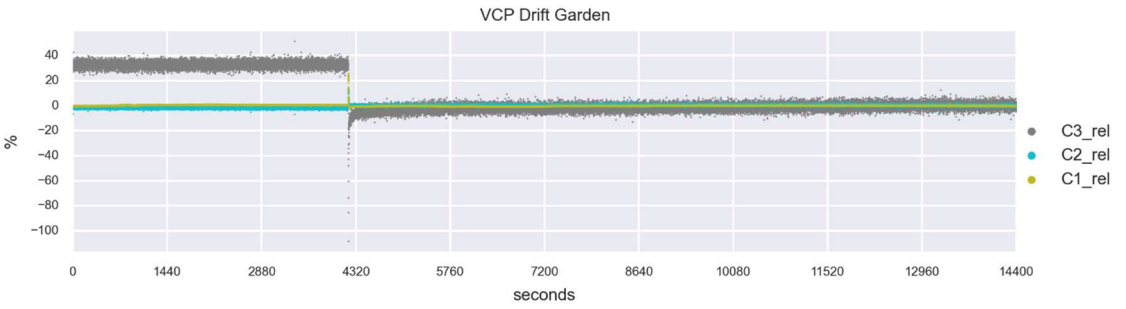

Figure 153: VCP Drift Garden experiment showing the relative quadrature-phase measurements over a four-hour period in a variable temperature and humidity environment.

As Figure 152 and Figure 153 show, all the coils exhibited a change in response around *t*=4204 seconds due to the accidental knocking. However, the time it took for the measurements to settle after the accidental knocking varied between the coils. Because the accidental knocking produced a different effect in the separate coils, the correction of the accidental knocking effect required manual individual correction of the respective coils. First, the extreme values occurring near the accidental knocking time were eliminated. Then, the median of a window of measurements directly either side of the accidental knocking was calculated. A ratio of the different medians before and after the accidental knocking provided the adjustment coefficient, which was applied to the measurements occurring before the accidental knocking. However, even though this correction was done on an individual coil basis, deriving an effective adjustment for all of the coils proved problematic for several reasons. One reason was instrument noise, which

affected the accuracy of the median background value, demonstrated in VCP C2 (Figure 154).

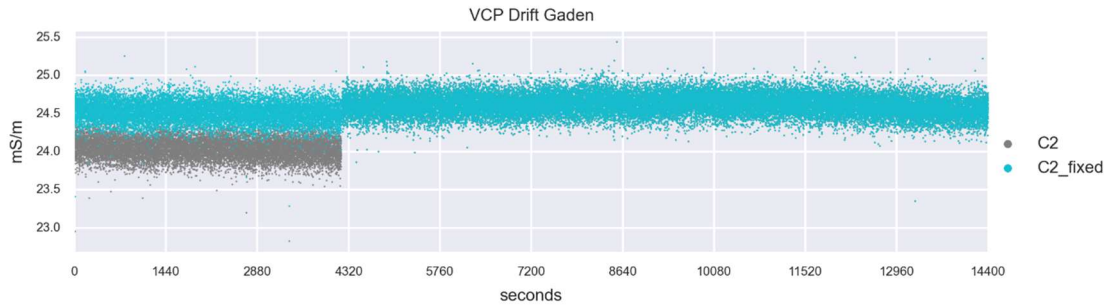

Figure 154: VCP Drift Garden experiment showing the C2 and fixed C2 quadrature-phase measurements after the instrument accidental knocking at t=4204 seconds.

Instrument drift was also problematic for deriving an effective instrument adjustment. For some coils, changes due to drift were difficult to separate from changes due to the accidental knocking, which created a disjointed effect, as seen in VCP C1 (Figure 155).

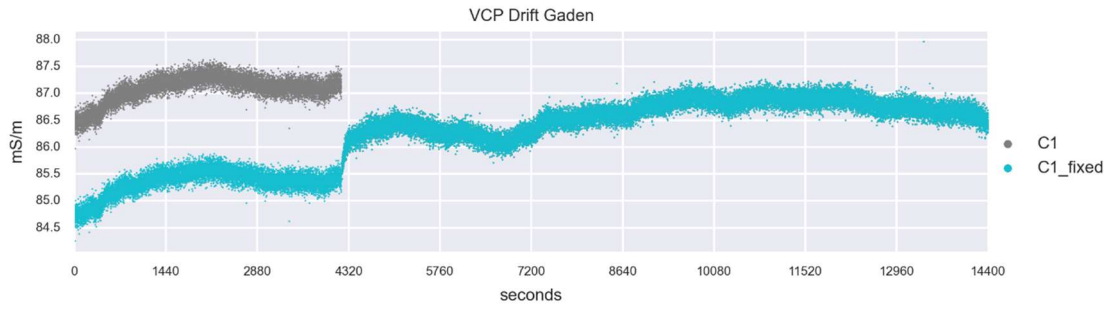

Figure 155: VCP Drift Garden experiment showing the C1 and fixed C1 quadrature-phase measurements after the instrument accidental knocking at t=4204 seconds.

Another consequence of the instrument drift is the difficulty in determining if the drift proceeding the accidental knocking was exacerbated or directly caused by the accidental knocking. The accidental knocking potentially introduced changes into the instrument's behaviour that are difficult to understand or predict. This potential instability is evident in VCP I2 (Figure 156). In contrast to the VCP results, the HCP I2 configuration showed less changeable drift and instead exhibited an overall downward trend in measurements.

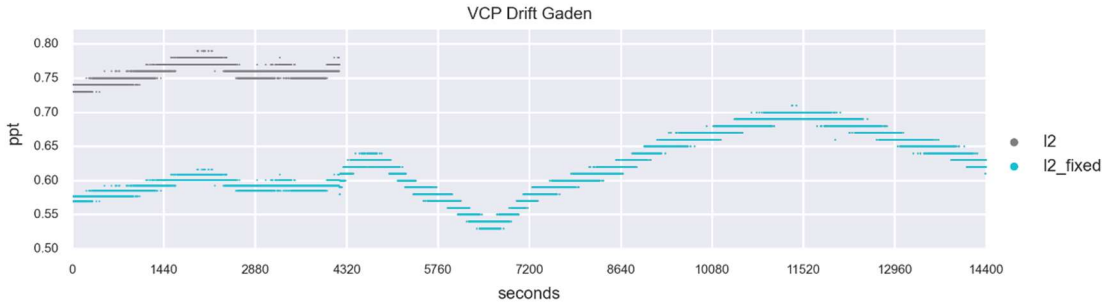

Figure 156: VCP Drift Garden experiment showing the I2 and fixed I2 measurements after the instrument accidental knocking at t=4205 seconds.

5.4 Drift Experiments vs. Fieldwork Results: Manifestation of Drift in Field Survey

The dynamic environment experiments demonstrated the tendency of the instrument's measurements to change in the presence of fluctuating external variables. However, in the presence of fluctuating external variables during field survey, the instrument's measurements tended to change in a predictable manner. For example, the Markenfield Hall Grid 1a in-phase greyscales exemplify a quadratic tendency towards drift, with a marked change from darker grey to white as the measurement values decrease (Figure 157). A quadratic tendency for the in-phase drift is also seen in the warm-up drift and static environment experiments, where, like the field results, the I1 datasets exhibit drastic changes in measurements with time. As the instrument was recalibrated at the end of every traverse, this drift occurs across the lines and obscures the features detected at the southern end of the grid.

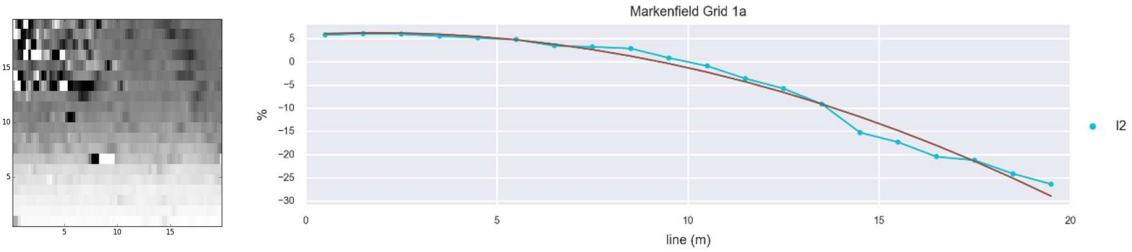

Figure 157: (left) I2 greyscale of Markenfield Grid 1a. Data are plotted +/-0.5 SD from white (low) to black (high) in comparison to (right) the relative change of the individual line's medians, fit with a 2nd order polynomial function where $R^2 = 0.98$.

Similar behaviour is also observed in the unprocessed in-phase VCP and HCP datasets from Lister Park. In the example VCP I2 dataset shown below (Figure 158), the median values of the lines increase as the survey progresses. Plotting

the median line values versus the position in the grid reveals a quadratic increase in instrument baseline values.

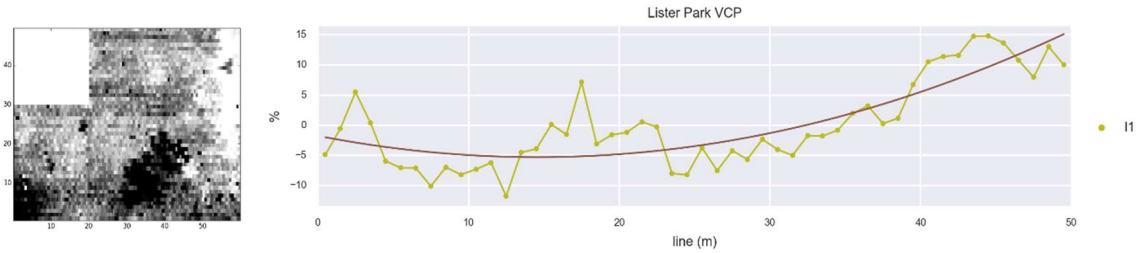

Figure 158: VCP I2 greyscale of Lister Park. Data are plotted +/-0.5 SD from white (low) to black (high) in comparison to (right) the relative change of the individual line's medians, fit with a 2nd order polynomial function where $R^2 = 0.69$

A quadratic tendency to drift is experienced in the quadrature-phase as well. For example, the Fountains Abbey C2 results are presented below (Figure 159).

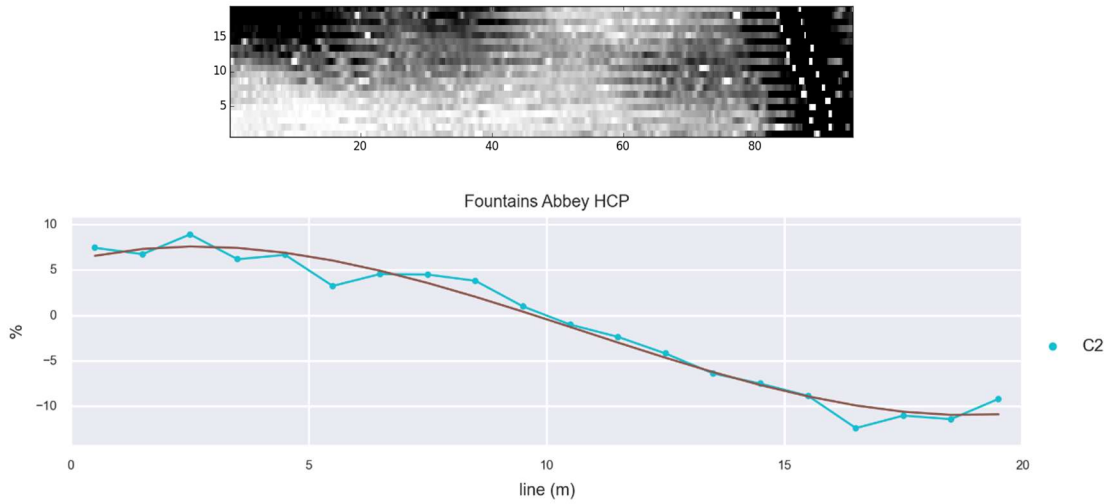

Figure 159: (top) C2 greyscale of HCP Fountains Abbey Gridded results. Data are plotted +/-0.5 SD from white (low) to high (black) in comparison to (bottom) the relative change of the individual line's medians, fit with a 2nd order polynomial function where $R^2 = 0.97$.

However, not all of the behaviour of instrument drift was consistent across all fieldwork results. At Menston, the instrument's background measurements show drift along the grid, but not in a constant trend occurring across the lines. Instead, drift is manifested as several line chunks across the grid (Figure 160). This behaviour is different from the steady tendency towards drift observed at Markenfield Hall and Fountains Abbey.

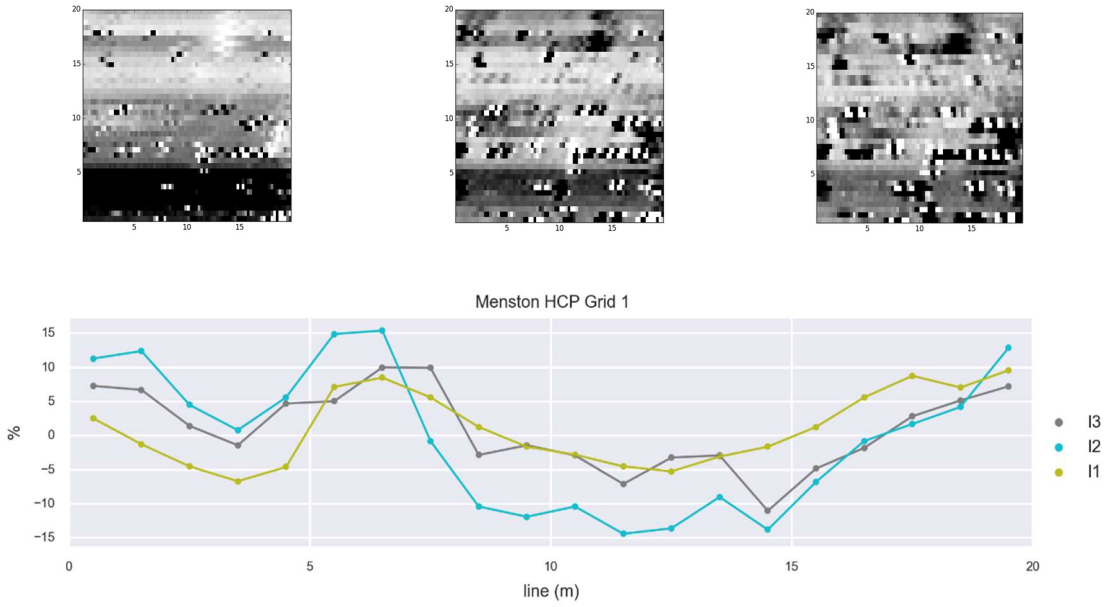

Figure 160: (top row: left to right) I1, I2 and I3 greyscales of the 2012 Menston HCP Grid 1, results plotted to +/- 0.5 SD from white (low) to black (high). In comparison to (bottom row) the relative change of the individual line's medians for the respective configurations.

And finally, not all the field results demonstrate a tendency towards drift. In contrast to the Markenfield Hall in-phase results presented above, the quadrature-phase results of the same grid do not demonstrate a temporal drift. Instead, the relative changes in the median values across the lines correlate with the detection of different archaeological features. In this dataset, no identifiable drift is observed as the configurations maintain a constant baseline level between detection of the different features (Figure 161).

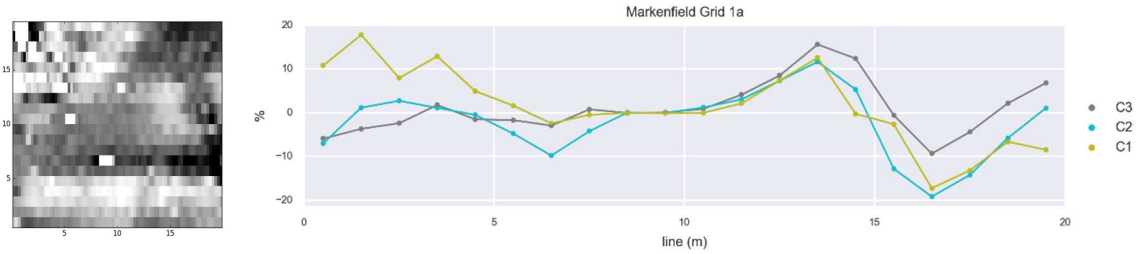

Figure 161: (left) C2 greyscale of Markenfield Grid 1a. Data are plotted +/-0.5 SD from white (low) to black (high). In comparison to (right) the relative change of the individual's lines for the respective configurations.

Temporal instrument drift was monitored at Linton at a reference calibration spot throughout the day. A baseline measurement was initially collected at t=0 minutes before the collection of Grid 1, with subsequent reference measurements collected after each 20m x 60m grid was surveyed. Results show the in-phase

drifted to a greater magnitude of change than the quadrature-phase (Figure 162), but the quadrature-phase still exhibited changes (Figure 163).

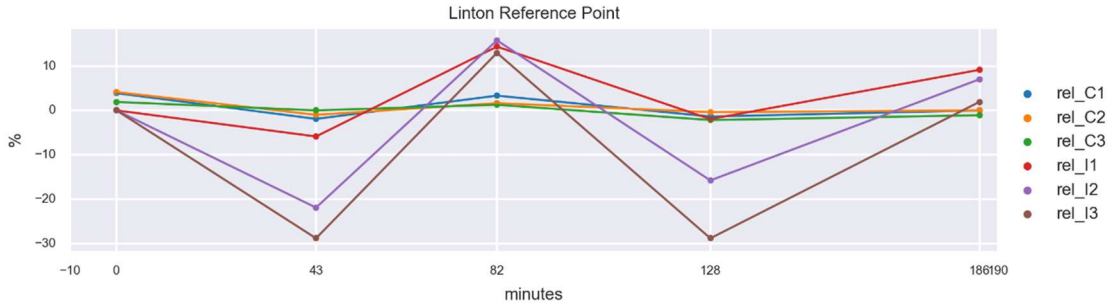

Figure 162: Linton calibration point drift showing the fluctuation of the relative in-phase and quadrature-phase calibration point measurements through the day in variable temperature and humidity.

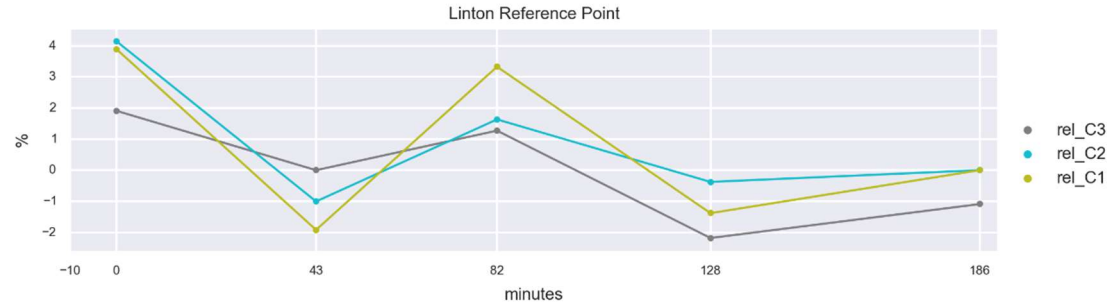

Figure 163: Linton calibration point drift showing the fluctuation of the relative quadrature-phase calibration point measurements through the day in variable temperature and humidity.

Plotting the reference measurements versus temperature and humidity demonstrates these respective variables are not well correlated with the changes to the in-phase (Figure 164) and quadrature-phase (Figure 165) baseline measurements.

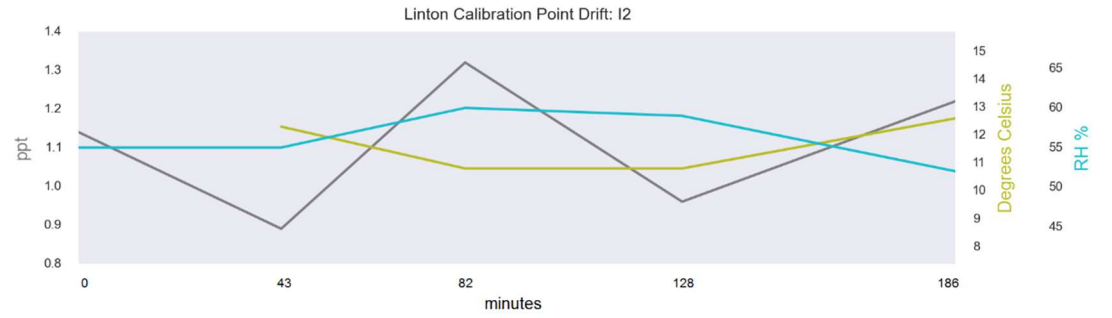

Figure 164: Linton calibration point drift showing the lack of correlation between the change in I2 measurements with changes in temperature and relative humidity through the day. The first temperature measurement is omitted due to a sensor error.

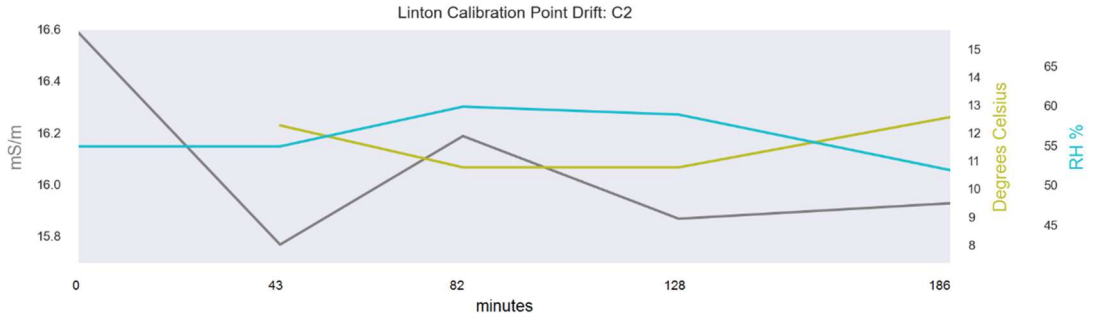

Figure 165: Linton calibration point drift showing the lack of correlation between the change in C2 measurements with changes in temperature and relative humidity through the day. The first temperature measurement is omitted due to a sensor error.

5.5 EM Instrument Drift Conclusions

The results of the drift experiments and the field surveys found no predictable correlation between changes in measurements with ambient temperature or relative humidity. This is not to say change in temperature and relative humidity do not influence measurement values, because as the warm-up experiments show, they do. Instead, there is likely a number of known and unknown variables that contribute to measured values. For instance, measured ambient air temperature and humidity may be different to the temperature of the ground surface. Other factors, such as surface moisture, could introduce a temperature differential between the bottom and the top of instrument. A temperature differential effect could potentially be the cause of the drift in the VCP Drift Lab 3 experiment, as the instrument was rotated 90°, parts of its case that would have been touching the worktop surface for 1+ hours, would have been exposed to the air, causing a noticeable “warm up” drift effect that was seen in the HCP Drift Amp experiments.

While drift was evident in the experiment and field results, external effects, such as moving or knocking the instrument made a bigger impact on the stability of measurements than any temporal drift did. During continuous data collection in field surveys, the instrument is regularly subjected to knocks, hits, or jostles due to instrument operation or survey obstacles. If during field surveys, these jostles were to have as great of an impact on the measured values as they had in the Drift Garden experiment, continuous survey data would be riddled with these effects and make the method ineffective for field survey. While undoubtedly these actions do introduce effects into continuous survey data, the impact is lessened

by the instrument's recalibration at the end of each line. For example, during data collection at Markenfield Grid 2, the operator tripped early into Line 6 and continued data collection down the line. The accidental knocking and knocking of the instrument produced a noticeable effect on that line, particularly in the area boxed in red in Figure 166, where there is a distinct single-line gap within the high conductivity rectilinear anomaly.

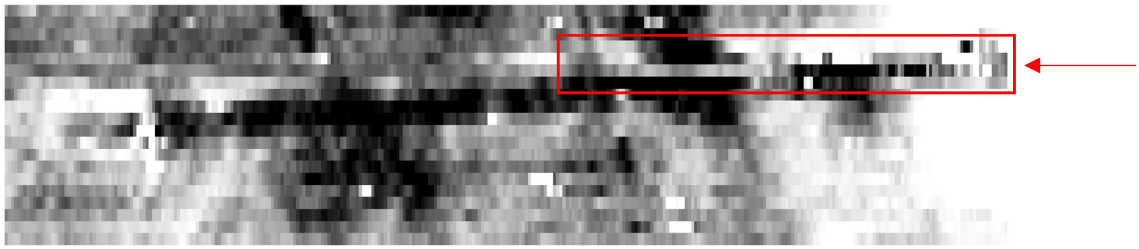

Figure 166: HCP C3 Markenfield Grid 2 showing the effect of instrument accidental knocking and knocking on collected measurements in the field. Red arrow indicates the occurrence of the tripping within the line. Data are plotted to +/-1 SD from low (white) to high (black).

The abrupt, drastic jumps observed in the baseline measurements of the warm-up (Figure 134) and dynamic environment (Figure 150; Figure 151) experiments are difficult to identify in the field results. Overall, drift was quantifiable primarily between the lines, but not within the lines. The recalibration of the instrument at the end of each every traverse likely neutralised the effects of any abrupt jumps within the line. Therefore, the instrument's recalibration has a significant effect on the output results. The following experiments in the proceeding section target this recalibration and how it effects instrument measurements.

5.6 Calibration Experiments

The first of the calibration experiments was simple in design in order to target the effect of the instrument recalibration. Temperature and relative humidity were measured every minute and remained relatively constant. The instrument and temperature sensor had been left to adjust to ambient outside temperature for 30 minutes before the experiment began to allow the measurements to stabilise to ambient survey conditions. For the HCP Cal Amp 3 experiment, the instrument was left stationary and recalibrated every minute for 10 minutes. Six minutes into the experiment, the instrument was rotated 180° before being recalibrated. Every minute thereafter, the instrument was rotated 180° before being recalibrated to simulate a field survey where in zig-zag data collection, the instrument is rotated after the recalibration at the end of each line. The instrument's centre remained

fixed during these rotations. For the larger R3 configurations, this should result in the same soil volume being measured regardless of rotation; this conjecture was confirmed by the experiment results as there were no significant changes in measured values between instrument rotation and recalibration in the C3 (Figure 167) and I3 results (Figure 168).

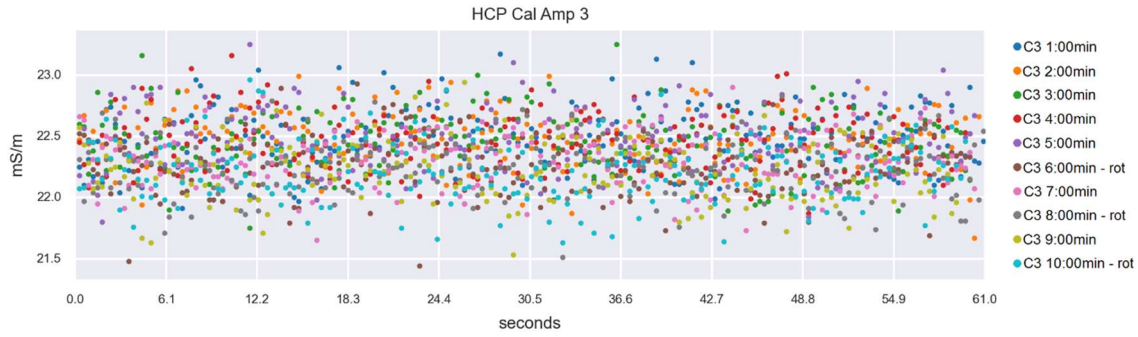

Figure 167: HCP Cal Amp 3 experiment showing the relative C3 measurements across a 60-second period. –rot indicates the interval when the instrument was rotated 180° to the control orientation.

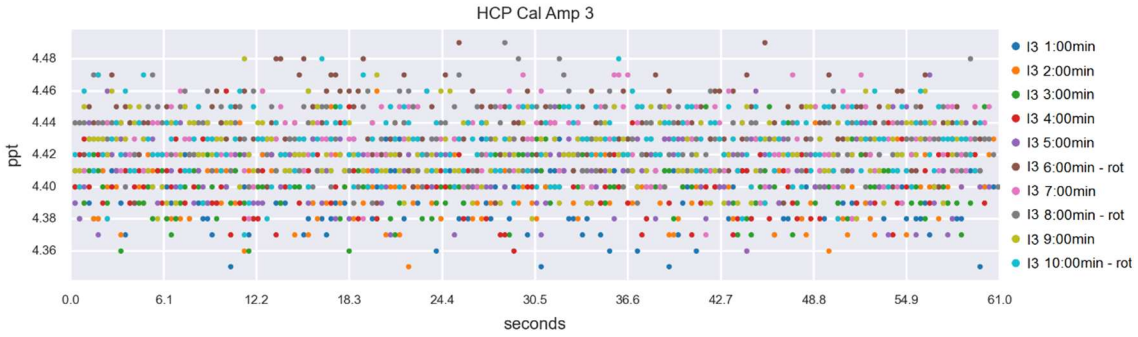

Figure 168: HCP Cal Amp 3 experiment showing the relative I3 measurements across a 60-second period. –rot indicates the interval when the instrument was rotated 180° to the control orientation.

In contrast to the larger coil separations, C1 experiences significant changes in measured values with the instrument's rotation after the recalibration. The median C1 measurements remain stable with calibration until the instrument is rotated 180° at the 6:00 minute mark (Figure 169). This measurement corresponds with an 18.6% increase in value from the preceding baseline measurements. When the instrument is rotated 180° back to the control orientation, a 17.3% decrease is seen, returning the measurement closer to the baseline values measured from 1:00-5:00 minutes.

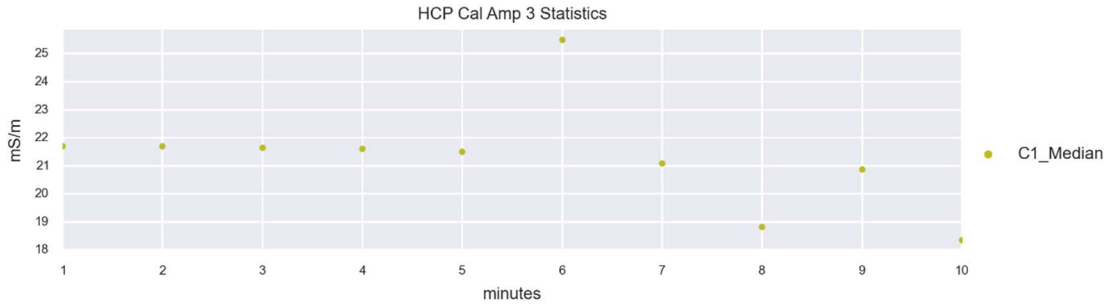

Figure 169: HCP Cal Amp 3 experiment showing the median C1 measurements for each 60-second interval across a 10-minute period. The instrument was recalibrated every 60 seconds and from t=300 seconds, the instrument was rotated 180° every 60 seconds thereafter. The baseline measurements jump with instrument rotation.

Not only does the median value change when the instrument is rotated, but the measurements experience a noticeable drift in the 180° rotation as well. This drift is not seen in the non-rotated orientations (Figure 170).

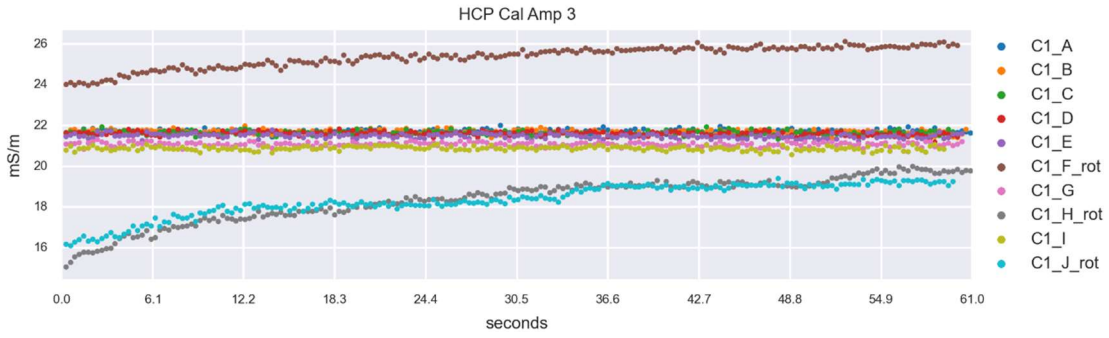

Figure 170: HCP Cal Amp 3 experiment showing the C1 measurements across a 60-second period. –rot indicates the interval when the instrument was rotated 180° to the control orientation.

I1 does not show the distinct change in median values with rotation nor does it experience increased drift for the rotated orientation (Figure 171).

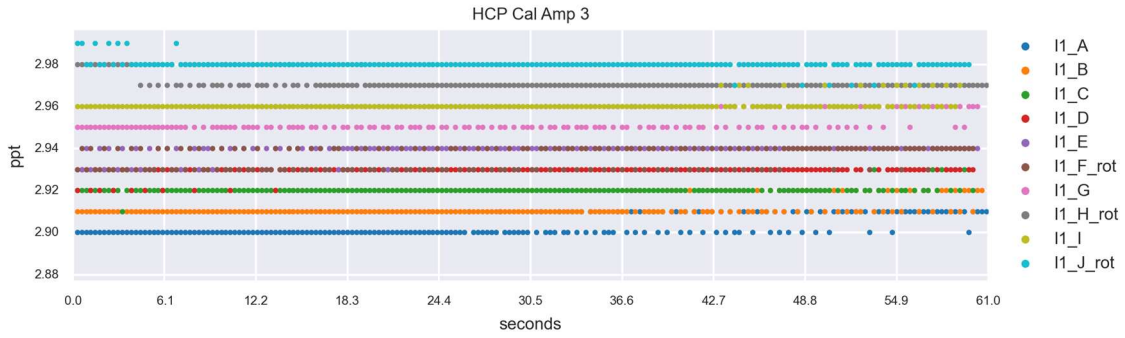

Figure 171: HCP Cal Amp 3 experiment showing the I1 measurements across a 60-second period. –rot indicates the interval when the instrument was rotated 180° to the control orientation.

Instead, the in-phases' median values illustrate a tendency towards linear change with time, regardless of instrument rotation (Figure 172). This is contrary to the drift amp and drift lab experiments, where a tendency for quadratic change is observed (e.g. Figure 128; Figure 132).

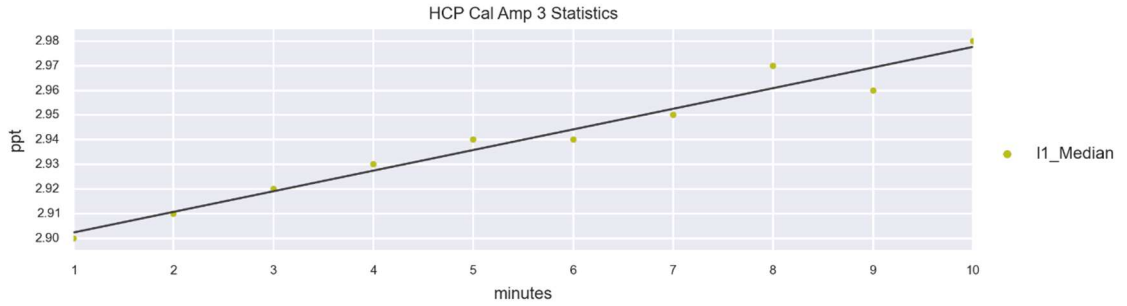

Figure 172: HCP Cal Amp 3 experiment showing the median I1 measurements for each 60-second interval across a 10-minute period. The instrument was recalibrated every 60 seconds and from t=300 seconds, the instrument was rotated 180° every 60 seconds thereafter. The baseline measurements jump with instrument rotation. Measurements are fit with a first-order polynomial function, with $R^2 = 0.96$.

The HCP Amp Flip 1 experiment was a follow-up to the HCP Cal Amp 3 experiment, except it targeted the effects of the rotation of the instrument with the recalibration. The main difference between the two experiments, is that the cable tethering the sensor and handset rotated with the instrument in HCP Amp Flip 1 experiments; as a result, unlike the HCP Cal Amp 3 experiment, the cable was not twisted over the instrument and alternated sides with the rotation. The cable was known to interfere with the collected measurements.

Plotting the XY responses over the experiment's entire duration illustrates the jumps in background values between the rotations. The magnitude of jumps is greater for the quadrature-phase (Figure 173). Although these rotations do not exhibit as significant of drift to what was observed in the HCP Cal Amp 3 experiment (Figure 174).

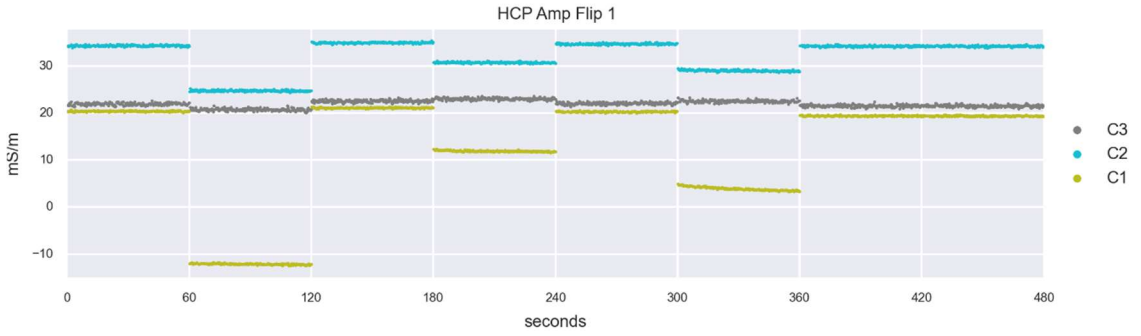

Figure 173: HCP Amp Flip 1 experiment showing the quadrature-phase measurements vs. time across an 8-minute period. Instrument was rotated every 60 seconds, which correlates with jumps in the baseline measurements for the C1 and C3 configurations.

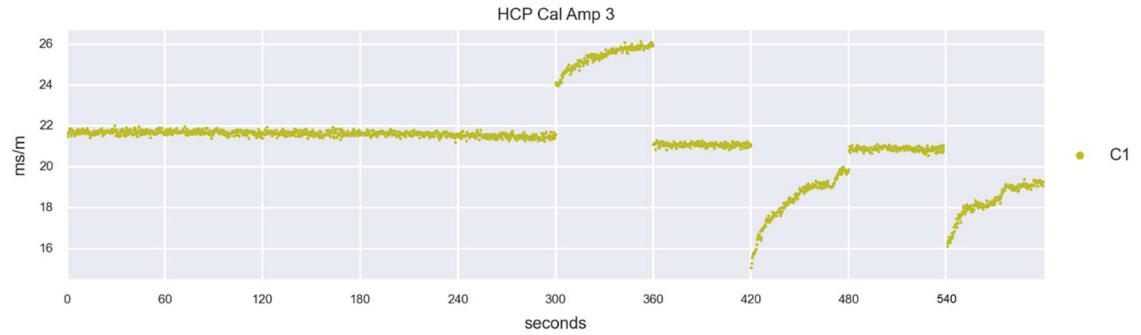

Figure 174: HCP Cal Amp 3 experiment showing the median C1 measurements for each 60-second interval across a 10-minute period. The instrument was recalibrated every 60 seconds and from t=300 seconds, the instrument was rotated 180° every 60 seconds thereafter. The baseline measurements jump with instrument rotation.

Compared to the quadrature-phase results (Figure 174), the in-phase responses from the HCP Cal Amp 3 experiment maintained relatively stability and do not exhibit the same extreme jumps with the instrument rotations (Figure 175).

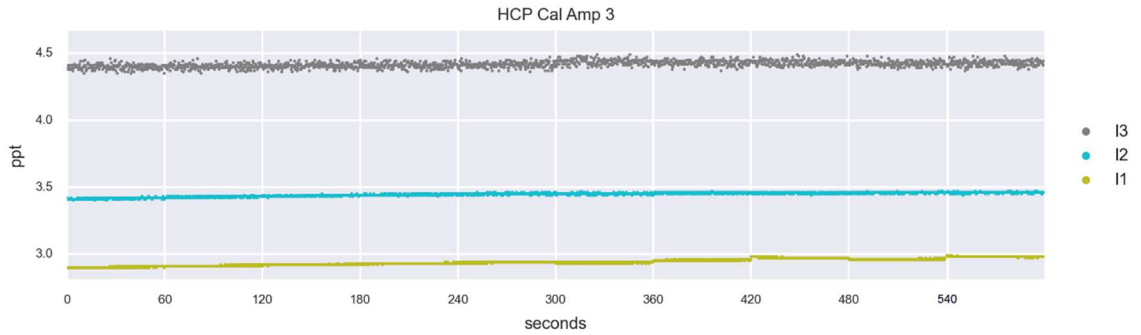

Figure 175: HCP Cal Amp 3 experiment showing the in-phase measurements vs. time for the duration of the entire experiment. Instrument was recalibrated every 60 seconds and from t=300 seconds, the instrument was rotated 180° every 60 seconds thereafter. The baseline measurements demonstrate an increase with each rotation.

However, the HCP Amp Flip 1 in-phase results exhibit the same noticeable jumps as the quadrature-phases, but not to the same magnitude (Figure 176).

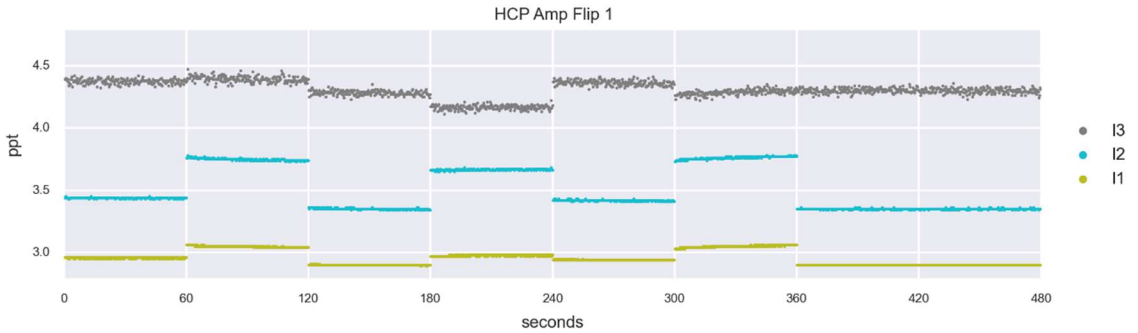

Figure 176: HCP Amp Flip 1 experiment showing the in-phase measurements vs. time across an 8-minute period. Instrument was rotated every 60 seconds, which correlates with jumps in the baseline measurements for all configurations.

5.7 Calibration Experiments vs. Field Data

The calibration experiments established that the recalibration of the instrument helps to maintain a consistent baseline level. However, when the instrument is rotated, to simulate a field traverse, the rotation introduces a new baseline level and, in some cases, introduces a measurement instability. This rotation effect could account for the striping between lines, which is visible in the unprocessed field results.

In the calibration experiments, the effect of the rotation had the greatest impact on the R1 results. The R1 coils has the smallest separation between the transmitting coil, in comparison to the other coils. As a result, R1 will measure a different soil volume when the instrument is rotated, unlike R2 and R3, which will measure a relatively similar soil volume. While this explanation is convincing as an explanation for the experimental results, it does not hold up for the field results. For example, at Lister Park, the most pronounced striping occurs in the R3 configuration, not the R1 configuration (Figure 177).

Figure 177: Selected Lister Park VCP in-phase and quadrature-phase results, displaying the variation of data striping. From left-right: I3, I1, C1.

Plotting the median value of the survey lines for the Lister Park I3 configuration (Figure 178) reveals a behaviour of alternating jumps and drops between adjacent traverses, similar to what was measured in C1 in the HCP Cal Amp 3 experiment (Figure 73).

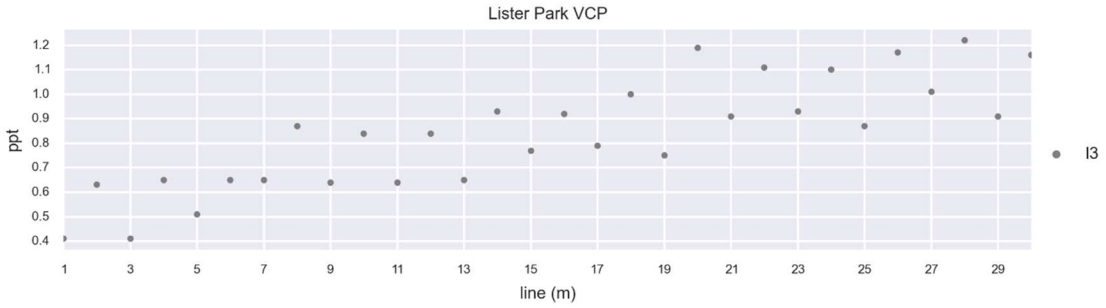

Figure 178: Lister Park VCP I3 results. The median values of individual lines are plotted against the line number.

A further issue, which is not addressed in the calibration experiments, is the calibration imbalances between adjacent grids. For example, in the unprocessed Fountains Abbey results, grid imbalances are visible in the combined greyscale image as breaks between survey grids, where temporal drift and recalibration exacerbate the differences between the background values. Figure 179 shows the changes in background values at lines 10 and 20. Figure 180 shows the response form and magnitude of these changes.

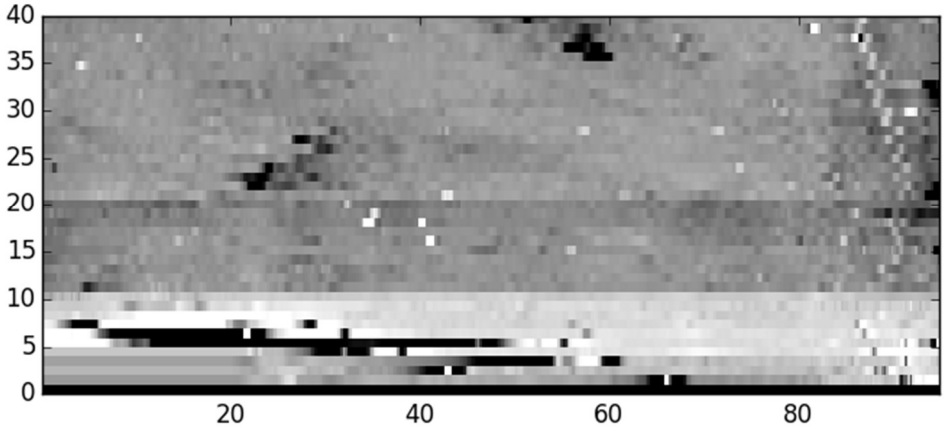

Figure 179: HCP I2 greyscale of Fountains Abbey highlighting the changes in the baseline values of the separate grids.

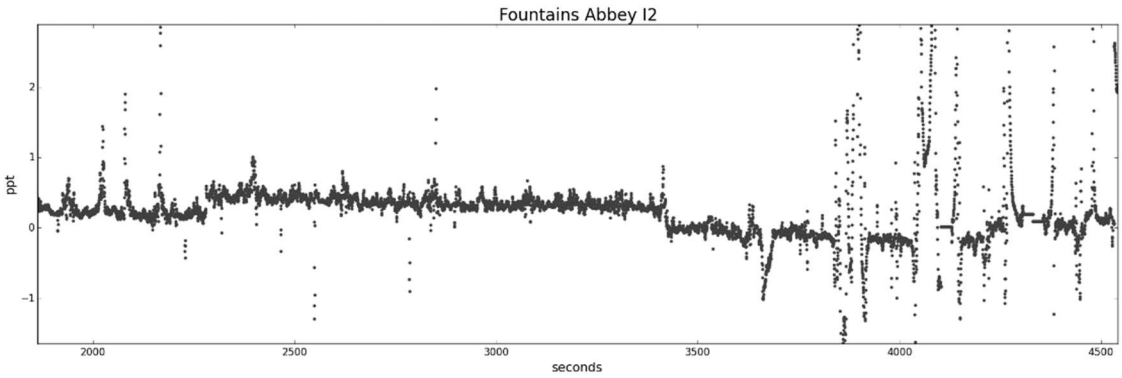

Figure 180: HCP I2 vs time showing the response form of grid imbalances.

5.8 Calibration Conclusions

Comparison of the experimental and field results indicates the effect of the instrument's recalibration and rotation at the end of the traverse in the field is less predictable than the behaviour demonstrated in the experimental results. The calibration itself does not introduce instrument instability, it is the rotation of the instrument which introduces instability. The calibration at the end of the line corrects these instabilities (Figure 174).

The following experiments target the effect of instrument elevation to derive methods to compensate for changes in instrument height, such as different operators.

5.9 Elevation Experiments

The quadrature-phase results of the Pool Elevation experiment (Figure 181) confirm the findings of Sudduth et al. (2001) and Beamish (2011), that apparent electrical conductivity decreases with increased elevation over a homogeneous half space (Figure 182).

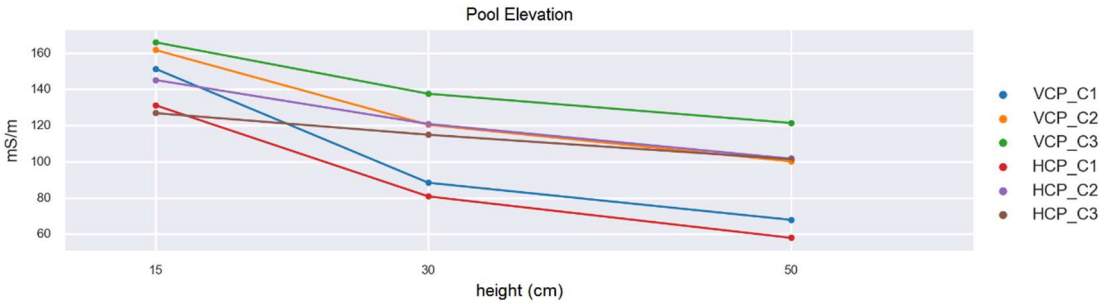

Figure 181: The decrease in VCP and HCP quadrature-phase measurements with increased instrument height in the Pool Elevation experiment.

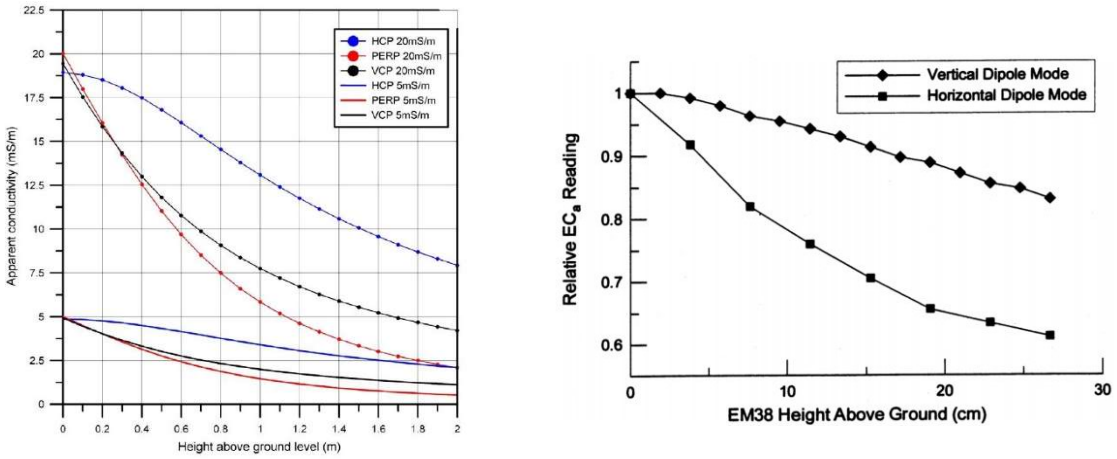

Figure 182: Charts showing the decrease in electrical conductivity measurements in the quadrature-phase as the instrument height increases. From (left) Beamish (2011) and (right) Sudduth et al. (2001).

While the LIN criteria are specifically derived to be applicable for approximating subsurface conductivity from the received EM signal, due to the intrinsic relationship between the quadrature-phase and in-phase, it would be reasonable to predict that changes in the quadrature-phase due to elevation differences could impact the in-phase results as well. The Pool Elevation experiment demonstrates the in-phase measurements also decrease with increased elevation (Figure 183), but typically exhibit a less dramatic change than their counterpart quadrature-phase measurements (Figure 184).

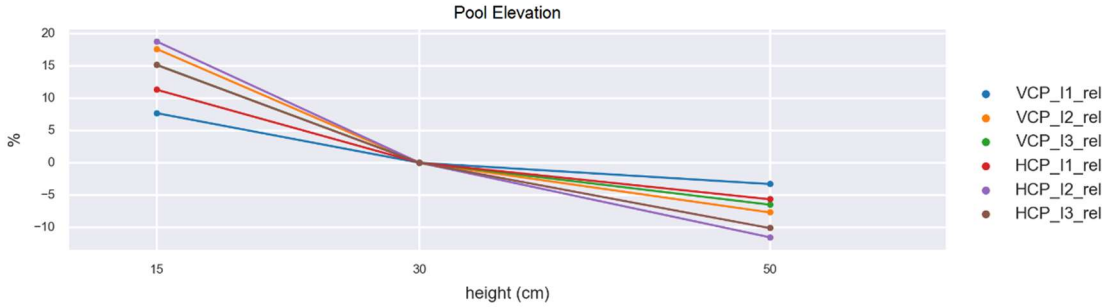

Figure 183: The relative decrease in VCP and HCP in-phase measurements with increased instrument height in the Pool Elevation experiment.

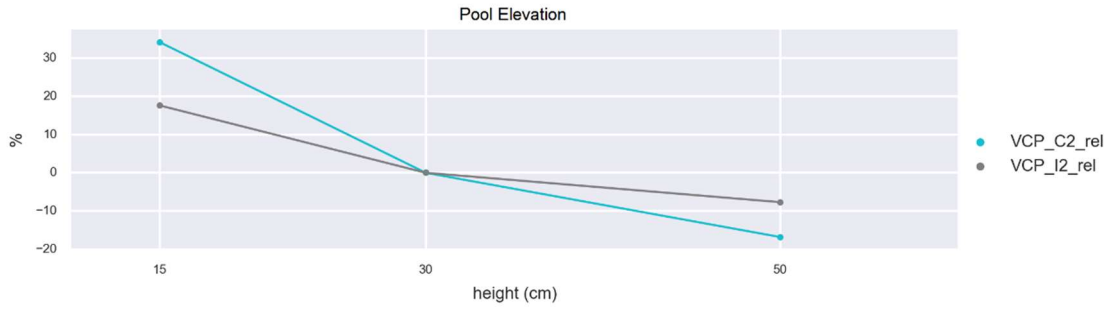

Figure 184: Comparison of the relative decrease in VCP C2 and I2 measurements with increased instrument height in the Pool Elevation experiment.

While the previous experiments demonstrated a tendency for the different datasets within the same coil orientation (e.g. VCP or HCP) to behave similarly, the elevation experiment reveals greater behavioural similarities between the analogous HCP-VCP coils (Figure 185) than within the same coil orientation (Figure 186). However, additional instrument heights would still be required to derive any confident conclusions of this behaviour, to more accurately measure the trend of response.

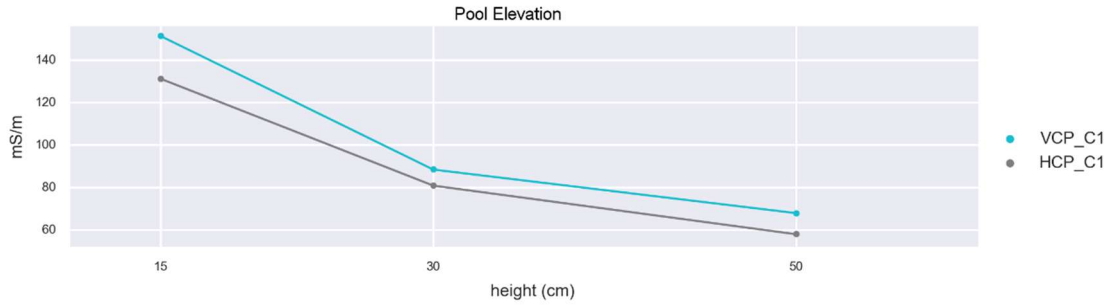

Figure 185: Comparison of the decrease in VCP and HCP C1 measurements with increased instrument height in the Pool Elevation experiment.

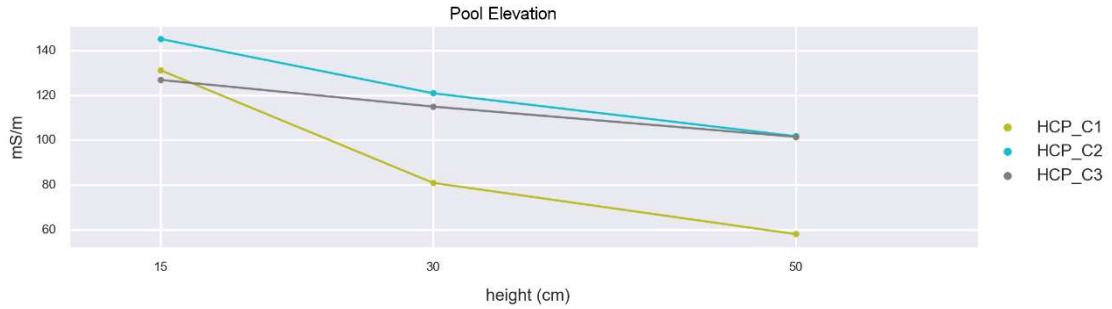

Figure 186: Comparison of the decrease in HCP quadrature-phase measurements with increased instrument height in the Pool Elevation experiment.

Overall the Pool Elevation results confirm the uniqueness of the respective coil orientations (VCP vs. HCP), the individual phases and the individual configurations. As such, any adjustments for offset effects must take these factors into consideration, instead of applying an all-encompassing correction.

5.10 Elevation Experiments vs. Field Data

Changes in the instrument's baseline measurements with elevation changes were also observed in the field results. At Linton, switching between instrument operators during a handheld survey strategy introduced pronounced changes to the background measurements. The strong banding in Figure 187 corresponds with different operators taking over survey; the operators were at different heights. Figure 188 shows the response form and magnitude of this effect.

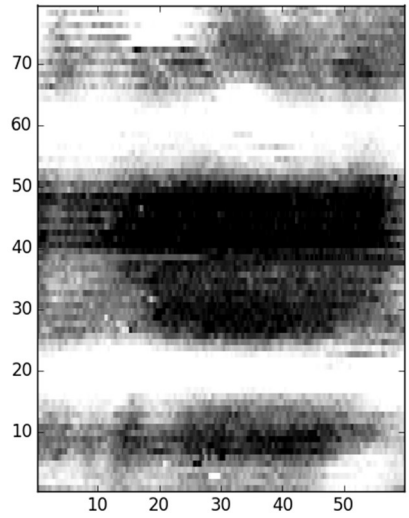

Figure 187: VCP I3 greyscale at Linton. The banding along the grid indicates where a change in instrument operator occurred.

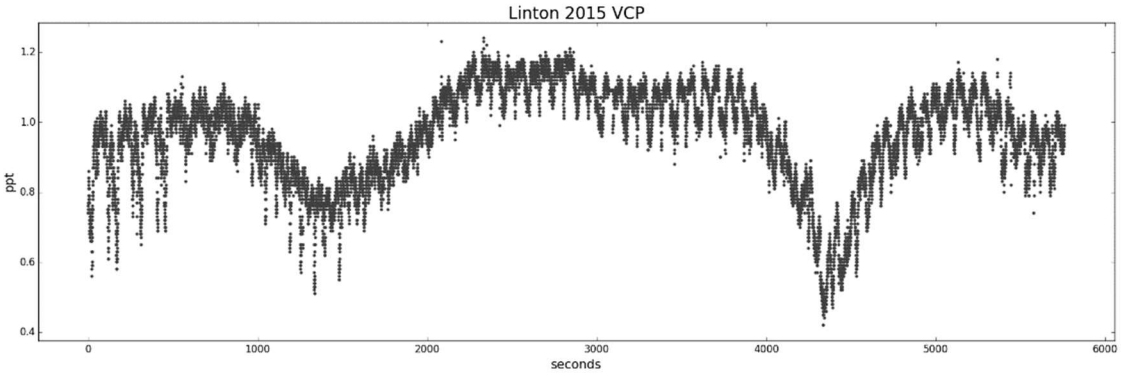

Figure 188: VCP I3 vs time at Linton showing the response form of variable instrument height. Minor variations between adjacent traverses represent the effect of recalibrating the instrument before it is rotated for the next traverse.

Abrupt elevation changes within the traverse also produced discrete bands within the line. For example, sudden elevation or orientation changes of the instrument caused by avoidance of surface obstacles or due to undulating terrain introduced many discrete high-contrast bands in the Linton results. Figure 189 shows these bands within VCP I3, correlating where the ground conditions featured sudden steep drops and surface obstacles. Figure 190 shows the magnitude and form of these types of responses.

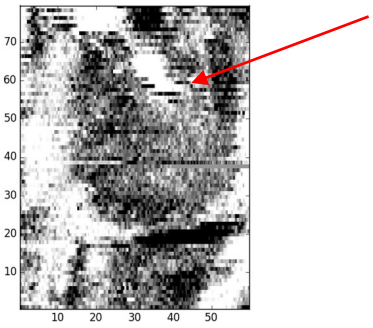

Figure 189: VCP I3 greyscale at Linton, with a rolling-median and zero-median traverse applied to correct for the wide banding introduced by the different instrument elevation between operators. The red arrow indicates discrete banding caused by the sudden change in instrument elevation and orientation around obstacles. The associated XY trace is presented below in Figure 190.

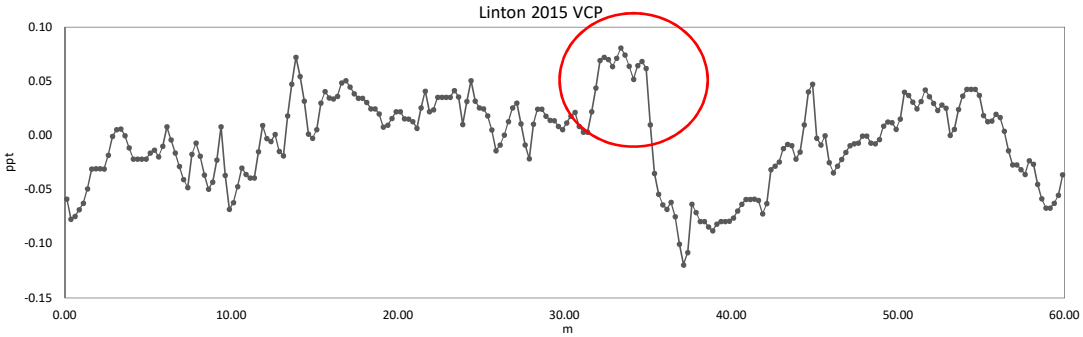

Figure 190: Selected traverse from VCP I3 at Linton. Isolated banding is outlined in red to illustrate the response form and magnitude caused by the sudden change in strument elevation and orientation around obstacles.

5.11 Elevation Conclusions

Comparison of the experiment and field results demonstrates the importance of maintaining a constant instrument height and position over the ground surface. While the presence of survey obstacles or variable ground height within a traverse cannot be controlled, the impact of the relative heights of the instrument operators should be considered when selecting an instrument apparatus and survey strategy; this will be fully explored in the following chapter.

5.12 Experiment Conclusions

Analysis of the cumulative experiment results with the fieldwork results concludes that many of the observed data issues can be mitigated or eliminated by adhering to consistent operator of the instrument. The following chapter will use these cumulative results to develop an effective methodology for instrument operation to reduce some of the issues highlighted in the preceding chapter. For those issues that cannot be entirely mitigated through accurate instrument set-up and consistent instrument operator, a processing strategy will be developed to rectify these issues.

Chapter 6 EM Methodology for the Collection, Processing and Visualisation of High-Quality Data to Ensure an Accurate Archaeological Characterisation of the Geophysical Results

The cumulative fieldwork and experimental results highlight the importance for accurate instrument set-up and consistent operation during field survey in order to minimise the introduction of drift, grid imbalances and other erroneous measurements into the resulting output. The analysis of the cumulative EM work presented in Chapter 4 and 5 has developed the following methodology, to answer research question 1. The methodology advises best practices for the collection, processing and visualisation of CMD Mini Explorer data to produce outputs that accurately represent subsurface conditions.

6.1 Best Field Operation Practices for the Collection of High-Quality Data

The foundation for the accurate characterisation of any geophysical dataset is formed by the collection of high-quality measurements in the field. Accurate instrument set-up and data collection will help reduce the introduction of erroneous measurements and data artefacts. The following EM field operation practices are supported by the cumulative results of the field survey and experimental work and satisfy research objective 1a.

6.1.1 Warm-Up Time

Before any data collection is commenced, the instrument must be given sufficient time to adjust to ambient survey temperature. The time required for the instrument's measurements to stabilise to survey conditions will vary depending on the temperature difference between the survey temperature and the previous environment the instrument had been adjusting to. The drift experiments were conducted during winter and tested the instrument under extreme temperature differences (i.e. differences of up to 17°C from inside to outside temperature). The results of the warm-up drift experiments recommend a full 30 minutes for the instrument to adjust to ambient survey conditions, under extreme conditions. However, fieldwork conducted during spring and early autumn found a warm-up of only 15 minutes was sufficient for the instrument to adjust to ambient to survey conditions, a result of the warmer seasonal temperatures. To determine if the instrument has been given sufficient time to warm or cool to ambient survey

conditions, the instrument measurements should be monitored in the datalogger's "search mode" function to establish whether the measurements have stabilised or are still increasing or decreasing.

6.1.2 Selecting an Effective Instrument Apparatus

The instrument has been operated within handheld, sledge-based and cart-based systems for the collection of field measurements. The telescopic handle requires an operator to physically suspend the instrument over the ground surface; the sledge contains the sensor within tubing to glide across the ground surface; and the cart-based system mounts the sensor at a fixed height above the ground surface. All three of these different apparatuses were tested during fieldwork; although only sledge-based and handled results are presented in the thesis text itself. The results of the cart-based surveys will be referenced in-text and can be viewed in the digital archive. Each one of these operational apparatuses has its advantages and disadvantages. Choosing which apparatus to employ should be considered on a site-specific basis.

- **Uneven Terrain** – For sites with uneven terrain or low-lying obstacles, a cart-based system will facilitate collection of the best quality data. The suspension of the instrument at a constant height above the ground surface means the instrument is less susceptible to knocks from obstacles and variable terrain cover. The handheld system, operated using the instrument's time-based sampling mode, was found to be the worst strategy for sites with uneven and variable ground cover, as it required the diligence of the operator to maintain the sensor at a fixed height above the ground surface. Sudden displacement of the instrument around obstacles can introduce discrete bands within the traverse. The handheld system was a more effective apparatus in the face of survey obstacles when the sensor was operated in manual data collection mode. In manual collection, the instrument is triggered to sample by the operator, which allows the sensor to be positioned on or over obstacles before collecting measurements. This strategy was found to be effective over the ruins at Fountains Abbey, where the instrument could be easily manoeuvred around extant remains (see Fountains Abbey 2014, digital archive). However, manual data collection is significantly slower than time-based

sampling. The time required to cover the 20m x 20m grid at Fountains Abbey was comparable to that of a parallel twin-probe survey; whereas a time-based survey was completed in less than half the time of a manual survey. Thus, manual data collection is not an efficient strategy for larger areas or high-resolution surveys.

- **Multiple Operators** - Cart-based systems produced the best-quality data when multiple operators were collecting measurements, because the sensor height was maintained at a fixed elevation from the ground surface (see Linton 2016, digital archive). The sledge system was the second-best apparatus for surveys with multiple operators. While the sledge also maintained the instrument at a fixed height above the ground surface, Purvis' (2003) sledge system requires a cable to connect the sensor to the datalogger. This cable can affect the collected measurements if the position of the cable relative to the coils is variable (refer to the calibration experiments in sections 5.6-5.8). The handheld system was concluded to be the worst apparatus to employ with multiple operators. Differences in operator height introduced elevation differences between the sensor and the ground surface, evident in the results as banding across the grid (refer to the elevation experiments in sections 5.10-5.12).

- **Even Terrain** - For sites with relatively even terrain, the handheld system operating in time-based sampling, with Bluetooth linkage between the sensor and the datalogger, produced the best results. At sites with even terrain, such as Lister Park, the sensor was able to skim across the top of the ground surface. The less distance between the sensor and the ground surface results in the sensor measuring a greater portion of subsurface, rather than the intermediate air gap; this not only facilitates superior depth penetration, but reduces the quantity of noisy data spikes as well. The sledge-based system also worked well on even terrain, but the requirement for a physical cable tethering between the sensor and the datalogger sometimes introduced interference with the collected measurements. However, the handheld system was more fatiguing to operate than the sledge-based system, as the operator must suspend the instrument through physical exertion; handheld operator can get be tiring

over larger sites. Cart-based systems also worked effectively over even terrain and produced high-quality results. However, the elevated sensor height above the ground surface often resulted in the R1 coil measuring a greater percentage of the air gap between the sensor and the ground surface, rather than the subsurface itself. Measuring the air gap produced noisier and less informative results.

6.1.3 Instrument Calibration

For grid-positioned data collection, a consistent reference zero-point to revisit throughout the survey was not effective for correcting instrument drift. The fieldwork and experiment results demonstrated instrument drift tended towards a quadratic change. If the instrument tended towards a linear drift, a consistent reference point could be more effective for correcting any changes; however, with a quadratic tendency towards drift, it would be difficult for the operator to measure enough reference points throughout the day to achieve an accurate model for the temporal change in measurements. For GPS-positioned surveys, tie-in lines are only as effective as the accuracy of the measurements collected within the tie-in lines themselves. The experiment results revealed the sensor is prone to random, sporadic jumps in background measurements. As these jumps are not predictable and difficult to isolate in the field results, any jumps would affect the accuracy of the calibration line. The calibration experiments and field results confirm the CMD Mini Explorer's built-in recalibration at the end of every traverse is helpful for limiting these jumps to only those lines in which they occur.

GF Instruments' datalogger is programmed to recalibrate the sensor at the end of every traverse. At the end of the traverse, the operator and the instrument should rotate to face the direction of the next traverse before the initiating the recalibration. As the calibration experiments demonstrated, the rotation of the sensor *after* its recalibration, not the calibration process in itself, introduces striping between adjacent traverses. This is a similar effect to heading errors experienced in the collection of zig-zag magnetometer data. By recalibrating the instrument in the orientation it will be facing for the next line of measurements, data striping from this "EM heading error" will be reduced. The instrument's end-of-line recalibration was also effective for reducing drift within the line, but drift

across the lines was still present in some of the field results. However, drift across the lines was straightforward to correct with subsequent data processing.

6.1.4 Selecting an Effective Grid Size

The field results reveal that using multiple grids within a single survey area creates imbalances between adjacent grids due to different baseline values. The 2012 VCP NW-SE results at Menston (see section 4.5.4) exemplify these grid imbalances and the difficulties of correcting such an effect. The 2012 VCP NW-SE survey at Menston collected measurements using the time-based sampling strategy in 20m x 20m grids over a 40m x 60m survey area. The iron plot markers buried within the topsoil produced overwhelming responses in both phases of the instrument, which significantly affected the baseline responses of each individual grid. The small grid sizes and the extreme differences between the individual grids' baseline levels made balancing the grids' baseline levels difficult, despite manual arithmetic modification of the individual grids' backgrounds and bespoke edge-matching algorithms (e.g., Figure 191). Subsequent surveys at Menston that utilised a grid size that matched the dimension of the survey area did not suffer from these grid imbalance effects (see Figure 121 in section 4.5.4).

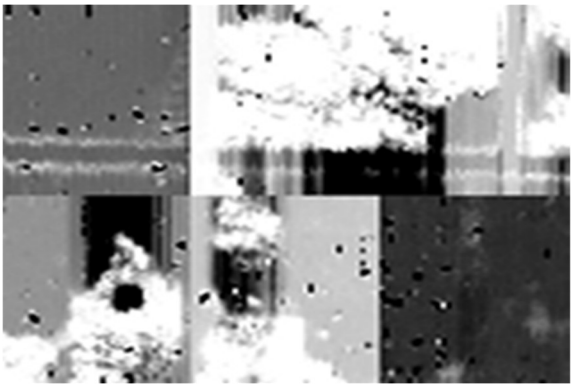

Figure 191: Menston 2012 HCP I1 greyscale (+/-1SD), highlighting the imbalances between the grids due to extreme differences in baseline measurements, caused by the varying concentration of highly magnetic within each grid.

6.1.5 Selecting an Effective Sampling Strategy

In time-based sampling mode, the accuracy of the positional referencing relies on the operator to walk at a constant pace and accurately update the position intervals. Updating the user-defined position before or after the reference marker will reduce the positional accuracy along the line and can introduce staggering effects between adjacent traverses. The GF Instruments' datalogger allows for

the interval of reference points to be pre-set by the operator. It is tempting to therefore assume that closer-spaced reference points would increase the overall positional accuracy because there would be a smaller set of positions to rubberband across. This assumption is not necessarily correct. Figure 192 shows the greyscale of HCP C1 results over a 20m x 20m grid using 0.5m line spacing and identifying reference measurements every 1m along the line. Staggering was noticeably more pronounced with the reference measurements every 1m than in datasets with reference measurements every 20m (Figure 192).

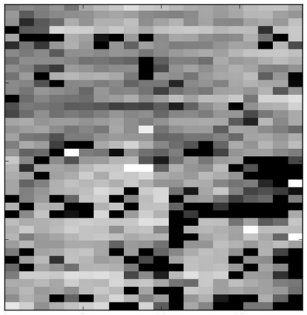

Figure 192: Greyscale of Menston HCP C1 results, showing significant staggering issues when the user-updated reference position was set to 1m.

The field operation steps above are summarised into a workflow diagram presented at the end of this section (Figure 193). Adhering to the field operation steps above will help to improve the quality and accuracy of the data collected, but not all the effects from site-specific field conditions and obstacles can accounted for by accurate instrument set-up and collection. Data processing steps can help rectify any remaining data issues. As part of this research, a data processing workflow and software to accompany the field operation workflow were developed to satisfied objective 1b, as no dedicated software or standard processing steps were available. Through the range of different types of fieldwork sites and scheme of experimental work, a comprehensive understanding of the behaviour and responses of the instrument has been thoroughly developed. The starting point for any data processing using time-sampled measurements is to resample the data into a gridded format to visualise the result in an image format.

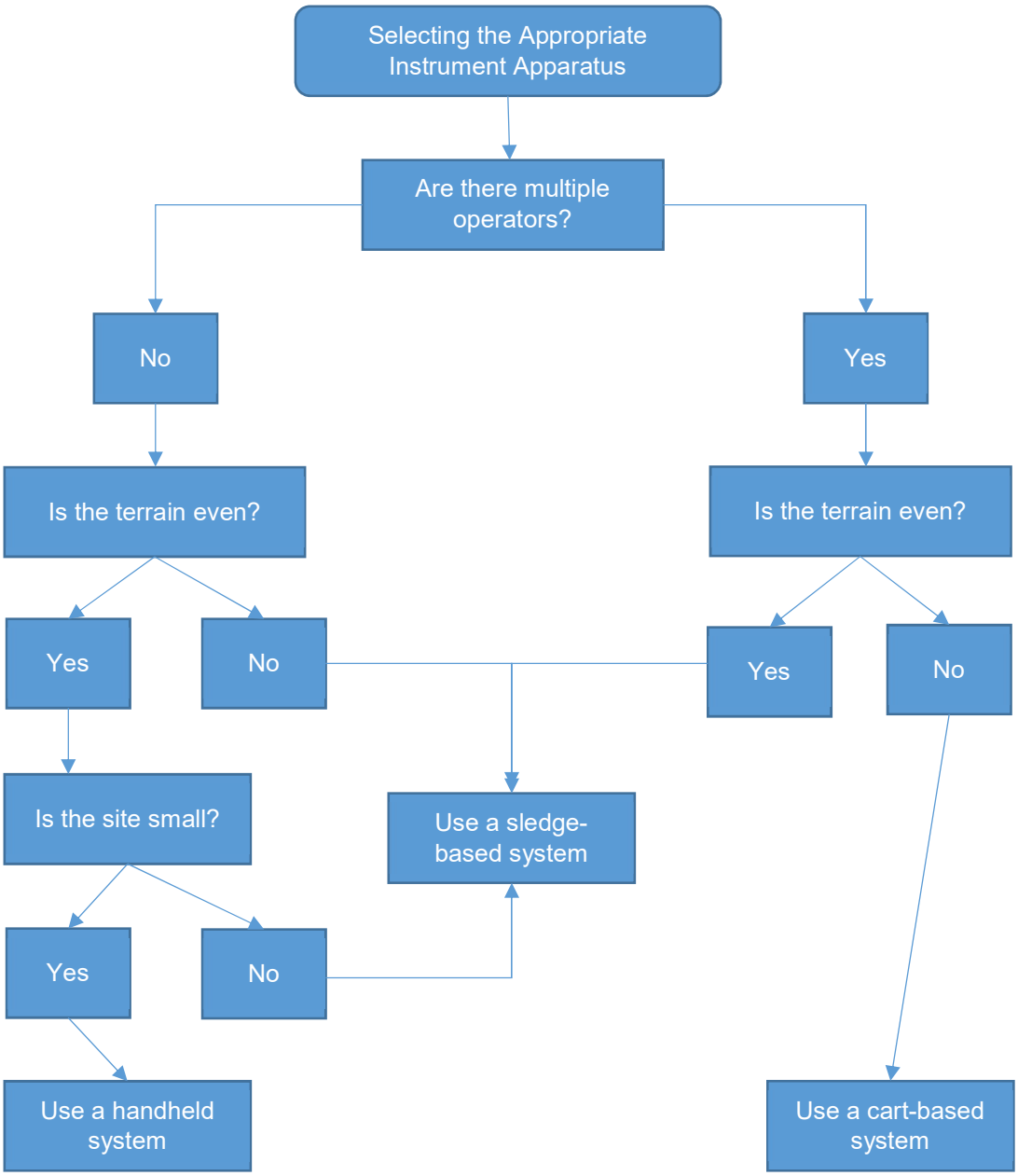

Figure 193: Flowchart for selecting the most appropriate instrument apparatus for the site conditions.

6.2 Resampling Time-Based Data into a Positionally Accurate Measurement Grid

Since the field data for this thesis were primarily collected using time-based sampling across lines within a grid, the time-based measurements had to be resampled onto a regular grid for processing and visualisation. The following section describes the algorithms for pre-processing and gridding the time-based measurements into a format suitable for visualisation The code is written specifically for the CMD Mini Explorer's output format, meeting research objective 1b. The CMD Mini Explorer datasets are exported as xyz files where x = the line

number, y = the user-updated position along the line, and z = the measurement value. However, the general algorithm steps can also be applicable to other time-based datasets with some modification. The regridding algorithms were initially developed as part of ArchaeoPY (Gaffney et al. 2015; Harris et al. 2015b; Pope-Carter et al. 2014b) and a user-interface was developed as part of this thesis to make the software more user-friendly; this thesis also added a blanking grid function to accommodate the results from Lister Park. A step-by-step summary of the ArchaeoPY CMD regridding algorithm will follow below; the full transcript of the code can be found in Appendix 2.

1. **Fix the End of Traverse** – The CMD Mini Explorer's xyz output denotes the end of a traverse with the last user-identified y-position and leaves the z-measurements blank. The x-position is automatically advanced at the end of each traverse before the subsequent traverse is collected. The end-of-traverse rows are identified by analysing the column containing the x-positions and identifying where the x-position in one row does not equal the x-position in the previous row. The code then takes the y-position in this row and pastes this value into the final measurement of the traverse; as a result, the final user-identified positions is the final position recorded in the traverse. The rows containing the blank measurements at the end of the line are then deleted.

2. **Rubberband Data Along the Traverse** - The user-identified reference y-positions need to be converted to actual positional measurements along the traverse. When the code is run, the input dataset is analysed line-by-line. The number of samples in a line is determined and a 1D interpolation between the button presses is performed, providing unique, local y-positions to all the measurements.

3. **Resample Data at Regular Intervals -** The regridding process requires the measurements to be sampled at regular intervals. While the rubberbanding provides local y-positions for all the measurements, these y-positions are derived from the time-interval and may not have a regular sampling distance due to inconsistent pacing and how instrument averages collected measurements. In the ArchaeoPY software's user-

interface, the user inputs the desired x and y sampling intervals. The user's input for the y sampling interval is applied to the measurements along the line using a 1D interpolation to produce a regular sampling interval.

4. **Grid Data** - Once the data have been resampled at regular intervals, the z data is extracted from the xyz columns and reshaped into the user-defined grid dimensions from the input x and y sampling intervals. The final gridded form of the datasets is used to visualise the results in an image format.

5. **Account for Coil Separations –** The ArchaeoPY software grids the data using the y-position as the measurement centre for the sensor. However, the measurement centre of the sensor is not the measurement centres for the individual R1, R2 and R3 volumes. Therefore, for zig-zag data collection, when the instrument heading will alternate between the transmitting coil and R3, staggering effects may be apparent between adjacent traverses. These staggering effects are separate from pacing inconsistencies because they manifest as a more uniform offset across the grid; whereas pacing inconsistencies were often limited to specific lines. Because of this uniformity across the grid, a user-defined adjustment was added and subtracted to alternating traverses to account for the offset of the measurement centre. In general, the smaller the coil separation, the larger the adjustment is required; whereas with the larger coil separations, a similar soil volume is still being measured despite the rotation of the instrument. However, the amount of adjustment required was found to vary between the type of site

   Regridding of the fieldwork results found that sites with earthen features, such as Markenfield (see 3.3.4.3) and Linton (3.3.4.4) required smaller adjustments of the separate coils' measurement centres. Sites with large concentrations of ferrous and other highly magnetic material required larger adjustments to the separate coils' measurements centres. This type of material is typical of modern sites, such as Lister Park (see 3.3.4.1) and Menston (see 3.4.4.5), but was also present at Fountains Abbey (see 3.3.4.2) where modern intervention laid services and cabling. The reasons

for the amount of positional adjustment required for these different types of sites likely is a result of the type of material composing the measured features. Ferrous and other highly magnetic material produce strong, high-contrast responses, which can overwhelm the signal through multiple coils. Changes in the in-phase that correlate with a coincident change in the quadrature-phase is a known phenomenon that has been attributed to the magnetic viscosity of the measured material, which can produce a time lag in the quadrature-phase. This complex relationship is explored in the Geonics Technical No. 36, but is still poorly understood (McNeill, 2013); consequently, quantifying the impact of magnetic viscosity on measured EM outputs is outside the realms of this thesis, but is likely a contribution to the greater adjustment required at modern sites. Furthermore, the relative size and magnitude of the response will also make any positional inaccuracies more noticeable. In contrast, with earthen features, the signal is generally weaker in magnitude and generated by a feature much larger than the coil separation, which may result in any staggering effects blending in to the surrounding measurements.

The accuracy of the regridding algorithm for positioning the time-based measurements into the expected grid positions was tested using synthetic data. Synthetic data was produced in an xyz format identical to the output from the GF Instruments' datalogger, except the z measurements were replaced with the actual sampling position along the line (Figure 194).

x[m]	y[m]	z1	z2	z3	z4	z5	z6
0.5	0	8.25	8.25	8.25	8.25	8.25	8.25
0.5	0	8.5	8.5	8.5	8.5	8.5	8.5
0.5	0	8.75	8.75	8.75	8.75	8.75	8.75
0.5	0	9	9	9	9	9	9
0.5	0	9.25	9.25	9.25	9.25	9.25	9.25
0.5	0	9.5	9.5	9.5	9.5	9.5	9.5
0.5	0	9.75	9.75	9.75	9.75	9.75	9.75
0.5	10	10	10	10	10	10	10
0.5	10	10.25	10.25	10.25	10.25	10.25	10.25
0.5	10	10.5	10.5	10.5	10.5	10.5	10.5
0.5	10	10.75	10.75	10.75	10.75	10.75	10.75
0.5	10	11	11	11	11	11	11
0.5	10	11.25	11.25	11.25	11.25	11.25	11.25
0.5	10	11.5	11.5	11.5	11.5	11.5	11.5
0.5	10	11.75	11.75	11.75	11.75	11.75	11.75
0.5	10	12	12	12	12	12	12
0.5	10	12.25	12.25	12.25	12.25	12.25	12.25
0.5	10	12.5	12.5	12.5	12.5	12.5	12.5
0.5	10	12.75	12.75	12.75	12.75	12.75	12.75
0.5	10	13	13	13	13	13	13

Figure 194: Synthetic CMD Mini Explorer xyz dataset with z = the sampling position along the line.

The ArchaeoPY CMD software regridded the synthetic xyz onto regular grid positions (Figure 195).

	A	B	C	D	E	F	G	H	I	J	K	L	M	N	O	P	Q	R	S	T
1	0.00	0.25	0.50	0.75	1.00	1.25	1.50	1.75	2.00	2.25	2.50	2.75	3.00	3.25	3.50	3.75	4.00	4.25	4.50	4.75
2	0.00	0.25	0.50	0.75	1.00	1.25	1.50	1.75	2.00	2.25	2.50	2.75	3.00	3.25	3.50	3.75	4.00	4.25	4.50	4.75
3	0.00	0.25	0.50	0.75	1.00	1.25	1.50	1.75	2.00	2.25	2.50	2.75	3.00	3.25	3.50	3.75	4.00	4.25	4.50	4.75
4	0.00	0.25	0.50	0.75	1.00	1.25	1.50	1.75	2.00	2.25	2.50	2.75	3.00	3.25	3.50	3.75	4.00	4.25	4.50	4.75
5	0.00	0.25	0.50	0.75	1.00	1.25	1.50	1.75	2.00	2.25	2.50	2.75	3.00	3.25	3.50	3.75	4.00	4.25	4.50	4.75
6	0.00	0.25	0.50	0.75	1.00	1.25	1.50	1.75	2.00	2.25	2.50	2.75	3.00	3.25	3.50	3.75	4.00	4.25	4.50	4.75
7	0.00	0.25	0.50	0.75	1.00	1.25	1.50	1.75	2.00	2.25	2.50	2.75	3.00	3.25	3.50	3.75	4.00	4.25	4.50	4.75
8	0.00	0.25	0.50	0.75	1.00	1.25	1.50	1.75	2.00	2.25	2.50	2.75	3.00	3.25	3.50	3.75	4.00	4.25	4.50	4.75
9	0.00	0.25	0.50	0.75	1.00	1.25	1.50	1.75	2.00	2.25	2.50	2.75	3.00	3.25	3.50	3.75	4.00	4.25	4.50	4.75
10	0.00	0.25	0.50	0.75	1.00	1.25	1.50	1.75	2.00	2.25	2.50	2.75	3.00	3.25	3.50	3.75	4.00	4.25	4.50	4.75

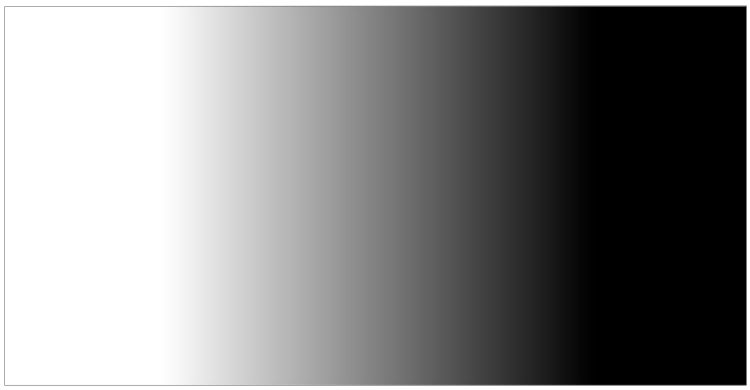

Figure 195: (top) the ArchaeoPY CMD software's regridded synthetic xyz dataset where z = the sampling position along the line. (bottom) The resulting greyscale from the regridded synthetic data.

The gridded synthetic data demonstrates the ArchaeoPY CMD code is resampling and reshaping the input xyz measurements into an accurate gridded output. While the synthetic data provides an idealised example of perfect data being regridded into the exact measurements positions within the grid, data collection in real-world environments is rarely ideal. To assess the efficacy of the ArchaeoPY CMD code for real world data collection, selected field data were run through the software with the z measurements replaced with the time position along the line. A control dataset was first run, using the results from the HCP Cal Line 1 experiment, where the data were collected in a controlled, field environment. The HCP Cal Line 1 experiment collected measurements over the same line, 20m in length, using a 0.3second sampling interval. The test line was located on the University of Bradford amphitheatre, which provided a firm, flat surface of mowed grass. Data collection was executed with a focused intent to maintain a constant pace and keep the instrument at a fixed position above the ground surface. Despite the concerted effort to minimise any operational effects on the collected results, the greyscale visualises the pacing inaccuracies as subtle banding and staggering between adjacent traverses (Figure 196).

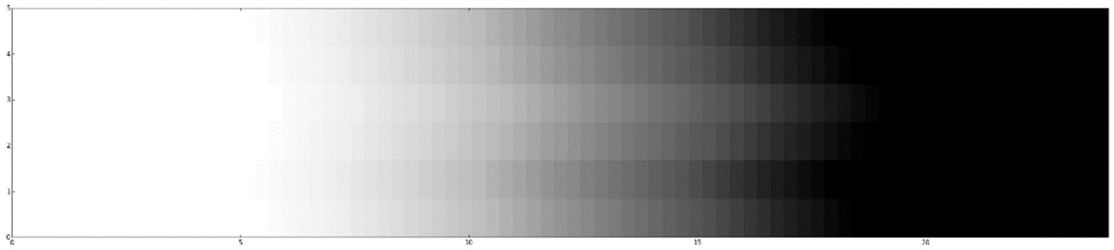

Figure 196: Greyscale of lines collected as part of the HCP Cal Line 1 experiment. Z measurements have been replaced with the time position along the line to visualise how pacing inaccuracies impact regridding and visualisation results.

The 2015 Lister Park HCP results (lines 20–39) were selected as an example of field data collected under non-controlled, real-world survey conditions. Lines 20-39 were orientated perpendicular to the slope of the terrain, which was under mowed grass cover. The ground surface was variable in firmness: soft and muddy in some areas and firmer in others. Compared to the Amphitheatre's survey environment in the HCP Cal Line 1 experiment, Lister Park provided less than ideal survey conditions. The variable ground surface and the slope of the survey area affects the ability to walk at a constant, even pace. The resulting greyscale image visualises the pacing differences between the traverses as banding across the grid (Figure 197). However, these pacing inaccuracies are likely exacerbated in this test, as the greyscale uses only the starting and final positions as reference points; whereas normally the collected field data would use the user-identified positional references, recommended every 20m, to help reduce these inaccuracies. This is confirmed by comparison with the greyscale of the HCP I3 results, which does show striping and staggering issues, but not to the extent as the z = time greyscale would suggest (Figure 198).

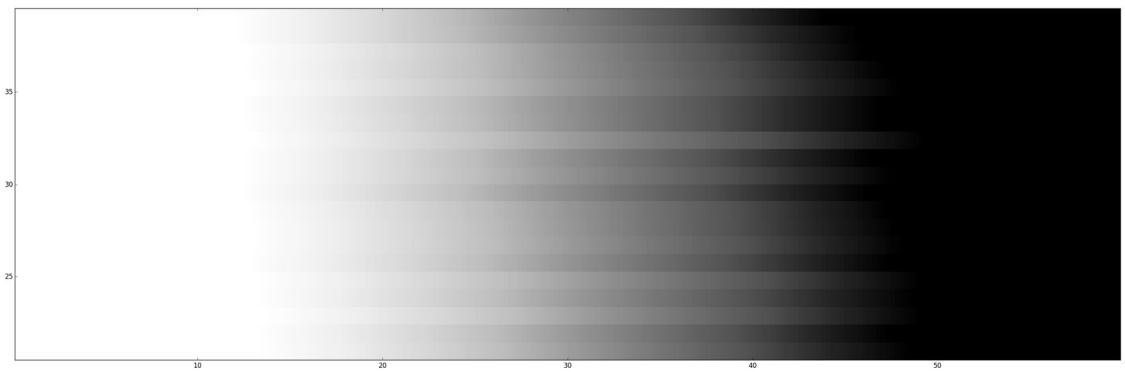

Figure 197: Greyscale of 2015 Lister Park HCP results. Z measurements have been replaced with the time position along the line to visualise how pacing inaccuracies impact regridding and visualisation results.

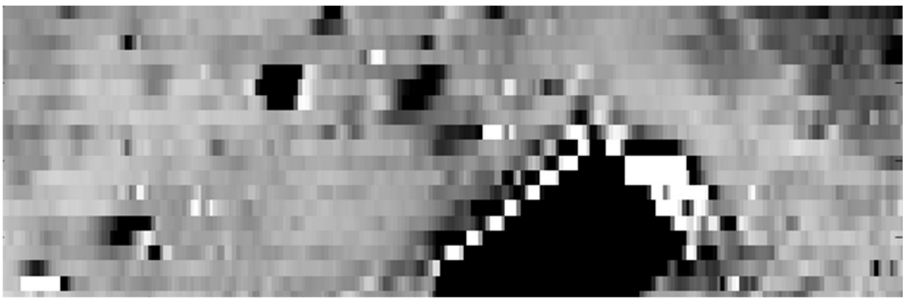

Figure 198: Greyscale of 2015 Lister Park HCP I3 results, showing less positional inaccuracies than the regridding of the time-positions in Figure 197.

Even the best datasets, collected under ideal survey conditions and with the due diligence taken to ensure quality data collection, can bear the effects of operator induced data issues. While the operator should be mindful to minimise these effects, post-data collection processing and mitigate many of the operator induced issues.

6.3 Data Processing and Correction Steps to Produce an Effective Image for Interpretation

Standard processing steps for magnetic and earth resistance data focus on correcting erroneous measurements and reducing data noise to enhance anomalies of potential archaeological origin. Processing methods for electromagnetic data are not comprehensive discussed in archaeological geophysics guidelines (Armin et al. 2015; David et al. 2008). Some archaeological geophysics books suggest the processing steps for quadrature-phase and in-phase data should be like those applied to earth resistance and magnetic data, respectively (Clay 2006; Gaffney and Gater 2003). At face value, the basis for these assertions is that the quadrature-phase and in-phase datasets measure similar physical properties to what earth resistance and magnetic methods measure. The problem with this recommendation, is that many of the steps for earth resistance and magnetic data processing are applied to correct for the specific behaviour or effects of the instruments themselves—not necessarily a reflection of some actual physical property. While the quadrature-phase can provide an inverse approximation for earth resistance under LIN conditions, the EM sensors themselves share many similarities to the operation requirements of magnetometers, and need to be calibrated or zeroed before operation. The requirement to calibrate the EM sensor can introduce striping

between adjacent traverses and imbalances between grids' baseline measurements. Positional inaccuracies, introduced or exacerbated by irregular survey pacing and offset coil measurements centres, can also affect the resulting quadrature-phase and in-phase datasets. Therefore, earth resistance processing methods may not be comprehensive to correct for all of the sensor and operator induced issues that can manifest in the quadrature-phase results. To this end, a selection of quadrature-phase and in-phase datasets were processed using standard earth resistance and gradiometer processing steps, to see if these workflows were effective for EM results. This analysis answers research objective 1b.

EM data were first resampled to regular intervals and imported into Geoplot v.4.0, a standard commercial processing package primarily used to handle earth resistance and magnetic data. Quadrature-phase data were processed using the Geoplot manual's standard steps for earth resistance data, while in-phase data were processed using the Geoplot manual's standard steps for fluxgate gradiometer data (see Geoscan Research 2005).

6.3.1 Processing Test 1: Lister Park

The targeted features at Lister Park are comprised of highly conductive and magnetic materials. The EM data were collected continuously with one operator, making it free of any grid edge effects or any other major errors (Figure 199). The quadrature-phase results reveal a high-contrast response over the paddling pool and lower-contrast responses over other structural features of the lido complex. Processing on this dataset focused on enhancing the lower-contrast features and correcting minor instrument noise and operator effects.

The first step for earth resistance processing as listed in the Geoplot manual (Geoscan 2005) is to remove erroneous measurements ("despiking"), caused by dry soil conditions or poor electrode-to-soil contact. A user-defined window will scan the dataset and replace any measurements falling outside a user-defined threshold range with the mean of the measurements within the window. Geoplot's despiking algorithm helps reduce some of the noise in the quadrature-phase dataset (Figure 200), but simultaneously curbs some of the ferrous responses representing archaeological remains. Following the despiking, a destaggering

algorithm was applied. Destaggering corrects for pacing irregularities by shifting traverses by a user-defined amount. Destaggering is not a standard processing step for manually-collected earth resistance datasets, but is applied for cart-based surveys. In the EM results, the destaggering helps to correct some of the positional inaccuracies introduced by operator pacing errors (Figure 201). Following the corrections of erroneous measurements and positional accuracies, the Geoplot manual recommends applying a high-pass filter to remove background geology to improve the clarity of archaeological features. A uniform high-pass filter with a 5x5 window was applied to the EM datasets to enhance the archaeological features (Figure 202). The high-pass filter does reveal the inner structuring of the paddling pool, which is not visible in the unfiltered dataset, but also obscures the railing response and the low-contrast anomalies adjacent to the paddling pool feature. The high-pass filter also struggles with the high-contrast ferrous anomaly in the southwest corner of the survey area—extending the extent of its response. These outcomes of the high-pass filter are similar to the results seen in the earth resistance data, where discrete anomalies are enhanced while broad background variation is stripped. However, as part of removing the background soil variation, the broad ambiguous response over the main pool that likely reflects some constituent material, is removed as well. The application of the high-pass filter produced mixed results on this particular dataset and was too harsh for preserving the more ephemeral features. The mixed success of the high-pass filter suggest that a more sophisticated filter, similar to the high-pass filter, but one that preserves subtle and low-contrast detail, could be beneficial for quadrature-phase data. Finally, the interpolation of the y-measurements was applied to the high-pass filtered data. The Geoplot manual recommends the application of this step to enhance the visibility of larger, low-contrast features. In the EM results, the interpolation of the y-measurements struggled with the paddling pool feature and obscures the pattern of response of the railing feature (Figure 203). The final figure (Figure 204) shows the data removed through the processing steps. The removed data is primarily represented by the high-contrast and ferrous type anomalies over the paddling pool and scattered across the site. The band of low conductivity extending SW-NE across the site has been removed as well. Overall, the standard earth resistance processing steps have not appropriate for the quadrature-phase results at Lister Park, nor added further interpretative value to the final image.

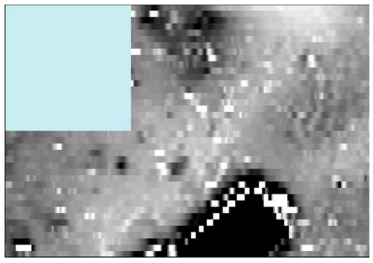

Figure 199: Unprocessed HCP C3 data from Lister Park.

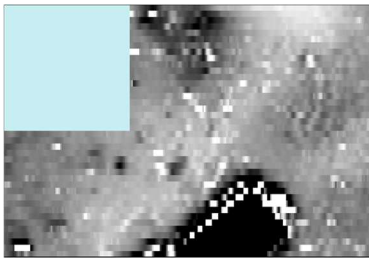

Figure 200: Lister Park HCP C3 data despiked in Geoplot.

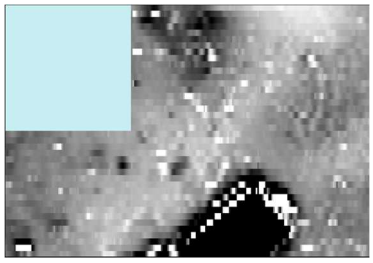

Figure 201: Lister Park HCP C3 data despiked and destaggered in Geoplot.

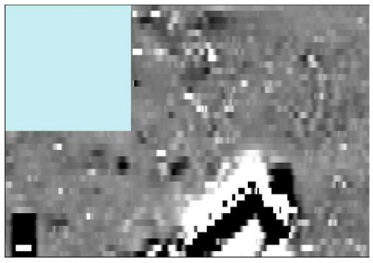

Figure 202: Lister Park HCP C3 data despiked, destaggered, and high-pass filtered in Geoplot.

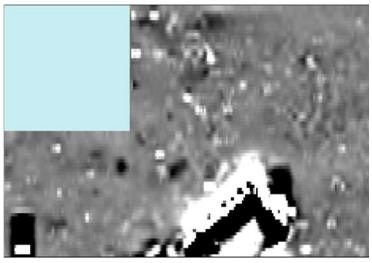

Figure 203: Lister Park HCP C3 data despiked, destaggered, high-pass filtered and interpolated in Geoplot.

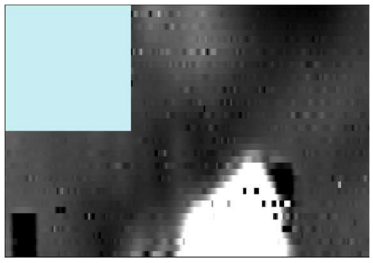

Figure 204: Data removed through processing of Lister Park HCP C3 data in Geoplot.

A gradiometer processing workflow following the Geoplot manual's recommended processing steps was applied to the in-phase results of the same survey. The Geoplot gradiometer processing workflow recommends clipping then removing spikes produced by discrete ferrous material. The in-phase data were initially despiked (Figure 206), which does help to enhance the overarching dataset trends. A zero-mean traverse followed the despiking, to correct for striping between adjacent traverses caused by variations in the baseline values (Figure 207). A programme bug would not allow for thresholds to be applied, but regardless of this issue, the zero-mean traverse proved effective for correcting instrument drift, as well as the banding issues at the bottom of the image. However, the zero-mean traverse left a processing artefact to the right of the paddling pool, which is likely a result of the inability to apply thresholds as part of the filter. The Geoplot manual recommends applying the destaggering algorithm to correct for pacing inaccuracies between adjacent traverses. The destaggering algorithm was not found effective for this dataset and is not presented below. Instead, the final processing step applied was the interpolation of the y-positions (Figure 208), which the manual recommends to enhance larger, weak features. Figure 209 visualises the data removed through processing steps, which looks

primarily related to instrument noise and drift. Overall, the magnetic data processing steps were more effective when applied to in-phase data at Lister Park, than the earth resistance processing steps were for the quadrature-phase data. Both quadrature-phase and in-phase datasets benefit the most from the zero-mean traverse, but the other processing steps were found to be less important for producing an interpretable image.

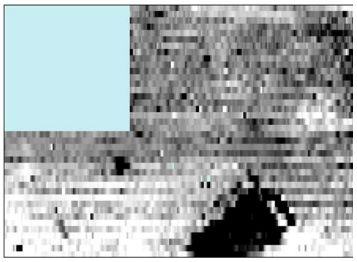

Figure 205: Unprocessed HCP I1 data from Lister Park.

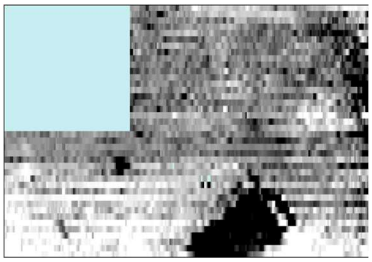

Figure 206: Lister Park I1 data despiked in Geoplot.

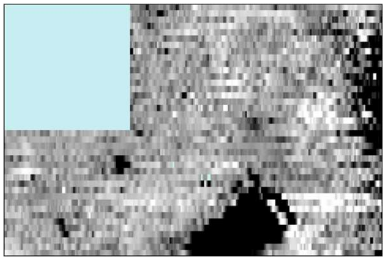

Figure 207: Lister Park I1 data despiked and with a zero mean-traverse in Geoplot.

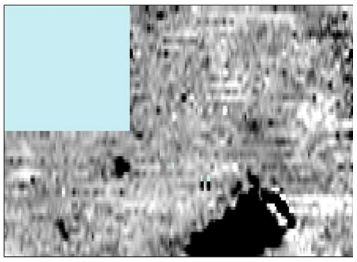

Figure 208: Lister Park I1 data despiked, with a zero-mean traverse and interpolated in the y-direction in Geoplot.

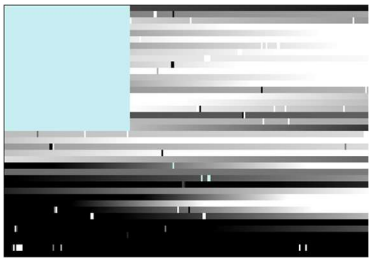

Figure 209: Lister Park I1 data removed through processing in Geoplot.

6.3.2 Processing Test 2: Linton 2015

Unlike Lister Park, there are no modern features in the survey area at Linton. Linton is comprised of earthwork features in a pasture landscape. As a result, the EM quadrature-phase survey should primarily be responding to soil variations between the earthwork features, detecting differential compaction and moisture retention, as well as the differential fill in the earthwork construction. Compared to the Lister Park results, the Linton results offer an extra challenge because data were collected by four individuals, who stopped between collecting grids. The instrument was carried at different heights above the ground surface, with inconsistent pacing between the different operators. Unlike the Lister Park results (Figure 199), the unprocessed Linton data exhibits striping and banding effects, due to differences in instrument operation and elevation (Figure 210). Isolated,

discrete bands within the lines are almost certainly caused by sudden displacement of the instrument over the undulating terrain or around surface obstacles. As with the Lister Park results, a standard earth resistance processing workflow was applied to the quadrature-phase results. The data were initially despiked (Figure 211), which smoothed some of the isolated noise. Geoplot's destaggering algorithm was then applied, but was not effective for improving most of the positional inaccuracies; as such, it is not presented below. Data were high-pass filtered to enhance the archaeological signal (Figure 212), but as with the Lister Park results, certain signals were enhanced but other archaeological signals were also removed (Figure 213). The final processing result (Figure 214), is not sufficiently corrected for instrument and operational noise to provide accurate or useful archaeological interpretations. None of these processing steps, nor any of the standard processing steps for earth resistance data, proved effective for correcting the striping and banding in the results. Geoplot's zero-mean traverse was tested on the results (Figure 215) because it is commonly used to correct similar issues seen in magnetic data. While the zero-mean traverse does not correct all of the striping effects, the prominent band of striping is successfully removed. The success of the zero-mean traverse demonstrates that a mixed magnetic and earth resistance approach to processing quadrature-phase results is more effective than just an earth resistance approach.

Figure 210: Unprocessed HCP C3 data from Linton.

Figure 211: Linton HCP C3 data despiked in Geoplot.

Figure 212: Linton HCP C3 data despiked and high-pass filtered (10x10 uniform) in Geoplot.

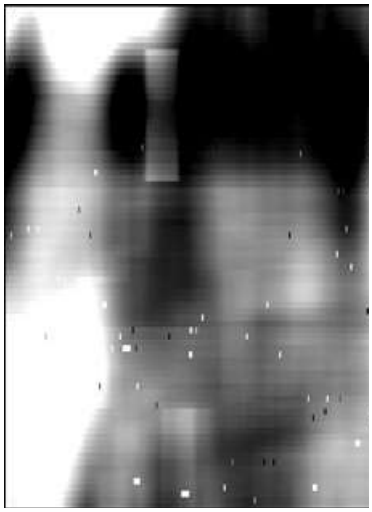

Figure 213: Linton HCP C3 data removed through processing in Geoplot.

Figure 214: Linton HCP C3 data despiked, high-pass filtered and interpolated in Geoplot.

Figure 215: Linton HCP C3 data despiked and with a zero-mean traverse in Geoplot.

The gradiometer processing workflow was applied on the in-phase HCP I3 dataset from the same survey at Linton in 2015. Compared to the Lister Park in-phase results, the Linton in-phase results show increased banding and striping between the traverses (Figure 216). Geoplot's despiking algorithm has smoothed some of the spurious instrument noise (Figure 217). As with the counterpart Linton quadrature-phase results (Figure 215), a zero-mean traverse corrected most of the banding (Figure 218). While the final processed image (Figure 219) is a more useful image for interpretation than its quadrature-phase counterpart (Figure 214), some of the shorter, discrete bands within the line are not fixed in the processing. Figure 220 shows the gradiometer processing workflow primarily removed instrument noise and the wide banding. While these processing steps improve the quality of image, further data processing is still needed to correct all of the operational effects.

Figure 216: Unprocessed VCP I3 data from Linton.

Figure 217: Linton I2 data despiked in Geoplot.

Figure 218: Linton I2 data despiked and with a zero-mean traverse in Geoplot.

Figure 219: Linton I2 data despiked, with a zero-mean traverse applied and interpolated in Geoplot.

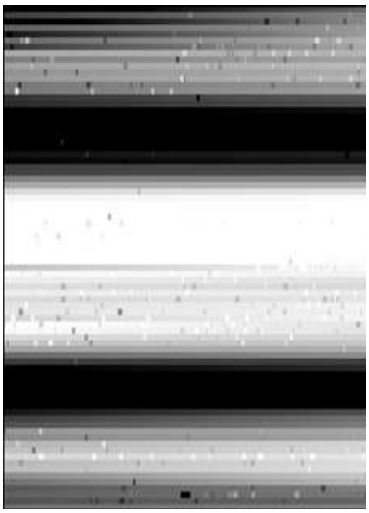

Figure 220: Linton I2 data removed through processing in Geoplot.

These preceding examples demonstrate how standard earth resistance and magnetic gradiometer processing workflows are not wholly effective for electromagnetic quadrature-phase and in-phase datasets, respectively. This thesis has instead concluded that a simple, two-staged approach for processing CMD Mini Explorer data corrects the major issues encountered, including instrument drift, striping between adjacent traverses, and variable sensor height. The approach commences with the application of a zero-median traverse, which was found to correct the majority of data issues.

6.3.3 Zero-Median Traverse

A zero-mean/median traverse is a standard processing algorithm for magnetic data, used to correct for minor baseline imbalances between adjacent traverses. The algorithms work well for magnetic gradiometer data, because gradiometer data are bipolar in nature, and should have a mean of zero. While EM data are not inherently based around a mean of zero nor are bipolar in nature, a zero-median traverse was found to be the single most effective processing step for the correction a range of different data issues. As such, a zero-median traverse was written into the ArchaeoPY CMD regridding software, by the author, and applied after the data were gridded. The algorithm operates by running through the gridded data line by line, subtracting the line's median from each measurement. This effectively reduces striping between adjacent traverses caused by instrument recalibration, by adjusting the baseline values of the different traverses to a common level (Figure 220; Figure 221). The global median of the grid is added back in to the measurements at the end, to return the scale of the measurements to the pre-zero-median level. A justification for applying a zero-median traverse to the EM data although it is not inherently based around zero, is the data processing sought to produce an effective image to be able to interpret the results and was less concerned with the absolute value of the measurement itself. The precedent for this justification is derived from processing strategies for earth resistance methods, where high-pass filters are standardly applied to enhance the archaeological features, at the expense of fundamentally changing the absolute measurement value and producing bipolar data in non-bipolar dataset.

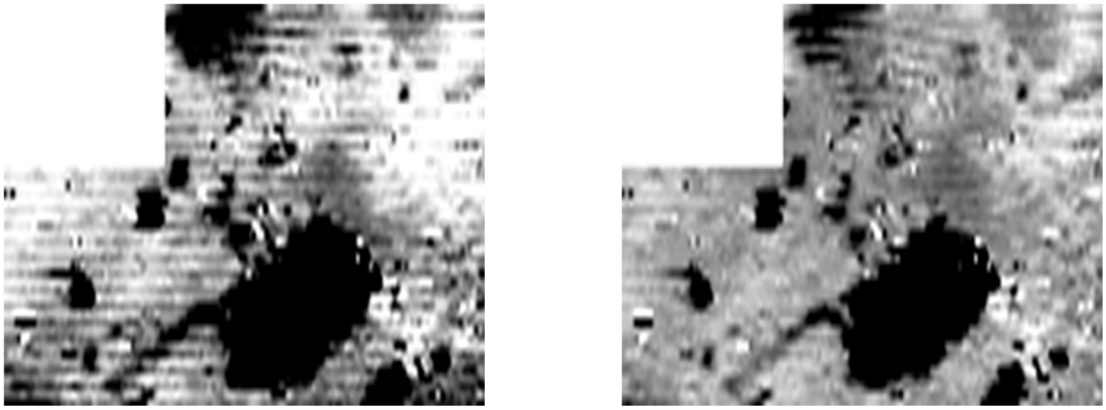

Figure 221: Lister Park VCP I3, unprocesssed (left) and corrected with a zero-median traverse (right).

Figure 222: Lister Park VCP I2, unprocessed (left) and corrected with a zero-median traverse (right).

The zero-median traverse was also found to alleviate other data issues introduced through operational effects, including instrument elevation effects. Figure 223 shows the Linton HCP I3 data, which was collected by four different surveyors changing every 20m. Changes in instrument height above the ground surface between the operators produce distinct bands across the grid. A zero-median traverse alleviates the elevation effects (Figure 223) by balancing the baseline values of the traverses within the grid.

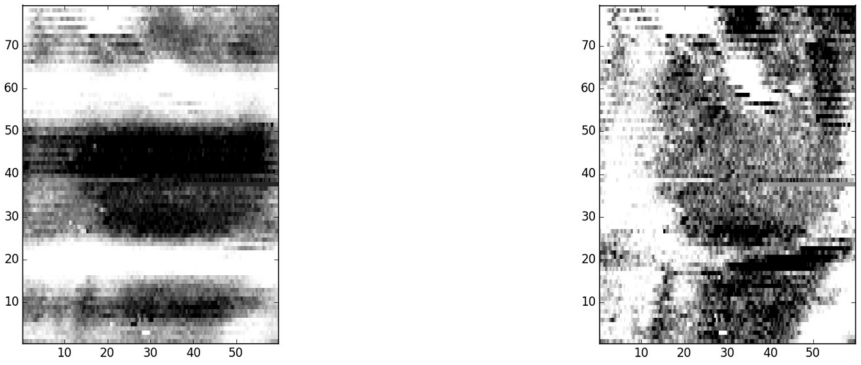

Figure 223: Unprocessed HCP I3 dataset from Linton 2015 (left) and HCP I3 corrected with zero-median traverse (right).

In sledge-based instrument operation, the relative position of the cable that tethers the sensor to the datalogger could affect the output measurements. The low conductivity banding near the southern end of the grid in Figure 224 occurs where the instrument operators switched several lines into the grid. The banding terminates in the centre of the grid when the operators switched back. The application of a zero-median traverse on the dataset corrects most of this banding, revealing the anomalies within this area.

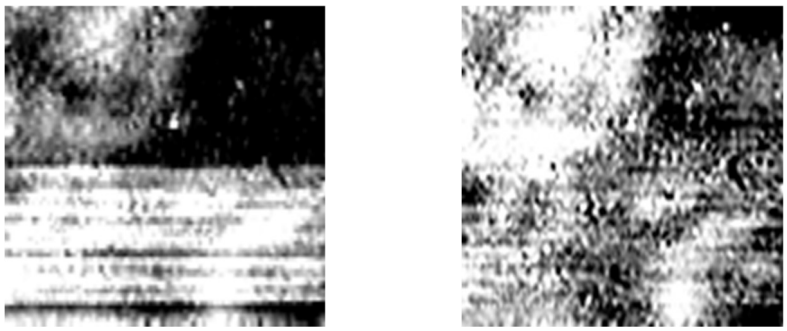

Figure 224: Unprocessed HCP C2 dataset from Linton (left) and HCP C2 corrected with a zero-median traverse (right).

The zero-median traverse was also effective for correcting temporal drift that occurred across the traverses (Figure 225; Figure 226).

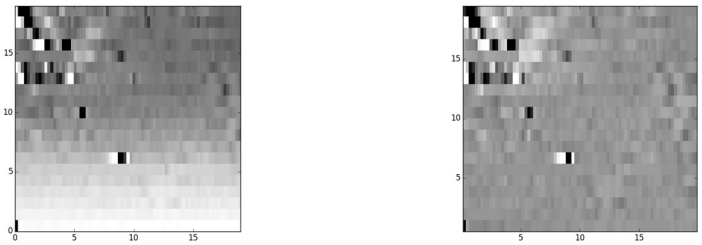

Figure 225: Unprocessed HCP I1 grid from Markenfield Hall (left) and HCP I1 corrected for drift with a zero-median traverse.

Figure 226: Unprocessed HCP I1 dataset from Lister Park (left) and HCP I1 corrected for drift with a zero-median traverse.

At sites where the quality and positional accuracy of the collected data was high, the zero-median traverse was found to effectively correct the majority of the data issues produced by instrument drift, end of line recalibration and elevation effects. At sites where the quality and positional accuracy of collected data were not as

high, additional processing steps were required. With these datasets, a rolling-median was applied before the zero-median traverse to further improve data quality.

6.3.4 Rolling-median

A rolling-median, also known as a weighted moving average, is commonly applied on time-series data to reduce short-term fluctuations in order to enhance overall data trends. If short-term fluctuations are considered as “data noise,” then a rolling-median could help to enhance archaeological features from surrounding noise. Although the CMD Mini Explorer’s data output is represented in an xyz positional format, the measurements are collected on a time-triggered interval and stored as an ordered time series— a suitable format for a rolling-median. Therefore, unlike the zero-median traverse, the rolling-median was applied to the z-data before it was gridded. A rolling-median was selectively applied to datasets where data quality and positional accuracy were poor. It was only used on two datasets in the entire set of fieldwork results: Fountains Abbey I2 and I3. The effect of the rolling-median was always compared against unprocessed data or datasets with a zero-median traverse. The objective of this comparison was to ensure only the least amount to data processing were applied to improve the data into an interpretable format. A rolling-median algorithm was written into the ArchaeoPY CMD regridding software, by the author, and applies the following steps:

1. A tree structure for the input datasets is generated to efficiently query data points and the nearest associated points within a defined window. The window size is defined by user input.

2. The collected measurements are clipped within a user-defined threshold range. Measurements occurring below or above the limits of the threshold range are replaced with a NaN, or “not a number,” datatype.

3. The rolling-median algorithm then calculates the median within a user-defined window around each data point. The window’s median is subtracted from the measurements within the window to derive the resulting output.

The application of the rolling-median on the fieldwork results could not conclude an appropriate “one-sized fits all” strategy for its application on the different types of sites and survey strategies. Determining the algorithm’s appropriate window size and threshold range is dependent on many factors, including the relative size of the targeted features, the magnitude of the anomalous responses (both archaeological and non-archaeological in origin), and the orientation of the feature relative to the instrument. The relative orientation of the instrument with respect to the buried feature is particularly important for those features occurring in-line with the traverse, they can be obscured or removed as the window runs along the line. Figure 227 - Figure 230 illustrate how the window size and threshold range affects the resulting output of the rolling-median on the Lister Park in-phase datasets. The unprocessed greyscale (Figure 227) has been gridded but has not had a zero-median traverse or rolling-median applied. Banding across the grid is indicative of instrument drift; individual measurements spikes within the line introduce data noise.

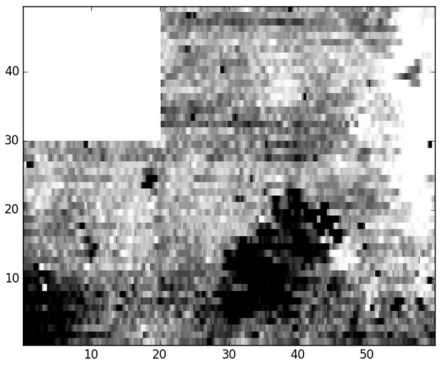

Figure 227: Unprocessed Lister Park VCP I1 dataset.

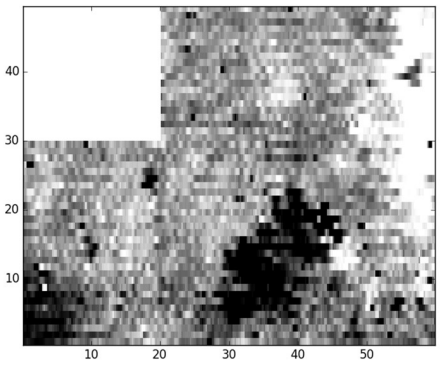

Figure 228: Lister Park VCP I1 dataset with a rolling-median: window = 60; thresholds = 25-75 percentile.

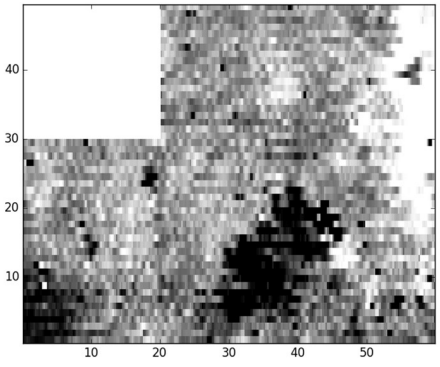

Figure 229: Lister Park VCP I1 with a rolling-median: window = 20; thresholds = 25-75 percentile.

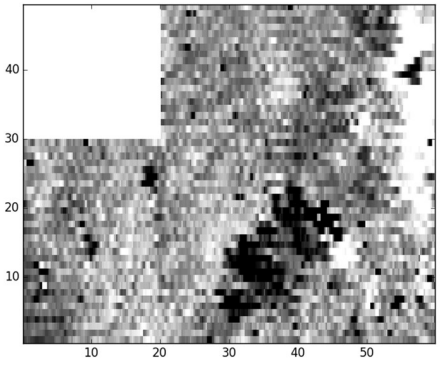

Figure 230: Lister Park VCP I1 dataset with a rolling-median: window = 60; thresholds = 5-95 percentile.

Figure 228 and Figure 229 both use thresholds to clip the data to a range within the 25th-75th percentiles, using a window size of 60 measurements and 20 measurements, respectively. Both filters reduce the magnitude of the banding and striping effects, but do little to improve the interpretable quality of the image. Decreasing the thresholds to clip the data to a range within the 5th-95th percentiles corrects the banding and minimises striping between adjacent traverses (Figure 230); the rolling-median with the 5-95th percentile thresholds also improves the relative contrast of low-contrast to high-contrast features, improving the delineation of the footprint of the women's changing room and main pool edge in the in-phase results. However, the same input parameters for a rolling-median applied to the quadrature-phase dataset, could not cope with the magnitude of response over the paddling pool feature, and produces a halo around the feature (Figure 231). Therefore, what is effective for one dataset from the same survey, may not be appropriate for another one.

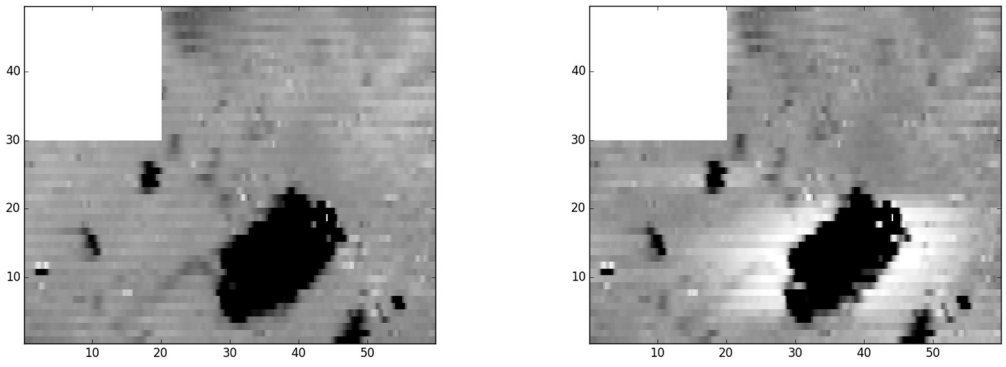

Figure 231: Unprocessed Lister Park VCP I3 dataset (left) and the VCP I3 dataset after the application of a rolling-median (window = 60; thresholds = 5-95 percentile).

The rolling-median was more effective at sites with earthen features, like Linton, and helped to create a more balanced contrast between low-contrast and high-contrast anomalies (Figure 232).

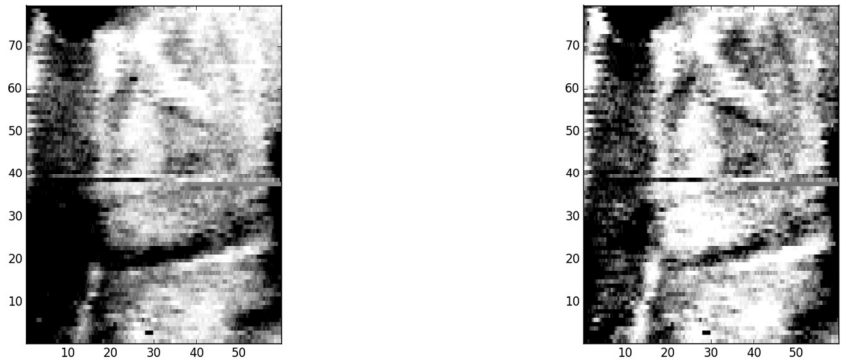

Figure 232: Unprocessed Linton HCP C3 dataset (left) and the HCP C3 dataset after the application of a rolling-median (window = 60; thresholds = 5-95 percentile).

6.3.5 Data Processing Conclusions

The preceding sections demonstrate how the standard processing steps utilised for earth resistance and magnetic data processing are not wholly sufficient for the EM datasets, given the unique operational and instrument factors linked with EM survey. The datasets from the different EM coils and phases were found to have variable and unique issues that were not necessarily consistent across the survey; these issues were primarily the result of environmental conditions and operator-induced effects, such as inconsistent pacing, poor recalibration, or movement of the sensor, rather than a product of instrument instability. The individual attention required to effectively process the different datasets was found to be time consuming, as the different datasets required different measurement centre adjustments and input parameters for the processing algorithms; still, the processing methodology presented in the preceding subsection was consistent across the field results and the basic steps were effective at the range of different sites. The recommendation for applying a zero-median traverse and/or a rolling-median to improve the clarity of the collected EM results is not exhaustive of all the processing techniques that may be effective on EM data, but this thesis takes a minimalistic approach to processing, only applying processing steps where explicitly necessary. A number of the EM datasets, including the Markenfield quadrature-phase results and the 2014 Menston results, were of good enough quality to not warrant any data processing. This thesis sought to understand how the resulting EM outputs represent the properties of the subsurface, in order facilitate a more effective comparison with the complementary magnetic and earth resistance datasets. However, more advanced filters and processing techniques could potentially be of use to highlight

or supress desired signals in the results. This advanced processing work falls outside of the focus of this thesis, but would be an important topic to address for future research.

6.4 Analysis and Visualisation of EM Datasets

To derive an accurate interpretation of any geophysical results, the data must be displayed in a useful and informative format. Data visualisation is now primarily accomplished using greyscale images to provide an easy-to-interpret planar view of the dataset. Visualisation of magnetic and earth resistance greyscales has been standardised, to an extent, given the existence of dedicated processing packages to manage the results. Earth resistance and Geoscan FM gradiometer data typically are typically displayed to +/- 1 standard deviation. The justification for this plotting range is derived from the Gaussian curve, where the statistically important data falls within this range. Data outside of this range likely represents noise or, in the magnetic results, overwhelming ferrous responses, and are considered less informative for understanding the targeted archaeological features. Bartington Instruments magnetic datasets are often visualised at tighter absolute ranges (e.g. -1 to 2nT; -2 to 3nT) than Geoscan FM datasets are. The difference in plotting levels can be attributed to Bartington system's electronic high-pass filter and the 1m sensor separation, which produces a more pronounced high-pass filtered effect than the Geoscan gradiometers, with their 0.5m sensor separation (Bartington and Chapman 2004).

In contrast to these magnetic and earth resistance sensors, the CMD Mini Explorer has a greater dynamic range of measurement values. As the range and distribution of the EM measurements will vary depending on the nature of the subsurface material encountered, particularly if there are any ferrous or other highly magnetic and conductive features present, the most effective plotting range is dependent on site-specific considerations. In CMD Mini Explorer datasets, mindful adjustment of the plotting levels can enhance or subdue specific features or anomalies. For example, at Fountains Abbey, the presence of modern services in the EM results means these features overwhelm the neighbouring responses at a tighter plotting range. At a wider plotting range, the individual features within the cellarer's yard and the outer wall of the cellarer's yard can be identified, but the response of the guest hall and the railway bed are subdued.

However, this presents a trade-off as the guest hall and railway bed have brighter contrast in the tighter plotting range, but the responses of the services and magnetic debris in the cellarer's yard obscure the eastern end of site.

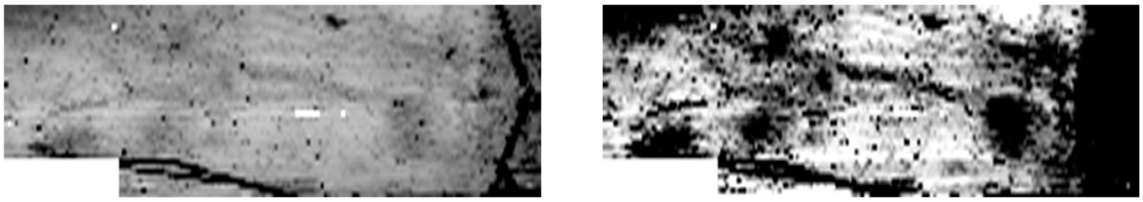

Figure 233: Comparison of the effects of different plotting ranges on the enhancement or suppression of features on a different order of magnitude. The Fountains Abbeys C1 dataset on the left is plotted to -6.68 to 6.48 mS/m, while the same dataset on the right is plotted at 0.80 to 3.42 mS/m.

Given the number of different datasets output from the CMD Mini Explorer, interpreting the results, both individually and in consideration with one another, can be overwhelming—especially if multiple plotting ranges are used for each individual dataset. The results of the fieldwork found that at the majority of sites, taking an arithmetic mean of the respective R1, R2 and R3 datasets produced a comprehensive composite image, highlighting the overall important aspects of the individual datasets, while simultaneously smoothing some of the discrete noise in the individual results. When the anomalous responses demonstrated good presence with depth and occurred between the datasets, such as the guest hall at Fountains Abbey (Figure 74; Figure 78) or the lido complex in the Lister Park quadrature-phase (Figure 55), normalising the individual datasets was found to be effective for limiting the over-contribution of any particular coil. In contrast, when the majority of the anomalous responses occurred in only one or two of the datasets and one of the datasets exhibited increased noise (most often exhibited in the R1 coils), as seen at Linton (Figure 104; Figure 107) and in the Lister Park in-phase results (Figure 61), not normalising the datasets before taking the mean was more effective for enhancing the archaeological features. Taking the inverse of the quadrature phase datasets when combing the EM datasets with different methods was not found to was not found to be effective for improving the combined image clarity. This had little effect on the combined results from Fountains Abbey (Figure 80; Figure 81) and Markenfield Hall (Figure 96), where the earth resistance datasets tended to dominate the combined results. While resistivity and electrical conductivity are theoretically inverse

properties, the cumulative fieldwork and experimental results of this these demonstrate that this inverse relationship does not strictly hold, particularly since the EM instruments are not solely measuring subsurface electrical conductivity.

Analysis of the fieldwork results also explored the application of principal component analysis (PCA) for creating an overall composite image. For most of the fieldwork sites, the PCA was less effective than the arithmetic mean for producing a composite representative image of the input datasets; however, the PCA was a valuable tool for enhancing the archaeological characterisation of the EM results. The separate principal component images highlighted and obscured different features within the results, which aided in the understanding of what different features comprise the overall image. PCA was particularly effective at Linton (Figure 104; Figure 107), where there was a distinct difference between the anomalies detected at the shallower and deeper depths. The transformation of the datasets onto the principal components also helped to highlight many low-contrast features, which were less explicit in the individual datasets and the mean results, such as the in-phase results at Lister Park (Figure 61). PCA was most effective on those sites that demonstrated variability between the R1, R2 and R3 datasets PCA was less effective on sites where near-surface noise dominated two of the datasets, as these responses were highlighted in the first and second components; this resulted in the poor performance of the PCA in the Fountains Abbey results (Figure 74; Figure 78) and with Lister Park quadrature-phase results (Figure 55).

Overall, the arithmetic mean and PCA on the EM results offered additional interpretative value; both methods have been incorporated into an EM visualisation workflow, as they were helpful for simplifying the interpretation of the 6 unique datasets the survey produces. Figure 234 presents a summary workflow of the visualisation and analysis of EM datasets, meeting research objective 1b.

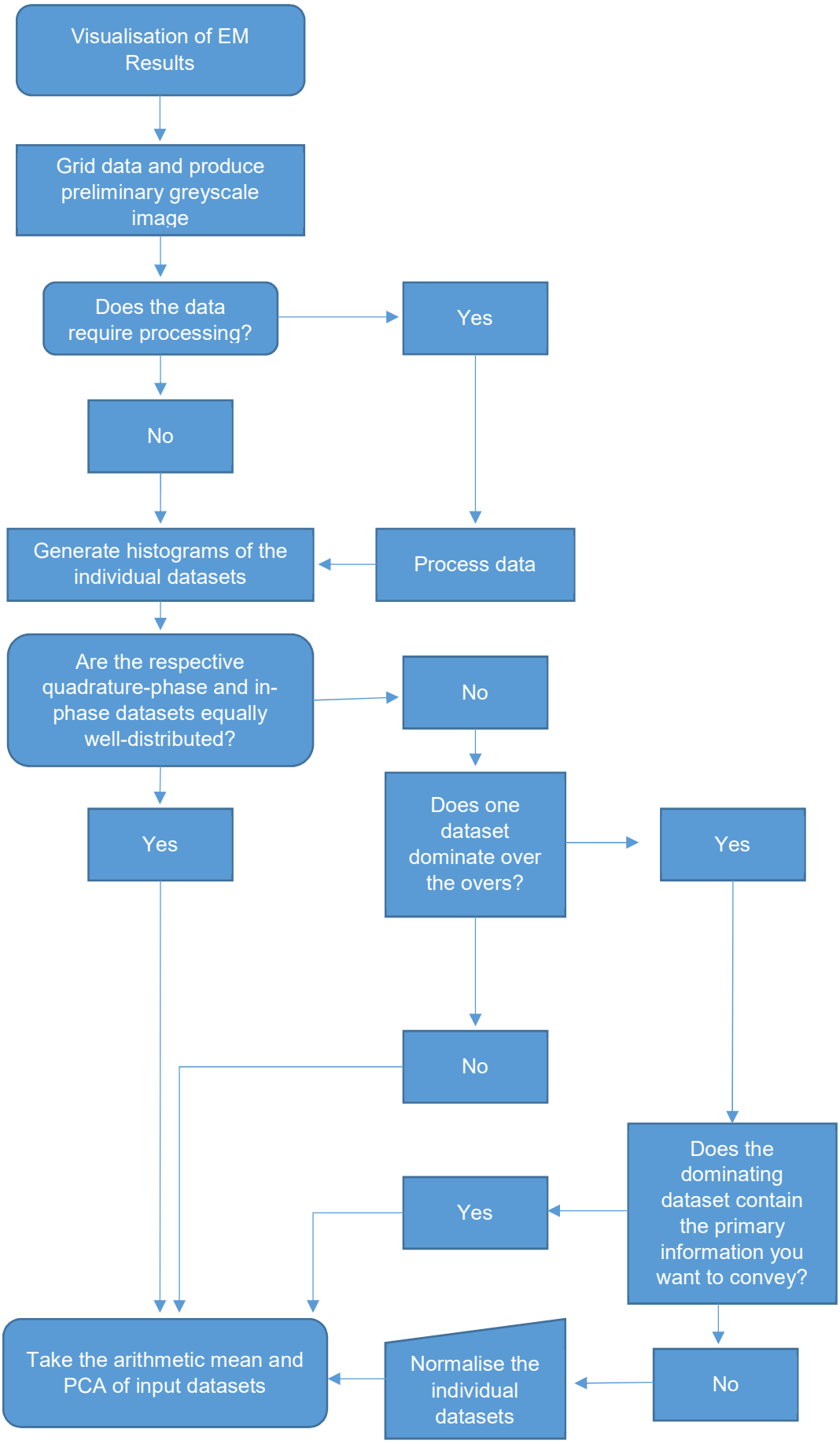

Figure 234: Flowchart for the visualisation steps for EM datasets.

6.5 EM Methodology Conclusions

The workflows presented in the preceding sections are supported by the cumulative fieldwork and experimental results of this thesis. The results have led to a better understanding of the impact of external variables on the instrument measurements. Overall, operator and environmental effects were found to have more of an impact on collected measurements than any instrument instability or drift issue. As a result, the field operation practices emphasise the importance of diligent survey procedure to ensure the collection of fundamentally accurate measurements. The data processing and visualisation methodologies have taken a straightforward, “less is more” strategy to data processing and visualisation, which should establish greater confidence in the reliability of the method. While the EM datasets required greater individual attention than their earth resistance and magnetic counterparts over the same sites, this was a result of the greater number of individual datasets produced by the EM survey. Generally, when best field operation practices were adhered to, the data output from the CMD Mini Explorer required little to no further processing. At most of the field sites, if further data processing were required to produce an interpretable image, a simple zero-median traverse was effective to mitigate a variety of data issues—most of which were operator induced in the first place.

Chapter 7 Defining the Role of EM methods Within a British Archaeological Geophysics Approach

The fulfilment of the aim of this research has been planned through the establishment of the research questions and their associated objectives. The answers to the research questions are discussed below, with the supporting work conducted in accordance with the research objectives. The culmination of the answers to these research questions will lead to the fulfilment of the aim: to develop the role of EM methods for British archaeology within a combined magnetic and earth resistance approach, in order to develop a comprehensive characterisation of archaeological remains.

7.1 Research Question 1: what is the most effective methodology for the collection, processing and visualisation of electromagnetic induction data?

The fully developed methodology for the collection, processing and visualisation of EM data is presented in Chapter 6. The methodology is separated into four separate aspects of EM work: field operation, gridding of data, data processing and correction, and the analysis and visualisation of results.

The fieldwork and experimental results demonstrated the critical importance of field operation practices for laying the foundation for the proceeding work. The collection of high-quality and positionally accurate measurements in the field minimises the need for further data processing and improves interpretation confidence. To ensure field results are collected to a high standard, it is important to consider any site-specific considerations or requirements of the field survey before commencing survey work. When collecting data, the operator should ensure the instrument is maintained at a fixed position above the ground surface, is calibrated in the direction of the upcoming traverse, and is walked at an even pace. While external variables, such as weather and ground conditions, can impact the collected measurements, operator introduced effects had a greater impact on instrument measurements and were often difficult to correct through data processing. In contrast, instrument drift proved relatively straightforward to correct through processing. Adhering to the best operation practices outlined in 6.1 and consistent operation of the instrument throughout the survey will minimise the introduction of data issues and errors.

Despite rigorous collection methods, none of the datasets collected during this thesis' field surveys are free from imperfections; most required minimal data processing, at the very least, to produce an accurate interpretative image. Standard processing workflows for earth resistance and magnetic gradiometer data were not found to be wholly effective for correcting quadrature-phase and in-phase datasets, respectively (see sections 6.3.1-2). The EM datasets need a bespoke approach, given the dynamic range of the instrument and its ability to detect both conductive and magnetically enhanced features. Generally, the EM datasets required less processing steps than what is recommended for earth resistance and magnetic gradiometer data. For the majority of the sites, a zero-median traverse was effective for correcting most of the data issues that manifested in both the in-phase and quadrature-phase (see section 6.3.3). Most of the data issues were introduced through the instrument operator or the site's ground surface conditions, as opposed to an instrument instability.

The visualisation of the EM results also required a bespoke approach to the standard methodology employed for the visualisation of magnetic and earth resistance data. Owing to the high dynamic range of the EM instrument, the plotting ranges for the greyscale images varied greatly depending on the type of archaeology present at the site—especially if ferrous material was present (see section 6.4). The output of six unique datasets from the CMD Mini Explorer provides a considerable amount of information to interpret, both as a lateral view and for providing a vertical discrimination of feature depth extent. Combination of the respective in-phase and quadrature-phase R1, R2 and R3 datasets, using an arithmetic mean and principal component analysis (PCA), was important for realising the full potential of the results. The PCA was an effective tool as an interpretative aid (see section 6.4). The transformation of the data onto the principal components highlighted different aspects of the variability between the individual input datasets, which was useful for better understanding of how the different datasets related to one another. Furthermore, the principal components often enhanced less explicit or obscured features that were difficult to identify in the individual datasets. Overall, PCA offered significant interpretative value and was harnessed to grasp the important information contained within the separate datasets. On the other hand, PCA was found to be less effective for producing a

representative composite image of the constituent datasets; any noise or significantly high-contrast responses were typically highlighted in the principal components and obscured the overarching archaeological features. Instead, a simple arithmetic mean of the respective in-phase and quadrature-phase R1, R2 and R3 datasets was more effective for creating a composite image that demonstrated the key features within the results (see section 6.4).

Adhering to these methodologies should ensure the collected, processed and visualised EM data are representative of the buried archaeology and not dominated by the influence of external, unrelated variables, such as operator-induced error and instrument drift. In the absence of the contributing external variables, the nature of the EM measurements and how they relate to buried archaeology can be more accurately understood. This follows into the next research question, which sought to better relate collected EM measurements to the feature generating the measured response.

7.2 Research Question 2: how do the resulting electromagnetic induction measurements relate to buried archaeology at a range of typical British sites?

EM methods proved to be effective over a range of different types of archaeology across a variety survey environments, demonstrated by the results in Chapter 4. The instrument proved its effectiveness in working in the presence of modern, ferrous material at the sites of Lister Park, Menston and Fountains Abbey. Comparison of the quadrature-phase and in-phase responses confirm that ferrous material produces high-contrast responses in both phases. However, despite the high-contrast nature of the ferrous response, the anomalies representing these features are not broad or blown-out in form. The EM responses over modern features, such as services and ferrous debris, more accurately delineated the true extent of the generating feature than the corresponding magnetic results did. This was useful for the delineation of the extent of debris material at Lister Park; whereas in the magnetic results, an analytic signal was required to reduce the anomalous response to the source target. Furthermore, the discrete response of ferrous material in the EM data allows for the interpretation of weaker signals closer in proximity to the modern features than could be discerned in the magnetic data. For example, as

demonstrated at Fountains Abbey and Lister Park, the spatial sensitivities of the EM instrument were advantageous over the magnetometer results in the presence of modern services and scattered near-surface debris. The near-surface ferrous material produces overwhelming responses in the magnetic and shallower EM datasets, which obscures the delineation of the archaeological features. However, the spatial sensitivity of the EM instrument allows for multiple exploration depths to be measured. As a result, the near-surface ferrous responses disappear with increased depth, allowing improved interpretation of the underlying archaeology. Therefore, an advantage of EM methods in the presence of modern interference is their vertical discrimination, which allows the instrument to measure beneath these high-contrast modern material, which is not possible with the bulk exploration depth of magnetometers.

In the absence of ferrous or other very high-contrast material, the quadrature-phase and in-phase responses show relative independence from one another and better represent the electrical conductivity and magnetic susceptibility properties of the features they are detecting. The separation of the phases is exemplified at Linton and Markenfield Hall, where the quadrature-phase and earth resistance detect complementary aspects of the same features, while the in-phase and magnetic results also detect similar aspects of the same features.

The successful detection of features exhibiting poor magnetic enhancement varied by site. At Markenfield Hall, the EM in-phase excelled over the magnetometer results, revealing trackway features and ridge and furrow ploughing responses. These features were distinguishable by the magnetic susceptibility within the fill material, which the magnetometers failed to detect. On the other hand, at Fountains Abbey, the magnetic results provided much better detection of the buried guest hall feature, which was constructed from weakly magnetic sandstone material. The in-phase struggled to coherently define the guest hall feature, although anomalies that correlate with the position of the feature have been identified. The poor performance of the in-phase over the guest hall at Fountains Abbey may therefore be a product of the survey collection strategy. The differences between these sites at Markenfield Hall and Fountains Abbey, is that a Markenfield Hall, the features were defined by earthen material, while at Fountains Abbey, the features were comprised of insulating material. EM

methods have a reputation for being poor at detecting resistive structures, given the nature of the induction of the electromagnetic wave. However, this explanation is not supported by the Lister Park results. In the EM in-phase results at Lister Park, linear anomalies correlating with wall features are detected, which indicates the method is able to detect resistive features. Furthermore, the quadrature-phase at Fountains Abbey delineates the full extent of the guest hall's structural remains. Therefore, resistive structures are not inherently impossible to detect, but their detection may depend on the surrounding site conditions.

Overall the EM methods were found to produce comprehensive detection of a range of different types of features at all the sites. The advantage of the EM methods is their ability to measure magnetic properties in addition to the electrical conductivity properties, which allowed for a range of different features and anthropogenic activity to be detected. The results at Fountains Abbey and Lister Park provide examples this ability, as not only are the structural remains detected, but areas of enhancement that reflect potential anthropogenic activity are detected as well. The site of Menston further exemplifies this capability, because the EM methods were the only geophysical method to detect the full extent and spread of the material separate from the plot markers. Furthermore, the spatial sensitivities of the instruments at some sites, like Linton, for instance, allowed the detection of unique responses at separate depths. This is an obvious advantage to the magnetic and earth resistance results, which only measured one bulk soil volume.

In regards to the accuracy of the EM anomaly for representing the source feature, the EM results provide coherent anomaly forms across the range of different feature types. Temporal drift was not present in all the EM results. No consistent correlation between changes in measurements with changes to ambient air temperature and/or humidity could be demonstrated either. When the instrument did show drift, it tended to be in the in-phase results, which is supported by the experimental results being less stable and less consistent than the quadrature-phase. The behaviour of the drift usually manifested as a quadratic tendency to change across the lines. Correction of the drift between the traverses was straightforward with the application of a zero-median traverse. Drift within the line was difficult to identify in the EM results, as well as the random, sporadic jumps

observed in the experimental phase of this research. Random knocks, accidental knocking and minor rotation of the sensor did not impact the field measurements noticeably either. The impact of these effects is reduced or confined to a single line due to the instrument's recalibration at the end of each line. Any lingering effects were often found to be corrected in the zero-median traverse.

Overall, the instrument demonstrated good stability in field operation, as well as the experimental results, especially when appropriate survey strategies and attentive instrument operation were adhered to. The outcome of the field and experiment results suggests that previous problems and notions of the instrument's instability were likely to be exacerbated or arise from by operational practices. With this in mind, the EM datasets can be effectively integrated with different geophysical methods to derive a more comprehensive understanding of the nature of the instrument and to accurately characterise the archaeological features.

7.3 Research Question 3: how can the individual magnetic, earth resistance and EM techniques be effectively used in combination to better assess and characterise buried archaeology?

Integration of the EM results with the complementary earth resistance and magnetic datasets was important for developing a comprehensive archaeological characterisation of the buried remains. Several graphical integration and data combination approaches were tested at the different sites to determine the most effective integration strategies. The diversity of the results concluded that no single integration strategy was more or less effective than another, as the success of the integration depended on the nature of the buried archaeology and the responses it produced in the different instruments.

7.3.1 Applications for GIS Integration

A GIS integration strategy was found to be the most flexible integration technique. GIS analysis tools were effective for analysing where the different techniques were correlated or not correlated to one another. The geometry intersect tool was utilised to understand where the quadrature-phase and in-phase anomalies correlated, which helped to describe what type of material or feature the instrument is responding to. The relationships between the earth resistance and

quadrature-phase datasets, as well as between the magnetic and in-phase datasets, were also understood through intersection analysis. Anomalies correlating with the complementary technique provided an indication of when the EM results represented the physical properties they are meant to be a proxy for.

The geometric intersection tool was critical for the Menston analysis, to determine the correlation and spread of the discrete grave anomalies detected by the different methods. Intersection analysis was not suitable for all sites, however. For example, intersection analysis had limited application at Lister Park, because in the magnetic results, many of the structural features were not defined by anomalies, but instead defined by the absence of anomalies. Still, the GIS environment was effective beyond exploiting the analytical tools. In addition to the analysis tools, the GIS environment was also effective for data integration by simply overlaying of the different methods' interpretations. This was important for Fountains Abbey where the vertical changes of features with depth was more important than a two-dimensional lateral view. Separating the different methods into relative exploration depths and overlaying the separate interpretations provided a comprehensive understanding of features changes with depth.

7.3.2 Applications for Image Integration Using Colour Channels

The graphical integration approach of producing a CMYK image with the colour channels representing the individual datasets produced mixed results. On sites where each constituent dataset produced unique, high-contrast results, the CMYK integration was effective. This was demonstrated at Lister Park and Linton, where each of the different methods were responding to different aspects of the same features. At both sites, the earth resistance provided a detailed lateral map of the structural plan or edges of the archaeological features. The detection of feature edges was less clear in the EM and magnetic results, but these methods detected material not evident in the earth resistance results, including areas of anthropogenic enhancement. When the individual datasets were overlaid against one another, the resulting image revealed areas of enhancement bounded within the coherent structural features in the earth resistance data (Figure 66; Figure 111).

The CMYK integration was less effective on sites where the different datasets detected the same aspects of the same features or had low-contrast responses. The resulting image blended these layers into a muddied response, or one particular dataset would dominate the others. This result was observed at Fountains Abbey and Markenfield Hall, where the same high-contrast features dominated two or more of the datasets and the resulting overlay was indistinguishable from an individual result (Figure 80; Figure 96).

7.3.3 Effectiveness of Data Combination Integration

The GIS-based and CMYK image overlay approaches were designed to integrate the different results through visual methods. The data combination approaches targeted the actual measurement values themselves and sought to further enhance or obscure aspects of the different datasets. The application of the arithmetic mean and principal component analysis on the geophysical methods had two objectives: the first sought to reduce the dimensionality of the combined methods by creating an image that represented the key features of the input datasets. The second sought to characterise the nature of the buried archaeology by understanding the relationships and differences between the different results.

The arithmetic mean of the different methods was straightforward to implement. It was most effective for generating a representative image on those sites where high-contrast, near-surface noise was detected in only one or two of the datasets because the contribution from the other datasets would obscure much of this noise. In contrast, the PCA would highlight this high-contrast noise and obscure the archaeological features, as demonstrated at Lister Park. The arithmetic mean was also more effective at those sites where the different methods were responding to different aspects of the same features. This is exemplified at Lister Park, where structural outlines are delineated in the earth resistance and EM methods, but the nature of the constituent fill of these features is better understood in the magnetic and EM results. As a result, when the mean of the methods is taken, the enhancement areas within the magnetic and EM results are visualised within the defined wall features contributed by the earth resistance data. The mean was least effective on sites where the different methods were detecting the same aspects of the same features, as the datasets with the highest contrasted of responses would dominate the composite image—despite the

datasets being normalised before combination. This was seen at Fountains Abbey, where all the methods are detecting the structural outline of the guest hall building. The PCA was also effective for dimensionality reduction and producing a representative composite image, but at sites where the mean of the methods was not effective. At Fountains Abbey, the PCA produces composite images that better represent the range of constituent datasets, as opposed to the arithmetic mean, which primarily reflects the earth resistance results. The PCA offers the additional interpretative benefit in that it delineates the individual pillar bases of the southern pillar row; whereas in the input datasets, these features are difficult to individually discern due to noise or lack of detection.

At sites where each input dataset is distinct from one another, the PCA is useful for understanding how the different datasets relate and differ to one another. At Lister Park, the PCA indicates which datasets have the most variance, which is useful for relating what properties the EM datasets are representing. At Linton, the PCA and mean results present unique datasets from one another. The arithmetic mean results provide the most balanced composite image, while the first principal component enhances the delineation of weaker features, which are lost beneath the broad trend across the site. In contrast, the second and third principal component highlight larger-scale trends within the results, both broad anthropogenic features and background variation.

The overall concept of integrating the geophysical methods was effective within this research and demonstrated the value that integration methods can offer for developing a comprehensive archaeological characterisation of the geophysical results. However, the testing of the different integration strategies demonstrates there is no “one-size-fits-all” strategy for integration techniques. The effectiveness of the integration technique depended on the type of material present and the scale of the measured features. The discussion above demonstrates how it is possible to have an idea on what integration technique will be most effective on the input datasets, but the strategy fundamentally depends on what information the integration should extract or convey.

7.4 EM Methods: Bridging the Gap Between Earth Resistance and Magnetic Methods

This thesis demonstrates the effectiveness of EM survey over a range of different environments with different types of archaeology. The success across this diversity of sites should instil a greater sense of confidence and reliability in the application of EM for British archaeology. At most of the sites, the application of the standard earth resistance and magnetic methods was successful as well, often detecting different aspects of the same features. As a result, the earth resistance and magnetic results generally presented distinct, complementary data. Whereas, by comparison, the EM results detected a range of features, many of which were uniquely presented in either the earth resistance and magnetic data. In this aspect, the EM results were more comprehensive than the standalone earth resistance or magnetometer surveys, because they could both measure electrical conductivity and magnetic susceptibility properties simultaneously. Lister Park, Menston, and Fountains Abbey exemplified the wealth of information the quadrature-phase and in-phase results can provide, because many of the measured features had distinct electrical or magnetic properties. Still, EM survey should not be considered a direct proxy for earth resistance or magnetometer survey, because the magnitude and form of the detected features is distinct to the other methods. Furthermore, over the earthen sites in particular, the EM results detected many unique features that were not detected in either of the earth resistance and magnetic methods.

The EM surveys also provided vertical discrimination of features by measuring three exploration depths. In the presence of ferrous material, the EM's multiple exploration depths was able to disentangle the overlying modern features and ferrous disturbances from the surrounding and underlying archaeological activity. At Lister Park, Fountains Abbey, and Linton, the EM results revealed distinct changes of features with depth, which were not possible to discern within the bulk measurements of the earth resistance and magnetic methods. At these sites, the vertical discrimination of the EM results was able to tie in the earth resistance and magnetic results with the sequencing of the study area.

Overall, the wealth of information contained within the six unique EM datasets, bridged the gap between the earth resistance and magnetic results at most of the

test sites. The EM results naturally fit within an integrated strategy using complementary earth resistance and magnetic results and together provide a more holistic characterisation of the nature of the subsurface. While the EM results were crucial for linking the earth resistance and magnetic results for a comprehensive narrative of the site, the research in this thesis proves that the EM method can provide a strong narrative in its own right. The reliability of the EM results through this research and their contribution to a greater archaeological characterisation, warrants further application of this method—both in its own right and with complementary techniques. The cumulative work of this research proves the effectiveness of EM methods over British archaeology, justifying its potential for more regular application within the UK. Given the wealth of information provided by the quadrature-phase and in-phase results of EM surveys, there is much potential for further research into EM application.

7.5 Scope for Further Work

This thesis has demonstrated the reliability of EM survey over a range of different environments, but the test sites were limited to within Yorkshire. Further comprehensive testing schemes should be taken across the country, especially under a range of different types of soils and geology.

Survey with the instrument was undertaken in the spring and autumn months. Testing over the same location in the University's amphitheatre revealed a range of different baseline measurements, indicating a potential dependency on measurement values to seasonal temperatures or soil conditions. Seasonality impact on earth resistance measurements has been discussed at length within the published literature, but less so for EM survey. If the EM instrument is measuring interstitial moisture content within earthen features, it is plausible that seasonal conditions could have an impact on the measured response.

The work at Fountains Abbey highlighted the limitations of the integration strategies employed for this research. The multiple exploration depths employed at the site revealed different features at deeper depths. Three-dimensional integration strategies for EM data should be explored to more effectively convey both the lateral and vertical extents of features. An approach similar to that of Watters (2006), which combines two-dimensional and three-dimensional

datasets could be effective for visualising sites with features changes with depth (see section 2.6.1; Figure 28). This would provide a good route to explore the integration of ground penetrating radar (GPR) or ERT data, which could be useful for more accurately quantifying the vertical changes observed through the EM datasets.

There is scope for further geophysical techniques to be incorporated into an integrated multi-method and EM framework. For example, integrating magnetic susceptibility with EM and magnetic datasets could prove informative for more accurately characterising the processes resulting in the magnetic enhancement of the source feature.

This thesis took a minimal, “less-is-more” approach to EM data processing—using data processing solely to correct for data issues that could impact the accuracy of the interpretation. The PCA highlighted components of the datasets that were not explicit when viewed as individual results. Therefore, the further potential to explore higher level filters and signal processing algorithms to enhance or extract information contained within the results could be effective to realise the full potential of the EM datasets.

Bibliography

Abraham, J.D., Deszcz-Pan, M., Fitterman, D.V. and Burton B.I. (2006) Use of a handheld broadband EM induction system for deriving resistivity depth images. Symposium on the Application of Geophysics to Engineering and Environmental Problems.

Andrenelli, M.C., Magini, S., Pellegrini, S., Perria, R., Vignozzi, N. and Costantini, E.A.C. (2013) The use of the ARP© system to reduce the costs of soil survey for precision viticulture. *Journal of Applied Geophysics* 99, 24-34.

Ard, V., Mathe, V., Leveque, F. and Camus, A. (2015) A comprehensive magnetic survey of a Neolithic causewayed enclosure in west-central France for the interpretation of archaeological features. *Archaeological Prospection* 22, 21-32.

Arisoy, M. (2014) Edge detection of archaeomagnetic data: A study from the city of Pisidia Antiocheia, Turkey. *Archaeological Prospection* 21, 293-300.

Aspinall, A. and Saunders, M. (2005) Experiments with the square array. *Archaeological Prospection* 12, 115-129.

Aspinall, A., Gaffney, C. F. and Schmidt, A. (2008) *Magnetometry for archaeologists.* Geophysical methods for archaeology. Lanham: AltaMira Press.

Bartington, G. and Chapman, C. (2004) A high-stability fluxgate magnetic gradiometer for shallow geophysical survey application. *Archaeological Prospection* 11, 19-34.

Beamish, D. (2011) Low induction number, ground conductivity meters: a correction procedure in the absence of magnetic effects. *Journal of Applied Geophysics* 75, 244-253.

Becker, H. (2009) Caesium-magnetometry for landscape-archaeology. In Campana, S. and Piro, S. (editors) *Seeing the Unseen: Geophysics and Landscape Archaeology.* London: Taylor & Francis Group. 129-166.

Benech, C. and Marmet, E. (1999) Optimum depth of investigation and conductivity response rejection of the different electromagnetic devices measuring apparent magnetic susceptibility. *Archaeological Prospection* 6, 31-45.

Benech, C., Tabbagh, A. and Desvignes, G. (2002) Joint inversion of EM and magnetic data for near-surface studies. *Geophysics* 67 (6), 1729-1739.

Bevan, B. (1996) The magnetic anomaly of a brick foundation. *Archaeological Prospection* 1, 93-104.

Black, G. and Johnston, R. (1962) A test of magnetometry as an aid to archaeology. *American Antiquity* 28 (2), 199-205.

Black, D. and Scollar, I. (1969) Spatial filtering in the wave-vector domain. *Geophysics* 34 (6), 916-923.

Bonsall, J., Fry, R., Gaffney, C., Armit, I., Beck, A. and Gaffney, V. (2013a) Assessment of the CMD Mini-Explorer, a new low-frequency multi-coil electromagnetic device, for archaeological applications. *Archaeological Prospection* 20, 219-231.

Bonsall, J., Gaffney, C. and Armit, I. (2013b) Preparing for the future: a reappraisal of archaeo-geophysical surveying on Irish National Road Schemes 2001-2010.

Boschi, F. (2011) Geophysical survey of the *Burnum* archaeological site, Croatia. *Archaeological Prospection* 18, 117-126.

Brinon, C., Simon, F. and Tabbagh, A. (2012) Rapid 1D/3D inversion of shallow resistivity multipole data: examples in archaeological prospection. *Geophysics*, 198-201.

British Geological Survey (2016) Geology of Britain viewer. http://mapapps.bgs*.ac.uk/geologyofbritain/home.html?*

Callegary, J.B., Ferre, T.P.A and Groom, R.W. (2012) Three-dimensional sensitivity distribution and sample volume of low-induction-number electromagetic-induction instruments. *SSAJ* 76 (1), 85-91.

Campana, S. and Dabas, M. (2011) Archaeological impact assessment: the BREBEMI Project (Italy). *Archaeological Prospection* 18 (2), 139-148.

Carr, C. (1982) *Handbook on soil resistivity surveying.* Evanston: Center for American Archaeology Press.

Cella, F., Paoletti, V., Florio, G. and Fedi, M. (2015) Characterizing elements of urban planning in Magna Graecia using geophysical techniques: the Case of Tirena (Southern Italy). *Archaeological Prospection* 22 (3).

Cheyney, S. (2012) *3D quantitative interpretation of archaeo-magnetic surveys: application of mathematical modelling to determine depths and physical characteristics of buried materials.* PhD Thesis. University of Leicester.

Cheyney, S., Hill, I. and Linford, N. (2011) Advantages to using the pseudogravity transformation to aid edge detection of total field archaeomagnetic datasets. *Archaeological Prospection* 18, 81-93.

Clark, A. (1996) *Seeing beneath the soil : prospecting methods in archaeology.* Revised paperback edition. Routledge: London.

Clay, R. (2006) Conductivity survey: a survival manual. In Johnson, J. (editor) *Remote sensing in archaeology: an explicitly North American perpsective.* Tuscaloosa: University of Alabama Press. 79-108.

Cocchi, L., Stefanelli, P., Carmisciano, C. and Tont (2012) Marine archaeogeophysical prospection of Roman Salapia settlement (Puglia, Italy): Detecting ancient harbour remains. *Archaeological Prospection* 19, 89-101.

Constable, S., Parker, R. and Constable, C. (1987) Occam's inversion: a practical algorithm for generating smooth models from electromagnetic sounding data. *Geophysics* 52 (3), 289-300.

Dabas, M. (2009) Theory and practice of the new fast electrical imaging system ARP. In Campana, S. and Piro, S. (editors) *Seeing the Unseen: Geophysics and Landscape Archaeology.* London: Taylor & Francis Group. 105-128.

Dabas, M., Anest, A., Thiesson, J. and Tabbagh, A. (2016) Slingram EMI devices for characterizing resistive features using apparent conductivity measurements: check of the DualEM-421S instrument and field tests. *Archaeological Prospection*.

Dalan, R., Bevan, B., Goodman, D., Lynch, D., De Vore, S., Adamek, S., Martin, T., Holley, G. and Michlovic, M. (2011) The measurement and analysis of depth in archaeological geophysics: tests as the Biesterfeldt Site, USA. *Archaeological Prospection* 18, 245-265.

David, A., Linford, N., Linford, P. and Martin, L. (2008) Geophysical survey in archaeological field evaluation: research and professional service guidelines (2nd edition). Historic England.

Dechezlepretre, T., Dabas, M. and Gruel, K. (2009) Automatic magnetic mapping of the oppidum of Boviolles (Meuse, France). In Marguerie, D. and Lanos, P. (eds) Memoire du sol, espace des hommes. Paris: Presses Universitaires De Rennes. 51-54.

De Smedt, P., Van Meirvenne, M., Meerschman, E., Saey, T., Bats, M., Court-Picon, M., De Reu, J., Zwertvaegher, A., Antrop, M., Bourgeois, J., De Maeyer, P., Finke, P.A., Verniers, J. and Crombe, P. (2011) Reconstructing palaeochannel morphology with a mobile multicoil electromagnetic induction sensor. *Geomorphology* 130, 136-141.

De Smedt, P., Saey, T., Lehouck, A., Stichelbaut, B., Meerschman, E., Islam, M., Van De Vijver, E. and Van Merivenne, M. (2013) Exploring the potential of multi-receiver EMI survey for geoarchaeological prospection: a 90 ha dataset. *Geoderma* 199, 30-36.

De Smedt, P., Saey, T., Meerschman, E., De Reu, J., De Ciercq, W. and Van Meirvenne, M. (2014a) Comparing apparent magnetic susceptibility measurements of a multi-receiver EMI sensor with topsoil and profile magnetic susceptibility data over weak magnetic anomalies. *Archaeological Prospection* 21 (2), 103-112.

De Smedt, P., Van Meirvenne, M., Saey, T., Baldwin, E., Gaffney, C. and Gaffney, V. (2014b) Unveiling the prehistoric landscape at Stonehenge through multi-receiver EM. *Journal of Archaeological Science* 50, 16-23.

Delefortrie, S., De Smedt, P., Saey, T., Van De Vijver, E. and Van Merivenne, M. (2014) An efficient calibration procedure for correction of drift in EMI survey data. *Journal of Applied Geophysics* 110, 115-125.

Di Maio, R., La Manna, M. and Piegari, E. (2016) 3D reconstruction of buried structures from magnetic, electromagnetic and ERT data: example from the archaeological site of Phaistos (Crete, Greece). *Archaeological Prospection* 23 (1), 3-13.

Doneus, M. and Neubauer, W. (1998) 2D combination of prospection data. *Archaeological Prospection* 5, 29-56.

Dos Santos, V. and Porsani, J. (2011) Comparing performance of instrument drift correction by linear and quadratic adjusting in inductive electromagnetic data. *Journal of Applied Geophysics* 73, 1-7.

Evans, M. and Heller, F. (2003) *Environmental magnetism: principles and applications of enviromagnetics.* International Geophysics Series. London: Academic Press.

Fassbinder, J. (2015) Seeing beneath the farmland, steppe and desert soil: Magnetic prospecting and soil magnetism. *Journal of Archaeological Science* 56, 85-95.

Gaffney, C. F. and Gater, J. (2003) *Revealing the buried past : geophysics for archaeologists.* Stroud: Tempus Publishing.

Gaffney, C., Gaffney, V., Neubauer, W., Baldwin, E., Chapman, H., Garwood, P., Moulden, H., Sparrow, T., Bates, R., Locker, K., Hinterleitner, A., Trinks, I., Nau, E., Zitz, T., Floery, S., Verhoeven, G. and Doneus, M. (2012) The Stonehenge Hidden Landscape Project. *Archaeological Prospection* 19: 147-155.

Gaffney, C., Harris, C., Pope-Carter, F., Bonsall, J., Fry, R. and Parkyn, A. (2015) Still searching for graves: an analytical strategy for interpreting geophysical data used in the search for “unmarked” graves. *Near Surface Geophysics* 13 (6), 557-569.

Geoscan Research (2005) Geoplot instruction manual: main section. Version 1.97. http://www.geoscan-research.co.uk/Gp300Short5andUSB.pdf

GF Instruments (2016) Short guide for electromagnetic conductivity mapping and tomography. http://www.gfinstruments.cz/version_cz/downloads/CMD_ Short_guide_ Electromagnetic _conductivity_mapping-10-10-2016.pdf. Accessed 12 December 2016.

Gheyle, W., Saey, T., Van Hollebeeke, Y., Verplaetse, S., Note, N., Bourgeois, J., Van Merivenne, M., Van Eetvelde, V. and Stichelbaut, B. (2016) Historic aerial photography and multi-receiver EMI soil sensing, complementing techniques for the study of a Great War conflict landscape. *Archaeological Prospection*.

Habberjam, G. (1979) *Apparent resistivity observations and the use of square array techniques.* Geoexploration Monographs. Vol. 1. Berlin: Gerbrueder Borntraeger.

Harris, C. (2011) *Evaluating the trapezoid array's effectiveness for archaeological prospection*. MSc Dissertation. University of Bradford.

Harris, C. and Gaffney, C. (2014) Fountains Abbey: BCAP report 2014/2015.

Harris, C., Gaffney, C., Pope-Carter, F., Bonsall, J., Fry, R. and Parkyn, A. (2015a) High Royds: an integrated, analytical approach for mapping the unmarked burials at a pauper cemetery. In *11th International Conference on Archaeological Prospection.* 15-19 September 2015 Warsaw.

Harris, C., Pope-Carter, F., Sparrow, T. and Gaffney, C. (2015b) ArchaeoPY: constructing and utilising open source software for archaeological geophysics. In *Computer Applications and Quantitative Methods in Archaeology (CAA) Annual Conference.* 30 March – 3 April 2015 Siena.

Henry, E., Laracuente, N., Case, J. and Johnson, J. (2014) Incorporating multistaged geophysical data into regional-scale models: a case study from an Adena burial mound in central Kentucky. *Archaeological Prospection* 21 (1), 15-26.

Heritage Gateway, 2016. http://www.heritagegateway.org.uk/gateway/

Hesse, A. (1999) Multi-parametric survey for archaeology: how and why? or how and why not? *Journal of Applied Geophysics* 41, 157-168.

Jolliffe, I. (1986) *Principal component analysis.* Springer Series in Statistics. New York: Springer-Verlag New York Inc.

Jordan, D. (2009) How effective is geophysical survey? A regional review. *Archaeological Prospection* 15 (2), 77-90.

Keay, S., Earl, G., Hay, S., Kay, S., Ogden, J. and Strutt, K. (2009) The role of integrated geophysical survey in the assessment of archaeological landscapes: the case of Portus. *Archaeological Prospection* 16, 154-166.

Klehm, C. and Ernenwein, E. (2016) Iron Age transformation at Mmadipudi Hill, Botswana: identifying spatial organization through electromagnetic induction survey. *African Archaeological Review* 33, 45-59.

Kvamme, K. (2001) Current practices in archaeogeophysics: magnetics, conductivity, and ground-penetrating radar. In Goldber, P., Holliday, V.T. and Ferring, C.R. (editors) *Earth Sciences and Archaeology*. 353-384.

Kvamme, K. (2003) Multidimensional prospecting in North American Great Plains village sites. *Archaeological Prospection* 10, 131-142.

Kvamme, K. (2006a) Magnetometry: nature's gift to archaeology. In Johnson, J. (editor) *Remote Sensing in Archaeology: an Explicitly North American Perpsective.* Tuscaloosa: The University of Alabama Press. 205-233.

Kvamme, K. (2006b) Integrating multidimensional geophysical data. *Archaeological Prospection* 13, 57-72.

Landry, D., Ferguson, I., Milne, S. and Park, R. (2015) Combined geophysical approach in a complex Arctic archaeological environment: a case study from the LdFa-1 Site, Southern Baffin Island, Nunavut. *Archaeological Prospection* 22, 157-170.

Linford, N. (1998) Geophysical survey at Boden Vean, Cornwall, including an assessment of the microgravity technique for the location of suspected archaeological features. *Archaeometry* 40 (1), 187-216.

Linford, N. (2004) From hypocaust to hyperbola: ground-penetrating radar surveys over mainly Roman remains in the UK. *Archaeological Prospection* 11, 237-246.

Linington, R. (1963) The application of geophysics to archaeology. *American Scientist* 51 (1), 48-70.

Loke, M., Chambers, J., Rucker, D., Kuras, O. and Wilkinson, P. (2013) Recent developments in the direct-current geoelectrical imaging method. *Journal of Applied Geophysics* 95, 135-156.

Lowe, K.M. and Fogel, A.S. (2010) Understanding northeastern Plains Village sites through archaeological geophysics. *Archaeological Prospection* 17, 247-257.

Lueck, E. and Ruehlmann, J. (2013) Resistivity mapping with GEOPHILUS ELECTRICUS--information about lateral and vertical soil heterogeneity. *Geoderma* 199, 2-11.

MacLeod, I., Jones, K. and Dai, T. F. (1993) 3-D analytic signal in the interpretation of total magnetic field data at low magnetic latitudes. *Exploration Geophysics* 24, 679-688.

Mather, P. M. and Koch, M. (2011) *Computer Processing of Remotely-Sensed Images.* Chichester: John Wiley & Sons, Ltd.

McNeill, J. (1980) Technical note TN-6: electromagnetic terrain conductivity measurement at low induction numbers. Geonics Limited.

McNeill, J. (2013) Technical note TN-35: archaeological mapping using the Geonics EM38B to map terrain magnetic susceptibility (with selected case histories). Geonics Limited:

Mohamed-Ali, M., Herbich, T., Grzymski, K. and Hobbs, R. (2012) Magnetic gradient and electrical resistivity tomography surveys in Meroe, the capital city of the Kush Kingdom, Sudan. *Archaeological Prospection* 19, 59-68.

Mojica, A., Pastor, L., Camerlynck, C., Florsch, N. and Tabbagh, A. (2014) Magnetic prospection of the pre-Columbian archaeological site of El Cano in the cultural region of Gran Cocle, Panama. *Archaeological Prospection* 21, 201-211.

Moorhouse, S. (2006) The Threshfield Pasture Historic Landscape Project: an interim report.

Mozzi, P., Fontana, A., Ferrarese, F., Ninfo, A., Campana, S. and Francese, R. (2016) The Roman city of Altinum, Venice Lagoon, from remote sensing and geophysical prospection. *Archaeological Prospection* 23, 27-44.

Neubauer, W. and Eder-Hinterleitner, A. (1997) 3-D interpretation of postprocessed archaeological magnetic prospection data. *Archaeological Prospection* 4, 191-205.

Panissod, C., Dabas, M., Hesse, A., Jolivet, A., Tabbagh, J. and Tabbagh, A. (1998) Recent developments in shallow-depth electrical and electrostatic prospecting using mobile arrays. *Geophysics* 63 (5), 1542-1550.

Papadopoulos, N., Tsokas, G., Dabas, M., Yi, M., Kim, J. and Tsourlos, P. (2009) Three-dimensional inversion of automatic resistivity profiling data. *Archaeological Prospection* 16, 267-278.

Papadopoulos, N., Tsourlos, P., Tsokas, G. and Sarris, A. (2006) Two-dimensional and three-dimensional resistivity imaging in archaeological site investigation. *Archaeological Prospection* 13, 163-181.

Parchas, A. and Tabbagh, A. (1978) Simultaneous measurement of electrical conductivity and magnetic susceptibility of the ground in the EM prospecting. *Archaeophysika* 10, 682-691.

Payne, A. (1996) The use of magnetic prospection in the exploration of Iron Age hillfort interiors in Southern England. *Archaeological Prospection* 3, 163-184.

Pope-Carter, F., Attwood, G., Gaffney C. and Gater J. (2014a) CartEasyN—moving from 2D tiles to three-dimensional data collection and analysis in magnetometry. In *Recent Work in Archaeological Geophysics: 2014 Meeting.* London 2 December 2014. NSGG. 61-64.

Pope-Carter, F., Harris, C., Sparrow, T. and Gaffney, C. (2014b) ArchaeoPY: constructing and utilising open source software for archaeological geophysics. In *Recent Work in Archaeological Geophysics: 2014 Meeting.* London 2 December 2014. NSGG. 20-22.

Powlesland, D. (2009) Why bother? Large scale geomangetic survey and the quest for 'real archaeology'. In Campana, S. and Piro, S. (editors) *Seeing the Unseen: Geophysics and Landscape Archaeology.* London: Taylor & Francis Group. 167-182. NSGG.

Purvis, S.T. (2014) CMD Mini Explorer: assessing the capabilities of a multi-coil instrument. MSc Dissertation: University of Bradford.

Robinson, D., Lebron, I., Lesch, S. and Shouse, P. (2004) Minimizing drift in electrical conductivity measurements in high temperature environments using the EM-38. *Soil Science Society of America* 68 (2), 339-345.

Rogers, M.B., Faehndrich, K., Roth, B. and Shear, G. (2010) Cesium magnetometer surveys at Pithouse Site near Silver City, New Mexico. *Journal of Archaeological Science* 37, 1102-1109.

Saey, T., De Smedt, P., Monirul Islam, M., Meerschman, E., Van de Vijver, E., Lehouck, A. and Van Meirvenne, M. (2012) Depth slicing of multi-receiver EMI measurements to enhance the delineation of contrasting subsoil features. *Geoderma* 189-190, 514-521.

Saey, T., Van Meirvenne, M., De Smedt, P., Neubauer, W., Trinks, I., Verhoeven, G. and Seren, S. (2013) Integrating multi-receiver electromagnetic induction measurements into the interpretation of the soil landscape around the school of gladiators at Carnuntum. *European Journal of Soil Science* 64, 716-727.

Saey, T., Delefortrie, S., Verdonck, L., De Smedt, P. and Van Meirvenne, M. (2014) Integrating EMI and GPR data to enhance the three-dimensional reconstruction of a circular ditch system. *Journal of Applied Geophysics* 101, 42-50.

Saey, T., De Smedt, P., Delefortrie, S., Van De Vijver, E. and Van Merivenne, M. (2015) Comparing one- and two-dimensional EMI conductivity inverse modeling procedures for characterizing a two-layered soil. *Geoderma*, 12-23.

Saey, T., Note, N., Gheyle, W., Stichelbaut, B., Bourgeois, J., Van Eetvelde, V. and Van Merivenne, M. (2016) EMI as non-invasive survey technique to

account for the interaction between WWI relicts and the soil environment at the Western front. *Geoderma* 265, 39-52.

Schmidt, A. (2013) *Earth resistance for archaeologists. Geophysical methods for archaeology*. Lanham: AltaMira Press.

Schotsmans, E., Van de Vijver, K., Wilson, A. and Castex, D. (2015) Interpreting lime burials. A discussion in light of lime burials at St. Rombout's cemetery in Mechelen, Belgium (10-18th centuries). *Journal of Archaeological Sciences: Reports* 3, 464-479.

Scollar, I. (1969) Some techniques for the evaluation of archaeological magnetometer surveys. *World Archaeology* 1, 77-89.

Scollar, I., Tabbagh, A., Hesse, A. and Herzog, I. (1990) *Archaeological prospecting and remote sensing.* Cambridge: Cambridge University Press.

Simpson, D., Lehouck, A., Verdonck, L., Vermeersch, H., Van Merivenne, M., Bourgeois, J., Thoen, E. and Docter, R. (2009) Comparison between electromagnetic induction and fluxgate gradiometer measurements on the buried remains of a 17th century castle. *Journal of Applied Geophysics* 68, 294-300.

Soilscapes (2016) Soilscapes. Cranfield Soil and Agrifood Institute. http://www.landis.org.uk/soilscapes/

Solem, J. E. (2012) *Programming Computer Vision with Python.* Sebastopol: O'Reilly.

Stampolidis, A. and Tsokas, G. (2012) Use of edge delineating methods in interpreting magnetic archaeological prospection data. *Archaeological Prospection* 19, 123-140.

Sudduth, K., Drummond, S. and Kitchen, N. (2001) Accuracy issues in electromagnetic induction sensing of soil electrical conductivity for precision agriculture. *Computers and Electronics in Agriculture* 31, 239-264.

Tabbagh, A. (1984) On the comparison between magnetic and electromagnetic prospection methods for magnetic features detection. *Archaeometry* 26 (2), 171-182.

Tabbagh, A., Desvignes, G. and Dabas, M. (1997) Processing of Z gradiometer magnetic data using linear transforms and analytical signal. *Archaeological Prospection* 4, 1-13.

Terron, J., Mayoral, V., Salgado, J., Galea, F., Perez, V., Odriozola, C., Mateos, P. and Pizzo, A. (2015) Use of soil apparent electrical resistivity contact sensors for the extensive study of archaeological sites. *Archaeological Prospection* 22, 269-281.

Thiesson, J., Dabas, M. and Flageul, S. (2009) Detection of resistive features using towed slingram electromagnetic induction instruments. *Archaeological Prospection* 16, 103-109.

Tite, M.S. and Mullins, C.E. (1973) Magnetic viscosity, quadrature susceptibility and multi-frequency dependence of susceptibility in single domain assemblies of magnetite and maghemite. *Journal of Geophysical Research* 78, 804-809.

Tsokas, G. and Hansen, R. (2000) On the use of complex attributes and the inferred source parameter estimates in the exploration of archaeological sites. *Archaeological Prospection* 7, 17-30.

Tsokas, G., Tsourlos, P. and Szymanski, J. (1997) Square array resistivity anomalies and inhomogeneity ratio calculated by the finite element method. *Geophysics* 62 (2), 426-435.

Tsokas, G.N., Tsourlos, P.I., Stampolidis, A, Katsonopoulou, D. and Soter, S. (2009) Tracing a major Roman road in the area of Ancient Helike by resistivity tomography. *Archaeological Prospection* 16, 251-266.

Verhegge, J., Missiaen, T. and Crombe, P. (2016) Exploring integrated geophysics and geotechnics as a palaeolandscape reconstruction tool: archaeological prospection of (prehistoric) sites buried deeply below the Scheldt Polders (NW Belgium). *Archaeological Prospection*.

Viberg, A., Trinks, I. and Liden, K. (2011) A review of the use of geophysical archaeological prospection in Sweden. *Archaeological Prospection* 18 (1), 43-56.

Von Frese, R. R. B. and Noble, V. E. (1984a) Magnetometry for archaeological exploration of historical sites. *Historical Archaeology* 18 (2), 38-53.

Von Frese, R. R. B. (1984b) Archaeomagnetic anomalies of midcontinental North American archaeological sites. *Historical Archaeology* 18 (2), 4-19.

Watters, M. (2006) Geovisualization: an example from the Catholme ceremonial complex. *Archaeological Prospection* 13, 282-290.

Welham, K., Fleisher, J., Cheetham, P., Manley, H., Steele, C. and Wynne-Jones, S. (2014) Geophysical survey in sub-Saharan Africa: magnetic and electromagnetic investigation of the UNESCO World Heritage Site of Songo Mnara, Tanzania. *Archaeological Prospection* 21, 255-262.

Weymouth, J. (1986) Geophysical methods of archaeological site surveying. *Advances in Archaeological Method and Theory* 9, 311-395.

Wunderlich, T., Wilken, D., Andersen, J., Rabbel, W., Zori, D., Kalmring, S. and Byock, J. (2015) On the ability of geophysical methods to image medieval turf buildings in Iceland. *Archaeological Prospection* 22 (3), 171-186.

Appendix 1 – Processing steps
Lister Park: processing steps

Method	Configurations	Processing Steps
Earth Resistance	Geoscan Research FM256 on MSP25: Alpha and Beta Averaged	Despike and Destagger on Individual Datasets Average Datasets Despike on averaged datasets High-pass Filter
	Gamma	Despike
Magnetic	Geoscan Research FM256 on MSP25	Destagger
EM	HCP Quadrature-Phase	Zero-median Traverse
	HCP In-Phase	Zero-median Traverse
	VCP Quadrature-Phase	Zero-median Traverse
	VCP In-Phase	Zero-median Traverse

Fountains Abbey: processing steps

Method	Configurations	Processing Steps
Earth Resistance	Twin-Probe	Despike Edge-Match High-pass Filter
	Geoscan Research FM256 on MSP25: Alpha and Beta Averaged	Despike Destagger High-pass Filter
Magnetic	CartEasyN	Zero-median Traverse
	Geoscan FM256 on MSP25	Zero-median Traverse Despike Destagger
EM	VCP I1	Zero-median Traverse
	VCP I2	Rolling-median (thresholds=25-75 percentile; window=60) Zero-median Traverse
	VCP I3	Rolling-median (thresholds=10-95 percentile; window=60) Zero-median Traverse
	VCP C1	Zero-median Traverse
	VCP C2	Zero-median Traverse
	VCP C3	Rolling-median (thresholds=25-75 percentile; window=60)

Markenfield Hall: processing steps

Method	Configurations	Processing Steps
Earth Resistance	Geoscan Research MSP25: Alpha and Beta Averaged	Despike and Destagger on Individual Datasets Despike on averaged datasets
Magnetic	Geoscan Research FM256 on MSP25	Zero-median Traverse Despike Destagger
EM	HCP In-Phase	Zero-median Traverse
	HCP Quadrature-Phase	None

Linton: processing steps

Method	Configurations	Processing Steps
Earth Resistance	Alpha and Beta Averaged	Despike and Destagger on Individual Datasets Despike on averaged datasets
Magnetic	Bartington Grad601-2	Zero-median Traverse Destagger
EM	HCP In-Phase and Quadrature-Phase	Zero-median Traverse

Menston: processing steps

Method	Configurations	Processing Steps
Earth Resistance	Twin-Probe	Despike Edge Match High-pass Filter
	Trapezoid	Despike High-pass Filter
Magnetic	CartEasyN	Zero-median Traverse
	Geoscan Research FM256	Zero-median Traverse Destagger
EM	2012 HCP & VCP Quadrature-Phase	None
	2012 HCP & VCP In-Phase	Multiply grids to balance Edge-Match
	2014 HCP Quadrature-Phase	None
	2014 VCP C1	Zero-median Traverse

Method	Configurations	Processing Steps
	2014 VCP C2 & C3	None
	2014 HCP & VCP In-Phase	None

Appendix 2 – ArchaeoPY CMD Regridding Code